DIVERSITY OF MAMMALIAN ACTOMYOSIN FUNCTIONS: EVALUATION OF THE INTERACTIONS OF MYO5 ACTIN MOTOR PROTEINS AND SPIRE ACTIN NUCLEATORS

DISSERTATION ZUR ERLANGUNG DES DOKTORGRADES DER NATURWISSENSCHAFTEN (DR. RER. NAT.) DER FAKULTÄT FÜR BIOLOGIE UND VORKLINISCHE MEDIZIN DER UNIVERSITÄT REGENSBURG

vorgelegt von

Jasmin Michelle Karreis

aus

Ulm

im Jahr

2025

Das Promotionsgesuch wurde eingereicht am:

Die Arbeit wurde angeleitet von:

Prof. Dr. Eugen Kerkhoff

_____

Jasmin Karreis

Selbstständigkeitserklärung

Ich, Jasmin Karreis, geboren am 17.02.1993 in Ulm, erkläre hiermit, dass ich die vorliegende Arbeit ohne unzulässige Hilfe Dritter und ohne Benutzung anderer als der angegebenen Hilfsmittel angefertigt habe.

Die aus anderen Quellen direkt oder indirekt übernommenen Daten und Konzepte sind unter Angabe der Quelle gekennzeichnet. Insbesondere habe ich nicht die entgeltliche Hilfe von Vermittlungs- bzw. Beratungsdiensten (Promotionsberater oder andere Personen) in Anspruch genommen.

Die Arbeit wurde bisher weder im In- noch im Ausland in gleicher oder ähnlicher Form einer anderen Prüfungsbehörde vorgelegt.

Regensburg, den

_____ _____

Ort, Datum Jasmin Karreis

Meinem Opa, Dr. Heinz Bär (1927-2013)

Table of content

Abstract VIII

Zusammenfassung IX

1 Introduction 11

1.1 Cell polarisation and intracellular vesicle transport 11

1.2 Intracellular transport along microtubules and actin filaments 11

1.3 Actin and actomyosin force generation 12

1.4 Actin filament generation 13

1.5 The SPIRE actin nucleator 14

1.5.1 mitoSPIRE1 15

1.5.2 The SPIRE-formin actin nucleator complex 16

1.6 The RAB GTPases as regulators of intracellular transport 17

1.7 Transport along microtubule tracks 18

1.7.1 The myosin class-5 actin motor proteins 19

1.7.2 Regulation of myosin 5 motor activity and function 22

1.8 MYO5 – SPIRE cooperation in intracellular vesicle transport 24

1.8.1 SPIRE1 and MYO5A cooperate in melanosome transport 28

1.8.2 SPIRE1/2 and MYO5B function in oocytic vesicle movement 29

1.8.3 von Willebrand factor release – MYO5C:SPIRE1:RAB3/27 30

1.9 Evolution of the SPIRE-MYO5 interaction 30

1.10 Aim of thesis 33

2 Materials and methods 34

2.1 Multiple SPIRE protein sequence alignments 34

2.2 Agarose gel electrophoresis 35

2.3 DNA extraction from agarose gels following the protocol of Machery-Nagel 35

2.4 Measurement of DNA concentrations (according to (Welz)) 36

2.5 PCR technique: amplification of cDNA fragments for cloning (according to (Welz)) 36

2.6 Cloning of plasmid DNA expression vectors (according to (Welz)) 37

2.6.1 Restriction digest 37

2.6.2 Ligation 38

2.6.3 Transformation of *Escherichia coli* bacterial cells 38

2.6.4 Plasmid DNA extraction and purification from bacterial cells 39

2.6.5 Plasmid-MINI-purification (MiniPrep) for control digests following the protocol for Spin MiniPrep of QIAGEN 39

2.6.6 Plasmid-MINI-purification (MiniPrep) for sequencing following the protocol for MiniPrep of QIAGEN 40

2.6.7 Plasmid-Maxi-purification (MaxiPrep) following the protocol for MaxiPrep of QIAGEN 40

2.6.8 Control digests 41

2.6.9 DNA sequencing 41

2.7 Cell culture techniques (according to (Welz)) 42

2.7.1 Thawing cells 42

2.7.2 Freezing cells 42

2.7.3 Poly-L-Lysine coating of 6-well plates 43

2.7.4 Seeding cells 43

2.7.5 Transfection of eukaryotic cells 44

2.7.6 Transfection of eukaryotic cells using Lipofectamine2000 reaction 44

2.7.7 Transfection of eukaryotic cells using jetOPTIMUS® reaction (following the protocol of jetOPTIMUS® transfection reagent (Polyplus^{+})) 45

2.8 Western blotting (according to (Welz)) 45

2.8.1 Sodium dodecyl sulfate polyacrylamide gel electrophoresis (SDS PAGE) 45

2.8.2 Western blotting – protein transfer 45

2.8.3 Western blotting – Ponceau S staining 46

2.8.4 Western blotting – antibody treatment 46

2.8.5 Antibody protocols 46

2.9 Production and purification of recombinant proteins in *E.coli* bacteria 47

2.9.1 Purification of GST-NTEV-Hs-MYO5A/B/C-GTD (according to (Welz)) 47

2.9.2 Purification of His_6-mScarlet-I-Hs-SPIRE1/2-linker (according to (Welz)) 49

2.9.3 Bradford assay to measure protein concentrations 51

2.10 GST-pulldown from HEK 293 cell lysates (according to (Welz)) 52

2.11 GST-pulldown experiments with purified proteins (according to (Welz)) 53

2.12 Supernatant depletion assay in a quantitative manner (according to (Pylypenko et al. 2016; Pollard 2010)) 53

2.13 Cell fixation and labelling of intracellular structures: Immunostaining and fluorescence microscopy (according to (Welz)) ... 56

2.14 Colocalisation analysis ... 57

2.15 RNA sequence analysis ... 57

3 Results ... 58

3.1 RNA expression analysis ... 58

3.2 Constructs used in this thesis ... 61

3.3 Protein purification for protein interaction studies ... 64

3.4 Interaction of mammalian MYO5 and SPIRE proteins ... 66

3.5 Quantitative analysis of the mammalian MYO5 and SPIRE isoform interaction ... 71

3.6 Analysis of cellular colocalisation studies of MYO5 ... 77

3.7 Evolution of the SPIRE-MYO5 interaction site ... 79

4 Discussion ... 83

4.1 *In silico* RNA expression pattern in humans ... 83

4.2 Differentiation of cellular functions of SPIRE1 and SPIRE2 ... 86

4.3 Colocalisation studies of MYO5-cc-GTD with SPIRE1 and SPIRE2 ... 88

5 References ... 90

6 Supplement ... 105

6.1 Sequence related data ... 105

6.2 Overview on cloning vectors ... 113

6.2.1 pAcGFP1-C1 ... 113

6.2.2 pGEX-4T1-NTEV ... 114

6.2.3 pProEX-HTb ... 115

6.3 Expression vectors used in this thesis ... 116

6.3.1 Eucaryotic expression vectors ... 116

6.3.2 Bacterial expression vectors ... 116

6.4 Single graphs of RNA expression pattern ... 118

6.5 Single graphs and raw data of the quantitative pulldown assays: MYO5 – SPIRE interaction ... 120

6.6 Colocalization images of whole cells with insets of GFP-MYO5-cc-GTD with mScarlet-I-SPIRE1/2-ΔKW in HeLa cells 126
6.7 Buffers, solutions and media 130
6.8 SDS polyacrylamide gels 131
6.9 Primer 132
6.10 Antibodies 132
6.10.1 Primary antibodies 132
6.10.2 Secondary antibodies 133
6.11 Chemicals and reagents 133
6.11.1 Restriction endonucleases 133
6.11.2 DNA polymerases 133
6.11.3 Enzymes 133
6.11.4 Chemicals 134
6.12 Cell culture media, reagents and supplements 135
6.13 Kits 135
6.14 Equipment 136
6.15 Disposable materials 136
7 List of abbreviations 138
8 List of figures 142
9 List of tables 144
10 Acknowledgements 145

Abstract

This study immerses into the evolutionary and functional diversity of myosin class-5 actin motor proteins (MYO5) and SPIRE actin nucleators, with a particular emphasis on their collaboration in intracellular transport processes. These processes involve the movement of organelles along actin filaments facilitated by MYO5. RAB GTPases act as key regulators by recruiting MYO5 and SPIRE proteins to organelle membranes. SPIRE and MYO5 interact through a conserved binding site, forming complex structures that coordinate actin filament formation and motor activity at organelle membranes. SPIRE proteins, cooperating with FMN-subfamily formin proteins, drive actin network assembly. In melanocytes, RAB27A, MYO5A, SPIRE1, and FMN1 mediate melanosome transport, while SPIRE1/2, FMN2, and MYO5B facilitate vesicle movement in oocytes. SPIRE1/MYO5C interaction aids Weibel-Palade Body release in endothelial cells. The exact mechanisms of cell-type-specific complex formation remain unclear. A crucial interaction is the binding of SPIRE's globular tail binding motif to MYO5's globular tail domain. This thesis investigates the isoform-specific interactions of mammalian SPIRE (SPIRE1, SPIRE2) and MYO5 (MYO5A, B, C) proteins, using GST-pulldown assays and cell localisation experiments. Additionally, evolutionary insights were gained through similar experiments with proteins from single-celled holozoa (Choanoflagellate) and early branching animals (sea anemone).

The protein interaction studies performed here show that in mammals, SPIRE2 exhibits a stronger binding affinity for MYO5 isoforms compared to SPIRE1. The study also places these findings in an evolutionary context, showing that in unicellular holozoa and early branching animals the SPIRE/MYO5 interaction compares to mammalian SPIRE2/MYO5 interactions. Cellular investigations using fluorescence microscopy revealed no differences in the co-localization of SPIRE1/2 and MYO5 on vesicle surfaces, despite the differences in binding strengths.

In conclusion, the findings provide strong evidence that mammalian SPIRE1 and SPIRE2 proteins exhibit different affinities for MYO5 proteins. Considering the relatively high binding strength between choanoflagellate and sea anemone proteins, those affinity differences might have developed during evolution and the vertebrate diversification into different SPIRE and MYO5 isoforms suggesting that quantitative and qualitative differences in protein complex formation account for the increased biological complexity of vertebrate SPIRE/MYO5 transport functions. However, these results show only a part of the whole image. Different affinities between other complex partners (SPIRE-RAB, MYO5-RAB) surely sum up to the final complex dynamics in all possible ways.

Zusammenfassung

Die Studie befasst sich mit der evolutionären und funktionellen Vielfalt der Myosin-class-5-Motorproteinen (MYO5) und den SPIRE-Aktin-Nukleatoren, mit besonderem Fokus auf ihrer Zusammenarbeit bei intrazellulären Transportprozessen. Diese Prozesse umfassen den Transport von Organellen entlang von Aktinfilamenten, der durch MYO5 ermöglicht wird. RAB-GTPasen fungieren als Schlüsselregulatoren, indem sie MYO5- und SPIRE-Proteine an Organellmembranen rekrutieren. SPIRE und MYO5 interagieren über eine konservierte Bindestelle und bilden komplexe Strukturen, die die Bildung von Aktinfilamenten und die Motoraktivität an Organellmembranen koordinieren. SPIRE-Proteine treiben in Zusammenarbeit mit FMN-subfamily-Forminproteinen die Bildung von Aktin-Netzwerken voran.

In Melanozyten vermitteln RAB27A, MYO5A, SPIRE1 und FMN1 den Transport von Melanosomen, während SPIRE1/2, FMN2 und MYO5B den Vesikeltransport in Oozyten fördern. Die Interaktion zwischen SPIRE1 und MYO5C unterstützt die Freisetzung von Weibel-Palade-Körperchen in Endothelzellen. Die genauen Mechanismen der zelltypspezifischen Bildung dieser Komplexe bleiben jedoch unklar. Eine entscheidende Interaktion ist die Bindung des globular-tail-binding Motivs von SPIRE an die globular-tail binding domain von MYO5.

Diese Arbeit untersucht die isoformspezifischen Interaktionen der Säugetierproteine SPIRE (SPIRE1, SPIRE2) und MYO5 (MYO5A, B, C) mithilfe von GST-Pulldown-Assays und Zelllokalisierungsexperimenten. Zusätzlich wurden evolutionäre Einblicke durch ähnliche Experimente mit Proteinen von einzelligen Holozoen (Choanoflagellaten) und frühen Vielzellern (Seeanemonen) gewonnen.

Die durchgeführten Protein-Interaktionsstudien zeigen, dass SPIRE2 bei Säugetieren eine stärkere Bindungsaffinität zu MYO5-Isoformen aufweist als SPIRE1. Diese Befunde werden in einen evolutionären Kontext gestellt, wobei gezeigt wird, dass die SPIRE/MYO5-Interaktion bei einzelligen Holozoen und frühen Vielzellern der Interaktion von SPIRE2 und MYO5 bei Säugetieren ähnelt. Zelluläre Untersuchungen mittels Fluoreszenzmikroskopie ergaben jedoch keine Unterschiede in der Kolokalisation von SPIRE1/2 und MYO5 auf Vesikeloberflächen, trotz der Unterschiede in der Bindungsstärke.

Zusammenfassend liefern die Ergebnisse deutliche Hinweise darauf, dass die Säugetierproteine SPIRE1 und SPIRE2 unterschiedliche Affinitäten zu MYO5-Proteinen aufweisen. Angesichts der relativ hohen Bindungsstärke zwischen Proteinen von Choanoflagellaten und Seeanemonen könnten sich diese Affinitätsunterschiede im Laufe der Evolution entwickelt haben. Die Diversifikation der Wirbeltiere in verschiedene SPIRE- und MYO5-Isoformen deutet darauf hin, dass quantitative und qualitative

Unterschiede in der Proteinkomplexbildung zur erhöhten biologischen Komplexität der SPIRE/MYO5-Transportfunktionen bei Wirbeltieren beitragen. Dennoch stellen diese Ergebnisse nur einen Teilaspekt dar. Unterschiede in den Affinitäten zwischen anderen Komplexpartnern (SPIRE-RAB, MYO5-RAB) beeinflussen mit Sicherheit die Dynamiken dieser Komplexe auf vielfältige Weise.

1 Introduction

1.1 Cell polarisation and intracellular vesicle transport

The intracellular transport of proteins, RNAs, membrane vesicles, organelles, signalling peptides and small molecules towards the cell membrane is the foundation of the structural diversity of eukaryotic cells and the establishment of cell polarity and communication (Martin-Belmonte and Perez-Moreno, 2012; Pollard and Cooper, 2009; Ross et al., 2008). Cytoskeletal components aid in the critical phase of transport and specify the localisation of these factors. Plasma membrane integration of receptors and other transmembrane proteins as well as the induced and constitutive secretion of substances into the extracellular space in eukaryotic cells requires initial sorting into membrane vesicles at the Golgi network. In addition it needs a subsequent transport by motor proteins along microtubule and actin filament tracks toward the cell periphery (E. Kerkhoff et al., 2001; Stenmark, 2009; Zhen and Stenmark, 2015).

1.2 Intracellular transport along microtubules and actin filaments

Microtubules and actin filaments as part of the cellular cytoskeleton provide the infrastructure to regulate and organise intracellular vesicle and organelle transport processes (Hammer and Sellers, 2012).

The so-called highways and local roads model commonly describes intracellular transport in animal cells (Figure 1) (Hammer and Sellers, 2012; Hume and Seabra, 2011; Langford, 1995). Here, microtubules provide routes for fast, long-range transport between the cell centre and the periphery driven by motor proteins of the dynein and kinesin families (Hammer and Sellers, 2012). The microtubule-dependent transport is less specific and flexible. Meanwhile, actin filaments and associated myosin motor proteins work downstream, pick up the cargo in the periphery, and transport them to the final destination (Hirokawa et al., 2009). These actin transport processes are rather slow and short-range, but they are more dynamic, flexible and specific (Hirokawa et al., 2009).

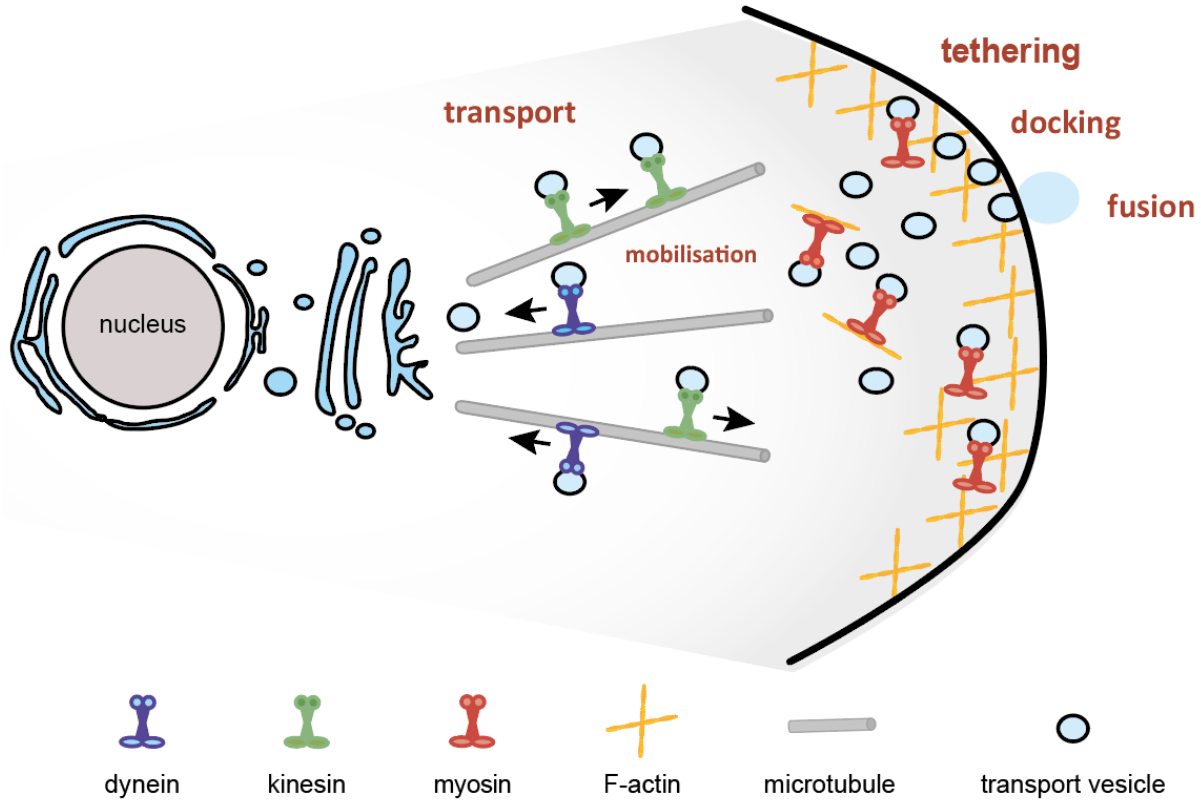

*Figure 1: **The highways and local roads model of mammalian exocytic transport processes.** Long-range transport on microtubule tracks via dynein (to the minus end) and kinesin (to the plus end) from the cell centre to the periphery. The vesicles are taken over at the cell cortex from myosin 5 motor proteins to move the vesicles the last distance from to the cell membrane on actin filaments (adapted from Tobias Welz, unpublished; (Hammer and Sellers, 2012)).*

1.3 Actin and actomyosin force generation

The actin cytoskeleton and associated myosin family motor proteins provide forces important for establishing the morphological diversity and dynamics of mammalian cells (Dominguez, 2009; Pollard, 2016; Rottner et al., 2017). Such actin-based mechanical forces can be generated by elongating actin filaments exerting pushing forces against intracellular structures (lamellipodia or filopodia, or endocytotic processes) (Rottner et al., 2017). Lamellipodia are actin-filament networks generated by migrating cells on flat or rigid substrates (Small et al., 2002). They are also known as membrane ruffles, and are thought to contain actin assembly machinery akin to micropinocytosis and phagocytosis (Rottner et al., 2017). Filopodia, or microspikes if embedded in the lamellipodium, are dynamic finger-like cell surface protrusions present in most cell types (Small et al., 2002). Filopodia play important roles in neural growth cone navigation and epithelial sheet fusion during morphogenesis (Millard and Martin, 2008; Viveiros et al., 2011). The cortical actin and actin stress fibres provide physical tension and cell stability, or a scaffold for myosin motor proteins sliding along intracellular actin structures to allow cell contractive forces (Rottner et al., 2017). Overall actin dynamics and actomyosin dependent force generation are therefore crucial to shape the cell membrane, and contribute to cell migration,

internalisation of substances, sensing of the environment and functions in intracellular membrane transport (Pollard and Cooper, 2009).

1.4 Actin filament generation

The actin cytoskeleton emerges from the assembly of globular actin (G-actin) into double helical filaments (F-actin) (Fujii et al., 2010; Holmes et al., 1990; Oda et al., 2009). These single actin filaments can be further assembled in terms of forming bundles or branched structures (Rottner et al., 2017). The assembly and disassembly of actin filaments are dynamic events, so they undergo a continuous turnover (actin treadmilling) that allows the dynamics and diversity of actin-mediated functions in the cell (Figure 2) (Blanchoin et al., 2014). Actin polymerisation is controlled by actin monomer-binding proteins such as profiling and Tß4 (Dominguez, 2009). Actin polymerisation is inhibited, due to relative instability of the actin dimer or trimer (Pantaloni and Carlier, 1993; Sept and McCammon, 2001; Xue and Robinson, 2013); it rather needs the initiation by actin nucleation factors (Dominguez, 2016; Pollard and Cooper, 2009; Quinlan and Kerkhoff, 2008). Eukaryotic cells use filament nucleators to stabilise actin polymerisation cores, the formation of which is rate-limiting (Dominguez, 2009). There are three major classes of nucleation factors (Figure 3) (Dominguez, 2016; Eugen Kerkhoff, 2006). First, the Arp2/3 complex, which is activated by nucleation promoting factors (NPFs) of the Wiskott–Aldrich syndrome protein (WASP)/WASP-family verprolin-homologous protein (WAVE) family, and which drives the formation of dendritically branched actin filament structures (Goley and Welch, 2006; Pollard, 2007; Pollard and Beltzner, 2002). Second, the formin proteins, which are characterised by the presence of the formin homology 1 (FH1) and 2, (FH2) domains (Wallar and Alberts, 2003). The FH2 domains of two proteins assemble into a donut-shaped dimer, where each of the subunits can bind two actin monomers (Pollard, 2007). The FH2 dimer moves processively with the growing actin filament and is provided with new actin monomers by the proline-rich FH1 domains in order to build unbranched filaments (Otomo et al., 2005; Romero et al., 2004; Vavylonis et al., 2006). The third class comprises the tandem WH2 (Wiskott–Aldrich syndrome protein homology region 2)-domain containing actin nucleators, which is a diverse group containing different types of proteins (Qualmann and Kessels, 2009). SPIRE proteins belong to this group, which promote initiation of actin filament generation by binding G-actin to two or more WH2 actin binding domains (Qualmann and Kessels, 2009).

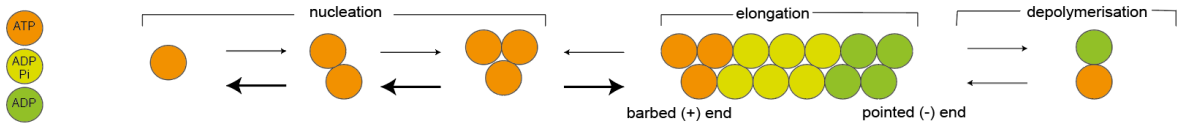

*Figure 2: **Actin filament polymerisation and depolymerisation**. (adapted from: (Dominguez, 2009). The actin filament is structurally and kinetically asymmetric. ATP-actin monomers add quicker at the barbed (or +) end, while nucleotide hydrolysis occurs throughout the filament. ADP-actin monomers dissociate primarily at the pointed (or -) end. Actin filament nucleators and actin nucleotide hydrolysis control the transition from monomeric to filamentous actin in cells. Nucleation, the creation of small actin oligomers (dimers, trimers, and tetramers), is rate limiting and hindered by actin monomer binding proteins. Thus, the function of filament nucleators is to stabilise the production of tiny actin oligomers can develop into actin filaments (Dominguez, 2009).*

1.5 The SPIRE actin nucleator

In humans, two *SPIRE* genes are identified that encode four SPIRE protein isoforms. The SPIRE actin nucleators are modular proteins with highly conserved functional domains that encode an N-terminal actin filament assembly module, comprising a kinase non-catalytic C-lobe domain (KIND) at the very N-terminal end, which mediates binding to formin (FMN) subfamily formin proteins via their formin SPIRE interaction (FSI) sequence (Pechlivanis et al., 2009). The FMN proteins as well as their interaction mechanism with SPIRE proteins are highly conserved in holozoa (animals and their closest single cell relatives) (formin-1 (FMN1), formin-2 (FMN2)), *Drosophila melanogaster* (Cappuccino (Capu)) (Quinlan et al., 2007; Quinlan and Kerkhoff, 2008), cnidaria (e.g. *Nematostella vectensis* FMN-short) or choanoflagellates (e.g. *Monosiga brevicollis* FMN) (Kollmar et al., 2024; Sebé-Pedrós et al., 2013), additionally a cluster of 2-4 G-actin-binding WASP-homology 2 (WH2) domains (Quinlan and Kerkhoff, 2005). This module is coupled to a C-terminal membrane-binding RAB-GTPase domain (FYVE_2 domain), comprised of a so-called SPIRE-box (SB, conserved among SPIRE proteins) and a FYVE-type zinc finger (Welz and Kerkhoff, 2023). Thus, SPIRE proteins are predominantly localised to intracellular membranes (especially exocytic, recycling and secretory vesicles, recycling endosome and TGN) by direct membrane binding and is further supported by their ability to interact with RAB GTPases at the vesicle membrane surface (Alzahofi et al., 2020; Kollmar et al., 2024). The formins are characterised by FH domains, FH1 is proline-rich, followed by a FH2 domain, which contains a region of 130 residues showing high homology (Schönichen and Geyer, 2010). The very C-terminus of mammalian formin, FMN1 and FMN2, contains a conserved sequence that interacts with SPIRE proteins (Pechlivanis et al., 2009; Schönichen and Geyer, 2010; Vizcarra et al., 2011; Zeth et al., 2011).

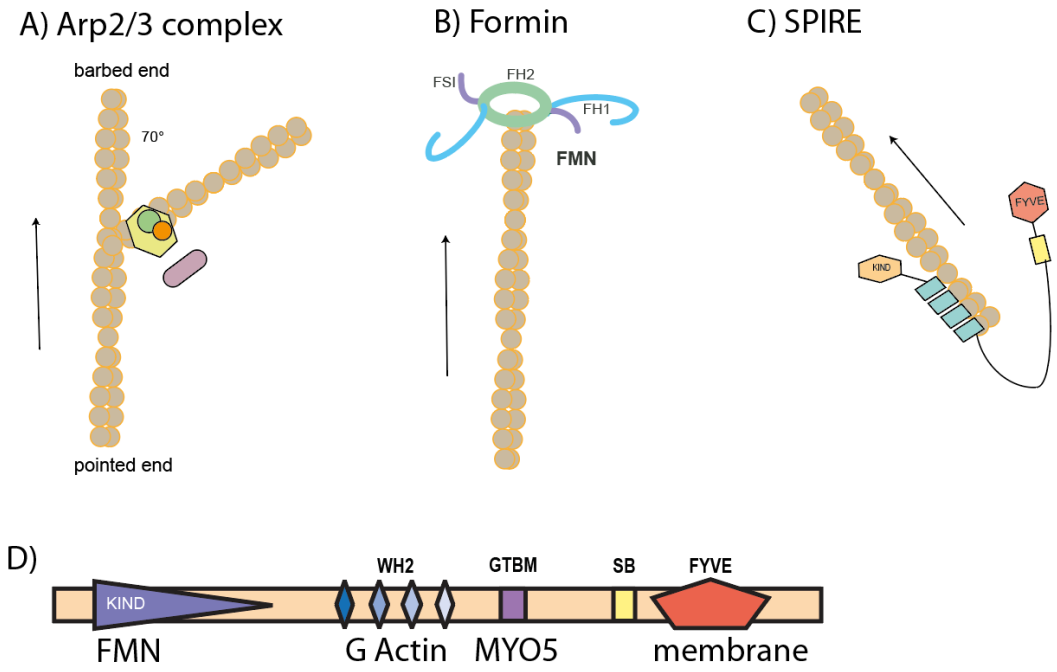

Figure 3: ***Actin nucleation factors and domain organisation of SPIRE:*** *SPIRE/FMN cooperation in actin filament nucleation elongation adapted from (Eugen Kerkhoff, 2006) A) the Arp2/3 complex forms new actin filaments by binding to pre-existing filaments and branching at a 70° angle. B) Formins, also known as modular proteins encode the formin homology 1 (FH1) and formin homology 2 (FH2) domains. Profilin-actin is bound by the proline-rich FH1 domain. The FH2 domain forms a ring-like dimer structure in which each FH2 domain binds two actins. Formins conrinue to be linked in a dimer with the filament's rapidly expanding barbed end. C) SPIRE proteins initiate actin polymerisation by the actin's attachment to a group of four WH2 domains arranged in the protein's middle. SPIRE proteins also initiate unbranched filaments, in line with formin proteins and D) domain organisation of SPIRE adapted from (Welz and Kerkhoff, 2023), actin nucleator KIND-domain interacts with FMN, WH2 regions are important for G-actin interaction, the GTBM is the MYO5 interaction site, SB (SPIRE box) and the FYVE domain interacts with membranes.*

The interaction of SPIRE with class-5 myosins (MYO5) has been discovered in 2016 (Pylypenko et al., 2016). This interaction is mediated by the globular tail domain binding motif (GTBM) and the MYO5 globular tail domain (GTD) (Welz and Kerkhoff, 2017, 2023). All those interactions contribute in a regulated manner to form membrane associated protein complexes that coordinate actin assembly and myosin 5 dependent force generation at vesicle membranes to drive organelle transport (Welz and Kerkhoff, 2023). Such mechanisms have been revealed to contribute to oocyte maturation (Pfender et al., 2011) and melanosome transport processes (Alzahofi et al., 2020) and the details of the involved protein interactions and complex formations will be described in the following sections (Pfender et al., 2011; Pleiser et al., 2014; Welz and Kerkhoff, 2023).

1.5.1 mitoSPIRE1

The control of mitochondria division and transport is another instance of force generation via elongation of SPIRE1-assembled actin filaments. A 58 amino acid short sequence motif, which is encoded by mouse SPIRE1 exon 13, that is alternatively spliced, selectively targets the mouse SPIRE1

protein to mitochondria, where it is integrated into the outer membrane of the mitochondria (Kollmar et al., 2019; Manor et al., 2015; Welz and Kerkhoff, 2023) (Figure 4). Actin filaments are assembled at the ER-mitochondria contact sites by mitoSPIRE1 (Manor et al., 2015), also called Spire1C, in conjunction with inverted of inverted formin-2 (INF2-CAAX isoform) (Manor et al., 2015), which is attached to the ER (endoplasmic reticulum) by a C-terminal farnesyl group (Korobova et al., 2013; Ramabhadran et al., 2011). Simulation results point to a model where actin structures arranged by mitoSPIRE1-INF2-CAAX can cause constriction of the mitochondria, which in turn promotes mitochondrial division at the ER-mitochondria contact sites (Manor et al., 2015). All of the functional and structural motifs of the vesicular SPIRE isoforms are present in the mitochondrial SPIRE1 isoform, which can also bind class-5 myosins (Kollmar et al., 2019; Straub et al., 2020; Welz and Kerkhoff, 2023). Given that MYO5 activity inhibits microtubule-based axonal transport of mitochondria in cultured *Drosophila* neurons (Pathak et al., 2010), one may be tempted to believe that mitoSPIRE1 could organise actomyosin structures at mitochondria, which may regulate mitochondrial motility (Pathak et al., 2010).

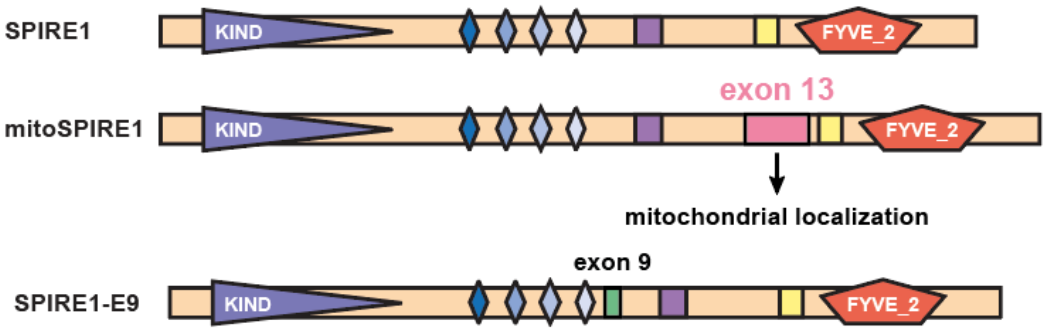

Figure 4: ***Isoforms of vertebrate SPIRE1*** adapted from: (Welz and Kerkhoff, 2023). A) schematic domain organisation of vertebrate SPIRE1 isoforms (shown are mammalian SPIRE from *Homo sapiens*): mitoSPIRE1, this isoform contains the alternatively spliced exon 13 (highlighted in pink) which is specifically targeted to the outer mitochondrial membrane. SPIRE1-E9, contains the alternatively spliced exon 9 (Welz and Kerkhoff, 2023).

1.5.2 The SPIRE-formin actin nucleator complex

Among the 15 vertebrate formins, the FMN subfamily formins have been shown to directly interact with SPIRE proteins. As described earlier, the KIND motif of the SPIRE protein interacts with the FSI (formin/ SPIRE interaction) sequence of the formin (Pechlivanis et al., 2009; Tittel et al., 2015). X-ray crystallography (Vizcarra et al., 2011; Zeth et al., 2011) revealed the structure of the SPIRE1 KIND domain in association with the FMN2-FSI peptide (Zeth et al., 2011). The SPIRE KIND domain interacts with FMN-subgroup formins and the C-terminal FYVE_2 zinc finger domain, also known as modified Fab1, YOTB/ZK632.12, VAC1, EEA1 (FYVE), or mFYVE (Tittel et al., 2015). The intramolecular KIND-FYVE_2 interaction competes with the intermolecular KIND-FMN-FSI

connection (Tittel et al., 2015). According to Tittel et al. (2015), SPIRE proteins adopt a cytoplasmic backfolded, autoinhibited conformation (Figure 7B) (Welz and Kerkhoff, 2023).

1.6 The RAB GTPases as regulators of intracellular transport

The RAS (Rat sarcoma virus) superfamily of small GTPases is divided in subfamilies based on their structure, sequence and function. The five subfamilies have distinct intracellular functions and comprise (signalling molecules), RHO (Ras homology) (cytoskeletal regulators), RAN (Ras-like nuclear) (nuclear transport), RAB (Ras-like in brain) and ARF (ADP-ribosylation factor) (both with functions in intracellular transport) (Rojas et al., 2012). The RAB GTPases form the largest RAS subfamily and are considered as the master regulators for intracellular transport (Rojas et al., 2012). RAB proteins can be subdivided into different functional groups (Klöpper et al., 2012). The secretory group includes RABs that localise and function on secretory vesicles for instance RAB3, RAB8, and RAB27. The complete membrane transfer mechanism can be split into five major steps (Stenmark, 2009): the budding and sorting process of proteins from vesicles, sometimes accompanied by vesicle coating and stabilising of the complex, the vesicle uncoating, the motility; transport of vesicles through the cell on the cytoskeleton, the vesicle tethering at the target membrane, often supported by tethering factors and SNARE complex proteins and the vesicle fusion with the target compartment (Fukuda, 2008; Stenmark, 2009). As most of the RAS superfamily members do, RAB GTPases cycle between an inactive (GDP-bound) and active (GTP-bound) state (Pfeffer, 2005; Stenmark, 2009; S. Wang et al., 2017), but also between a cytosolic and a membrane bound form (Müller and Goody, 2018). RABs are activated by guanine nucleotide exchange factors (GEFs) and inactivated by GTPase-activating proteins (GAPs) (Stenmark, 2009). GEFs allow the release of GDP and favour quick GTP loading due to the abundance of GTP in the cytoplasm (~1 mM) (Stenmark, 2009). GAPs accelerate the hydrolysis of GTP to GDP and inorganic phosphate (Pi) within the GTPase, which is necessary given the comparatively low intrinsic GTP hydrolysis activity of the GTPase itself (Bos et al., 2007; Reiner and Lundquist, 2018). Depending on binding of GDP or GTP, the switch regions (switch I and II) are known to undergo large conformational changes that influence their binding abilities and thus their function (Pfeffer, 2005; Stenmark, 2009). Individual RABs are targeted via their prenylated C-termini (Müller and Goody, 2018) to specific intracellular membranes and compartments, e.g. the endoplasmic reticulum (ER), Golgi apparatus, secretory vesicles, endosomes, or lysosomes (Stenmark, 2009). Considering their activity cycle and membrane targeting RAB proteins function as molecular switches as they recruit adaptor and effector proteins (Müller and Goody, 2018), such as vesicle coat proteins, motor proteins such as MYO5 and signalling proteins, towards the membrane surface which thereafter exert and regulate different steps of vesicle trafficking (Fukuda, 2008).

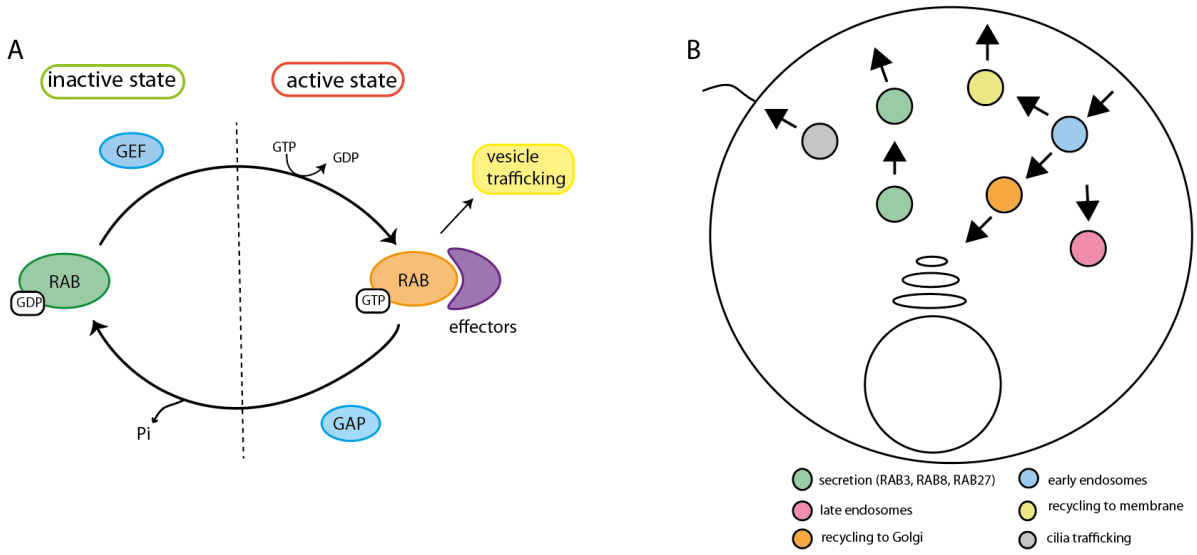

*Figure 5: **RAB GTPase cycle** adapted from (S. Wang et al., 2017) and **RAB-GTPase groups** schematically shown adapted from Kerkhoff, Welz and Kim, unpublished and (Klöpper et al., 2012). A) RABs alternate between an active GTP-bound form and an inactive GDP-bound form. RAB is activated by a guanine nucleotide exchange factor (GEF), which catalyses the transition from GDP-bound to GTP-bound state. Activated RAB facilitates vesicle trafficking by binding with particular effectors. RAB inactivation is caused by the natural GTP hydrolysis of RABs combined with the activating function of GTPase-activating protein (GAP). Effector dissociation from the RAB protein is caused by the conversion of active RABs into inactive states (S. Wang et al., 2017). B) RAB GTPases are divided in six groups (secretion, late endosomes, recycling to Golgi, early endosomes, recycling to membrane and cilia trafficking) depending on their function (Klöpper et al., 2012) and Kerkhoff, Welz and Kim unpublished.*

1.7 Transport along microtubule tracks

For cellular cargo transport, there exist two major groups of microtubule-associated motor proteins (Hirokawa et al., 2009). Kinesin motors are a vast set of motor proteins classified into 14 classes, including approximately 40 human genes (Dagenbach and Endow, 2004; Hirokawa et al., 2009; Miki et al., 2005). Kinesin motors travel undirectionally toward the microtubule plus end (Dagenbach and Endow, 2004) with some exceptions (kinesin-13, for example, Drosophila Ncd (nonclaret disjunctional), move minus end directed, while kinesin-13 may not move at all) (Dagenbach and Endow, 2004). Most of the kinesins are heavy chain dimers that serve as processive motors, meaning they move continuously along microtubules because their two motor heads attach sequentially to the microtubule tracks, providing for efficient cargo delivery. The classical kinesins (kinesin-1) are one type of processive kinesin. The members of the kinesin-1 family are able to move over long distances with a velocity of ~0.8 µm/s (Vale and Fletterick, 1997). The motor takes one-step every 10 ms, if we reflect on a step size of 8 nm (distance between two consecutive tubulin dimers) (Vale and Fletterick, 1997).

Dyneins belong to the ATPases Associated with Diverse Activities family and have a different evolutionary origin from kinesin and myosin motors (Vale, 2003). Dyneins consist of two classes: the axonemal dynein and the cytoplasmic dynein (Bhabha et al., 2016). The axonemal dynein is important for the regulation of microtubule sliding in axonemes of cilia and flagella in both directions (Bhabha et

al., 2016). Whereas the cytoplasmic dynein provides organelle movement and other cargoes, this dynein is divided in dynein1 and dynein2 and is involved in a variety of cellular functions. On the one hand cytoplasmic dynein1 i.e. transports mRNA-protein complexes, viruses and certain proteins towards the cell centre, on the other hand, cytoplasmic dynein2 is only involved in the cargo transport in the cilium (Bhabha et al., 2016).

The transport processed over longer distances can take place on the microtubules and for the final destination step underneath the cell membrane the myosin 5 motor proteins take over.

1.7.1 The myosin class-5 actin motor proteins

Myosin motor proteins are molecular motors that bind to actin filaments (Hammer and Sellers, 2012). These proteins play a role in a variety of cellular and subcellular activities, such as cell adhesion and migration, cell division, and cargo transport, including vesicle transport, which drives endocytic and exocytic trafficking (Hammer and Sellers, 2012). Myosin motors are ATPases that hydrolyse ATP. The ATP/ADP cycle regulates the interaction of the motor proteins with the actin filaments. The actin filament binding and conformational changes generate forces that are then employed to either modify the actin cytoskeleton, resulting in morphological changes, or to move along actin tracks, transporting cellular components (Hammer and Sellers, 2012; Hammer and Wagner, 2013).

The myosin superfamily includes one class of conventional myosins and over 30 kinds of unconventional myosins depending on motor domain sequence (Hammer and Sellers, 2012). Myosin II is a conventional myosin and the first type that has been described from the myosin superfamily (Hammer and Sellers, 2012). In muscle cells myosin II is responsible for skeletal muscle contraction (Hammer and Sellers, 2012). Class-5 myosin (MYO5) is the most well studied unconventional myosin in terms of cellular function, enzyme properties, and regulation (Hammer and Sellers, 2012). Members of the class-5 myosin (MYO5) proteins are actin dependent motor proteins which are capable to move processively along actin filaments in order to transport cargo through the cell along actin filaments, in comparison to the conventional myosin II that applies forces on actin in order to cause structural changes (Hammer and Sellers, 2012). Various regulatory mechanisms can activate myosin motor activity at specific sites (Hammer and Sellers, 2012).

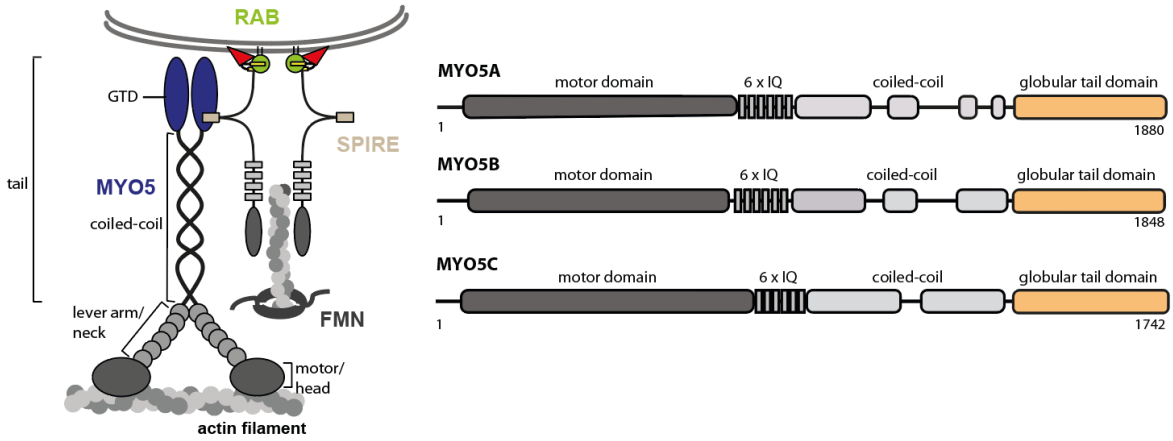

*Figure 6: **Mammalian class-5 myosin actin motor proteins :** the motor domain, also referred as head, is located N-terminal and binds to actin filaments mediating the actin-dependent ATPase activity. Followed by six IQ motifs (each known as neck) forming the lever arm, which is needed for forward motion. These IQ motifs also bind calmodulin light chains. The C-terminal tail contains of two parts: at the very C-terminal end, the globular tail domain (GTD) is located, which works as the cargo-binding domain and significant protein interaction site; and the coiled-coil region, which is needed for heavy chain dimerization. On the right site, the corresponding regions in MYO5A/B/C are shown schematically. Numbers indicate the numbers of the amino acids. Adapted from (Welz and Kerkhoff, 2017).*

There are three class-5 myosin genes in humans (MYO5A, B, C), but due to alternative splicing processes, there are more than three protein isoforms (Welz and Kerkhoff, 2017). The MYO5 heavy chain is composed of the N-terminal motor domain, which binds to actin filaments and harbours the actin dependent ATPase activity for force generation and movement (Welz and Kerkhoff, 2017). Six IQ motifs bind calmodulin light chains and an elongated coiled-coil region is required for heavy chain dimerization (Welz and Kerkhoff, 2017). The very C-terminal globular tail domain (GTD) is considered as the cargo binding domain (Welz and Kerkhoff, 2017). Both, the coiled-coil regions and the globular tail domain, bind distinct RAB GTPases (Welz and Kerkhoff, 2017)(Figure 6). In the case of MYO5A, the exons D and F, which encode sequences N-terminal adjacent to the globular tail domain are mediating protein interactions. The exon D is required for the binding of MYO5A to RAB8 and RAB10, on the other hand the exon F is involved in the process of melanosome transport (Seperack et al., 1995). Exon F supports the association of myosin 5A with melanophilin (MLPH) to form a functional complex with RAB27A (Strom et al., 2002; Welz and Kerkhoff, 2017). The globular tail domain of myosin 5A interacts with the RAB3 GTPase (Pavlos et al., 2010; Wöllert et al., 2011) which is a major regulator of exocytic synaptic vesicle transport (Jahn et al., 1994). Myosin 5A functions in melanosome transport (Hume and Seabra, 2011). Here it interacts with melanophilin (MLPH), which is targeted to melanosomes by its interaction with RAB27A (Alzahofi et al., 2020; Hume et al., 2002; Strom et al., 2002). In oocyte vesicle transport myosin 5B interacts with RAB11, but it interacts directly also with RAB8A and RAB10A (Bultema et al., 2014; Roland et al., 2009; Welz and Kerkhoff, 2017). The third mammalian class-5 myosin is myosin 5C, which in contrast to MYO5A and MYO5B does not bind to RAB11 because the four RAB11 contact site residues of MYO5A/B are substituted by non-homologous residues (Pylypenko

et al., 2013; Roland et al., 2009; Welz and Kerkhoff, 2017). However, MYO5C is also involved in exocytic vesicle transport; e.g. it colocalises with the Weibel-Palade bodies (WPB) (Holthenrich et al., 2019; Holthenrich et al., 2022). The exon D and exon E-like region of myosin 5C is critical for the binding to RAB8A and RAB10A (Bultema et al., 2014; Roland et al., 2009; Welz and Kerkhoff, 2017). RAB38 and the related RAB32, two RAB GTPases required for melanosome formation, share some binding sites (Bultema et al., 2014). RAB38 can bind to exon E-like and exon F-like and RAB32 can bind exon F-like (Bultema et al., 2014; Welz and Kerkhoff, 2017). These three MYO5 isoforms differ slightly in their binding to the actin filaments (Hammer and Wagner, 2013). MYO5A and MYO5B have their highest affinity to ADP ("high duty ratio"), while bound to actin and they can move processively on the actin filament (Hammer and Sellers, 2012). MYO5A and MYO5B can walk processively on actin filaments as single molecules (Hammer and Sellers, 2012; Hammer and Wagner, 2013). In contrast, MYO5C, as a single motor can only walk on actin bundles, shown by (Sladewski et al., 2016), before MYO5C has been described as a non-processive motor, but these experiments were only done on actin filaments.

Nearly all eukaryotic species have conserved class-5 myosins (MYO5 (Odronitz and Kollmar, 2007)). Humans have three myosin 5 genes: MYO5A, MYO5B and MYO5C. These genes encode the proteins myosin 5A (MYO5A), myosin 5B (MYO5B) and myosin 5C (MYO5C). Unlike myosin 5C (Berg et al., 2001; Mercer et al., 1991; Rodriguez and Cheney, 2002; L. Zhao et al., 1996), MYO5A and MYO5B proteins are expressed throughout the body (Roland et al., 2009), as well as in the brain. MYO5B exhibits robust expression in the hippocampus (Cheney et al., 1993; Espreafico et al., 1992; Kneussel & Wagner, 2013; Lisé et al., 2006; Rodriguez and Cheney, 2002; Tilelli et al., 2003), while MYO5A is more extensively dispersed across other brain regions (Tilelli et al., 2003). Both isoforms are found in the postsynaptic densities and dendritic spines within neuronal cells (Lisé et al., 2006; Tilelli et al., 2003). MYO5C is primarily expressed in epithelial cells and is found in large quantities in epithelial and glandular tissues, including the pancreas, prostate, mammary, stomach, colon, and lung (Rodriguez and Cheney, 2002). All three of the MYO5 isoforms have distinct splice variants that are expressed differently and mediate particular interactions and functions (Hódi et al., 2006; Huang et al., 1998; Lambert, J., et al., 1998; Mercer et al., 1991; Roland et al., 2009; Seperack et al., 1995; Wagner et al., 2006). MYO5 motors travel in the direction of the barbed end (plus end) of actin filaments (Provance, 1999). Their gliding velocities are generally between 0.2 and 0.8 µm/sec, with some exceptions to slower and faster movements (Watanabe et al., 2006). They move an order of magnitude slower than kinesins or dyneins (Nelson et al., 2014; Tóth et al., 2005; Watanabe et al., 2006).

1.7.2 Regulation of myosin 5 motor activity and function

MYO5 motor proteins' ability to function as processive motors on actin is tracked by demand regulatory systems that limit their activity and movement on F-actin when not required, such as when not coupled to cargo (Krementsov et al., 2004; Li et al., 2004; F. Wang et al., 2004; Yao et al., 2015). The full-length MYO5 motor has two different states. In an auto-inhibited, inactive form, the MYO5 dimer is back-folded such that its globular tail domains (GTD) attach to its motor domains (Krementsov et al., 2004; Li et al., 2004; Tittel et al., 2015; F. Wang et al., 2004; Yao et al., 2015). In this state, ATPase activity is inhibited, and the motor attaches weakly to actin filaments (Lu et al., 2006; Sato et al., 2007). Furthermore, the auto-inhibited motor is located in the cytoplasm and so does not associate with vesicles or other cargo (Lindsay et al., 2013). Activatory processes loosen the inhibitory GTD/ motor domain contacts, allowing MYO5 to adopt an open and extended conformation similar to the active state in which it binds cargo and F-actin. Increased intracellular Ca^{2+} ion concentrations open MYO5 dimers and promote ATPase activity *in vitro* (Li et al., 2004; Pylypenko et al., 2013; Pylypenko et al., 2016; Tittel et al., 2015). At the same time, high Ca^{2+} concentrations eventually lead to the dissociation of calmodulin light chains from the neck are, making it very flexible and hence unsuitable to drive the motor movement, resulting in MYO5A's inability to move on F-actin tracks (Lu et al., 2006). The binding of cargo to the globular tail domains may be the most physiologically relevant opening mechanism for MYO5 proteins (Yao et al., 2015; Zhang et al., 2018). The melanophilin (MLPH or Slac-2a) protein is an excellent example of this, as it binds to MYO5A's GTD, increases its ATPases activity, and aids its mobility on actin filaments *in vitro* (Pylypenko et al., 2013; Pylypenko et al., 2016; Yao et al., 2015).

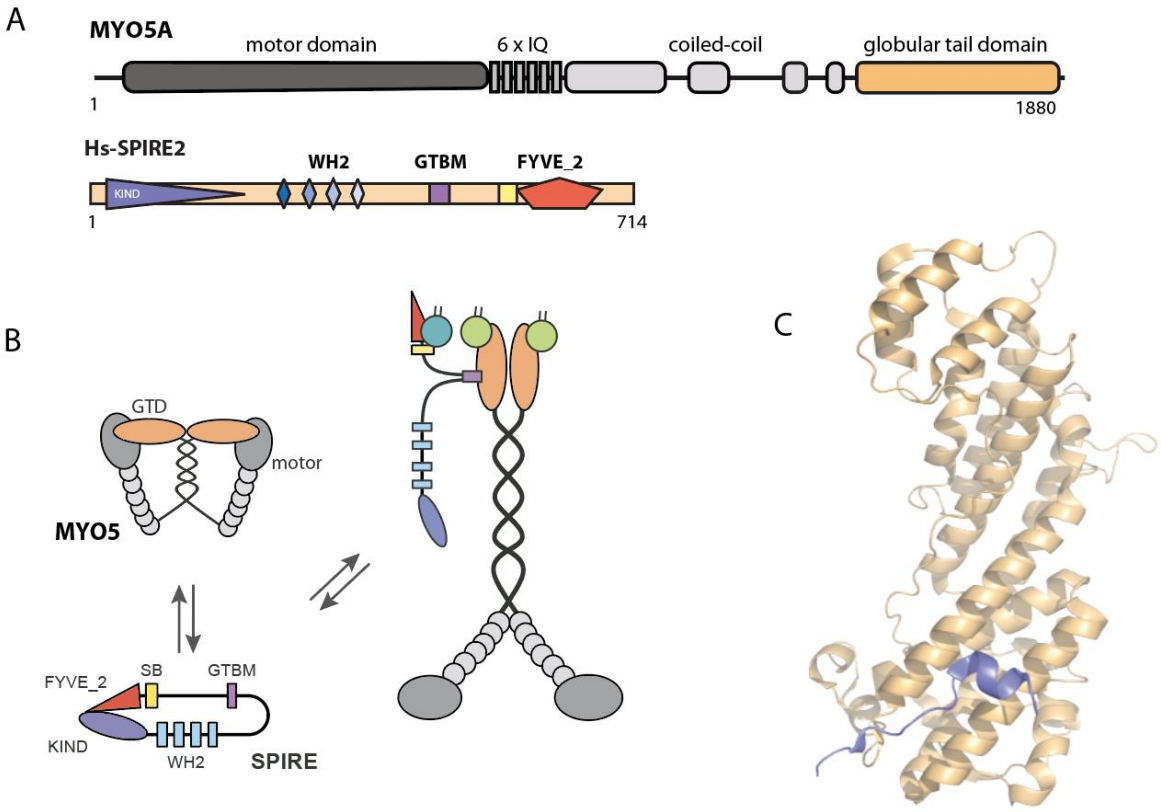

*Figure 7: **Structure and conformations of MYO5A and SPIRE2 adapted from (Pylypenko et al., 2016; Welz and Kerkhoff, 2023):** A) domains of MYO5A and SPIRE2; B) autoinhibited conformation of MYO5 and SPIRE and conformation after activation; C) crystal structure of Hs-MYO5A-GTD (light orange) / Hs-SPIRE2-GTBM (light purple).created with PyMol.*

Furthermore, it was recently established using electron microscopy, that MLPH is able to bind to the purified full-length back-folded MYO5A dimer and stimulate its opening into the extended conformation (Yao et al., 2015). Aside from the regulated opening and activation mechanisms for myosin 5 dimers, myosin motors are also subject to fine-tuned regulation while active, at least in some situations (Yao et al., 2015). Although myosin 5 proteins (such as mammalian MYO5A and MYO5B) are processive actin-based motors as dimeric molecules, it has been repeatedly observed that MYO5 proteins cluster at the cargo surface to form motor units (Gross et al., 2002; Nascimento et al., 1997; Tabb et al, 1998), in a manner similar to that described for Drosophila MYO5 (Provance, 1999) or mammalian MYO5C (Rodriguez and Cheney, 2002). This mechanical characteristic increases the run duration of motors on actin tracks but also decreasing their velocities when compared to single dimeric molecules (Conway et al., 2012; Hariadi et al., 2014; Klumpp and Lipowsky, 2005). This phenome might be explained by a hindrance caused by the asynchronous movement of the several motors and a load dependence of the motor kinetics, implying that the cargo itself can impact the motors' walking behavior to some extent (Nelson et al., 2014). Even the lipid content of the vesicular cargo can affect myosin movement (Nelson et al., 2014). A more fluid vesicle nature causes walking velocities higher than those at the single dimeric molecule level, even reaching unloaded motor velocities (Nelson et al., 2014). Conversely, more gel-like vesicle compositions reduced walking velocity (Nelson et al.,

2014). The melanophilin protein slows myosin 5A movement (~4-fold) while increasing the length of processive walks (~2-fold) compared to the solitary dimeric motor (Sckolnick et al., 2013). Overall, the motor's attachment duration to actin tracks is greatly extended, which facilitates melanosomes trafficking in melanocytes (Sckolnick et al., 2013). One plausible explanation for these data is that electrostatic interactions between MLPH and actin filaments cause MLPH to act as a tether, allowing the MYO5A motor to remain attached to the actin tracks for prolonged periods (Sckolnick et al., 2013). Moreover, an interconnection has been discovered in which motor proteins from several families collaborate to influence each other's processivity (Sckolnick et al., 2013). One example is the interaction of MYO5 with kinesin family motors in peripheral-directed transport (Ali et al., 2008). In this mechanism, MYO5 conducts a diffusional search along microtubules, which increases the run length of the kinesin motor coupled to the same cargo (Ali et al., 2008). For MYO5 motors on actin tracks, the identical phenomena occur in reverse. Electrostatic interactions within the non-specific motor-cytoskeleton connections, which may have a tethering character that reduces the diffusion rate of the cytoskeleton-specific motor, could explain the proposed mechanism for a mutual run length enhancement (similar to the MLPH effects on myosin 5A processivity mentioned previously (Yao et al., 2015)).

1.8 MYO5 – SPIRE cooperation in intracellular vesicle transport

MYO5 and SPIRE proteins were shown that they interact with each other and are involved in diverse intracellular functions, including melanosome transport, oocytic vesicle movement, asymetric spindle orientation or exocytotic vesicle transport (Alzahofi et al., 2020; Holthenrich et al., 2022; Pfender et al., 2011; Schuh, 2011). However, currently, little is known about the mechanism by which actin nucleators and motors are specifically recruited to membranes. Both, SPIRE and MYO5 proteins are effectors of RAB GTPases, which are thought to determine the membrane specificity of SPIRE/MYO5 cooperation. MYO5C does not interact with RAB11. SPIRE C-terminal sequences were also found to interact with RAB3, RAB8 and RAB27.

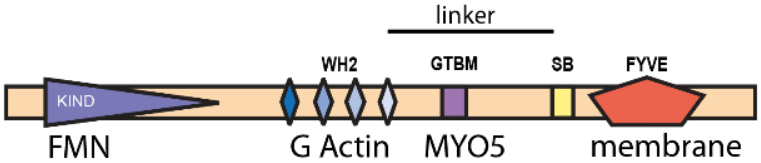

*Figure 8: **Diagram showing the general structure of the SPIRE protein**, showing the sequence motifs and highly conserved domains. Each domain mediates a specific interaction. Adapted from (Welz and Kerkhoff, 2023).*

Pylypenko et al (2016) confirmed an interaction of the MYO5 isoforms (MYO5A, MYO5B and MYO5C) with SPIRE2. MYO5A and MYO5B bind the central SPIRE2-linker region in a quit similar affinity way (Kd

~ 728 nM and 377 nM for MYO5A and MYO5B) (Pylypenko et al., 2016). It could be shown that the deletion of the KIND or WH2 domain of the SPIRE did not affect the binding of the two proteins (Pylypenko et al., 2013; Pylypenko et al., 2016). Deleting the linker region between WH2 domains and SPIRE-box (SB) entirely disrupted the connection, indicating the importance of the SPIRE central linker region in MYO5-GTD binding (Pylypenko et al., 2016) (Figure 3;Figure 8). MYO5A and MYO5B have substantially conserved GTDs that interact directly with RAB11 (Lindsay et al., 2013; Roland et al., 2009). Interestingly, GFP-tagged MYO5A-GTD interacts with SPIRE2. MYO5A and MYO5B perform overlapping physiological roles, including mobilising RAB11 recycling endosomes for AMPA receptor delivery into dendritic spines (Correia et al., 2008; Hammer and Wagner, 2013; Z. Wang et al., 2008). They also share interaction partners and are involved comparable RAB11-vesicle transport processes (Pylypenko et al., 2016).

Pylypenko et al (2016) have identified a globular tail binding motif (GTBM) in SPIRE proteins which is conserved over evolution. A central region of 26 amino acids in the middle part of the linker of SPIRE2 is important for the interaction with MYO5 (Pylypenko et al., 2016). To identify the protein interaction sites of SPIRE2 and MYO5A, the crystal structure of the protein complex was analysed to illustrate the stabilising interactions in atomic detail (Figure 7C). SPIRE1 and SPIRE2 proteins share conserved residues that interact with MYO5A-GTD (Pylypenko et al., 2016). The SPIRE2-GTBM peptide binds to the MYO5A-GTD in an extended conformation, generating a two-turn alpha helix at the end, between helices H3 and H5 (Pylypenko et al., 2016). SPIRE2-GTBM may be accommodated on the surface of MYO5A without causing conformational changes to the GTD, and the SPIRE-GTBM binding pocket is structurally preserved in MYO5B and MYO5C (Pylypenko et al., 2016). A binding experiment confirmed that MYO5C-GTD binds SPIRE2-GTBM with micromolar affinity (Pylypenko et al., 2016). The structural conservation of SPIRE-binding sites in the three myosin 5 isoforms explains SPIRE's promiscuity in binding to MYO5A, MYO5B and MYO5C (Pylypenko et al., 2016). Another interesting observed aspect was that the binding site of MYO5-GTD:SPIRE2 largely coincides with the one of melanophilin (MLPH) (Pylypenko et al., 2016). SPIRE2-GTBM and MLPH-GTBM bind to MYO5A-GTD bind with similar micromolar affinities. (Geething and Spudich, 2007; Pylypenko et al., 2016) Unlike SPIRE2-GTBM, which interacts with all three MYO5 isoforms, the MLPH-GTBM binding is MYO5A-specific (Pylypenko et al., 2016). The SPIRE-2 and MLPH-GTBM share some sequence similarities, and their N-terminal regions interact with MYO5A in a similar way (Pylypenko et al., 2016). The SPIRE-GTBM C-terminal portion anchors in the MYO5A hydrophobic cleft between helices H3 and H5 (Pylypenko et al., 2016). The apo-MYO5-GTD surface is designed to bind SPIRE-GTBM (Pylypenko et al., 2016). In contrast to SPIRE2-GTBM, MLPH-GTBM cannot fit on the surface of apo-MYO5A-GTD without conformational modifications (Pylypenko et al., 2016). Another finding, SPIRE2-GTBM and MLPH-GTBM have a similar distribution of charged residues along the sequence: the N-terminal part is positively charged, whereas

the C-terminal region, after the particular binding motif, has a cluster of negatively charged residues. The GTD recognises three features of the polypeptide chain: 1) The clusters of charged residues may aid in orienting the peptide relative to the GTD surface; 2) the extended N-terminal region can form hydrogen bonds with the GTD's backbone atoms; and 3) the motif's hydrophobic residues provide peptide anchoring in small surface pockets of the GTD (Pylypenko et al., 2016).

All these different interactions between MYO5s and SPIREs lead through the combinations of the interactions to different protein complex formations (Figure 9). In figure 15, a general motor protein complex containing MYO5, SPIRE, FMN and RAB GTPases at distinct vesicle membranes is shown. This complex plays a crucial role in intracellular transport processes and differs in myosin 5 motor protein, SPIRE as actin nucleator, FMN-formin and the membrane specific RAB GTPase.

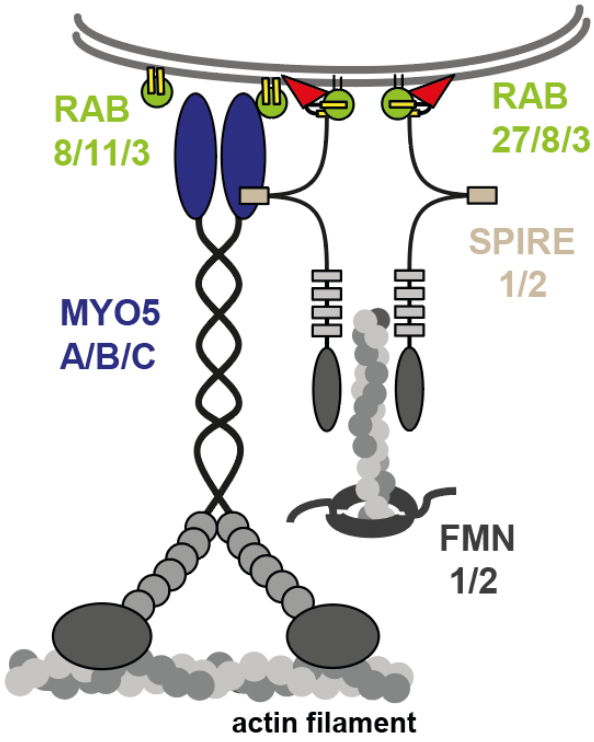

*Figure 9: **RAB/SPIRE/MYO5 motor protein complexes** at distinct vesicle membranes. The tripartite complex MYO5/ SPIRE/ RAB.*

Distinct protein complexes of SPIRE, MYO5 and RAB isoforms been shown to function in specific cellular processes in which they are thought to mediate actomyosin force generation (Welz and Kerkhoff, 2023).

Based on protein interaction data, cellular co-localisation and protein expression data the following complexes have been proposed: RAB27A/SPIRE1/MYO5A (melanosome transport) (Alzahofi et al.,

2020), RAB11/SPIRE1,2/MYO5B (oocytic transport) (Pfender et al., 2011; Schuh, 2011) and RAB3/27/SPIRE1/MYO5C (von Willebrand factor release in Weibel-Palade bodies (WPB)) (Holthenrich et al., 2022).

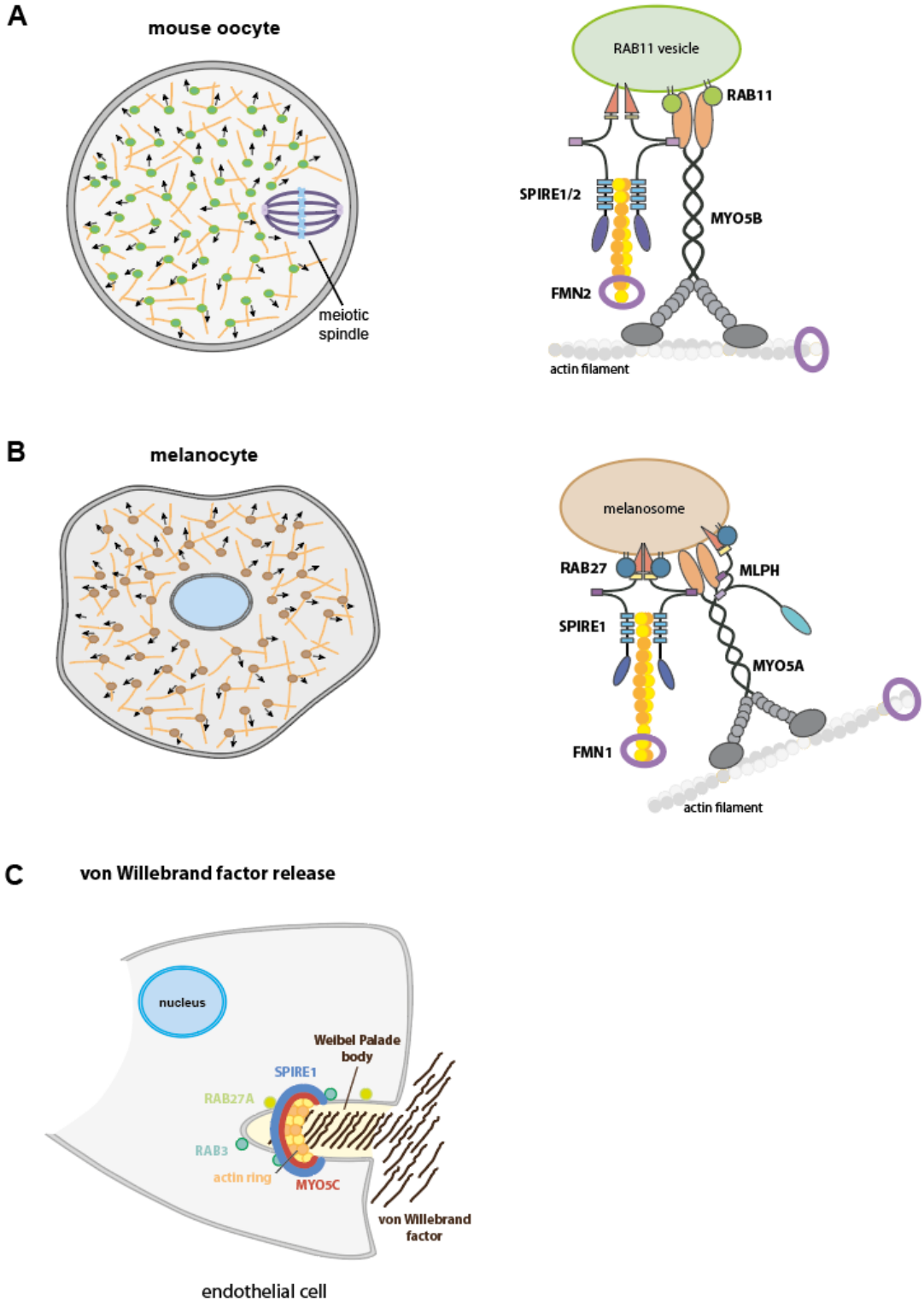

Figure 10: ***Different known protein complexes and their functions*** *. adapted from (Welz and Kerkhoff, 2023) A)* ***Melanosome transport:*** *The pigment-carrying melanosomes (brown dots) are transported peripherally from the cell centre to the membrane by an actin filament network in the cytoplasm (orange lines) that begins at the melanosome membrane (left side). The right side shows a model of the protein complexes that have been proposed to produce new actin filaments at the melanosome*

surface (involving RAB27A, SPIRE1, and FMN1) and to promote MYO5A-dependent transport along actin tracks (RAB27A, MLPH or SPIRE1, MYO5A). The "co-factor" that connects MYO5A and RAB27A is MLPH. The surrounding vesicle surfaces are the source of the actin filaments that are shown in grey. (Welz and Kerkhoff, 2023); B) ***Oocytic vesicle transport mechanisms*** *involve RAB11A vesicles originating at the surface (left side), where an actin filament network (depicted as orange lines) facilitates the movement of RAB11A vesicles (green dots) from the centre to the periphery in metaphase oocytes in mice. A protein complex, including of RAB11A, FMN2, SPIRE1 or SPIRE2, and MYO5B is proposed to assemble on the vesicle surface (right). Actin filaments (orange and yellow circles) are generated directly at the membrane by FMN2-driven elongation, following nucleation initiated through the cooperative interaction of SPIRE proteins and FMN2. This intricate actin filament network (shown in grey) serves as tracks for MYO5B-mediated transport of vesicles toward the membrane (Pfender et al., 2011; Schuh, 2011; Welz and Kerkhoff, 2023); C)* ***van Willebrand factor release in endothelial cells:*** *The externalisation of von Willebrand factor from Weibel-Palade bodies in endothelial cells is facilitated by SPIRE1 and MYO5C. Although the underlying mechanism is unknown, SPIRE1 and MYO5C accumulate at actin ring-like structures formed at the cortical externalisation sites (Holthenrich et al., 2022; Welz and Kerkhoff, 2023)*

1.8.1 SPIRE1 and MYO5A cooperate in melanosome transport

Melanocytes are specialised cells found on the skin's surface and in hair follicles (van den Bossche et al., 2006). They create melanin pigment to protect against and respond to environmental UV light (van den Bossche et al., 2006). Melanin is produced by melanocytes and stored in specialised organelles known as melanosomes (Hume and Seabra, 2011; Wasmeier et al., 2008). In melanocytes, a vesicle-originated actin filament mesh mediates the centrifugal dispersion of melanosome dense-core vesicles towards the plasma membrane (Alzahofi et al., 2020). RAB27A controls melanosome transport (Alzahofi et al., 2020); in this instance, it interacts with the C-terminal FYVE-type domain of SPIRE1 (Figure 10) and the FYVE2 domain of MLPH rather than the processive MYO5A motor. Actin filaments are produced as a result of SPIRE1/2 and FMN1 working together (Alzahofi et al., 2020). Melanophilin (MLPH) is also necessary for the actomyosin-dependent long-range transport of melanosomes (Alzahofi et al., 2020). Additionally, MLPH and SPIRE proteins share the FYVE_2 domain RAB27A interaction module and the closely related MYO5A-GTD-binding motif (Alzahofi et al., 2020; Pylypenko et al., 2013; Pylypenko et al., 2016), indicating that both proteins are involved in the targeting and activation of MYO5A. Furthermore, MLPH has an actin filament-binding motif at the C-terminal end of the protein (Welz and Kerkhoff, 2017), which may help actin filaments attach to melanosome membranes. It is proposed that actin filaments' pointed ends remain affixed to the melanosome membrane and that they extend peripherally into the cytoplasm in a modelling (Alzahofi et al., 2020). MLPH or even MYO5A may act as filament anchors at melanosomes membranes in addition to directly anchoring actin filaments by maintaining binding of the pointed ends via the SPIRE-WH2 cluster. In wild-type melanocytes, the distribution of melanosomes is uniformly throughout the cytoplasm. However, in SPIRE1/2 depleted cells, melanosomes accumulate around the nucleus (Alzahofi et al., 2020). The wild-type melanosome distribution is restored in double knockdown cells after adenovirus infection mediated transgenic expression of SPIRE1, whereas melanosome hyperdispersion was seen in the case of SPIRE2 expression (Alzahofi et al., 2020). In melanosomes next to MLPH exists another

protein, MYRIP (myosin and RAB interacting protein) interacting and activating MYO5A in skin melanosomes (Ramalho et al., 2009).

The human Griscelli syndrome (GS) is a rare autosomal recessive cutaneous condition, where RAB27, MYO5A and MLPH were found mutated and which is characterised by silvery-gray hair and hypopigmentation of the skin (Müller et al., 2008). It can be accompanied with primary neurological impairment (type 1; mutation in MYO5A; in mice: dilute phenotype) (Alzahofi et al., 2020; Hume and Seabra, 2011); immunologic impairment (type 2; mutation in RAB27A, in mice: ashen phenotype) (Alzahofi et al., 2020; Hume and Seabra, 2011), or be isolated (type 3; mutation in MLPH, in mice: leaden phenotype) (Alzahofi et al., 2020; Hume and Seabra, 2011). So the loss of any of these interacting proteins can result in a specific more or less severe phenotype (Müller et al., 2008).

1.8.2 SPIRE1/2 and MYO5B function in oocytic vesicle movement

In mouse oocytes, a cytoplasmic actin meshwork from RAB11 vesicles for peripheral vesicle transport was discovered (Pfender et al., 2011; Schuh, 2011). Actin filaments are produced at the surface of these vesicles by SPIRE1 and SPIRE2 working with FMN2, providing pathways for the long-distance movement of RAB11A vesicles in the direction of the oocyte cortex (Pfender et al., 2011; Schuh, 2011)(Figure 10). Here, the forces responsible for the RAB11A vesicles' motility are produced by MYO5B's processive actin filament sliding activity. Different surfaces of the MYO5B-GTD interact with RAB11A and SPIRE2 (Pylypenko et al., 2013; Pylypenko et al., 2016). Interaction studies indicate that MYO5B acts as a linker between the RAB11 GTPase sitting on the vesicle membrane and SPIRE1/2 in the mouse oocytes (Pylypenko et al., 2016). Thus, by creating a protein complex at the membrane surface, the associated MYO5B may coordinate targeting of the actin nucleation activity of SPIRE1 and SPIRE2 proteins to RAB11A vesicles. MYO5B has a key role in polarised epithelial cells (Bowman et al., 2022). In individuals with microvillus inclusion disease (MVID) nonsense and missense mutations in MYO5B was identified (Müller et al., 2008). MVID is a rare and severe autosomal recessive intestinal disease characterised by watery diarrhoea during infancy, which can be life-threatening (Müller et al., 2008).

A function of SPIRE, FMN, MYO5 and RAB11 proteins was also described in neuronal networks associated with memory and learning (Kollmar et al., 2024).

1.8.3 von Willebrand factor release – MYO5C:SPIRE1:RAB3/27

A recent study by Holthenrich et al. (2022) provides evidence for a role of SPIRE1 in secretory transport processes by demonstrating that SPIRE1 promotes the externalisation of von Willebrand factor from endothelial cells. Here, it has been discovered that MYO5C and SPIRE1 accumulate at actin ring structures at the Weibel-Palade body release sites (Holthenrich et al., 2022)(Figure 10). Weibel-Palade bodies are long, secretory granules that contain two main constituents: P-selectin, which aids in the recruitment of leukocytes during inflammation, and von Willebrand factor, which is involved in hemostasis (Goligorsky et al., 2009). It is currently unknown how the SPIRE1 protein functions in the von Willebrand factor externalisation process on a mechanistic level. Regarding this, it is crucial to remember that the study's human umbilical vein endothelial cells (HUVECs) lack the expression FMN1 and FMN2 (Holthenrich et al., 2022). This implies that SPIRE1 functions either autonomously of FMN-subgroup formins or in conjunction with another formin.

The Weibel-Palade bodies (WPB) are secretory cell organelles, which form at the trans-Golgi network (McCormack et al., 2017). WPB are storage granules of endothelial cells, which synthesise, store and release two principal molecules (P-selectin (Bonfanti et al., 1989; McEver et al., 1989), von Willebrand factor (Wagner et al, 1982)) and play a dual role in hemostasis (Nightingale and Cutler, 2013), inflammation and blood coagulation (van Mourik et al., 2002). The von Willebrand factor connects thrombocytes and the injured vessel wall and activates the thrombocytes (Shalmi and Goetze, 2021). The thrombocytes are one component of the blood whose function with other coagulation factors is to react to bleeding from blood vessel injury by clumping and initiating a blood clot (Springer, 2014). SPIRE1, RAB3, RAB27 and MYO5C function in the release of von Willebrand factor (VWF) in endothelial cells (Holthenrich et al., 2022). MYO5 and actin-binding protein MyRIP are recruited with RAB27A and its effectors to mature WPB, anchoring the WPB to the actin cortex until fully matured (Conte et al., 2016; Nightingale et al., 2009). RAB3B and RAB27A are localised at WPBs (Holthenrich et al., 2022). SPIRE1 and MYO5C interact in co-immunoprecipitation experiments and instead of an actin mesh, as in oocytes and melanocytes, may contribute to the formation of an actin ring structure that is crucial for VWF externalisation (Holthenrich et al., 2022). This exocytic vesicle process is SPIRE2 independent and FMN1/2 independent (Holthenrich et al., 2022). The exact underlying mechanisms remain unknown and need further investigation.

1.9 Evolution of the SPIRE-MYO5 interaction

The closest unicellular relatives of animals are choanoflagellates (Carr et al., 2008; Nicole King et al., 2008; Lang et al., 2002; Ruiz-Trillo et al., 2008). In addition to pointing out the striking structural similarities between choanoflagellates and the flagellated choanocytes of sponges, one of the earliest

multicellular animals, James Clark first described these unicellular flagellate protists in 1866 (Carr et al., 2008; Clark, 1866; Schultz et al., 2023). Therefore, it is hypothesised that living choanoflagellates resemble the single-celled ancestors of the animal kingdom (Brunet and King, 2017; N. King et al., 2004). Therefore, researching choanoflagellates may yield valuable information about the cell biology of animal origins (Brunet and King, 2017). The holozoans (animals and their closest single-celled relatives) origin of many synaptic proteins and the identification of neuronal vesicle transport protein homologs in choanoflagellates (Burkhardt, 2015) imply that a sophisticated cell signalling apparatus predated animal evolution. Furthermore, the sophisticated diversity of animal cells and their neuroendocrine communication systems may have evolved as a result of their development (Burkhardt et al., 2014; Burkhardt et al., 2011; Göhde et al., 2021).

According to earlier research, SPIRE proteins are conserved in both, mammals and insects, such as *Drosophila melanogaster*, and are crucial for the movement of organelles, such as vesicles in oocytes and melanosomes in melanocytes (Alzahofi et al., 2020; E. Kerkhoff et al., 2001; Pfender et al., 2011; Schuh, 2011; Wellington and Manseau, 1999; Welz and Kerkhoff, 2023). In Drosophila SPIRE plays a role in oocyte development (Dahlgaard et al., 2007; Quinlan, 2013). Using known SPIRE homologs from *Drosophila melanogaster* and humans as a starting point, eukaryotic genomes and transcriptomes were searched using TBLASTN (Altschul et al., 1997) to determine the origin of SPIRE proteins in evolution and their distribution across living species (Kollmar et al., 2024).

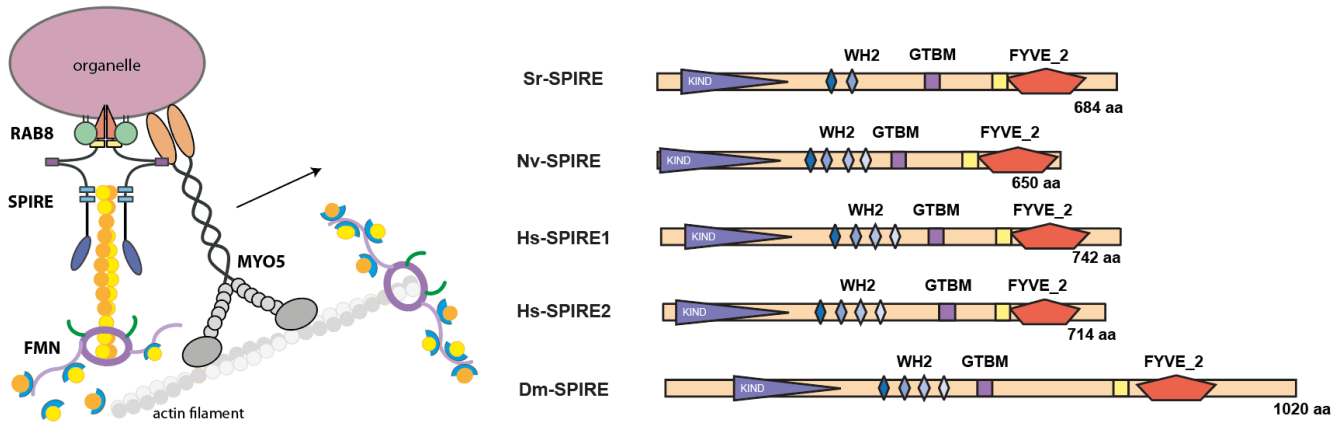

Figure 11: ***Model of a proposed RAB8/SPIRE/MYO5/FMN protein complex in choanoflagellates*** *from (Kollmar et al., 2024) A) Schematic model of the proposed choanoflagellate RAB8/SPIRE/MYO5/FMN protein complex at the surface of organelle membranes. B) A schematic representation of a choanoflagellate cell is shown aside indicating the intracellular organisation including Golgi system (G), nucleus (N) and food vacuoles (F) (Kollmar et al., 2024).*

Four major aspects regarding the evolution, retention, and duplication of SPIRE proteins in eukaryotes were highlighted by the analysis (Kollmar et al., 2024). SPIRE homologues are absent in fungi, plants, and amoebae, whereas they are present in most other holozoa, including multicellular animals and their closest unicellular relatives (Kollmar et al., 2024). Not all holozoa encode SPIRE proteins; for

example, nematodes and the unicellular filasterean *Capsaspora owczarzaki* do not express SPIRE (Kollmar et al., 2024). Throughout evolution, there have been multiple independent instances of SPIRE duplication and loss (Kollmar et al., 2024). For instance, among vertebrates, the coastal hagfish *Eptatretus burger*, an ancient jawless fish, has a single SPIRE gene, whereas more recent jawed vertebrates, like birds and reptiles, have three SPIRE genes (SPIRE1-3) (Kollmar et al., 2024). In mammals and bony fish (euteleosts), SPIRE3 has been lost independently, so these groups only kept SPIRE1 and SPIRE2 (Kollmar et al., 2024). Examining the invertebrates more closely, ctenophores (comb jellies), placozoans (*Trichoplax adhaerens*, small disc-like animals), mesozoans (wormlike parasites of marine invertebrates), platyhelmintes (flat worms) and nematodes (round worms) have lost SPIRE (Kollmar et al., 2024). The unicellular ichthyosporean *Amoebidium parasiticum*, a gene duplication event took place, which lead to two SPIRE genes, one of them encoding a SPIRE-like protein lacking the RAB GTPase/membrane binding FYVE_2 zinc finger domain (Kollmar et al., 2024).

The cooperative role of MYO5 motor proteins and SPIRE actin nucleators in organelles precedes with the evolution of animals, as demonstrated by the presence and interaction of SPIRE and MYO5 homologs in unicellular choanoflagellates (Kollmar et al., 2024). Actin filament assembly is efficiently started by choanoflagellate SPIRE, which can offset the role of mammalian SPIRE in organelle transport (Kollmar et al., 2024). The primary interactions of SPIRE proteins with MYO5, RAB GTPases, and FMN-subgroup formins are shared by mammals and choanoflagellates (Kollmar et al., 2024). Protein complexes known to date are conserved in choanoflagellates (Kollmar et al., 2024). In animals, the increased numbers of isoforms lead to more specific complexes, proteins in different contexts that have arisen during evolution (Kollmar et al., 2024). The choanoflagellate SPIRE has recently been identified as a RAB8 GTPase interacting protein (Kollmar et al., 2024). SPIRE, RAB8 and MYO5 have a functional relationship in both choanoflagellate and mammalian cells (Figure 11), as previously demonstrated (Kollmar et al., 2024). SPIRE2-GTBM-FYVE_2, RAB8A, and MYO5A-cc-GTD co-localise (Welz and Kerkhoff, 2023) at vesicular structures in human HeLa cells. In eukaryotic cells, RAB8 effects on the transit from the Golgi to the plasma membrane (Kollmar et al., 2024). The single-celled holozoan's RAB8 gene has a great number of duplications in metazoans, giving rise, among other things, to RAB3 and RAB27 GTPases in mammals (Kollmar et al., 2024). The interactions of the mammalian SPIRE1 protein with RAB3 and RAB27 GTPases have been characterised (Kollmar et al., 2019; Straub et al., 2020).

1.10 Aim of thesis

The aim of this thesis was to get a greater understanding of the principles of intracellular vesicle transport processes and the underlying molecular mechanisms that regulate vesicle trafficking. Upon the diversity of mammalian actomyosin functions, the interactions of MYO5 motor actin proteins and SPIRE actin nucleators are evaluated. The investigation is based on the conserved proteins and interactions. A basic vesicle complex localised of RAB8, MYO5, SPIRE and FMN in unicellular holozoa has been proposed which has evolved into numerous, specialised complexes in animals driven by gene duplications. This work focused on understanding these specialisations by means of the SPIRE/MYO5 interaction variances and specificities in mammals.

2 Materials and methods

2.1 Multiple SPIRE protein sequence alignments

As described in (Kollmar et al., 2024) a preliminary SPIRE-GTBM alignment was performed using ClustalW (Chenna et al., 2003) and afterwards manually refined. Based on this alignment the weblogo in this thesis was done. The SPIRE sequence alignment is available at CyMoBase (www.cymobase.org) (Odronitz and Kollmar, 2006). For the protein sequence alignment of the SPIRE-GTBM, additional multiple sequence alignments were performed using the Job Dispatcher EMBL's European Bioinformatics Insitute (EMBL-EBI, Hinxton, UK). The Calculations of the protein sequence identities and similarities of SPIRE-GTBM were done using the UniProt Align tool (UniProt Consortium). For the weblogo and an easier visualisation, the SPIRE-GTBM sequences of different vertebrate SPIRE1 and SPIRE2 were aligned using Jalview (version 2.11.4.1) (Clamp et al., 2004) and the weblogo was performed as mentioned in (Crooks et al., 2004) with the required sequences.

From the NCBI protein database, the respective protein sequences were obtained with the following accession numbers: Hs-SPIRE1: NP_064533.3, Hs-SPIRE2: CAD19439.1, Nv-SPIRE: XP_032234162.2, Sr-SPIRE: XP_004990203.1, Hs-MYO5A: NP_001369277.1, Hs-MYO5B: NP_001073936.1, Hs-MYO5C: NP_061198, Nv-MYO5: XP_048581654.1 and Sr-Myo5: XP_004997168.1.

For the weblogo generation the protein sequences were obtained from the database www.cymobase.org.

For the vertebrate SPIRE1 weblogo, 12 sequences from the following species were used: *Homo sapiens*, Hs; *Panthera leo*; Pat; *Canis lupus familiares*, Caf; *Felis catus*, Fc; *Bos taurus*, Bt; *Loxodonta africana*, La; *Equus caballus*, Eqc; *Mus musculus*; Mm; *Brachydanio rerio*, Br, A and B isoform; *Gallus gallus*, Ggg and *Xenopus tropicalis*, Xt.

For the vertebrate SPIRE2 weblogo, 10 sequences from the following species were used: *Homo sapiens*, Hs; *Panthera leo*; Pat; *Felis catus*, Fc; *Bos taurus*, Bt; *Loxodonta africana*, La; *Equus caballus*, Eqc; *Mus musculus*; Mm; *Brachydanio rerio* ,Br; *Gallus gallus*, Ggg and *Xenopus tropicalis*, Xt.

For the cnidarian SPIRE weblogo, 13 sequences from the following species were used: *Rhopilema esculentum*, Rhes; *Hydra magnipapillata*, Hm; *Hydra oligactis*, Hyo; *Clytia hemisphaerica*, Clh; *Podocoryna carnea*, Poc; *Hydractinia symbiolongicarpus*, Hysy; *Briareum asbestinum*, Bras; *Acropora millepora*, Acm; *Protes australiensis*, Poau; *Orbicella faveolata*, Orfa; *Stylophora pistillata*, Stp; *Nematostella vectensis*, Nv and *Anthopleura elegantissima*, Anel.

For the choanoflagellate SPIRE weblogo, 18 sequences from the following species were used: *Monosiga brevicollis*, Mb; *Choanoeca perplexa*, Chop; *Salpingoeca infusionum*, Sinf; *Hartaetosiga gracilis*, Hagr; *Hartaetosiga balthica*, Haba; *Salpingoeca rosetta*, Sr; *Microstomoeca roanoka*, Miro; *Codosiga hollandica*, Codh; *Salpingoeca dolichothecata*, Sado; *Salpingoeca urceolata*, Saur; *Salpingoeca punica*, Spun; *Mylnosiga fluctuans*, Mvfl; *Salpingoeca helianthica*, Sahe; S*alpingoeca kvevrii*, Sakv; *Didymoeca costata*, Didc; *Stephanoeca diplocostata*, Stdi; *Diaphanoeca grandis*, Digr and *Savillea parva*, Sapa.

2.2 Agarose gel electrophoresis

Agarose gel electrophoresis was used for the size separation of the PCR amplified DNA fragments, digested vectors and DNA inserts. Therefore, the PCR or restriction digest samples were mixed with 6x DNA loading buffer (10 mM Tris-HCl, pH 7.6, 0.03% Bromophenol blue, 60% glycerol, 60 mM EDTA). For the agarose gels, ultrapure agarose (ThermoFisher, Waltham, MA, USA) was solved in 0.5x TBE buffer (89 mM Tris, pH 7.6, 89 mM boric acid, 2 mM EDTA, pH 8.0) by shaking and heating. Agarose gels were used with suitable agarose concentrations (in the range between 1% and 2%), depending on the size of the expected DNA fragments. The gel electrophoresis was performed at 120 V for 23 min in 0.5x TBE buffer with a DNA ladder (6x Tri Track DNA loading buffer, 1kb ladder, Thermo Fisher, H_2O) in a BIORAD Mini-Sub cell GT gel chamber.

2.3 DNA extraction from agarose gels following the protocol of Machery-Nagel

For separating the DNA fragments via gel electrophoresis by size, the PCR was mixed previously with 6x DNA loading buffer (10 mM Tris-HCl, pH 7.6, 0.03% Bromophenol blue, 60% glycerol, 60 mM EDTA), loaded on a agarose gel and run for 23 min at 120 V. The desired DNA fragment was extracted from agarose gels using the NucleoSpin Gel and PCR Clean-up (250 preps) (Macherey-Nagel, Düren, Germany). The DNA fragment was cut out of the agarose gel, weighted and transferred into 200 µl binding buffer (NTI buffer) (per 100 mg gel, incubated at 52-56°C for 5-10 min and vortexed from time to time. The melted sample was loaded onto a column and centrifuged (11,000 x g, 1 min, room temperature, 22°C). Afterwards the silica column was washed using up to two times 650 µl neutralisation buffer (NT3 buffer) each and centrifuged (11,000 x g, 1 min, 22°C). Then the silica membrane was dried by centrifugation (11,000 x g, 2 min, 22°C) to elute the DNA. The column was placed in a new 1.5 ml tube with 30 µl elution buffer (NE buffer), incubated for 1 min at room temperature (RT, 22°C) and centrifuged (11,000 x g, 1 min, 22°C).

2.4 Measurement of DNA concentrations (according to (T. Welz))

The concentration of plasmid DNA, PCR amplified DNA fragments was measured by spectrophotometric analysis using the GeneQuant photometer (GE Healthcare Life Sciences, Freiburg, Germany). The DNA was diluted 1:200 in autoclaved water and transferred into a glass cuvette. The absorption of ultraviolet light (λ = 260 nm) by the DNA was measured and the concentration was calculated accordingly. The contamination of the DNA sample was estimated by measuring of sample absorption at 280 nm, since proteins absorb light at 280 nm. The ratio of absorbance at 260 nm and 280 nm ($A_{260/280}$) was calculated. An $A_{260/280}$-ratio around 1.8 is accepted as "pure" DNA.

2.5 PCR technique: amplification of cDNA fragments for cloning (according to (T. Welz))

AccuPrime Pfx DNA Polymerase (ThermoFisher; Table 21) was used for DNA fragment amplification for cloning. 50 ng of template DNA (here plasmid DNA) was applied. The elongation time for the DNA synthesis (t_E) was adapted to the length of the amplified DNA fragment (60 sec per 1000 bp). The temperature for the primer annealing (T_A) was normally set to 5°C lower than the calculated melting temperature of the primer. When oligonucleotide primer with high melting temperatures were used, DMSO (5% to 10%) was added. The oligonucleotide primers were designed oligonucleotides manually, containing also restriction site overhangs, and ordered as lyophilised oligonucleotides at Sigma-Aldrich (Taufkirchen, Germany). A list of all oligonucleotide primers used in this thesis can be found in the supplements, Table 17 on page 126 of supplements.

Table 1: Protocol of PCR-mixture

Reagents	Volume
template DNA	50 ng
Primer 5' (10 µM)	3 µl
Primer 3' (10 µM)	3 µl
10x Pfx Buffer	5 µl
Pfx DNA Polymerase	1 µl (2.5 units/ µl)
DMSO (optional)	5% - 10%
H_2O	Fill up to 50 µl
Total volume	50 µl

Table 2: PCR cycling protocol

Temperature	Time
95°C	5 min
95°C	1 min
T_A	30 sec
68°C	T_E
68°C	5 min
4°C	hold

T_A = 5°C less than primers melting temperature t_E = 60 sec for 1000 bp

2.6 Cloning of plasmid DNA expression vectors (according to (T. Welz))

2.6.1 Restriction digest

For the restriction digests, 2 µg plasmid DNA was incubated with restriction endonucleases (NEB) in an appropriate buffer (CutSmart; NEB) for 2.5 h at 37°C. 1 µl calf intestinal phosphatase (CIP; NEB) was added 1 h and 30 min before the end of the restriction digest. CIP removes the phosphate groups at the 5' ends of the DNA and thus prevents the re-ligation of the vector. Controls were used to control for the proper digestion: undigested vector and the vector digested with only one of the two enzymes. PCR amplified DNA fragments digested with restriction endonucleases were used as plasmid DNA inserts, usually 7 µl (depending on the band strength on the agarose gel) of the gel extracted DNA (from a total elution volume of 30 µl) (Table 3; Table 4). Following restriction digest, vector and inserts were separated by agarose gel electrophoresis and subsequently purified from the agarose gel for further processing.

Table 3 : Protocol for plasmid DNA vector digest. Enzyme : 2 µl for 5,000 U/ ml, 1 µl for 10,000 U/ ml, 0.5 µl for 20,000 U/ ml.

Reagent	**Volume**			
	Undigested	Enzyme 1	Enzyme 2	Double digest
Plasmid DNA	0.5 µg	0.5 µg	0.5 µg	2 µg
Enzyme 1	-	Enzyme dependent	Enzyme dependent	Enzyme dependent
Enzyme 2	-	Enzyme dependent	Enzyme dependent	Enzyme dependent
10x NEBuffer	3 µl	3 µl	3 µl	3 µl
H_20	Up to 30 µl	Up to 30 µl	Up to 30 µl	Up to 30 µl
Total volume	*30 µl*	*30 µl*	*30 µl*	*30 µl*

Table 4: Protocol for insert digest. Enzyme: 2 µl for 5,000 U/ ml, 1 µl for 10,000 U/ ml, 0.5 µl for 20,000 U/ ml.

Reagent	**Volume**
Linear DNA fragement (PCR fragment)	7 µl
Enzyme 1	Enzyme dependent
Enzyme 2	Enzyme dependent
10x NEBuffer	3 µl
H_20	Up to 30 µl
Total volume	*30 µl*

2.6.2 Ligation

In order to combine the digested vector and the digested insert DNA fragment T4 DNA ligase (NEB; Table 22) mediated ligation was performed in a thermocycler at 16°C, overnight (oN).

*Table 5：Protocol for ligation of digested plasmid DNA vectors and DNA- inserts. *) the DNA amount of the vector/ insert refer to the 30 µl elution volume and the used amount was estimated from the band strength on the agarose gel (ratio vector/ insert mostly 1:7).*

Reagent	**Volume**
Digested vector	1-2 µl (1-2 µg) (according to 30 µl elution volume and depending on the strength of the band on the agarose gel)
Digested insert fragment	3-7 µl * (~7 µg; according to 30 µl elution volume and depending on the strength of the band on the agarose gel)
10x T4 buffer (50mM Tris-HCl, 10mM $MgCl_2$, 1mM ATP, 10mM DTT; pH7.5)	2 µl
T4 DNA ligase	1 µl
H_20	Up to 21 µl
Total volume	*21 µl*

Following ligation, NEB10-beta rubidium chloride competent *E. coli* bacteria cells were transformed according to the standard transformation protocol (see below).

2.6.3 Transformation of *Escherichia coli* bacterial cells

The following chemo-competent *E.coli* strains were used for transformations: *E.coli* Rosetta (F– *ompT hsdS*B(rB– mB–) *gal dcm* pRARE2 *(*CamR), Novagen) were used for bacterial expression vectors, and NEB10-beta Competent *E. coli* (Δ*(ara-leu) 7697 araD139 fhuA* Δ*lacX74 galK16 galE15 e14-* φ*80*d*lacZ*Δ*M15 recA1 relA1 endA1 nupG rpsL* (StrR) *rph spoT1* Δ*(mrr-hsdRMS-mcrBC)*; NEB) for DNA vector cloning and plasmid DNA amplification and subsequent purification. The bacterial cells were thawed on ice. The complete ligation mixture (or ~ 1 µg of existing plasmid DNA for re-transformations) was added to the cell suspension (100 µl) and incubated for 1 h on ice, followed by a heat shock (42°C, 55 sec) to induce plasmid uptake. After 2 min incubation on ice, 900 µl LB_0 medium (lysogeny broth, recipe in the supplement) was added to the bacteria and incubated in a round-bottom tube for 1.5 h

at 37°C while shaking. After this step, the bacteria were pelleted by centrifugation (4,600 x g, 10 min, 22°C) and 800 µL of the supernatant was discarded. The bacterial cells were resuspended in the remaining supernatant, plated and cultured on respective agar selection plates overnight at 37°C.

2.6.4 Plasmid DNA extraction and purification from bacterial cells

After the successful plasmid DNA vector generation and following transformation of *E. coli* cells, single colonies were picked from the selection plate and incubated in LB medium, containing the specific antibiotics. Those were incubated at 37°C, overnight, while shaking to produce enough amounts of plasmid DNA. On the following day, the plasmid DNA was extracted and purified from the bacterial cells for further processing, including a control of the vector correctness by DNA-sequencing and long-term storage. The plasmid DNA was extracted from bacterial cells using Plasmid-Mini-Purification (MiniPrep; QIAGEN, Hilden, Germany) for control digests, Plasmid-Mini-Purification (MiniPrep, QIAGEN, Hilden, Germany) for sequencing or Plasmid-Maxi-Purification (MaxiPrep, QIAGEN, Hilden, Germany).

2.6.5 Plasmid-MINI-purification (MiniPrep) for control digests following the protocol for Spin MiniPrep of QIAGEN

After a successful vector generation and transformation of *E. coli* cells, single colonies were picked and incubated in 1.5 ml LB medium with respective antibiotics, and incubated overnight at 37° while shaking (150 rpm). On the next day, the overnight-culture was pelleted by centrifugation (4,600 x g, 10 min, 22°C). The supernatant was discarded. The bacterial pellet was resuspended in 250 µl resuspension buffer (P1 buffer; pH 7.4; 150 mM NaCl, 5 mM KCl, 2.5 mM $CaCl_2$, 1 mM $MgCl_2$, 10 mM HEPES, 3 mM glucose; QiaPrep Spin Miniprep Kit), 250 µl lysis buffer (P2 buffer; 2 mM NaCl, 55 mM KCl, 2.5 mM $CaCl_2$, 1 mM $MgCl_2$, 10 mM HEPES, 3 mM glucose) were added, mixed thoroughly by inverting 4-6 times and incubated for 5 min at RT. 250 µl neutralisation buffer (P3 buffer; pH 5.5; 3 M potassium acetate) was added, mixed thoroughly by inverting 4-6 times and centrifuged (4,600 x g, 10 min, 22°C). 500 µl of the supernatant were applied to a new 1.5 ml cup and 1 ml EtOH absolute was added. After inverting two times and a 5 min incubation step at room temperature, it was centrifuged (11,000 x g, 10 min, 22°C). The supernatant was decanted; the DNA pellet washed with 500 µl 70% EtOH and centrifuged (11,000 x g, 10 min, 22°C). The supernatant was decanted again, the rest was taken away carefully with a pipette and the pellet was air-dried for 5-10 min: incubate in a heat block at 52°C with an open lid. In the last step, the DNA was dissolved in 50 µl distilled water.

2.6.6 Plasmid-MINI-purification (MiniPrep) for sequencing following the protocol for MiniPrep of QIAGEN

Bacterial colonies were picked and incubated in 10 ml LB medium, with the respective antibiotics, and incubated oN at 37° while shaking. On the next day, the over-night-culture was pelleted by centrifugation (4,600 x g, 10 min, 22°C). The supernatant was discarded. The bacterial pellet was resuspended in 250 µl resuspension buffer (P1 Buffer, pH 7.4; 150 mM NaCl, 5 mM KCl, 2.5 mM $CaCl_2$, 1 mM $MgCl_2$, 10 mM HEPES, 3 mM glucose), 250 µl lysis buffer (P2 buffer; 2 mM NaCl, 55 mM KCl, 2.5 mM $CaCl_2$, 1 mM $MgCl_2$, 10 mM HEPES, 3 mM glucose) were added, mixed thoroughly by inverting 4-6 times until the solution turns blue (if using LyseBlue reagent), incubated for 5 min at room temperature. 350 µl neutralisation buffer (N3 buffer; pH 4.8; 4.2 M guanidine hydrochloride, 0.9 M potassium acetate) were added, mixed thoroughly by inverting 4-6 times, the solution will turn colourless (if using LyseBlue reagent) and centrifuged (16,000 x g, 10 min, 22°C). Then, 800 µl of the supernatant were applied to a QIAprep 2.0 spin column and centrifuged (16,000 x g, 1 min, 22°C) and the flow-through was discarded. The QIAprep 2.0 spin column was washed by adding 0.5 ml binding buffer (PB buffer; 5 M Gu-HCl, 30% isopropanol) and centrifuged (16,000 x g, 1 min, 22°C). The spin column was washed again by adding 0.75 ml washing buffer (PE buffer; 10 mM Tris-HCl, pH 7.5, 80% EtOH), centrifuged (16,000 x g, 1 min, 22°C) and the flow-through discarded again. To remove residual wash buffer and dry the membrane, the column was centrifuged (16,000 x g, 1 min, 22°C) and placed on a clean 1.5 ml microcentrifuge tube. To elute the bound DNA, 50 µl elution buffer (EB buffer; 10 mM Tris-Cl, pH 8.5) was added, incubated for 1 min at room temperature and centrifuged (16,000 x g, 1 min, 22°C).

2.6.7 Plasmid-Maxi-purification (MaxiPrep) following the protocol for MaxiPrep of QIAGEN

The day before, 100 ml LB_0 medium with respective antibiotics were inoculated with bacterial colonies oN at 37°C while shaking. The next day, the over-night-culture was pelleted at (4,600 x g, 15 min, 4°C). The supernatant was discarded and the bacterial pellet was resuspended in resuspension buffer (P1 buffer, 4°C; pH 7.4; 150 mM NaCl, 5 mM KCl, 2.5 mM $CaCl_2$, 1 mM $MgCl_2$, 10 mM HEPES, 3 mM glucose). 10 ml lysis buffer (P2 buffer; 2 mM NaCl, 55 mM KCl, 2.5 mM $CaCl_2$, 1 mM $MgCl_2$, 10 mM HEPES, 3 mM glucose) was added, mixed thoroughly by inverting 4-6 times and incubated at RT for 5 min. After incubation 10 ml neutralisation buffer (P3 buffer; pH 5.5, 3 M potassium acetate) were added, mixed by inverting 4-6 times and incubated on ice for 10 min, followed by a centrifugation step (4,600 x g, 10 min, 4°C). During this centrifugation step, a QIAGEN-tip was equilibrated by applying 10 ml equilibration buffer (QBT buffer; pH 7.0, 750 mM NaCl, 50 mM MOPS, 15% isopropanol (v/v), 0.15% Triton®X-100 (v/v)), allowing the column to empty by gravity flow. The supernatant was applied to the

QIAGEN-tip, allowing it to enter the resin by gravity flow. Afterwards the QIAGEN-tip was washed with 2x 30 ml wash buffer (QC buffer; pH 7.0, 1 M NaCl, 50 mM MOPS, 15% isopropanol (v/v)) and the bound DNA was eluted with 15 ml elution buffer (QF buffer; pH 8.5, 1.25 M NaCl, 50 mM Tris-Cl, 15% isopropanol (v/v)) into a clean 50 ml Falcon. The DNA was precipitated by adding 10.5 ml iso-propanol to elute the DNA and mixed, centrifuged afterwards (4,600 x g, 30 min, 4°C). The supernatant was decanted carefully, the DNA pellet washed with 5 ml EtOH (70%) and centrifuged (4,600 x g,10 min, 4°C). The supernatant was decanted again. In the last step, the pellet air-dried for 5-10 min and the DNA was redissolved in 300 µl Tris-EDTA pH 8.0.

2.6.8 Control digests

Control digests were performed to check newly generated and isolated plasmid DNA for successful DNA fragment insertion. First, plasmid DNA was extracted and purified from bacterial colonies, and subsequently incubated with respective restriction endonucleases to obtain specific DNA bands on agarose gels. A master mix containing buffer, restriction endonucleases and H_2O was prepared. 10 µl of plasmid DNA was incubated with 10 µl of the previously prepared master mix for 2 h at 37°C. The presence of specific DNA bands was subsequently checked by agarose gel electrophoresis.

Table 6: Protocol for digest.

Reagent	**Volume**
Plasmid DNA	10 µl
10x NEBuffer	2 µl
Enzyme 1	Enzyme dependent
Enzyme 2	Enzyme dependent
H_20	Up to 20 µl
Total volume	*20 µl*

2.6.9 DNA sequencing

For verification of the DNA sequence of the newly generated plasmid DNA, the prepped DNA was sent to and analysed by a commercially available DNA sequencing service (LGC Genomics, Berlin, Germany). The DNA was diluted to a concentration of 100 ng/ µl using autoclaved water. The primers used for the sequencing were provided by the sequencing service, or self-designed primers were sent with the probes. Nucleotide sequence alignments (Nucleotide BLAST; NCBI) with the corresponding target cDNA sequence were used to confirm the validity of the sequence, and the computer program Serial Cloner was used to analyse the correct translation reading frame of the proposed protein sequence.

2.7 Cell culture techniques (according to (T. Welz))

HEK 293 (human embryonic kidney) cells (ATCC 293, Manassas, Virginia, USA) and HeLa (cells of a probe of cervix tumour from patient Henrietta Lacks, ATCC CCL-2) cells were cultured in Dulbecco's Modified Eagle's Medium (DMEM; ThermoFisher) supplemented with 10% fetal calf serum (FCSIII; GE Healthcare Life Sciences, HyClone), 2 mM L-Glutamine (ThermoFisher), penicillin (100 units/ ml, ThermoFisher) and streptomycin (100 units/ ml, ThermoFisher) (from now on known as full medium, FM) at 37°C, 5% CO_2, 95% humidity and were passaged regularly at 80% confluency. For passaging, medium was removed and cells were washed once with 1x PBS (only in the case of HeLa cells) to get rid of residual serum. Cells were detached using trypsin-EDTA solution (0.05%; ThermoFisher) for 2-5 min (until the cells were detached) at room temperature. Trypsin-EDTA was inactivated by adding full medium. A fraction of the cell suspension was then transferred into a new culture dish containing fresh full medium, generally at a ratio of 1:10 for HEK 293 cells and 1:5 for HeLa cells.

2.7.1 Thawing cells

For long-term storage eukaryotic cells are kept in liquid nitrogen (-196°C). A stock of frozen cells was thawed rapidly at 37°C in a water bath and the cells were transferred into a 50 ml Falcon tube containing 15 ml of full medium (DMEM, 10% FCSIII, PenStrep, L-Gln) to dilute the DMSO. The cell suspension was centrifuged (800 x g, 6 min, 22°C). The supernatant was removed and the cells were resuspended in 1 ml pre-warmed full medium. The cell suspension was transferred into a 10 cm dish (Greiner Bio-One, Frickenhausen, Germany) containing 9 mL pre-warmed Full Medium. The cells were cultured at 37°C, 5% CO_2.

2.7.2 Freezing cells

For long-term storage eukaryotic cells are kept in liquid nitrogen (-196°C). For freezing the cells, first a specific Freezing Medium was prepared in the necessary amount containing DMEM supplemented with 20% FCSIII, 2 mM L-Glutamine, penicillin (100 units/ ml), streptomycin (100 µg/ ml) and 10% DMSO. DMSO and FCSIII work as cryoprotective agents that prevent the formation of ice crystals inside the cell. For a freezing event, normally eight 10 cm dishes with cells at a confluency at approximately 80% were used. The old medium was removed, the cells were washed with 1x PBS and detached with Trypsin-EDTA as described previously. The Full Medium was added to inactivate the Trypsin-EDTA and the cell suspension was collected and transferred into 5 ml Freezing Medium. After a centrifugation step (800 x g, 6 min, 22°C), the supernatant was removed and the cells were resuspended in 18 ml Freezing Medium. 1 ml aliquots of the cell suspension were transferred into cryovials (ThermoFisher,

Nunc). The vials were stored over-night in a cryo-box filled with isopropanol at -80°C to permit gradual freezing (-1°C per minute). The gradual freezing process prevents ice crystal formation inside the cells that would cause damage and induces cell shrinkage because of a loss of water. On the next day, the cryovials with the cells were transferred to the liquid nitrogen tank for long time storage.

2.7.3 Poly-L-Lysine coating of 6-well plates

Prior to seeding HEK 293 cells for transfections in 6-well plastic plates, the wells need to be coated with Poly-L-Lysine to prevent cell loss during multiple washing steps because of the weak HEK 293 cell adhesion capacity. Poly-L-lysine (Sigma-Aldrich) was diluted 1:10 in sterile water (Sigma-Aldrich). 1 ml of this solution was added per well and shortly incubated (10 min). The coating solution was removed and the wells were washed once with 1x PBS to get rid of residual solution and allowed to dry with a slightly open lid. Subsequently, cell seeding was performed as described in the following.

2.7.4 Seeding cells

The cells were seeded in 6-well plates and cover glasses in the respective densities one day before transfection. To seed cells, old medium was removed and cells were detached using Trypsin-EDTA as described above. 4 ml Full Medium were added per 10 cm dish to inactivate Trypsin-EDTA and the cells were transferred into a 50 ml Falcon tube and centrifuged (800 x g, 6 min, 22°C). The supernatant was removed and cells were resuspended in a respective volume of Full Medium, according to the expected cell number. 10 µl of the cell suspension was mixed with 10 µl Trypan Blue Solution (0.4%; Sigma-Aldrich) to differentiate between viable and dead cells. The living cells appear white and only these are counted using a Neubauer counting chamber, considering all four major squares and calculating the mean ($\bar{x}$). One major square, involving 4 x 4 minor squares, is 1 mm in length and 1 mm in width. The distance between cover glass and counting chamber is 0.1 mm. Considering this, the counted cell number per square is in a volume of 1 x 1 x 0.1 mm = 0.1 mm^3 = 0.1 µl. To compensate the dilution by Trypan Blue, the cell concentration is multiplied by 2. To normalise the concentration to ml volumes, the concentration is multiplied by 10^4 to get the number of cells per ml of cell suspension.

$$X\ [\text{cell number}/0.1\ \mu l] \times 2 \times 10^4 = \text{cell concentration}\ [\frac{cells}{ml}]$$

The volume of the cell suspension required to get the desired cell number was calculated as follows:

$$\frac{desired\ number\ of\ cells\ [cells]}{\text{cell concentration}\ [\frac{cells}{ml}]} = Y\ ml\ of\ cell\ suspension$$

The appropriate volume of the cell suspension was transferred into the respective culture plate or dish, which already filled with 2 ml Full Medium. Seeded cells were allowed to attach over night at 37°C, 5% CO_2.For the transfection with the jetOPTIMUS® reagent, the cells were seeded with a density of 1.25 x 10^5 cells per well in a 12-well dish.

2.7.5 Transfection of eukaryotic cells

For the experiments, the cells were transfected with different transfection reagents, Lipofectamin2000 and jetOPTIMUS®. The Lipofectamin2000 was used for the transfection for the pulldown assays; because this reagent is versatile, that has shown to transfect a wide range of adherent cell lines as well as cell lines in suspension. It has been widely used in science for knockdown experiments. The jetOPTIMUS® requires a lower volume and is highly efficient in difficult-to-transfect cell lines. For the transfection with jetOPTIMUS® a lower amount of reagent is needed.

2.7.6 Transfection of eukaryotic cells using Lipofectamine2000 reaction

The HEK 293 cells were seeded on 6-well plates in the respective densities (8 x 10^5 cells/well) for each pulldown assay experiment one day before transfection. The plasmid DNA was diluted in DMEM without supplements to receive a concentration of 5 µg/ml. 6 µl of Lipofectamine2000 Transfection Reagent (ThermoFisher) was mixed with 200 µl DMEM (per well) and incubated for 5 min at room temperature. Per sample, 200 µl of Lipofectamine2000 dilution and 0.5 µg plasmid DNA were mixed and filled up with DMEM up to 600 µl. This mixture was incubated for 20 min at room temperature. In the meantime, the seeded cells were washed two times with DMEM to get rid of any residual serum that would perturb transfections. After the incubation the complete transfection mix was transferred to the cells. The transfections were incubated for 5 hours at 37°C, 5% CO_2. After the incubation the transfection mix was removed and replaced by 2 ml fresh full medium. The 6-well plates were incubated at 37°C, 5% CO_2 for at least 24 hours to allow an efficient protein production.

2.7.7 Transfection of eukaryotic cells using jetOPTIMUS® reaction (following the protocol of jetOPTIMUS® transfection reagent (Polyplus^{+}))

The HeLa cells were seeded on 10 mm cover slips in 12-well plates in the respective densities (1.25 x 10^5 cells per well) for each experiment one day before transfection. The plasmid DNA was diluted in TE buffer (20 mM Tris, pH 8.8, 1 mM EDTA) to receive a concentration of 0.1 µg/µl. Per sample a total of 0.5 µg plasmid DNA (0.25 µg each in a double transfection) and 100 µl jetOPTIMUS® buffer were mixed, vortexed and spun down. To the mixture 0.5 µl jetOPTIMUS® reagent was added, vortexed, spun down and incubated for 10 min at room temperature. After the incubation, the transfection mix was added to the cells. The cells were incubated with the transfection solution at 37°C, 5% CO2 for at least 24 hours to allow an efficient protein production.

2.8 Western blotting (according to (T. Welz))

2.8.1 Sodium dodecyl sulfate polyacrylamide gel electrophoresis (SDS PAGE)

Protein preparations were mixed with SDS protein sample buffer (Laemmli buffer, composition in the supplement) and denatured at 95°C for 10 min. Proteins were separated on SDS polyacrylamide gels with respective concentrations (depending on the molecular weight of the proteins to be separated, between 7.5% and 15%) at 50 mA per gel in 1x SDS running buffer (250 mM Tris, 1.9 M glycine, 1% SDS). To obtain even separations for each lane, every lane was filled with the same volume of protein sample; in case of empty lanes, they were filled with the same volume of sample buffer. The Precision Plus Protein Standard (Dual Color; Bio-Rad, Munich, Germany) was used as a molecular weight marker.

2.8.2 Western blotting – protein transfer

Proteins were transferred from SDS gels to nitrocellulose membranes (Protran Nitrocellulose Transfer Membrane, 0.45 µm pore size; GE Healthcare Life Sciences) by using the Mini Trans-Blot Cell system (Bio-Rad) in 1x transfer buffer (25 mM Tris, 192 mM glycine, 20% methanol). Smaller proteins were typically transferred at 150 mA, room temperature for 2 h. Directly after the protein transfer, proteins were visualised by Ponceau S staining to check for equal loading of all lanes and showing the GST proteins in the pulldown assays. Unspecific antibody binding sites were blocked with 5% milk powder solution in 1x PBS, 0.05% Tween buffer (PBS-T) at room temperature for 1 h. After blocking, the blots were incubated with primary and secondary antibodies, and protein bands were visualised by chemiluminescence detection as described below.

2.8.3 Western blotting – Ponceau S staining

Ponceau S staining was performed to show the transfer efficiency of the Western blot and the loading of the GST-proteins. Membranes were incubated for 5 min in Ponceau S staining solution (5 % acetic acid, 0.1% Ponceau S) at room temperature and washed with deionised water to get clear bands without background. For complete destaining the membrane was washed in 1x PBST after taking a picture.

2.8.4 Western blotting – antibody treatment

After blocking with 5% milk powder solution, the membrane was incubated with the primary antibody according to concentration provided by the manufacturer, see chart below. To get rid of residual antibody solution, blots were washed three times in 1x PBST. Afterwards, the blot was incubated with the secondary antibody, coupled to HRP (horse-radish-peroxidase), according to the antibody protocols (2.8.5). To get rid of residual antibody solution, blots were washed three times in 1x PBST. Protein bands were visualised by chemiluminescence signals (Luminata Forte Western HRP Substrate; Merck Millipore, Darmstadt, Germany). The signal was detected with an ImageQuant LAS 4000 Lumineszent Image Analyser (GE Healthcare Life Sciences). Western blot images were processed using Adobe Photoshop and assembled in Adobe Illustrator.

2.8.5 Antibody protocols

Primary antibody	**Concentration and blocking solution**	**Incubation conditions**
Living Colors® Full-length GFP Polyclonal Antibody (Anti-GFP, rabbit ; Takara/Clontech, Saint-Germain-en-Laye, France)	1:100; 5% milk ≙ 1 µg/ml	oN, 4°C
Penta-His™ Antibody, BSA-free (QIAGEN)	1:1000; 5% milk ≙ 0.5 µg/ml;	oN, 4°C

Secondary antibody	Concentration and blocking solution	Incubation conditions
Donkey anti-rabbit, HRP-linked (GE Healthcare Life Sciences)	1:5000; 1.6% milk	1 h, RT
Sheep anti-mouse, HRP-linked (GE Healthcare Life Sciences)	1:5000; 1.6% milk	1 h, RT

2.9 Production and purification of recombinant proteins in *E.coli* bacteria

2.9.1 Purification of GST-NTEV-Hs-MYO5A/B/C-GTD (according to (T. Welz))

The bacterial expression vector pGEX-4T1-NTEV-Hs-MYO5A/B/C-GTD were expressed in *E. coli* Rosetta bacteria (Novagen). 20 ml of an overnight culture (37°C) was used to inoculate 1 l LB_0 medium (1:50), supplemented with 100 mg/l ampicillin, 34 mg/l chloramphenicol in an Erlenmeyer flask with chicanes. The bacteria were grown at 37°C while shaking (150 rpm) until an optical density at a wavelength of 600nm and a light path OD_{600} of around 0.8. When the suitable OD_{600} was reached the protein expression was induced by 0.2mM IPTG (Isopropyl-β-D-thiogalactopyranosid), and continued at 20°C for 18–20 h. Before and after induction a 1 ml sample was taken to check for protein induction by SDS-PAGE and Coomassie staining. For the Coomassie staining, the SDS-gel was stained for 30 min at 22°C with Coomassie staining solution. Afterwards, the gel was detained with deionised water in multiple steps, by cooking in the microwave, until the bands are visible without background stain. Following protein expression bacteria were harvested by pelleting by centrifugation (4,600 x *g*, 30 min, 4°C) and the bacterial pellet was washed in cold 1x PBST (1x PBS, 0.05% Tween20). Bacteria were pelleted again by centrifugation (4,600 x *g*, 30 min, 4°C), resuspended in 40 ml lysis buffer ((1x PBS, pH 7.8, 2 mM β-Mercaptoethanol, 2 mM $MgCl_2$, 5% glycerol (v/v), 0.05% Tween20), supplemented with 1 mM Phenylmethylsulfonylfluoride (PMSF;Sigma-Aldrich), 2 protease Inhibitor cocktail tablets (complete Mini, EDTA-free; Roche, Penzberg, Germany)) and subsequently lysed by ultra-sonication (6 x 30 sec, 6 cycles, 60% amplitude; Bandelin Sonopuls, HD 2070, Bandelin electronic, UW 2070, Berlin, Germany) on ice. The lysates were centrifuged (75,000 x g, 2 x 30 min, 4°C), after the first centrifugation step the supernatant is transferred to a new centrifugation tube. After the second centrifugation step, the cleared supernatant was incubated with 2 ml glutathione Sepharose 4B (GSH) beads (1:1 suspension) for 2 h at 4°C on a rotating wheel. The beads were pelleted (500 x *g*, 5 min, 4°C) and washed five times in 5 ml wash buffer (1x PBS, pH 7.8; 2 mM β-Mercaptoethanol; 2 mM $MgCl_2$; 5% glycerol (v/v); 0.05% Tween20). Bound proteins were eluted five times from the beads in 1ml elution buffer (20 mM Tris-HCl, pH 7.8, 150 mM NaCl, 2m M β-Mercaptoethanol, 2 mM $MgCl_2$, 5% glycerol (v/v), 20 mM glutathione) for 25 min per elution step. The eluted fractions were concentrated via Amicon 30K

centrifugal filters by centrifugation (4,000 x *g*, 10 min, 4°C) until ~1 ml protein solution is left. The eluted GST and GST-fusion proteins were further purified by fast protein liquid chromatography (FPLC, ÄKTA purifier) employing a 16/60 superdex200 gel filtration column (Cytiva). The concentrated protein solution was transferred in an Eppendorf tube and centrifuged (4,000 x g, 10 min, 4°C). After the centrifugation step the protein was loaded on the ÄKTApurifier (2 ml loop) using a syringe. The column was calibrated using gel filtration buffer (20 mM Tris-HCl, pH 7.8, 150 mM NaCl, 2 mM DTE, 2 mM $MgCl_2$, 5% glycerol (v/v); sterile filtered and de-gassed, 4°C) (1.5 CV(column volume), flow rate: 1 ml/ min). The protein solution was then placed onto the column and separated in gel filtration buffer according to a predetermined procedure (program see page 55; 1.2 CV, flow rate: 1ml/ min). 2-ml portions were automatically collected.

To control the process of the protein purification samples were taken after each step: pre-induction (1 ml), post-induction (1 ml), crude lysate (40 µl), clear lysate (40 µl), supernatant after beads (40 µl) and elution (40 µl) supplemented with Laemmli buffer (SDS sample buffer) and analysed by immunoblotting. The pre-induction sample was taken, right before the induction with 0.2 mM IPTG, 1 ml was taken from the bacterial culture, centrifuged at (11,000 x g, 1 min, 22°C) and resuspended in 50 µl 2x SDS sample buffer, from this solution 4 µl were loaded on the SDS-gel. The post-induction sample was taken, after the induction with 0.2 mM IPTG for 18 – 20 hours before the centrifugation step, 1 ml was taken from the bacterial culture, centrifuged (11,000 x g, 1min, 22°C) and resuspended in 100 µl 2x SDS sample buffer, from this solution 4 µl were loaded on the SDS-gel. The crude lysate sample was taken, after the sonification step, 40 µl were taken from the 40 ml lysate and mixed in 10 µl 5x SDS sample buffer, from this solution 4 µl were loaded on the SDS-gel. The clear lysate sample was taken, after the two high-speed centrifugation steps, 40 µl were taken from the 40 ml clear lysate and mixed with 10 µl 5x SDS sample buffer, from this solution 4 µl were loaded on the SDS-gel. The supernatant after bead incubation sample was taken, after the bead incubation step, 40 µl were taken from the 40 ml clear lysate and mixed with 10 µl 5x SDS sample buffer, from this solution 4 µl were loaded on the SDS-gel. The elution sample was taken, after the elution step from the beads, 40 µl were taken from the 10 ml clear lysate and mixed with 10 µl 5x SDS sample buffer, from this solution 1 µl were loaded on the SDS-gel. The taken samples during the protein purification sample process were denatured at 95°C for 5 min before loading on the 10% SDS gel. The different amounts of the Laemmli buffer are necessary to get a similar amount of protein in the sample and the loaded amounts are different for the same reason. By taking a sample after each step, it is possible to retrace at which step in the purification pipeline, a problem might arise.

Wash buffer **for GST-Hs-MYO5A/B/C-GTD**	- 1x PBS, pH 7.4 - 2 mM β-Mercaptoethanol - 2 mM $MgCl_2$ - 5% (v/v) Glycerol - 0.05% Tween20
Lysis buffer	- add freshly: 1 mM PMSF, complete Mini Protease Inhibitor Cocktail, 0.1% Triton-X100
Elution buffer **for GST-Hs-Myo5A/B/C-GTD**	- 20 mM Tris-HCl, pH 7.4 - 150 mM NaCl - 2 mM β-Mercaptoethanol - 2 mM $MgCl_2$ - 5% Glycerol - 20 mM Glutathion
Gelfiltration buffer **for GST-Hs- Myo5A/B/C-GTD**	- 20 mM Tris-HCl, pH 7.4 - 150 mM NaCl - 2 mM DTE - 2 mM $MgCl_2$ - 5% Glycerol - filter sterile, de-gas, store at 4°C

2.9.2 Purification of His_6-mScarlet-I-Hs-SPIRE1/2-linker (according to (T. Welz))

The bacterial expression vector pProEx-HTb-mScarlet-I-Hs-SPIRE1/2-linker was expressed in E. coli Rosetta bacteria. 20 ml of an overnight culture (37°C) was used to inoculate 1 l LB0 medium (1:50), supplemented with 100 mg/l ampicillin, 34 mg/l chloramphenicol. The bacteria were grown at 37°C until an OD600 was 0.8. Protein expression was induced by 0.2 mM IPTG, and continued at 20°C, 18–20 h. Before and after induction a 1 ml sample was taken for further analysed on a SDS gel. Bacteria were harvested by pelleting by centrifugation (4,600 x g, 30 min, 4°C) and the bacterial pellet was washed in cold 1x PBST (1x PBS, 0.05% Tween20). Bacteria were pelleted again by centrifugation (4,700 x g, 30 min, 4°C), resuspended in 40 mL lysis buffer (20 mM Tris-HCl, pH 8.0, 300 mM NaCl, 20 mM Imidazol, 5 mM β-Mercaptoethanol, supplemented with 1 mM Phenylmethylsulfonylfluoride (PMSF;

Sigma-Aldrich), 2 protease Inhibitor cocktail tablets (complete Mini, EDTA-free; Roche, Penzberg, Germany)), and subsequently lysed by ultra-sonication (6 x 30 sec, 6 cycles, 60% amplitude; Bandelin Sonopuls, HD 2070, Bandelin electronic, UW 2070, Berlin, Germany) on ice. The lysates were centrifuged (75,000 x g, 2 x 30 min, 4°C), and the cleared supernatant was incubated with 2 ml Ni-NTA Agarose beads (1:1 suspension) for 2 h, at 4°C on a rotating wheel. The beads were pelleted (500 x g, 5 min, 4°C) and washed five times in 5 ml wash buffer (20 mM Tris-HCl, pH 8.0, 300 mM NaCl, 20 mM Imidazol, 5 mM β-Mercaptoethanol). Bound proteins were eluted five times from the beads in 1 ml elution buffer (20 mM Tris-HCl, pH 8.0, 300 mM NaCl, 300 mM Imidazol; 5 mM β-Mercaptoethanol) for 25 min per elution step. The eluted fractions were concentrated via Amicon 30K centrifugal filters centrifuged (4,000 x g, 10 min, 4°C) until around 1 ml protein solution is left. The eluted His- mScarlet-I and His-mScarlet-I-fusion proteins were further purified by fast protein liquid chromatography (FPLC, ÄKTA purifier) employing a 16/60 superdex200 gel filtration column (Cytiva, Marlborough, Massachusetts, USA since 2020; before GE Healthcare Life Sciences, Chicago, Illinois, USA).The concentrated protein solution was transferred in an Eppendorf tube and centrifuged (4,000 x g, 10 min, 4°C). After the centrifugation step the protein was loaded on the ÄKTApurifier (2 ml loop) by a syringe. The protocol for the ÄKTA purifier is shown on page 55.

Wash buffer **for His_6-mScarlet-I-SPIRE-1/2-linker** **Lysis buffer**	- 20 mM Tris-HCl, pH 8.0 - 300 mM NaCl - 20 mM Imidazol - 5 mM β-Mercaptoethanol - add freshly: 1 mM PMSF, complete Mini Protease Inhibitor Cocktail, 0.1% Triton-X100
Elution buffer **for His_6-mScarlet-I-SPIRE-1/2-linker**	- 20 mM Tris-HCl, pH 8.0 - 300 mM NaCl - 300 mM Imidazol - 5 mM β-Mercaptoethanol
Gelfiltration buffer **for His_6-mScarlet-I-SPIRE-1/2-linker**	- 2x PBS, pH 7.2 - 10% Glycerol - filter sterile, de-gas, store at 4°C

Method used for Protein Purification using ÄKTA purifier system

```
Method: C:\UNICORN\Local\Fil\default\Method\Purification Protocolls\Sdex1660completerun2.m01

Main method:
¤  (Main)
  0.00  Base  Volume 120.637 {ml} HiLoad_16/60_Superdex_200_prep_grade
  0.00  Flow  0.500 {ml/min}
  0.00  ColumnPosition  Position7
  0.00  Alarm_Pressure  Enabled 0.45 {MPa} 0.00 {MPa}
¤  0.00  Block  Buffer_Equilibration
    (Buffer_Equilibration)
    0.00  Base  SameAsMain
    0.00  End_Block
  0.00  Flow  0.500 {ml/min}
  0.00  InjectionValve  Load
  0.00  PumpAInlet  A1
  0.00  OutletValve  WasteF1
¤  5.00  Block  Sample_Inject
    (Sample_Inject)
    0.00  Base  SameAsMain
    0.00  End_Block
  5.00  InjectionValve  Inject
  5.00  PumpAInlet  A1
  5.00  Flow  0.500 {ml/min}
  5.00  OutletValve  WasteF1
  5.00  AutozeroUV
¤  10  Block  Elution
    (Elution)
    0.00  Base  SameAsMain
    0.00  End_Block
  10.00  InjectionValve  Load
  10.00  OutletValve  F2
  10.00  Flow  0.500 {ml/min}
  10.00  Fractionation  30mm 40.000 {ml} FirstTube Volume
¤  50.00  Block  BlockElution2
    (BlockElution2)
    0.00  Base  SameAsMain
    0.00  End_Block
  50.00  Flow  0.500 {ml/min}
  50.00  InjectionValve  Load
  50.00  PumpAInlet  A1
  50.00  OutletValve  F2
  50.00  Fractionation  18mm 1.500 {ml} FirstTube Volume
¤  135.00  Block  END
    (END)
    0.00  Base  SameAsMain
    0.00  End_Block
```

*Figure 12: **Method of the Protein Purification using ÄKTA purifier system.***

2.9.3 Bradford assay to measure protein concentrations

To determine the concentration of purified proteins the Bradford assay was used. For this, a self-prepared Bradford solution with an initial calibration was used. Coomassie Plus Protein Assay Reagent (ThermoFisher) was mixed 2:1 with de-ionised water. A calibration curve was determined with water alone, Bradford solution alone and Bradford solution supplemented with BSA protein standard rising

from 1 µg/µl up to 15 µg/µl in 1 µg/µl steps. The absorptions were measured at 595 nm and a linear plot of the calibration values was calculated with:

$$y = ax + b$$

For the measurements of protein concentrations, 1 ml calibrated Bradford solution was adjusted to room temperature in a transparent plastic cuvette. Then 1 µl protein solution was added to the Bradford solution, mixed and incubated for 10 min at room temperature, kept in the dark. The absorption of the solution at 595 nm was measured and the mean of three measurements was used to calculate the concentration of the protein solution with:

$$x = (A_{595} - b) / a$$

2.10 GST-pulldown from HEK 293 cell lysates (according to (T. Welz))

HEK 293 cells were seeded on poly-L-lysine coated 6-well plates ($8x10^5$ cells per well) as described previously, one day before transfection. HEK 293 cells were transfected with expression vectors encoding pAcGFP1-C1, pAcGFP1-C1-Hs-SPIRE1-fl, pAcGFP1-C1-Hs-SPIRE2-fl, pAcGFP1-C1-Hs-SPIRE1-ΔKW and pAcGFP1-C1-Hs-SPIRE2-ΔKW, as described previously, in triplicates (the cells of three wells were subsequently pooled and treated as one sample). 24 hours post transfection, the cells were washed two times with 1x PBS to remove residual medium and serum. The cells were scraped off the wells using 333 µl lysis buffer (25 mM Tris-HCl pH 7.4, 150 mM NaCl, 5 mM $MgCl_2$, 10% (v/v) glycerol, 0.1% (v/v) Nonidet P-40, 1 mM PMSF, protease inhibitor cocktail (complete Mini, EDTA-free; Roche, Penzberg, Germany)) per well. The cells of three wells were pooled per sample and cells were lysed for about 40 min on a rotating wheel at 4°C. After lysis, the cell lysates were centrifuged (20.000 x g, 20 min, 4°C), to remove the insoluble debris. In the meantime, respective amounts of GSH-Sepharose 4B beads were washed three times; two times in lysis buffer and once in pulldown buffer (25 mM Tris-HCl pH 7.4, 150 mM NaCl, 5 mM $MgCl_2$, 10% (v/v) glycerol, 0.1% (v/v) Nonidet P-40). A 1:1 suspension of beads and pulldown buffer was prepared for further use. The cleared supernatant of the cell lysates was pre-incubated with 20 µl GSH-Sepharose 4B beads for 1 h, on a rotating wheel at 4°C to get rid of proteins with unspecific binding to the beads. 40 µl of the cleared supernatant were mixed with 5x Laemmli buffer and used as cleared lysates in Western blots to control for protein expression levels. For GST-pulldown assays, 50 µg GST-Hs-MYO5A, B, C-GTD proteins and 50 µg GST protein as a control, was coupled to 40 µl GSH-Sepharose 4B beads (1:1 suspension) in 500 µl pulldown buffer for 1 h on a rotating wheel at 4°C. The beads were pelleted by centrifugation (500 x g, 2 min, 4°C) and washed two times with pulldown buffer (500 µl each) by pelleting the beads each time (500 x g, 2 min, 4°C). After

the washing steps, the beads were pelleted again and any residual fluid was removed completely. The beads from the pre-incubation step were pelleted (500 x g, 4 min, 4°C) and the supernatant (cleared cell lysates) were transferred to the GST-protein coupled GSH-Sepharose 4B beads and incubated for 2 h on a rotating wheel at 4°C. The beads were pelleted (500 x g, 2 min, 4°C) and washed four times with pulldown buffer (500 µl each). After the washing steps the beads were pelleted finally by centrifugation (500 x g, 2 min, 4°C) and any residual fluid was removed completely with care. The bound proteins were eluted using 40 µl 1x Laemmli buffer and denatured for 10 min at 95°C. Potential protein interactions in pulldowns and the protein expression in cleared lysates were analysed by immunoblotting using appropriate antibodies.

2.11 GST-pulldown experiments with purified proteins (according to (T. Welz))

Appropriate amounts of GSH-Sepharose 4B beads were washed three times in pulldown buffer (25 mM Tris-HCl pH 7.4, 150 mM NaCl, 5 mM $MgCl_2$, 10% (v/v) glycerol, 0.1% (v/v) Nonidet P-40) and a 1:1 suspension of beads and the pulldown buffer was prepared for subsequent use. 50 µg GST-fusion proteins were coupled to 40 µl GSH-Sepharose 4B beads (1:1 suspension) in 500 µl pulldown buffer for 1 h on a rotating wheel at 4°C. After the coupling the beads were pelleted by centrifugation (500 x g, 2 min, 4°C) and washed two times with pulldown buffer (500 µl each) by pelleting the beads each time (500 x g, 2 min, 4°C). After the washing steps, the beads were pelleted again to remove any residual fluid completely. GST-protein coupled beads were incubated with 20 µg His_6-mScarlet-I-fusion proteins in 1 ml pulldown buffer for 2 h on a rotating wheel at 4°C. After the incubation the beads were pelleted (500 x g, 2 min, 4°C) and washed four times with pulldown buffer (500 µl each). After the washing steps, the beads were pelleted again and any residual fluid was removed completely with care. The bound proteins were eluted using 20 µl 1x Laemmli buffer and denatured for 10 min at 95°C. Potential proteins interactions in pulldown assays were analysed by immunoblotting using appropriate antibodies. For each protein different protein purifications steps were used to exclude “results depending on bad protein purifications”.

2.12 Supernatant depletion assay in a quantitative manner (according to (Pollard, 2010; Pylypenko et al., 2016))

The GST-pulldown assays were performed as described previously (see GST-pulldown experiments with purified proteins (according to (T. Welz)). Increasing amounts of GST-MYO5A/B/C-GTD fusion proteins were coupled to 40 µl GSH-Sepharose 4B beads (1:1 suspension) in 500 µl pulldown buffer for 1 h, at 4°C on a rotating wheel. Beads were pelleted by centrifugation (500 x *g*, 2 min, 4°C) and washed

two times with pulldown buffer, 500 µl per washing step, by pelleting beads each time (500 x *g*, 2 min, 4°C). Beads were pelleted again and any residual fluid was removed completely. GST-protein coupled beads were incubated with 100 nM His_6-mScarlet-I-Hs-SPIRE-1/2-linker peptide in SPECS buffer (1x PBS pH 7.2, 50 mM NaCl) for 2 h, at 4°C on a rotating wheel. Beads were pelleted by centrifugation (500 x *g*, 5 min, 4°C) and the supernatant was transferred into a new tube. The supernatant was centrifuged (20,000 x *g,* 10 min*,* 4°C) to remove potential debris that could disturb fluorescence measurements.
Each protein sample was allowed to adapt to room temperature for 20 min on the bench. The concentration dependent binding of GST-MYO5A/B/C-GTD to the His_6-mScarlet-I-Hs-SPIRE-1/2-linker was determined by fluorospectrometric analysis using the Varioskan™ LUX multimode microplate reader (Thermo Scientific™, Germany). The fluorescence measurements were performed in black 96 well plates, these absorb light and reduce background and crosstalk. During the measurement, the light was applied from above with an exposure time of 100 ms, a measurement protocol is shown in the supplement. The temperature for the incubation in the device was 22.9°C for 5 min, followed by a shaking step for 10 sec. The samples were measured as triplicates. The volume in the wells was 200 µl. The mScarlet-I red fluorescent protein was excited at 569 nm and the emission at 594 nm was recorded (excitation and emission maxima of mScarlet-I). The data were calculated as “fraction bound” compared to the fluorescence signals of His_6-mScarlet-I-Hs-SPIRE-1/2-linker alone, without any GST-MYO5-GTD protein (0 nM sample):

$$y = \frac{y_0 - y_c}{y_0}$$

With y_0 is the fluorescence signal of His_6-mScarlet-I-Hs-SPIRE-1/2-linker alone, without GST-MYO5-GTD and y_c is the signal at the respective GST-MYO5-GTD concentration.

Steps Data		
Protocol properties		
	Protocol name	QuantPD_MYO5A_SPIRE_triplett_8000nM
	Protocol description	
	Plate template	96-well BD Falcon, 370 ul, black plate
	Execution block type	plate
	Execution order	7
	Settle delay [ms]	0
	Well interval [ms]	0
Incubate1		
	Incubation time	0:05:00.0
	Temperature [°C]	22
	Wait	Wait until instrument has reached the target temperature
	Leave temperature	No
Shake1		
	Step duration	0:00:10.0
	ON time	0:00:00.0
	OFF time	0:00:00.0
	Speed [rpm]	600
	Diameter [mm]	1
	Shaking mode	End with ON time
Fluorometric1		
	Measurement technology	Fluorometric
	Optics	Top
	Measurement type	Normal
	Step duration	0:00:00.0
	Lag time	0:00:00.0
	Measurement time [ms]	100
	Bandwidth [nm]	5
	Dynamic range	Automatic
	Multipoint	Not in use
	Excitation [nm]	569
	Emission [nm]	593
BasicStatistics1		
	Statistics type	Combine replicates without dilution factors
BlankSubtraction1		
	Blank Type	average

*Figure 13: **Fluorometric measurement protocol and black 96 well plate layout** , shown for MYO5B-GTD/SPIRE2-linker.*

The data were further processed in SigmaPlot 11.0 software (Systat Software, Erkrath, Germany) and the equilibrium binding data were fitted according to the equation:

$$y = \frac{B_{max} * x}{K_d + x}$$

assuming a single binding site, and with $B_{\max}$ representing the maximal amplitude (maximal binding amplitude), K_d representing the equilibrium binding constant, and x representing the concentration of GST-MYO5-GTD. The binding curves saturated at 40% since the His_6-mScarlet-I-Hs-SPIRE-1/2-linker protein preparation contained C-terminal incomplete protein products, which are still fluorescent but cannot interact with MYO5-GTD. The SPIRE-1/2-linker region is predicted to be highly unstructured,

which may be the reason for the relative instability of the recombinant His_6-mScarlet-I-Hs-SPIRE-1/2-linker fusion protein, which complicated the quantitative measurement.

2.13 Cell fixation and labelling of intracellular structures: Immunostaining and fluorescence microscopy (according to (T. Welz))

HeLa cells were seeded in 12-well plates (1.25 x 10^5) on microscope cover glasses and on the next day transfected with the indicated expression vectors encoding fluorescently tagged proteins, as described above. Therefore, one day after transfection, cells were washed three times with 1x PBS (1 mL each) to remove residual medium and serum and fixed for 20 min at 4°C with 300 µl PFA (paraformaldehyde; 3.7% stock in 1x PBS; -20°C) per well. After fixation the PFA was removed and the cells were washed again three times with 1x PBS (1 ml each). Afterwards the cells were treated with 300 µl 0.2% Triton-X100 (in 1x PBS) per well at RT for 3.5 min for cell membrane permeabilisation. The Triton-X100 was removed and the cells were washed again three times with 1x PBS (1 ml each). The cover glasses were placed in the middle of the 12 well dish and any residual fluid was removed. For actin filament staining with phalloidin 670-Stain (Acti-stain™ 670, Cytoskeleton, Inc.). 0.7 µl of the phalloidin 670-Stain were centrifuged for at least 10 min at 13,000 x g in an Eppendorf tube (open lid) until the MetOH was evaporated, then resuspended in 0.5 µl fetal calf serum (FCSIII) and 49.5 µl 1x PBS and carefully pipetted on the cells to incubate at room temperature for 20 min in the dark. In parallel, the cell nucleus can be stained using 4',6-diamino-2-phenylindol (DAPI). Per well 0.05 µl DAPI stock solution and 50 µl of 1x PBS containing 1% FCS was carefully pipetted on the cells to incubate for 20 min at room temperature in the dark. If Phallodin and DAPI staining is performed at the same time on the cells, both reagents can be added together, therefore for one cover slip the Acti-stain was prepared as described above, then resuspended in 50 µl of 1x PBS containing 1% FCS, applying 50 µl of the staining solution per cover slip. During incubation, the mowiol solution (composition in the supplement Table 14) needs to be thawed and the object slides can be labelled. After incubation, the staining solution was also diluted in 1x PBS and then washed three times with 1x PBS (1 ml each). After the last washing step, each well was filled with 1 ml water and the coverslip was transferred with the cells upside down in 10 µl mowiol to the object slide, pressed carefully to prevent air bubbles. After the mowiol has hardened, the fixed cells were analysed were imaged using a Leica AF6000LX fluorescence microscope (Leica Microsystems, Wetzlar, Germany), outfitted with a Leica DFC350 FX digital camera (12-bit monochrom, 1.4 MPixel, 1392 x 1040 pixels, 6.45 x 6.45 µm pixel size) and a Leica HCX PL APO 63x/1.3 GLYC objective. 3D stacks were captured and processed using the LASX software module for Leica deconvolution. Leica software LASX was used to record the images. The images were then processed with Adobe Photoshop and assembled with Adobe Illustrator.

2.14 Colocalisation analysis

The extent of colocalisation of mScarlet-I-Hs-SPIRE-1/2-ΔKW and AcGFP1-C1-Hs-MYO5A/B/C-cc-GTD was analysed using the ImageJ (V2.0.0) plug-in Coloc2 (Pompey et al., 2013). Here, the colocalisation rate for signals of individual fluorescence channels within one image was indicated by the Pearson's Correlation Coefficient (PCC) (Costes et al., 2004) as a standard statistical measure to unravel a linear correlation between the intensity of different fluorescent signals. A PCC value of 1 indicates a perfect colocalisation (perfect positive correlation of signals), 0 indicates a random colocalisation (no correlation) and a PCC value of -1 indicates a mutually exclusive localisation (perfect negative correlation) of the analysed signals. To take the noise of each image into account and to gain an objective evaluation of PCC significance, a Costes significance test was performed (Costes et al., 2004). To do so, the pixels in one image were scrambled randomly and the correlation with the other (unscrambled) image was measured. PCC significance was observed when at least 95% of the randomised images show a PCC less than that of the original image, meaning that the probability for the measured correlation of two colours is significantly greater than the correlation of random overlap (Costes et al., 2004; Pompey et al., 2013).

2.15 RNA sequence analysis

RNA sequencing (RNA-seq) is a cutting-edge approach for measuring gene expression (mRNA abundance) and conducting differential gene expression analyses at high resolution using next-generation sequencing (NGS). A variety of factors affect gene quantification in RNA-seq, including sequencing depth, gene (transcript) length, RNA composition, and sample-to-sample variability. The data of the RNA sequencing were taken from the NCBI-Gene-Database (www.ncbi.nlm.nih.gov/gene/). The following genes were analysed for Homo sapiens: SPIRE1 (NP_064533.3; NM_020148.3), SPIRE2 (CAD19439.1; AJ422077.1), MYO5A (XM_011521607.1; XP_011519909.1), MYO5B (NM_001080467.2; NP_001073936.1), MYO5C (NP_061198; NM_018728.4), FMN1 (AAI07594.1) and FMN2 (AAI12336.1). The data are represented here in RPKM (reads per kilo base of transcript per million mapped reads) in a bar diagram for five different tissues: brain, colon, skin, small intestine and thyroid, because these tissues were mostly related to the content of this thesis.

3 Results

Different interactions and roles of the interaction of SPIRE and MYO5 were observed in the last years of investigation (Alzahofi et al., 2020; Holthenrich et al., 2022; Pylypenko et al., 2016; Schuh, 2011; Tittel et al., 2015). In the van Willebrand factor release in endothelial cells, at the Weibel-Palade bodies (WPB) SPIRE1 interacts with MYO5C, but SPIRE2 does not localise with Weibel-Palade bodies (Holthenrich et al., 2022). In melanosomes, SPIRE1 interacts with MYO5A and leads to melanosome dispersion, but SPIRE2 leads to hyperdispersion of the melanocytes (Alzahofi et al., 2020). Therefore, the analysis of the interaction of SPIRE1/2 and MYO5A/B/C in a qualitative and quantitative manner using GST-pulldown assays is the core of this thesis.

To get a first impression over the observed differences in SPIRE1/2 and MYO5A/B/C interaction, the expression of selected genes in different tissues were analysed. The existence of a database of *in silico* data of many genes raises the possibility to compare the expression of genes of the SPIRE complex. Therefore, the human genes of the three isoforms of *MYO5A/B/C*, of *SPIRE1/2* and *FMN1/2* were chosen, because they were already described as parts of a SPIRE complex (Alzahofi et al., 2020; Holthenrich et al., 2022; Pfender et al., 2011; Pylypenko et al., 2016; Schuh, 2011; Tittel et al., 2015). The chosen tissues represent the tissues where the complexes function skin for the melanosome transport (Alzahofi et al., 2020), ovary for the oocytic vesicle movement (Schuh, 2011; Tittel et al., 2015), thyroid for the vWF release (Holthenrich et al., 2022) and the small intestine because the cause of MVID is a mutation in MYO5B (Müller et al., 2008) and the pancreas is coupled to insulin production in ß-cells .

3.1 RNA expression analysis

The RNA-sequencing (RNA-seq) data are the new gene expression microarrays used for transcriptome profiling (S. Zhao et al., 2020; Y. Zhao et al., 2021). The in silico RNA sequence (RNA seq) analysis is based on collected data on the RNA expression pattern in different tissues. For this database, the data are measured in RPKM, this stands for “reads per kilo base of transcript per million mapped reads”. RPKM is a normalised expression unit, this unit is necessary, because raw counts are not comparable between samples or conditions, because longer transcripts have more reads compared to shorter transcripts with a similar expression level (S. Zhao et al., 2020). Therefore, a database with collected RNA expression pattern exists, which can be used for *in silico* RNA seq.

For the *in silico* analysis of the relative RNA expression of different genes in six different tissues, the used RNA sequence data are from the NCBI gene database to compare the expression patterns. The

six tissues were chosen, because they represent the nearest the tissues where the investigated may have a cell biological function. The expression of *SPIRE1*, *SPIRE2*, *MYO5A*, *MYO5B* and *MYO5C* genes in small intestine, skin (melanocytes), thyroid (endothelial cells), brain, ovary and pancreas were investigated. In addition, we also investigated the expression of the genes of SPIRE interacting FMN1/2 proteins. Within the compared tissues, the RNA expression of eleven genes in six different tissues was analysed using the NCBI-gene database, the gene was searched and the RPKM and the depending standard error of mean was used to create a graph for further analysis. The investigated genes were *MYO5A*, *MYO5B*, *MYO5C*, *SPIRE1*, *SPIRE2*, *FMN1* and *FMN2* in brain, skin, small intestine, thyroid, ovary and pancreas (Figure 14). The RNA expression in the different tissues were expected because the i.e. *SPIRE1* and *SPIRE2* were shown to be expressed in different tissues (Pleiser et al., 2010; Schumacher et al., 2004). The expression of *SPIRE1* is highest in brain and the thyroid, lower in small intestine and skin. *MYO5A* expression is highest in the brain and the small intestine; in the other five tissues, it is lower. The expression of *MYO5B* is high in small intestine and the thyroid. The high expression of *MYO5B* in the intestinal tract is not surprising because the problem of the known microvillus inclusion disease (MVID) is an atypical microvillus phenotype caused by a *MYO5B* mutation (Müller et al., 2008). The expression of *MYO5C* is high in the small intestine, thyroid and the pancreas, as expected in endothelial cells. In some cases, the expression pattern in the observed tissue is higher or lower than expected, but the data on the RNA expression is for the whole tissue and possibly the expression differs in the single cells.

In the following, each tissue is represented on its own with the nine RNA expression levels.

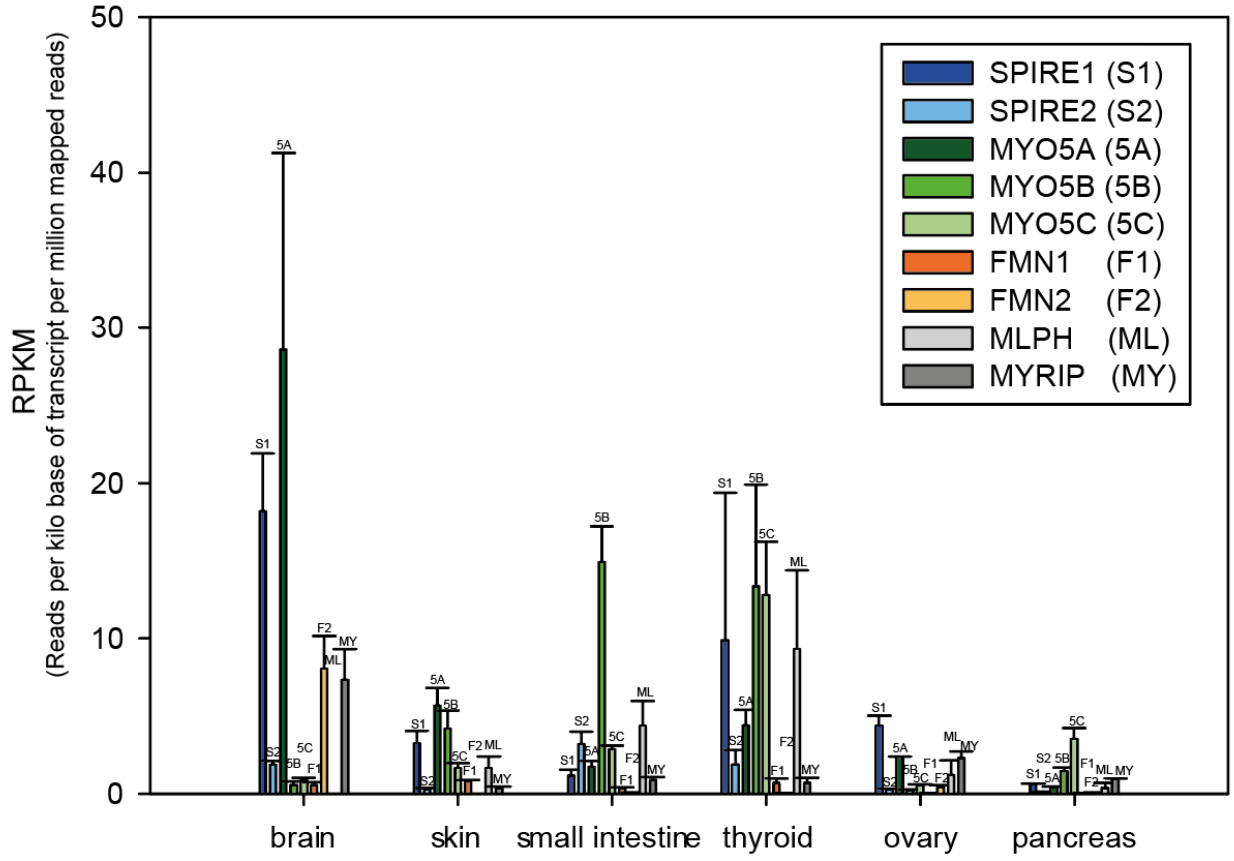

*Figure 14: **RNA expression of SPIRE1, SPIRE2, MYO5A, MYO5B, MYO5C, FMN1, FMN2, MLPH and MYRIP** in six different tissues: brain, skin, small intestine, thyroid, ovary and pancreas in humans. Error bars represent SEM. Data from the in silico RNA-seq data base from the NCBI. The single graphs of the different tissues are shown in the supplement (Figure 34).*

In the brain *SPIRE1*, *MYO5A*, *FMN2* and *MYRIP* are expressed at high levels. These proteins are also known to be involved in learning and memory formation processes in neuronal networks. *FMN2* is also expressed in higher levels than the other analysed RNAs. *FMN2* mutants are described in cases of human intellectual disability.

In the skin *SPIRE1*, *MYO5A* and *MYO5B* are expressed at the highest level. *MYO5A* is expressed higher than *MYO5B* and *MYO5C*; *MYO5A* is expressed the highest, this expression pattern was expected because *MYO5A* for example functions in the melanosome transport, so *MLPH* is also expressed in the skin.

In the small intestine, *MYO5B* is expressed at high levels. *MYO5B* functions together within oocyte maturation with *SPIRE1* and *RAB11A* (Pfender et al., 2011; Schuh, 2011; Tobias Welz et al., 2014; Welz and Kerkhoff, 2023), the RNA expression of *SPIRE1* and *MLPH* is at higher levels. Mutations in *MYO5B* refers to a microvilli inclusion disease (MVID) (Bowman et al., 2022; Hess et al., 2021; Müller et al., 2008; Vogel et al., 2016).

In the thyroid *SPIRE1*, *MYO5B*, *MYO5C*, *MYO5A* and *MLPH* are expressed at high levels. *SPIRE1*, *MYO5B* and *RAB11A* build a known tripartite complex involved in the asymmetric oocyte division: the asymmetric positioning of the metaphase spindle and polar body extrusion (Pfender et al., 2011; Welz, Kerkhoff, 2023).

In the ovary, *SPIRE1*, *MYO5A, MLPH* and *MYRIP* are expressed at high levels. *MYO5A* and *SPIRE1* interact in the asymmetric oocyte division with *RAB11A*, so the high RNA expressions were expected (Pfender et al., 2011).

In the pancreas *SPIRE1*, *MYO5A*, *MYO5B, MYO5C* and *MYRIP* are expressed at high levels. There the ß-cells secret the insulin to regulate the blood sugar together with glucagon. The high expression level of *MYO5C* was expected.

In summary, in the brain *SPIRE1*, *MYO5A, FMN2* and *MYRIP* are expressed the highest, in the skin these are *SPIRE1*, *MYO5A* and FMN1, in the small intestine *SPIRE2*, *MYO5B* and *FMN1* and in the thyroid *SPIRE1*, *MYO5B/C* and *FMN1*. In the ovary *SPIRE1* and *MYO5A* and in the pancreas *SPIRE1*, *MYO5B* and *MYO5C* are expressed at highest levels.

3.2 Constructs used in this thesis

In order to characterise and analyse the interaction of the myosin motor protein myosin 5 and the actin nucleation factor SPIRE the following eukaryotic expression vectors encoding a fluorescent-tagged proteins MYO5A, MYO5B, MYO5C, SPIRE1 and SPIRE2, full length and mutants were produced. Additionally prokaryotic expression vectors encoding Glutathione-S-transferase (GST) or His_6-mScarlet-I tagged and untagged MYO5A, MYO5B, MYO5C, SPIRE1, SPIRE2 proteins were generated. For a better understanding throughout the results part, all proteins and protein fragments are presented in Figure 15; Figure 16 and Figure 17. In the supplements a detailed list of all the expression vectors, including information about vector backbone, amino acid boundaries, restriction sites used for cloning, respective sites, the method of protein purification and the purpose of each plasmid (Table 10; Table 11).

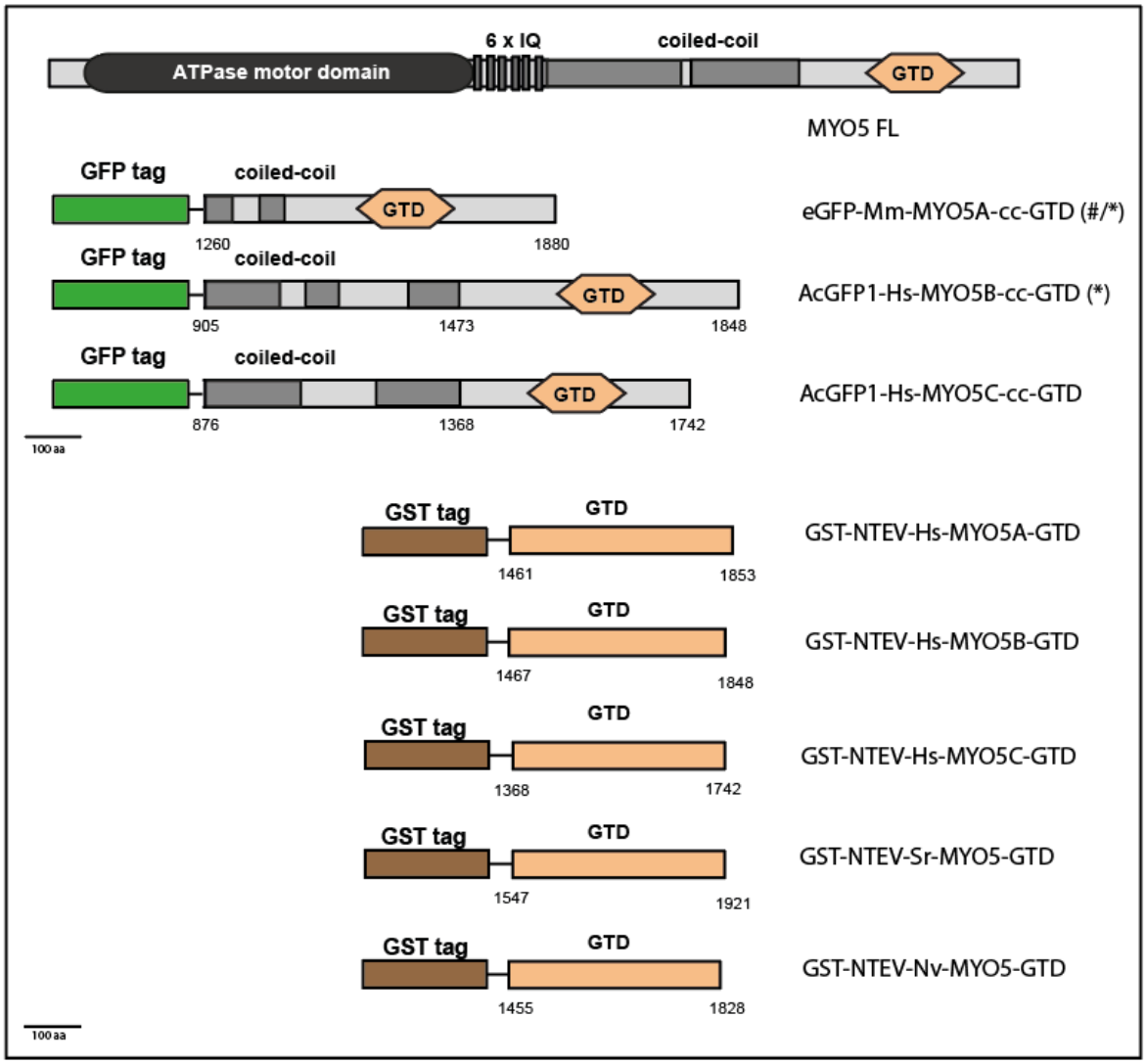

*Figure 15: **Overview on mammalian myosin 5A, myosin 5B and myosin 5C protein fragments used in this thesis**. Numbers indicate amino acids. (#) This expression vector was generated and kindly provided by the lab of Alistair Hume, University of Nottingham, UK. (*) These expression vectors already existed in the lab of Eugen Kerkhoff. eGFP-mm-MYO5A-cc-GTD and AcGFP1-Hs-MYO5B/C-cc-GTD in the following GFP-mm/Hs-MYO5A/B/C-cc-GTD; cc, coiled-coil; GTD, globular tail domain; Hs, Homo sapiens; Sr, Salpingoeca rosetta; Nv, Nematostella vectensis; aa, amino acid; FL, full length.*

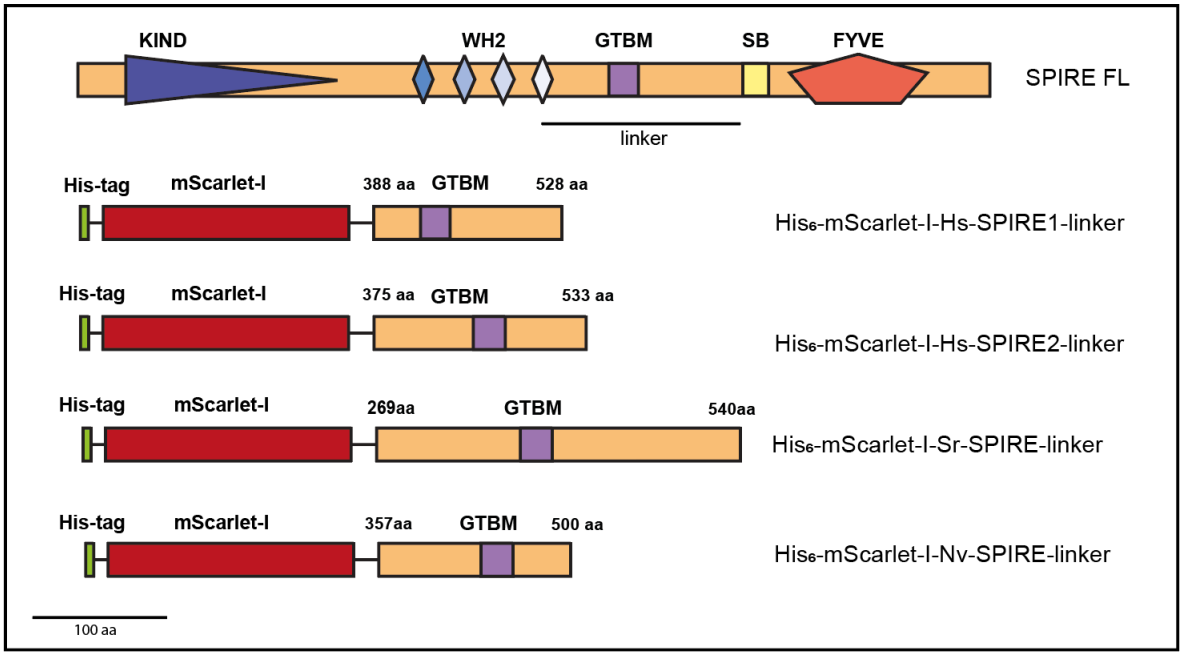

*Figure 16: **Overview on SPIRE1/2-linker, Sr-SPIRE-linker, Nv-SPIRE-linker protein fragments used in this thesis**. Numbers indicate amino acids. GTBM, globular tail binding domain; Hs, Homo sapiens; Sr, Salpingoeca rosetta; Nv, Nematostella vectensis; aa, amino acid.*

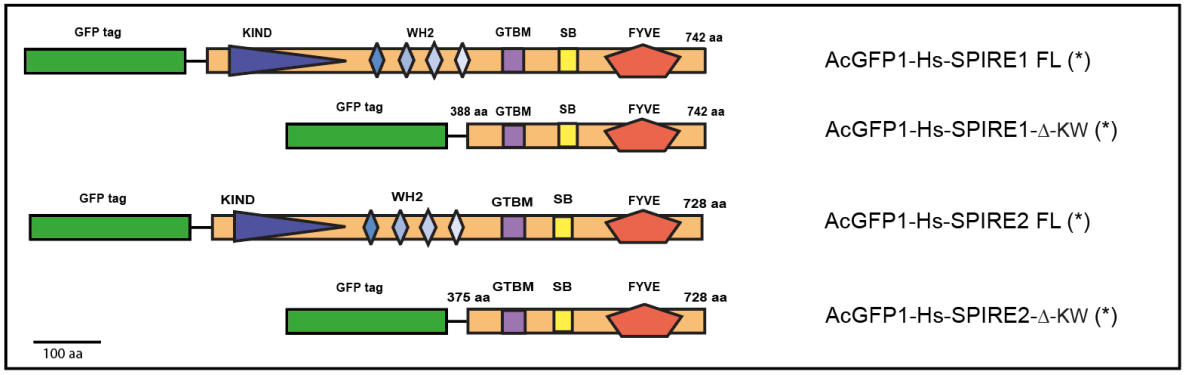

*Figure 17: **Overview on SPIRE1/2 protein fragments used in this thesis**. These constructs were used for the GST-pulldown assays from HEK 293 lysates. Number indicate amino acids. (*) The expression vectors already existed in the lab of Eugen Kerkhoff. GTBM, globular tail domain; SB, SPIRE-box; FL, full-length; ΔKW, deletion of KIND-/ and WH2-domain; aa, amino acid.*

The sequence correctness of the cloned vectors were confirmed by DNA sequencing (LGC Genomic Biosearch Technologies) and the correct expression of the purified GST-Hs-MYO5A/B/C-GTD, GST-Sr/Nv-MYO5-GTD, His_6-mScarlet-I-Hs-SPIRE1/2-linker, His_6-mScarlet-I-Sr/Nv-SPIRE-linker proteins were confirmed by mass spectrometry analysis. This analysis was done by the group of the Mass Spectrometry facility of Dr. Astrid Bruckmann at the Institute of Biochemistry I of the working group of Prof. Meister at the University of Regensburg.

3.3 Protein purification for protein interaction studies

For the protein interaction studies, namely the qualitative and quantitative GST-pulldown assays, the proteins were purified to have the pure protein after the bacterial expression process. An example of an overview of the two-step protein purification using GSH-beads via GST affinity, followed by a size exclusion chromatography using an ÄKTA purifier system is shown for GST-NTEV-Hs-MYO5B-GTD (Figure 18). After each step a sample ranging from 40 µl up to 1 ml was taken and mixed with 2x / 5x SDS sample buffer, denatured and analysed by gel electrophoresis using SDS-PAGE. This method is commonly used for protein analysis; the proteins are separated depending on their size.

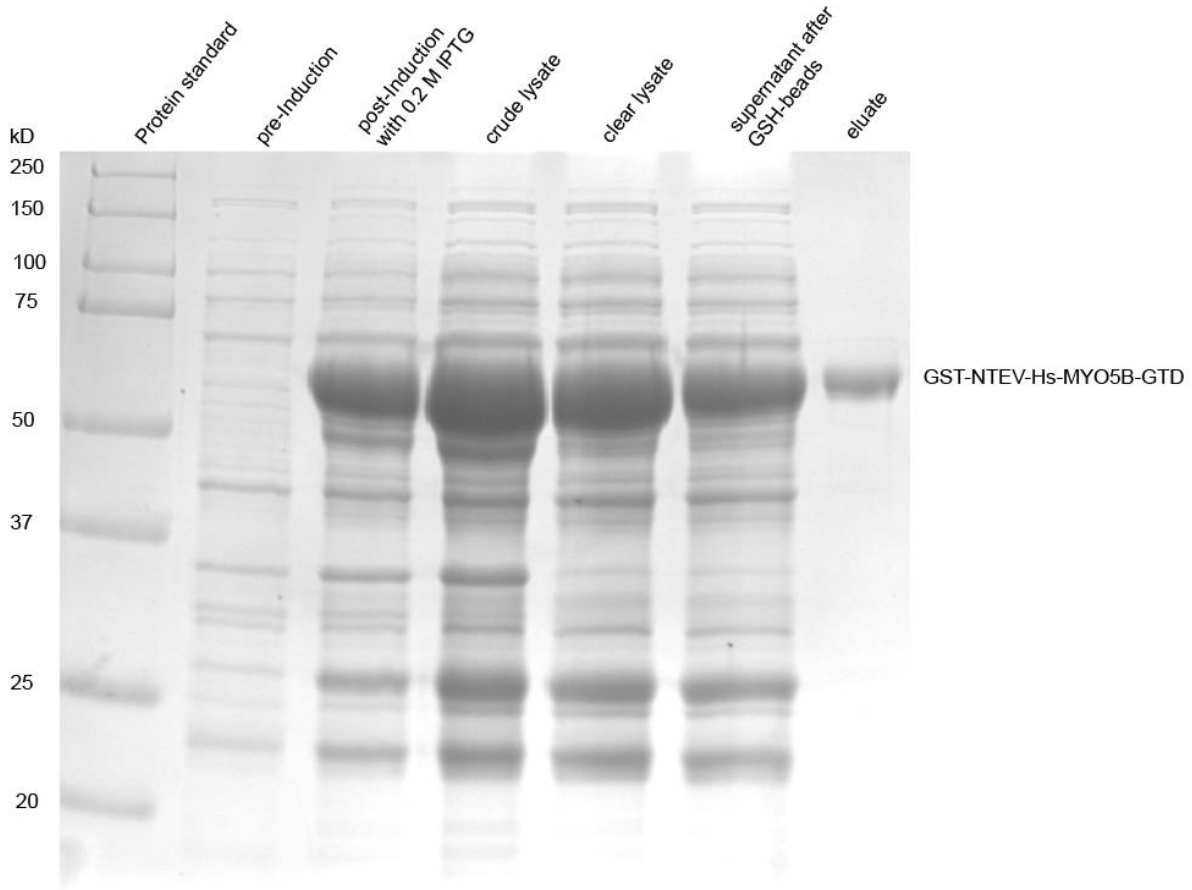

Figure 18: ***Protein purification steps of GST-NTEV-Hs-MYO5B-GTD****. Pre-Induction, post-Induction, crude lysate, clear lysate, supernatant after GSH-beads each 4 µl loaded and eluate loaded 1 µl. To control the process of the protein purification samples were taken after each step: pre-induction (1 ml), post-induction (1 ml), crude lysate (40 µl), clear lysate (40 µl), supernatant after beads (40 µl) and elution (40 µl) supplemented with Laemmli buffer (SDS sample buffer) and analysed by immunoblotting. The pre-induction sample was taken, right before the induction with 0.2 mM IPTG, 1 ml was taken from the bacterial culture, centrifuged at 11,000 x g and resuspended in 50 µl 2x SDS sample buffer, from this solution 4 µl were loaded on the SDS-gel. The post-induction sample was taken, after the induction with 0.2 mM IPTG for 18 – 20 hours before the centrifugation step, 1 ml was taken from the bacterial culture, centrifuged at 11,000 x g and resuspended in 100 µl 2x SDS sample buffer, from this solution 4 µl were loaded on the SDS-gel. The crude lysate sample was taken, after the sonification step, 40 µl were taken from the 40 ml lysate and mixed in 10 µl 5x SDS sample buffer, from this solution 4 µl were loaded on the SDS-gel. The clear lysate sample was taken, after the two high-speed centrifugation steps, 40 µl were taken from the 40 ml clear lysate and mixed with 10 µl 5x SDS sample buffer, from this solution 4 µl were loaded on the SDS-gel. The supernatant after bead incubation sample was taken, after the bead incubation step, 40 µl were taken from the 40 ml clear lysate and mixed with 10 µl 5x SDS sample buffer, from this solution 4 µl were loaded on the SDS-gel. The elution sample was taken, after the elution step from the beads, 40 µl were taken from the 10 ml clear lysate and mixed with 10 µl 5x SDS sample buffer, from this solution 1 µl were loaded on the SDS-gel.*

Here an example of a purification profile for His_6-mScarlet-I-Nv-SPIRE-linker is shown (Figure 19). The protocol of the used purification program is shown in the material and method section (page 51).

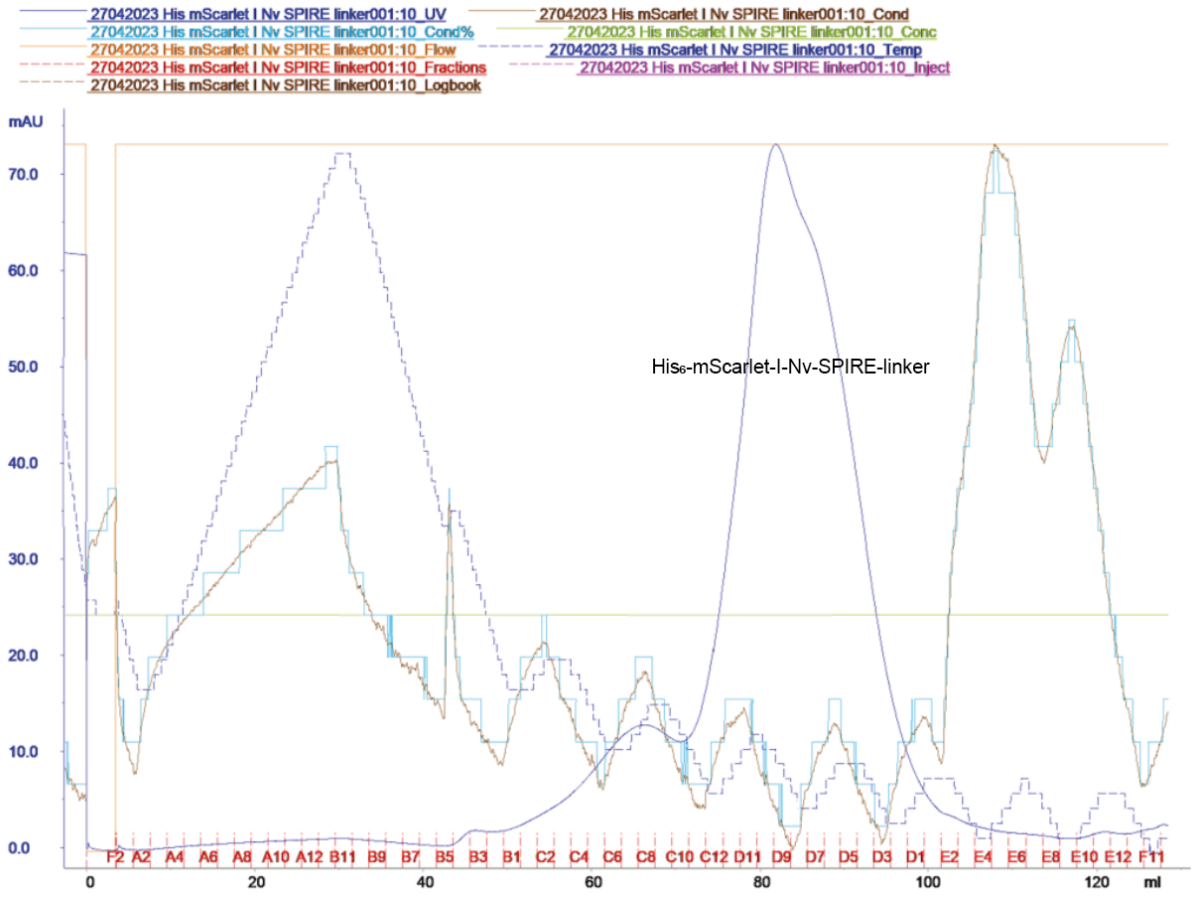

Figure 19: ***Chromatogram for size exclusion chromatography of His_6-mScarlet-I-Nv-SPIRE-linker.*** *The fractions D12-D5 (fractions collected in 15 ml tubes) were analysed by Coomassie staining and pooled for further purification steps. mAU, milli absorption unit, ml of the column volume, when the sample is eluted from the column.*

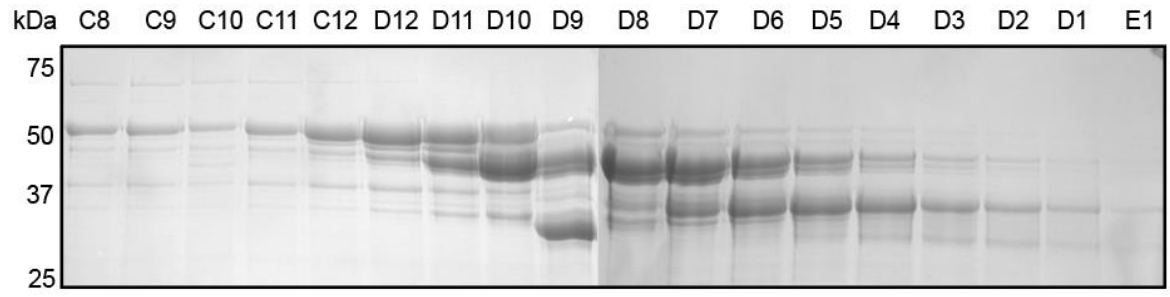

Figure 20: ***SDS-PAGE of His_6-mScarlet-I-Nv-SPIRE-linker after size exclusion chromatography.*** *The fractions of D12-D5 correspond to the molecular size of His_6-mScarlet-I-Nv-SPIRE-linker, around 46 kD and were pooled for further processing., kDa, kilo Dalton.*

The Coomassie brilliant blue staining of the proteins was done to test the final protein quality and purity. The Coomassie dye serves as a protein loading control. The dye attachs itself to the basic side chains of the amino acids and leads to sequence-non-specific protein staining in SDS-gels. All seven

purified proteins appeared quite clean and specific protein bands appeared at the correct size in SDS-polyacrylamide gel ectrophoresis. The GST-tagged MYO5-GTD proteins are around 68 kDa in size, His_6-mScarlet-I tagged SPIRE1/2-linker proteins are around 42 kDa in size, GST is 25 kDa and His-mScarlet-I around 27 kDa (Figure 21).

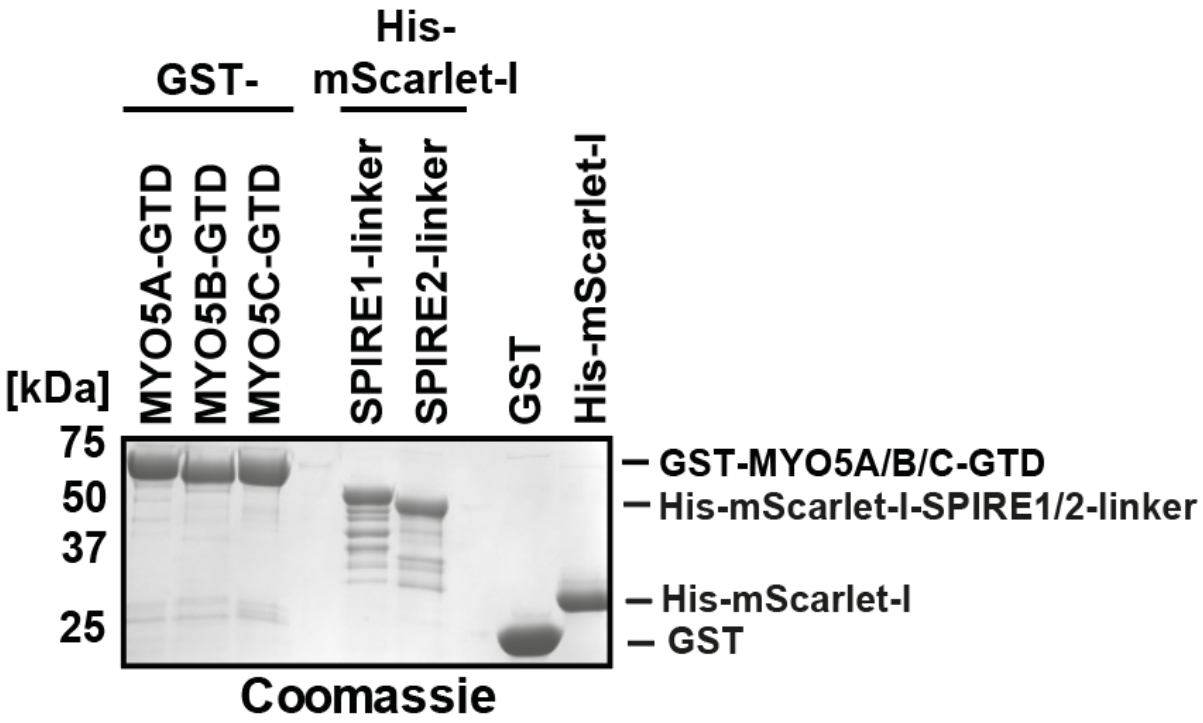

Figure 21: ***Protein quality control of used purified proteins:*** *GST-Hs-MYO5A-GTD, GST-Hs-MYO5B-GTD, GST-Hs-MYO5C-GTD, His-mScarlet-I-SPIRE1-linker, His-mScarlet-I und GST. The purified proteins GST-tagged MYO5A/B/C-GTD, mScarlet-I-SPIRE1/2-linker, GST and mScarlet-I were loaded on a 10% SDS gel, separated by size and afterwards stained using Coomassie brilliant blue, a dye to stain protein after a SDS-PAGE. GTD, globular tail domain.*

3.4 Interaction of mammalian MYO5 and SPIRE proteins

So far, findings have shown that SPIRE proteins coexist in a protein complex with MYO5A, MYO5B and MYO5C, regulated by the MYO5-GTD and the SPIRE-GTBM. Nonetheless, the creation of a protein complex containing SPIRE and MYO5 proteins could be mediated or supported by other proteins and complex members, and this does not necessarily imply a direct contact between the two. The interaction of MYO5C and SPIRE2 has not been analysed before. Therefore, the interactions between MYO5A/B/C-GTD were analysed with SPIRE1 and SPIRE2 using the same interaction study method, so the gained results can be compared. Because if different interaction methods are used, the experiment conditions differ, the results are different, and they cannot be compared.

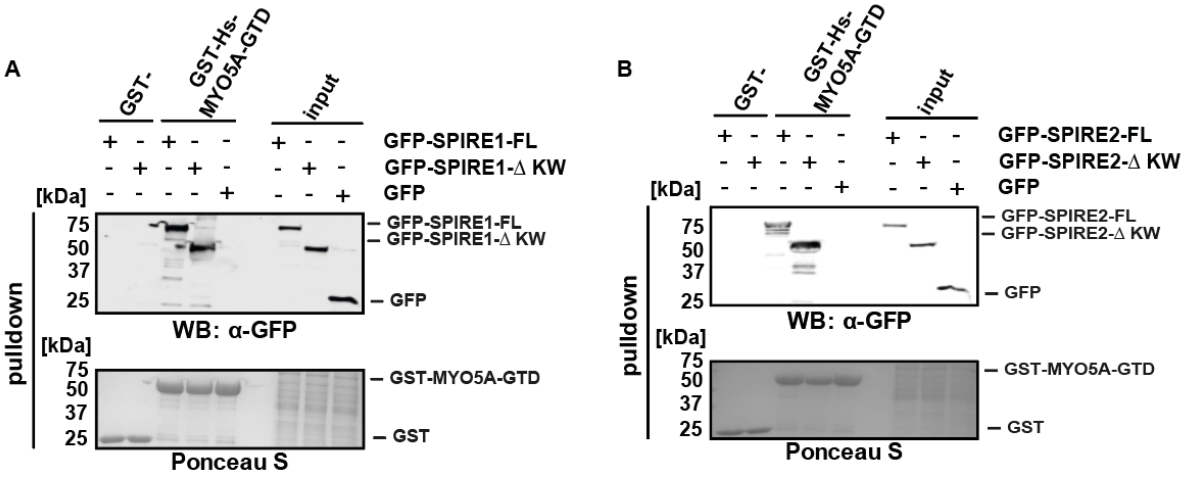

*Figure 22: **SPIRE1 and SPIRE2 interact with MYO 5A-GTD**. GST-Pulldown assays employing bacterially expressed GST-MYO5-GTD and lysates of HEK 293 cells transfected with plasmids expressing AcGFP1 (GFP) in the following referred as GFP, GFP-tagged-SPIRE1/2 full length (FL) and deletion mutants (GFP-SPIRE1/2-Δ-KW). Ponceau S staining shows equal loading of GST-fusion proteins. N = 5 experimental repeats, a representative experiment is shown. GTD, globular tail domain; FL, full-length; ΔKW, deletion of KIND- and WH2-domain; WB, Western blot.*

As a first attempt, a GST-pulldown experiment was performed, employing GST-MYO5-GTD proteins purified from bacteria and lysates from HEK 293 cells transiently expressing AcGFP1-tagged SPIRE proteins, in the following referred as GFP-SPIRE proteins. To have a look at these observations in more detail and assay the full-length SPIRE proteins for interaction with MYO5-GTD, an initial GST-pulldown from HEK 293 cell lysates could show that a GST-tagged MYO5A globular tail domain protein (GST-MYO5A-GTD) is able to pull the SPIRE1 protein from cell lysates (Figure 22A). These findings confirm the co-existence of MYO5A-GTD and SPIRE1 proteins in a protein complex. The GST-tagged MYO5A (GST-MYO5A-GTD) pulls the SPIRE1 full length protein as well as the SPIRE1-ΔKW from cell lysates as expected, considering the well-established GTBM-GTD interaction of SPIRE and MYO5 proteins (Kollmar et al., 2024; Welz and Kerkhoff, 2023). Therefore, the shorter and easier to handle GFP-SPIRE1-ΔKW constructs was used for the experimental repeats. No interactions were observed for GFP, GST and buffer controls.

Similarly, an initial GST-pulldown from HEK 293 cell lysates could show that a GST-tagged MYO5A globular tail domain protein (GST-MYO5A-GTD) is able to pull the SPIRE2 protein from cell lysates (Figure 22B*)*. These findings confirm the co-existence of MYO5A-GTD and SPIRE2 proteins in a protein complex. The GST-tagged MYO5A (GST-MYO5A-GTD) pulls the SPIRE2 FL protein as well as the SPIRE2-ΔKW from cell lysates. Therefore, the shorter and easier to handle GFP-SPIRE2-ΔKW constructs was used for the experimental repeats. No interactions were observed for GFP, GST and buffer controls.

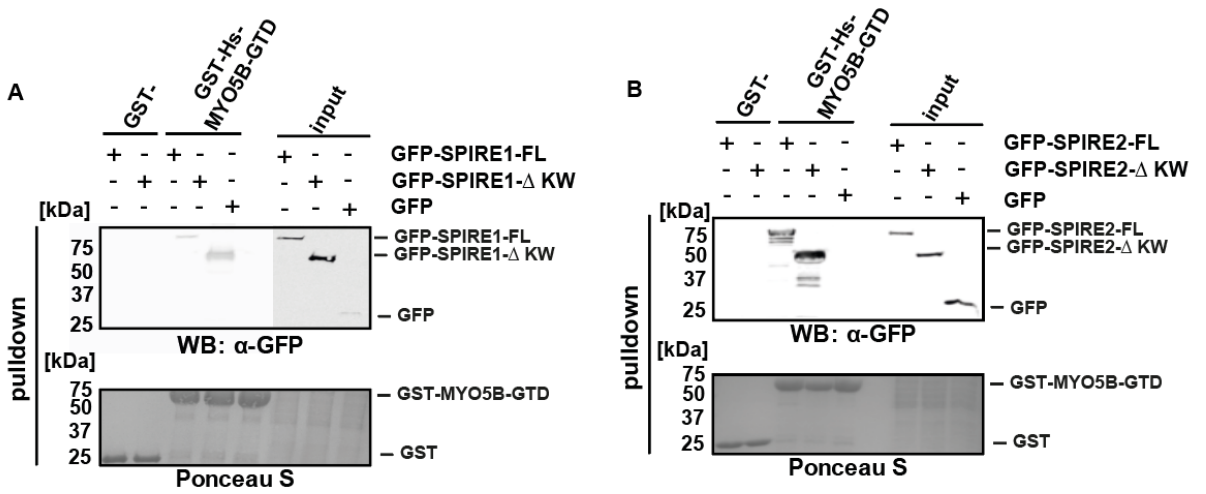

*Figure 23: **SPIRE1 and SPIRE2 interact with MYO5B-GTD**. GST-Pulldown assays employing bacterially expressed GST-MYO5-GTD and lysates of HEK 293 cells transfected with plasmids expressing GFP-tagged-SPIRE full length (FL) and deletion mutants. GST-Hs-MYO5B-GTD with GFP-SPIRE1/2-FL, GFP-SPIRE1/2-Δ-KW and GFP. Ponceau S staining shows equal loading of GST-fusion proteins. N = 5 experimental repeats, a representative experiment is shown. GTD, globular tail domain; FL, full-length; ΔKW, deletion of KIND- and WH2-domain; WB, Western blot.*

I further analysed MYO5B-GTD and MYO5C-GTD for interaction with the full-length SPIRE1 and SPIRE2 proteins. A GST-tagged MYO5B globular tail domain protein (GST-MYO5B-GTD) is able to pull the SPIRE1 protein from cell lysates (Figure 23A). These findings confirm the co-existence of MYO5B-GTD and SPIRE1 proteins in a protein complex. The GST-tagged MYO5B (GST-MYO5B-GTD) pulls the SPIRE1 full-length protein as well as the SPIRE1-ΔKW from cell lysates. Therefore, the shorter and easier to handle GFP-SPIRE1-ΔKW constructs was used for the experimental repeats. No interactions were observed for both, GST and buffer controls.

A GST-pulldown from HEK 293 cell lysates could show that a GST-tagged MYO5B globular tail domain protein (GST-MYO5B-GTD) is able to pull the SPIRE2 protein from cell lysates (Figure 23B). These findings confirm the co-existence of MYO5B-GTD and SPIRE2 proteins in a protein complex. The GST-tagged MYO5B (GST-MYO5B-GTD) pulls the SPIRE2 full-length protein as well as the SPIRE2-ΔKW from cell lysates. The shorter and easier to handle GFP-SPIRE2-ΔKW constructs was used for the experimental repeats. No interactions were observed for GFP, GST and buffer controls.

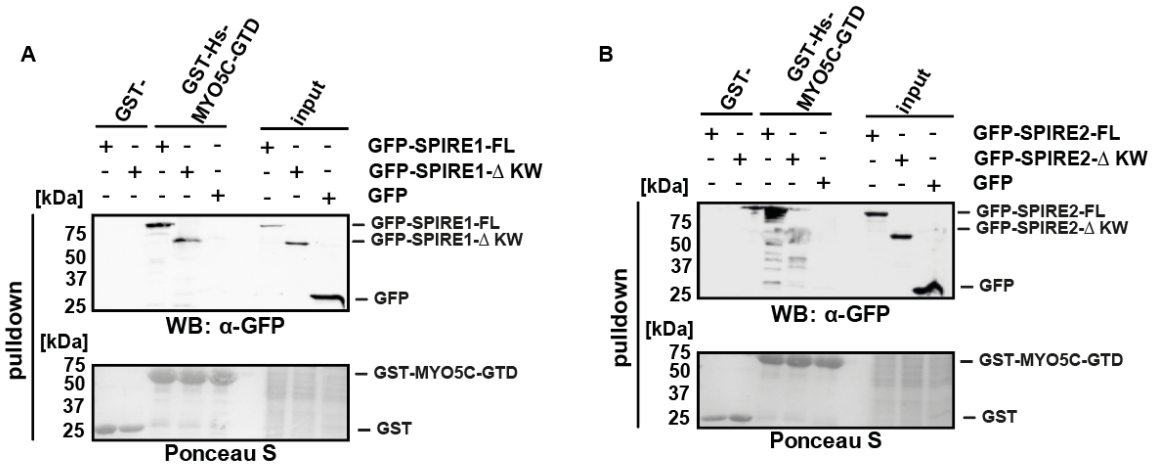

*Figure 24: **SPIRE1 and SPIRE2 interact with MYO5C-GTD**. GST-Pulldown assays employing bacterially expressed GST-MYO5-GTD and lysates of HEK 293 cells transfected with plasmids expressing GFP-tagged-SPIRE1/2 full length (FL) and deletion mutants. GST-Hs-MYO5C-GTD with GFP-SPIRE1/2-FL, GFP-SPIRE1/2-Δ-KW and GFP. Ponceau S staining shows equal loading of GST-fusion proteins. N = 5 experimental repeats, a representative experiment is shown. GTD, globular tail domain; FL, full-length; ΔKW, deletion of KIND- and WH2-domain; WB, Western blot.*

Next to MYO5A-GTD and MYO5B-GTD also a GST-tagged MYO5C globular tail domain protein (GST-MYO5C-GTD) is able to pull the SPIRE1 protein from cell lysates (Figure 24A). These findings confirm the co-existence of MYO5C-GTD and SPIRE1 proteins in a protein complex. The GST-tagged MYO5C (GST-MYO5C-GTD) pulls the SPIRE1 full-length protein as well as the SPIRE1-ΔKW from cell lysates. Therefore, the shorter and easier to handle GFP-SPIRE1-ΔKW constructs was used for the experimental repeats. No interactions were observed for both, GST and buffer controls.

An initial GST-pulldown from HEK 293 cell lysates could show that a GST-tagged MYO5C globular tail domain protein (GST-MYO5C-GTD) is able to pull the SPIRE2 protein from cell lysates (Figure 24B*)*. These findings confirm the co-existence of MYO5C-GTD and SPIRE2 proteins in a protein complex. The GST-tagged MYO5C (GST-MYO5C-GTD) pulls the SPIRE2 full-length protein as well as the SPIRE2-ΔKW from cell lysates. The shorter and easier to handle GFP-SPIRE2-ΔKW constructs was used for the experimental repeats. No interactions were observed for GFP, GST and buffer controls.

The GST-pulldowns from lysates from HEK 293 cells transiently expressing the MYO5-GTD isoforms with the SPIRE1/2-ΔKW or full length constructs showed in all the experiments a stronger or even band with the SPIRE1/2-ΔKW construct, so because this construct is easier to express, it is sufficient, so these were used for experimental repeats.

To investigate a direct physical contact between SPIRE and MYO5 proteins, GST-pulldown experiments were conducted with bacterially expressed and purified recombinant SPIRE1/2-linker peptides and MYO5A/MYO5B/MYO5C-GTD proteins (Figure 25). GST-Hs-MYO5A-GTD, GST-Hs-MYO5B-GTD and

GST-Hs-MYO5C-GTD are all three capable of pulling a His_6-mScarlet-I-tagged SPIRE1/2-linker protein (mScarlet-I-SPIRE1/2-linker), indicated a direct protein interaction between SPIRE and MYO5, which may contribute to protein interactions (Pylypenko et al., 2016). To improve the results in the pulldown assay, GST and His_6- mScarlet-I proteins served as controls and showed no binding (Figure 26). For these pulldown experiments for each protein more than one batch of purified protein was used to exclude results depending on inactive protein forms because of bad protein purifications.

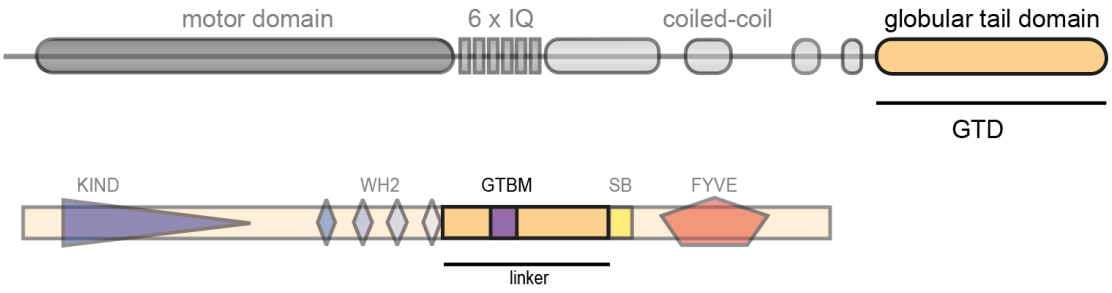

*Figure 25: **Schematic representation of GTD- and linker-region.** Interaction sites of SPIRE and MYO5 constructs; these proteins were employed in the qualitative binding assays. The regions for the interaction are notated. For MYO5 the globular tail domain (GTD) and for SPIRE the globular tail binding motif (GTBM).*

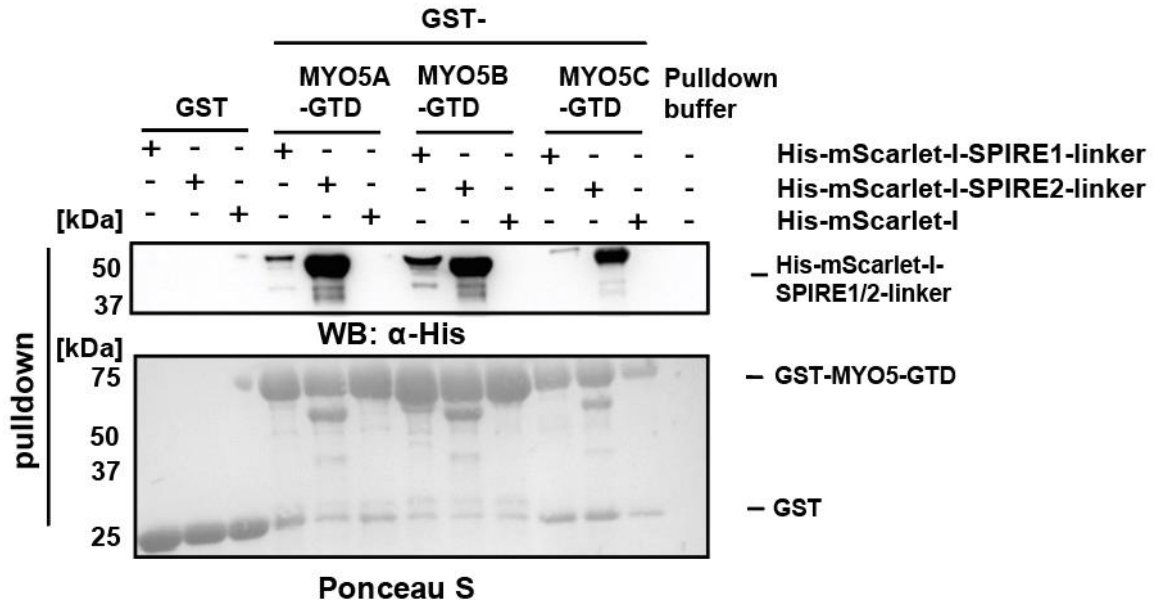

*Figure 26: **MYO5A/B/C-GTD interacts with SPIRE1/2-linker:** GST-Pulldown-Assay with purified GST-Hs-MYO5A/B/C-GTD with purified His-mScarlet-I-SPIRE1/2-linker and as a control functions GST, mScarlet-I and Pulldown buffer. GST-tagged proteins were immobilised on GSH-beads and incubated with His-mScarlet-I-SPIRE1/2-linker and His-mScarlet-I on a rotating wheel at 4°C. GTD, globular tail domain. Pulldown shown for Nv-/Sr-MYO5-GTD with Nv-/Sr-SPIRE-linker in the supplement.*

These findings manifest the co-existence of MYO5 and SPIRE proteins in a protein complex. The observed interaction was in all three cases of MYO5A/B/C-GTD stronger with SPIRE2 than with SPIRE1. No interactions were observed for controls: GST, mScarlet-I and pulldown buffer control. Since the SPIRE band in the case of all three MYO5 isoforms appeared stronger for the interaction with SPIRE2,

suggesting a higher affinity of MYO5 proteins for SPIRE2 over SPIRE1. These findings were analysed in more detail by means of quantitative interaction studies to unravel respective binding strengths.

3.5 Quantitative analysis of the mammalian MYO5 and SPIRE isoform interaction

So far, the findings have shown that SPIRE proteins coexist in a protein complex with MYO5A, MYO5B and MYO5C, regulated by the MYO5-GTD and the SPIRE-GTBM interaction. The band of SPIRE after the interaction with MYO5 appeared stronger with SPIRE2 than with SPIRE1 in western blot, so the next step was to analyse the binding affinity in a quantitative way using fluorescence spectroscopy. Nonetheless, the creation of a protein complex containing SPIRE and MYO5 proteins could be mediated or supported by other proteins and complex members, and this does not necessarily imply a direct contact between the two. The interaction of the MYO5 isoforms with SPIRE1 is not investigated in detail, so with this work new insights into these interactions were obtained.

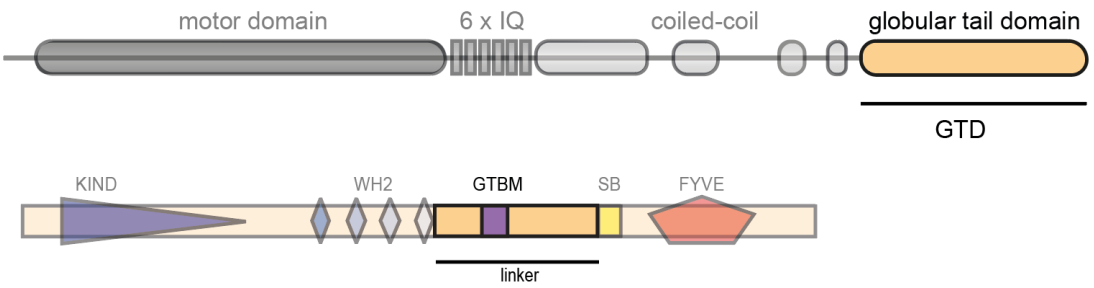

*Figure 27: **Schematic representation of GTD- and linker-region.** Interaction sites of SPIRE and MYO5 proteins; these proteins were employed in the quantitative binding assays. The regions for the interaction are notated in these proteins. For MYO5 the globular tail domain (GTD) and for SPIRE the globular tail binding motif (GTBM).*

To gain further insight into the interaction of MYO5 and SPIRE the dissociation equilibrium constants were determined. In a basic binding, bimolecular binding reaction: a molecule A binds to molecule B, forming a complex: A + B ⇆ AB. This complex AB dissociates, AB ⟶ A + B, AB is the only reactant and this reaction is a first order reaction with a rate of: Rate = k_- (AB) (Pollard, 2010). The dissociation rate constant is just the probability that the complex falls apart in a unit of time (Pollard, 2010). The equilibrium constant (K) is a number, that characterises the affinity of molecules for each other, so the rates of the forward and reverse binding reaction are equal: rate of binding = k_+ (A) (B) = k_- (AB) = rate of dissociation (Pollard, 2010). The equilibrium constant (K) is equal to the ratio of the forward and reverse rate constants or the ratio of the concentration of products to the concentrations of free reactants at equilibrium (Pollard, 2010). So the equilibrium constant (K) is equal to the ratio of the

forward and reverse rate constants or the ratio of the concentration of products to the concentrations of free reactants at equilibrium $K_{eq} = k_+/k_- = (AB_{eq})/(A_{eq})(B_{eq})$ (Pollard, 2010). So, the dissociation equilibrium constant (K_d) is described by the reciprocal of the expression of the equilibrium constant for a binding reaction $K_d = k-/k_+ = (A_{eq})(B_{eq})/(AB_{eq})$. The unit for this form of K_d is M, moles per litre (Pollard, 2010). Therefore, we can say the lower the value of the K_d, the stronger the reaction and the more completely reactants A and B are converted into product AB (Pollard, 2010). Often, the dissociation rate constant determines the affinity of the proteins to each other. To analyse the equilibrium binding data, the experiment has to include high concentration of B, so B can saturate A and the concentration of AB will reach a plateau. Without reaching this plateau, the amplitude of the reaction is unknown and without the amplitude, no equilibrium constant can be measured (Pollard, 2010).

A possible assay to measure this dissociation equilibrium constant is with an optical assay. In this assay, the difference in fluorescence intensity between the product compared to the reactants is measured (Pollard, 2010).

Therefore, a GST-pulldown assay was performed using GST-tagged MYO5-GTD proteins with increasing concentrations and His_6-mScarlet-I-tagged SPIRE1/2-linker proteins with a constant concentration (100 nM) at equilibrium (Figure 28). The dissociation equilibrium constants (K_d) for the His_6-mScarlet-SPIRE1/2-linker:MYO5A-GTD, His_6-mScarlet-SPIRE1/2-linker:MYO5B-GTD and His_6-mScarlet-SPIRE1/2-linker:MYO5C-GTD complexes were thus determined by fluorescence-spectroscopic measurements of the His_6-mScarlet-I-tagged SPIRE1/2-linker peptide with increasing concentrations of GST-MYO5A-GTD, GST-MYO5B-GTD and GST-MYO5C-GTD (Figure 28). Therefore, the difference in fluorescence intensity left after protein complex formation was measured. For the experiments different batches of all purified proteins were used to exclude “results depending on bad protein purifications”.

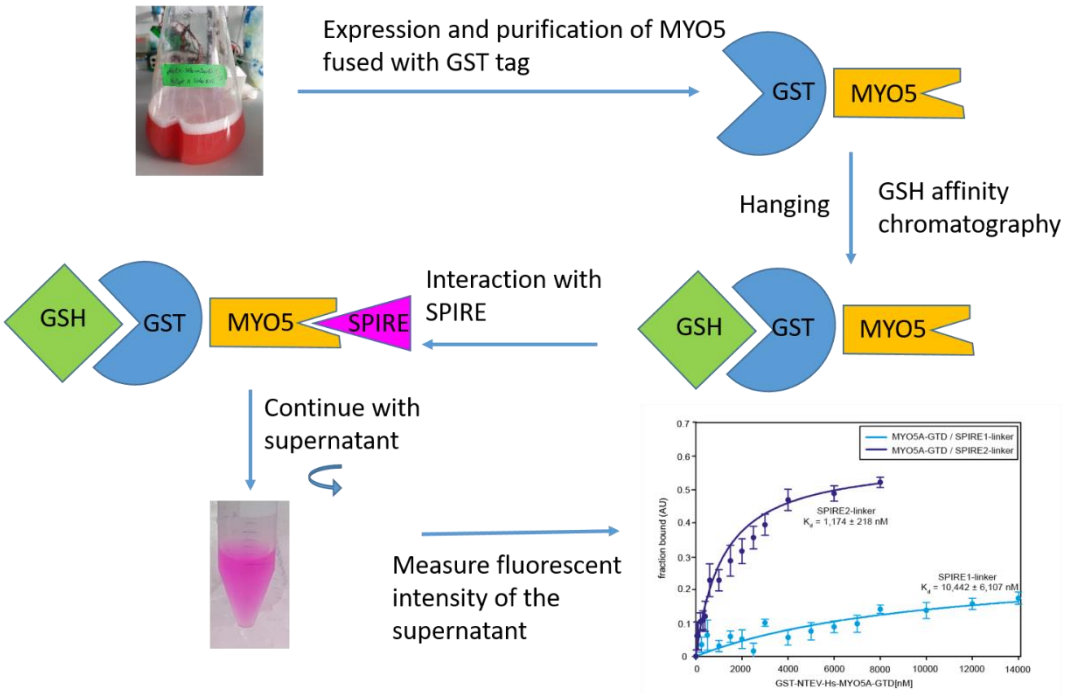

Figure 28: ***Scheme of the quantitative binding assay:*** *GST-pulldown assays were performed as described previously with increasing concentrations of GST-MYO5A/B/C-GTD fusion proteins and 100 nM His$_6$-mScarlet-I-SPIRE1/2-linker peptide in SPECS buffer (1xPBS, 50 mM NaCl). GST-MYO5A/B/C-GTD was immobilized on GSH-beads and fluorescently labelled m-Scarlet-I-SPIRE1/2-linker was added in a constant defined amount at equilibrium. The mixture of the two proteins and the beads was incubated on a rotating wheel for 2 hours, afterwards the beads were pelleted and the supernatant was centrifuged for 10 min at 20,000 x g to remove potential debris that could disturb the fluorescence measurement. The intensity of the fluorescence of the supernatant was measured using VarioskanTM (fluorescence spectroscopy); the graphs were built using Sigmaplot11 and the regression curve was generated, the scheme was created in Microsoft PowerPoint. Modified by (Pylypenko et al., 2016).*

The measured equilibrium dissociation constants (K_d) were compared to each other, so further details on the protein interaction of MYO5-GTD and SPIRE-linker can be gained. The K_d for the His$_6$-mScarlet-SPIRE1/2-linker:MYO5A-GTD, His$_6$-mScarlet-SPIRE1/2-linker:MYO5B-GTD and His$_6$-mScarlet-SPIRE1/2-linker:MYO5C-GTD complexes were determined by fluorescence-spectroscopic measurements of the His$_6$-mScarlet-I-tagged SPIRE1/2-linker peptide with increasing concentrations of GST-MYO5A-GTD, GST-MYO5B-GTD and GST-Myo5C-GTD (Figure 29).

The His$_6$-mScarlet-I-SPIRE1-linker: MYO5A-GTD has a K_d of 10,442 nM, while the His$_6$-mScarlet-I-SPIRE1-linker: MYO5B-GTD has a K_d of 37,151 nM and for the His$_6$-mScarlet-I-SPIRE1-linker: MYO5C-GTD no K_d could be measured, because the plateau and so also the amplitude necessary for determining the K_d was not reached. The His$_6$-mScarlet-I-SPIRE2-linker: MYO5A-GTD has a K_d of 1,174 nM, while the His$_6$-mScarlet-I-SPIRE2-linker: MYO5B-GTD has a K_d of 119 nM and for the His$_6$-mScarlet-I-SPIRE2-linker: MYO5C-GTD has a K_d of 633 nM (Figure 29D). The His$_6$-mScarlet-I-Sr-SPIRE-linker: Sr-MYO5-GTD has a K_d of 460 nM and for the His$_6$-mScarlet-I-Nv-SPIRE-linker: Nv-MYO5-GTD has a K_d of 3,444 nM. The binding curves for the interaction with SPIRE2-linker reached their plateau around 40%

and 50%. For the binding of SPIRE1-linker, the binding curves could not reach a saturation because of the instability of the contact of the proteins. The interaction between Sr-SPIRE-linker and Sr-MYO5 is the strongest and already existed in the choanoflagellates.

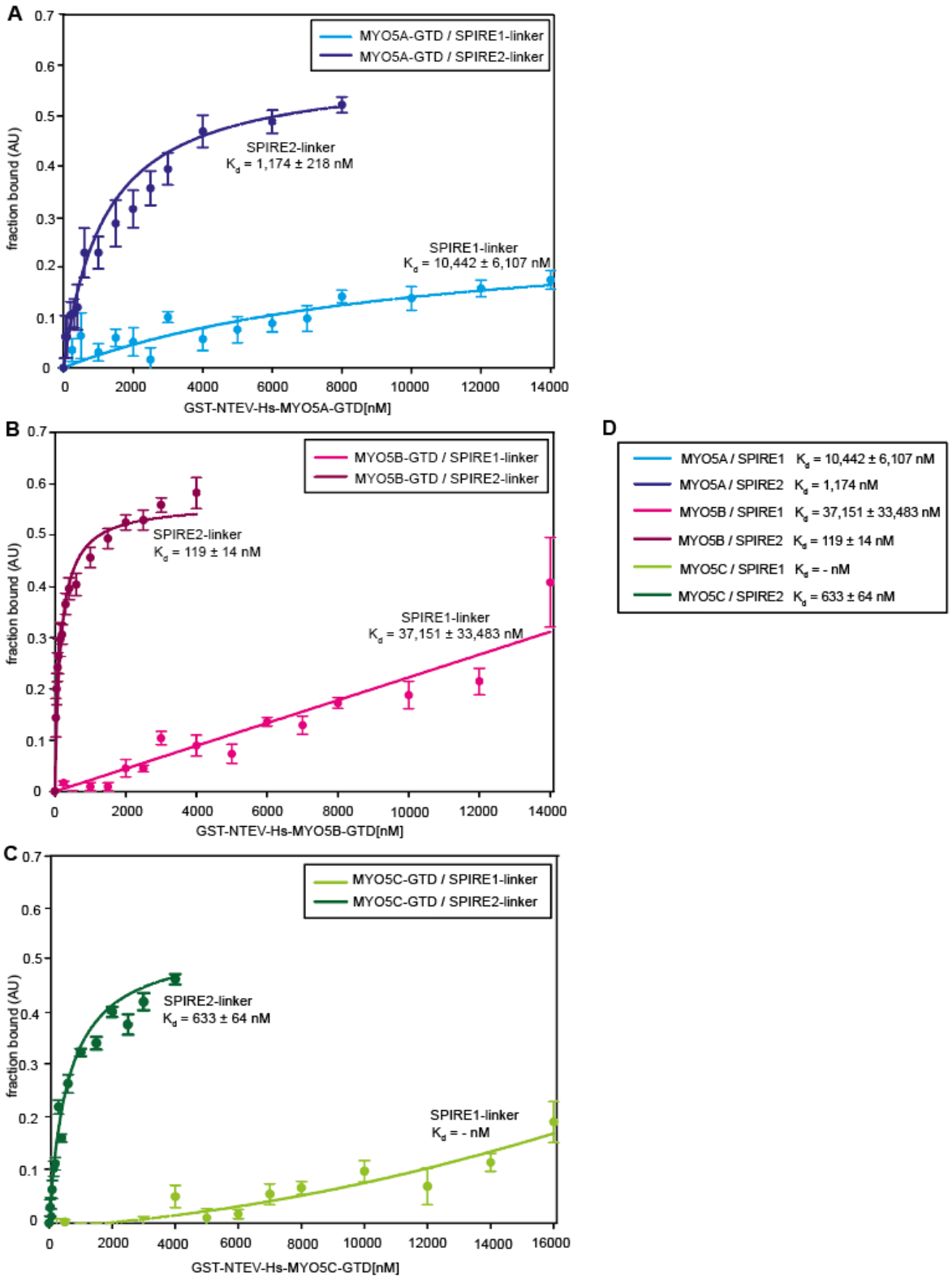

*Figure 29: **Quantitative binding assays of GST-NTEV-Hs-MYO5-GTD with His_6-mScarlet-I-Hs-SPIRE1/2-linker**. Fluorescence spectroscopy was performed to determine the equilibrium dissociation constant using increasing concentrations of GST-MYO5-GTD and constant concentrations of mScarlet-I-SPIRE-linker (100 nM) at equilibrium. A) GST-NTEV-Hs-MYO5A-GTD with His_6-*

mScarlet-I-Hs-SPIRE1-linker (light blue) and His_6-mScarlet-I-Hs-SPIRE2-linker (dark blue) B) GST-NTEV-Hs-MYO5B-GTD His_6-mScarlet-I-Hs-SPIRE1-linker (light pink) and His_6-mScarlet-I-Hs-SPIRE2-linker (dark pink) C) GST-NTEV-Hs-MYO5C-GTD with His_6-mScarlet-I-Hs-SPIRE1-linker (light green) and His_6-mScarlet-I-Hs-SPIRE2-linker (dark green) D) table showing the measured K_ds of GST-NTEV-Hs-MYO5-GTD with His_6-mScarlet-I-Hs-SPIRE1/2-linker. N= 5 experimental repeats. Graphs were generated with SigmaPlot 11 software, measurement points were set in the graph and a regression curve was created and added to the graph. GTD, globular tail domain; nM, nanomolar; Hs, Homo sapiens. The single graphs and the raw data are shown in the supplement.

In Figure 29A, the measured equilibrium dissociation constants (K_d) of the binding strengths of the binding MYO5A-GTD and SPIRE1 and SPIRE2 are shown. The affinity of MYO5A is higher with SPIRE2-linker than with SPIRE1-linker, so the interaction seems to be stronger with SPIRE2 that with SPIRE1.

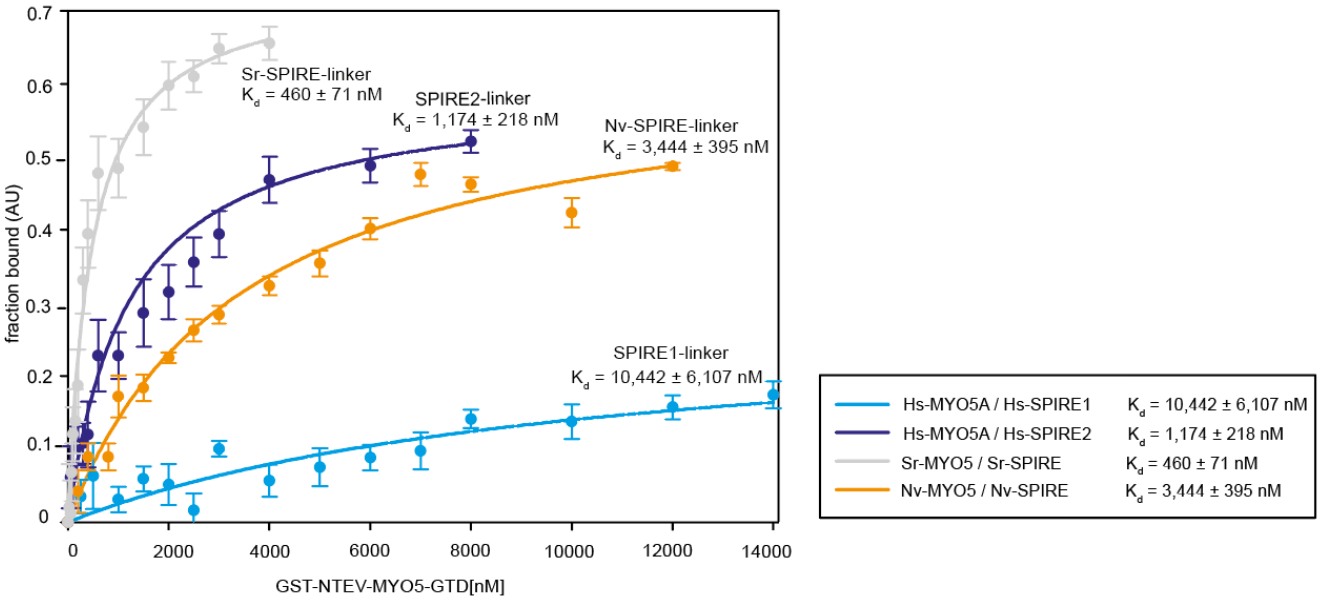

*Figure 30: **Quantitative pulldowns of GST-NTEV-Hs-MYO5A-GTD with His-mScarlet-I-Hs-SPIRE1/2-linker with the measured dissociation constants, K_d.** Fluorescence spectroscopy was performed to determine the equilibrium dissociation constant using increasing concentrations of GST-MYO5-GTD and constant concentrations of mScarlet-I-SPIRE-linker (100 nM) at equilibrium. GST-NTEV-Hs-MYO5A-GTD with His-mScarlet-I-Hs-SPIRE1-linker (light blue) and His-mScarlet-I-Hs-SPIRE1-linker (dark blue); GST-NTEV-Nv-MYO5-GTD with His-mScarlet-I-Nv-SPIRE-linker (orange) and GST-NTEV-Sr-MYO5-GTD His-mScarlet-I-Sr-SPIRE-linker (grey); N= 5 experimental repeats. Graphs were generated with SigmaPlot 11 software, measurement points were set in the graph and a regression curve was created and added to the graph. GTD, globular tail domain; nM, nanomolar; Hs, Homo sapiens; Nv, Nematostella vectensis; Sr, Salpingoeca rosetta. The single graphs and the raw data are shown in the supplement (Figure 36).*

In Figure 29B, the measured equilibrium dissociation constants (K_d) of the binding strengths of the binding MYO5B-GTD and SPIRE1 and SPIRE2 are shown. The affinity of MYO5B is higher with SPIRE2-linker than with SPIRE1-linker, so the interaction seems to be stronger with SPIRE2 that with SPIRE1.

In Figure 29C, the measured equilibrium dissociation constants (K_d) of the binding strengths of the binding MYO5C-GTD and SPIRE1 and SPIRE2 are shown. The affinity of MYO5C is higher with SPIRE2-linker than with SPIRE1-linker, so the interaction seems to be stronger with SPIRE2 that with SPIRE1.

In Figure 30, the measured equilibrium dissociation constants (K_d) of the binding strengths of the binding of SPIRE-linker and MYO5-GTD in *Salpingoeca rosetta*, *Nematostella vectensis* in comparison to the human MYO5A-GTD with SPIRE1/2-linker are shown. The affinity of Sr-MYO5 is higher with Sr-SPIRE-linker than Nv-MYO5 with Nv-SPIRE-linker, the interaction of Sr-MYO5 is the strongest in this thesis measured dissociation constants.

The finding that the value of the measured equilibrium dissociation constants of choanoflagellates and cnidarian are more similar to the K_d of human MYO5-GTD with SPIRE2-linker, takes into account that SPIRE2 is higher expressed in the small intestine in the epithelial cells, and a small intestine is also found earlier in evolution.

In Table 7 the measured equilibrium dissociation constants (K_d) of the binding strengths of the MYO5-GTD and SPIRE-linker interactions are shown. The plus and minus indicate the strength of the dissociation equilibrium constants.

Table 7: Overview of the measured equilibrium dissociation constants (K_d) of the MYO5-GTD: SPIRE-linker interactions and respective binding strengths according to qualitative pulldown Western blot results. + = binding; ++ = stronger binding, +++ = very strong binding; N =5.

	Hs-SPIRE1-linker	Hs-SPIRE2-linker	Nv-SPIRE-linker	Sr-SPIRE-linker
Hs-MYO5A-GTD	+ 10,442 ± 6,107 nM	+++ 1,174 ± 218 nM	-	-
Hs-MYO5B-GTD	+ 37,151 ± 33,483 nM	++ 119 ± 14 nM	-	-
Hs-MYO5C-GTD	+ -	+++ 633 ± 64 nM	-	-
Nv-MYO5-GTD	-	-	+ 3,444 ± 395 nM	-
Sr-MYO5-GTD	-	-	-	+ 460 ± 71 nM

In all the Hs-MYO5-GTD combinations, the binding of the MYO5-GTD with SPIRE2 is stronger and more specific than the binding with SPIRE1. The binding of MYO5-GTD and SPIRE-linker is the strongest in the case of *Salpingoeca rosetta (Sr),* so already in the choanoflagellates earlier in evolution and the binding of MYO5-GTD and SPIRE-linker in Nematostella and Salpingoeca is more similar to the Hs-MYO5-GTD with SPIRE2-linker.

Table 8: Comparison of measured dissociation constants (K_d) of the MYO5-GTD: SPIRE-linker interactions and binding strengths in comparison with already measured K_d from (Pylypenko et al., 2016).

	Hs-SPIRE1-linker	Hs-SPIRE2-linker	Hs-SPIRE2-linker Pylypenko 2016
Hs-MYO5A-GTD	+ 10,442 ± 6,107 nM	+++ 1,174 ± 218 nM	+++ 728 ± 113 nM
Hs-MYO5B-GTD	+ 37,151 ± 33,483 nM	++ 119 ± 14 nM	++ 377 ± 84 nM
Hs-MYO5C-GTD	+ -	+++ 633 ± 64 nM	-

The measured equilibrium dissociation constants (K_d) of the binding strengths of the MYO5A/B-GTD and SPIRE2-linker interactions have been measured in previous studies (Pylypenko et al., 2016). The results in this work are in a similar range of the K_d value (Table 8). For MYO5/SPIRE1-linker interactions, no data were published before this thesis.

3.6 Analysis of cellular colocalisation studies of MYO5

To address an interaction of MYO5A/B/C with the SPIRE1/2 in a cellular context, GFP-Hs-MYO5A/B/C-cc-GTD and mScarlet-I-Hs-SPIRE1/2-ΔKW constructs were transiently co-expressed in HeLa cells, microscope images were taken with a Leica fluorescence microscope and the images were processed with 3D-deconvolution at the Leica LASX software. The processed images with the observed colocalisation were analysed using the Pearson's Correlation Coefficient (PCC) with the Coloc2-macro in the Fiji ImageJ software (Costes et al., 2004; Pompey et al., 2013). The PCC value is a statistical measure to determine a linear relationship between the intensity of various fluorescent signals (Costes et al., 2004). A PCC value of 1 indicates a perfect colocalisation (perfect positive correlation of signals), 0 indicates a random colocalisation (no correlation) and a PCC value of -1 indicates a mutually exclusive localisation (perfect negative correlation) of the analysed signals (Costes et al., 2004).

The Pearson's correlation coefficient showed that SPIRE1/2 and Myosin5 proteins colocalise with each other *in vitro*, but not with the control mScarlet-I.

The microscopy pictures of the co-expression of MYO5A/B/C-cc-GTD with the SPIRE1/2-ΔKW (GFP-Hs-MYO5A/B/C-cc-GTD and mScarlet-I-Hs-SPIRE1/2-ΔKW) were the basis of the colocalisationanalysis.

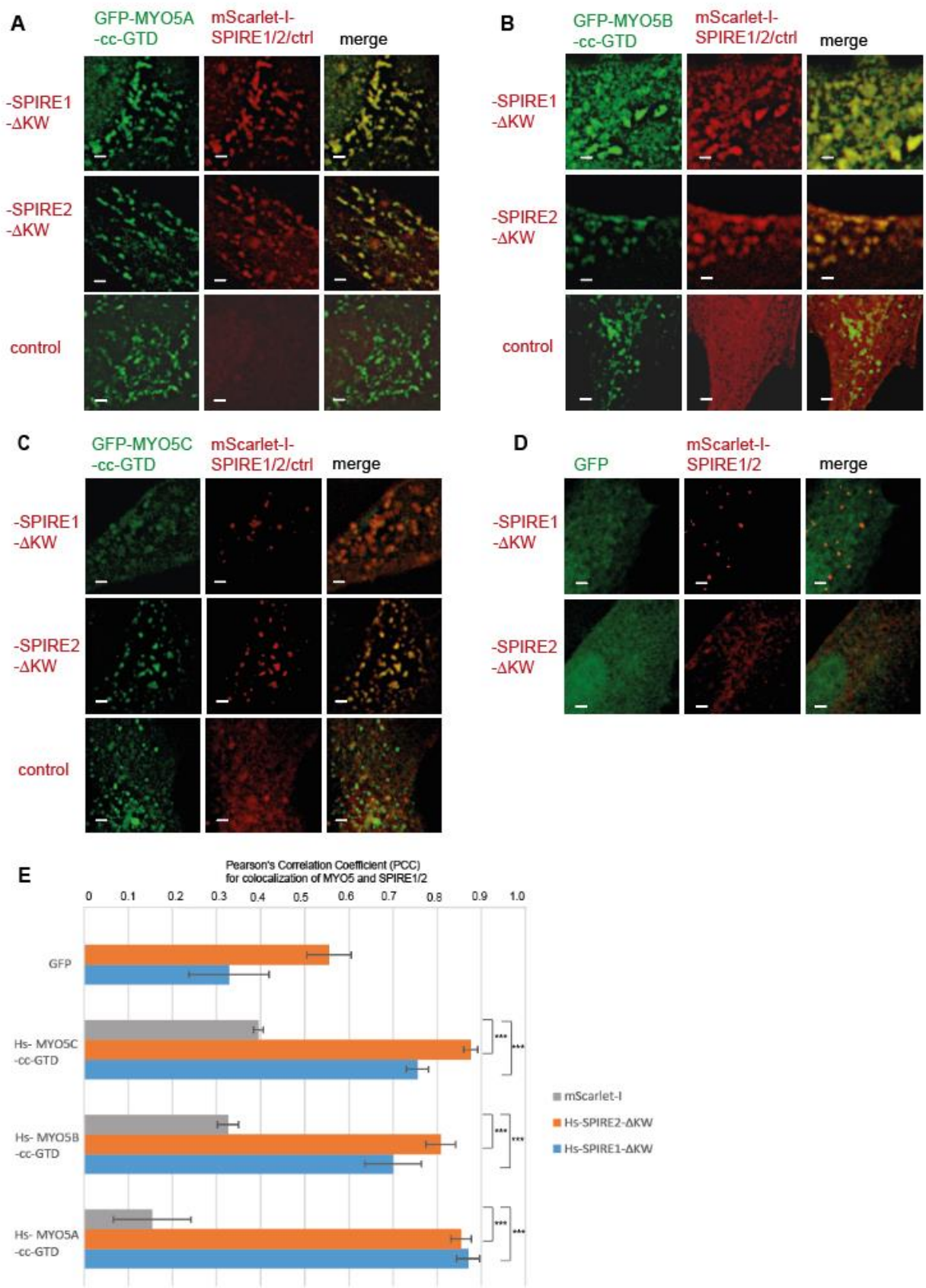

Figure 31: ***MYO5-cc-GTD and SPIRE1-ΔKW and SPIRE2-ΔKW colocalise at vesicle membranes. HeLa cells transiently expressing GFP-MYO5-cc-GTD, GFP, mScarlet-I-/-SPIRE1/2-ΔKW*** *GFP-tagged MYO5-cc-GTD (green) and mScalet-I-SPIRE1/2-ΔKW (red)* ***A****) GFP-tagged-MYO5A-cc-GTD does not colocalise with mScarlet-I (pm-Scarlet-I; red), GFP-tagged-MYO5A-cc-GTD colocalise with mScarlet-I-SPIRE1-ΔKW (pm-Scarlet-I-Hs-SPIRE1-ΔKW; red); GFP-tagged-MYO5A-cc-GTD colocalise with mScarlet-I-SPIRE2-ΔKW (pm-Scarlet-I-Hs-SPIRE2-ΔKW; red) at vesicle membranes when transiently co-expressed in HeLa cells, as indicated by*

overlapping punctae (merge; yellow, here only insets are shown; the whole cells are shown in the supplement (Figure 37-Figure 40). ***B)*** *GFP-tagged-MYO5B-cc-GTD does not colocalise with mScarlet-I (pm-Scarlet-I; red), GFP-tagged-MYO5B-cc-GTD colocalise with mScarlet-I-SPIRE1-ΔKW (pm-Scarlet-I-Hs-SPIRE1-ΔKW; red); GFP-tagged-MYO5B-cc-GTD colocalise with mScarlet-I-SPIRE2-ΔKW (pm-Scarlet-I-Hs-SPIRE2-ΔKW; red) at vesicle membranes when transiently co-expressed in HeLa cells, as indicated by overlapping punctae (merge; yellow, here only insets are shown; the whole cells are shown in the supplement).* ***C)*** *GFP-tagged-MYO5C-cc-GTD does not colocalise with mScarlet-I (pm-Scarlet-I; red), GFP-tagged-MYO5C-cc-GTD colocalise with mScarlet-I-SPIRE1-ΔKW (pm-Scarlet-I-Hs-SPIRE1-ΔKW; red); GFP-tagged-MYO5C-cc-GTD colocalise with mScarlet-I-SPIRE2-ΔKW (pm-Scarlet-I-Hs-SPIRE2-ΔKW; red) at vesicle membranes when transiently co-expressed in HeLa cells, as indicated by overlapping punctae (merge; yellow, here only insets are shown; the whole cells are shown in the supplement).* ***D)*** *GFP does not colocalise with mScarlet-I-SPIRE1-ΔKW (pm-Scarlet-I-SPIRE1-ΔKW; red) and GFP does not colocalise with mScarlet-I-SPIRE2-ΔKW (pm-Scarlet-I-Hs-SPIRE2-ΔKW; red) at vesicle membranes when transiently co-expressed in HeLa cells, as indicated by overlapping punctae (merge; yellow, here only insets are shown; the whole cells are shown in the supplement).* ***E)*** *Colocalisation of GFP-tagged MYO5-cc-GTD and mScarlet-I-tagged SPIRE1/2-ΔKW and as a control mScarlet-I. cc, coiled-coil domain; GTD, globular tail domain. The colocalisationof tagged proteins as described in was quantified for the indicated co-expressions by determining its Pearson's correlation coefficient (PCC) as shown in a bar diagram. Each bar represents the mean PCC value for at least 5 cells analysed. 5 cells were recorded for each condition and one representative cell is presented here, Error bars represent SEM. Graph was built with Microsoft Excel, Statistics was done using SPSS unpaired students t-test, to compare the mean PCC values of co-expression conditions with a confidence interval of 95%. ***, p < 0.001.* Scale bars *represent 5 µm. The images were processed with the Leica LASX software 3D-deconvoluted and Adobe Photoshop 2023; figure was assembled in Adobe Illustrator 2023;.*

SPIRE1/2 and MYO5 proteins were shown to interact directly with each other *in vitro*. The functional cooperation of SPIRE actin nucleators and specific RAB GTPases in vesicle transport processes was considered to be mediated by MYO5 actin motor proteins that link SPIRE and specific RABs to the same vesicle membranes, hence determining vesicle identity.

In Figure 31, the co-expression of GFP-tagged MYO5-cc-GTD (GFP-MYO5-cc-GTD), correspondingly, and mScarlet-I-tagged SPIRE1/2-ΔKW (mScarlet-I-Hs-SPIRE1/2-ΔKW) in HeLa cells disclosed that both, SPIRE1-ΔKW and SPIRE2-ΔKW, perfectly colocalise with MYO5-GTD, but not with the used control mScarlet-I (Figure 31A-C). In addition, a colocalisation of GFP and His-mScarlet-I-tagged SPIRE1/2-ΔKW (mScarlet-I-Hs-SPIRE1/2-ΔKW) could be excluded (Figure 31D).

The quantification of the colocalisation is shown in the graph (Figure 31E). The error bars define the SEM. A colocalisation is observed in the case of MYO5A/B/C-cc-GTD with SPIRE1/2-ΔKW, but not with mScarlet-I alone, SPIRE1/2-ΔKW with GFP. The observed differences in the colocalisation between the SPIRE1/2-ΔKW and the controls showed a statistical significance. For MYO5B/C-cc-GTD a tendency can be observed that the colocalisation with SPIRE2-linker is better. In contrast, for MYOA-cc-GTD, the colocalisation with SPIRE1/2-linker are almost the same. The colocalisation experiment proofed, that the observed interactions are possible due to intracellular proximity.

3.7 Evolution of the SPIRE-MYO5 interaction site

The MYO5 – SPIRE interaction was shown to be conserved across of evolution, therefore the known interaction site sequences of the two proteins for different species were aligned to see if there are conserved regions (Pylypenko et al., 2016). Therefore, weblogos of respective SPIRE-GTBM sequences were generated by Dr. Tobias Welz using the weblogo server (Crooks et al., 2004; Schneider and

Stephens, 1990). The weblogos represent the amino acid conservation for each residue of the compared sequences, they are stacked on top of each other (Schneider and Stephens, 1990). The frequency of the amino acids is shown proportional in the height of the letter and the most common one is on top (Schneider and Stephens, 1990). So, the most common amino acid sequence can be easily read, if the letters on top of the weblogo are read. Comparison of the choanoflagellate, cnidarian and vertebrate SPIRE-GTBMs shows only low sequence homology (Figure 32). For choanoflagellates 18 sequences were aligned, for cnidaria 13 sequences and for vertebrate SPIRE1 and SPIRE2, 12 or 10 sequences, respectively (Kollmar et al., 2024). However, the array of basic (blue), hydrophobic (green) and acidic residues (red) in the vertebrate GTBMs appears to be conserved in the cnidarian and choanoflagellate protein (Kollmar et al., 2024). The GTBM is a quite conserved sequence motif of 27 amino acids that binds to the globular tail domain of MYO5. The C-terminal hydrophobic residues of the GTBM in choanoflagellates are not dominant in cnidarian and move to the core in the mammalian SPIRE1 and SPIRE2. The results of the protein interaction assays depending on the differences in binding strength between mammalian SPIRE1 and SPIRE2 prompted the study of the GTBM sequence in more detail. The hydrophobic leucines in the middle of mammalian SPIRE2 are shown to contact MYO5A (Pylypenko et al., 2016). Mammalian SPIRE1 has leucines at the same position, so it may also contact MYO5A. These hydrophobic leucines are already present in the core region of choanoflagellates, but less conserved. The N-terminal basic residues in choanoflagellates stayed N-terminal in the cnidarian but moved to the middle part in mammalian SPIRE1 and SPIRE2. In mammalian SPIRE1 and SPIRE2, acidic residues evolved C-terminal, and is already present in cnidarian but less unambiguous.

In summary, the C-terminal hydrophobic cluster from choanoflagellate changes to an acidic cluster in vertebrate, mainly mammalian SPIRE1/2. Additionally, the N-terminal basic residues in the choanoflagellates and cnidaria moved to the middle of the GTBM sequence in mammalian SPIRE1/2.

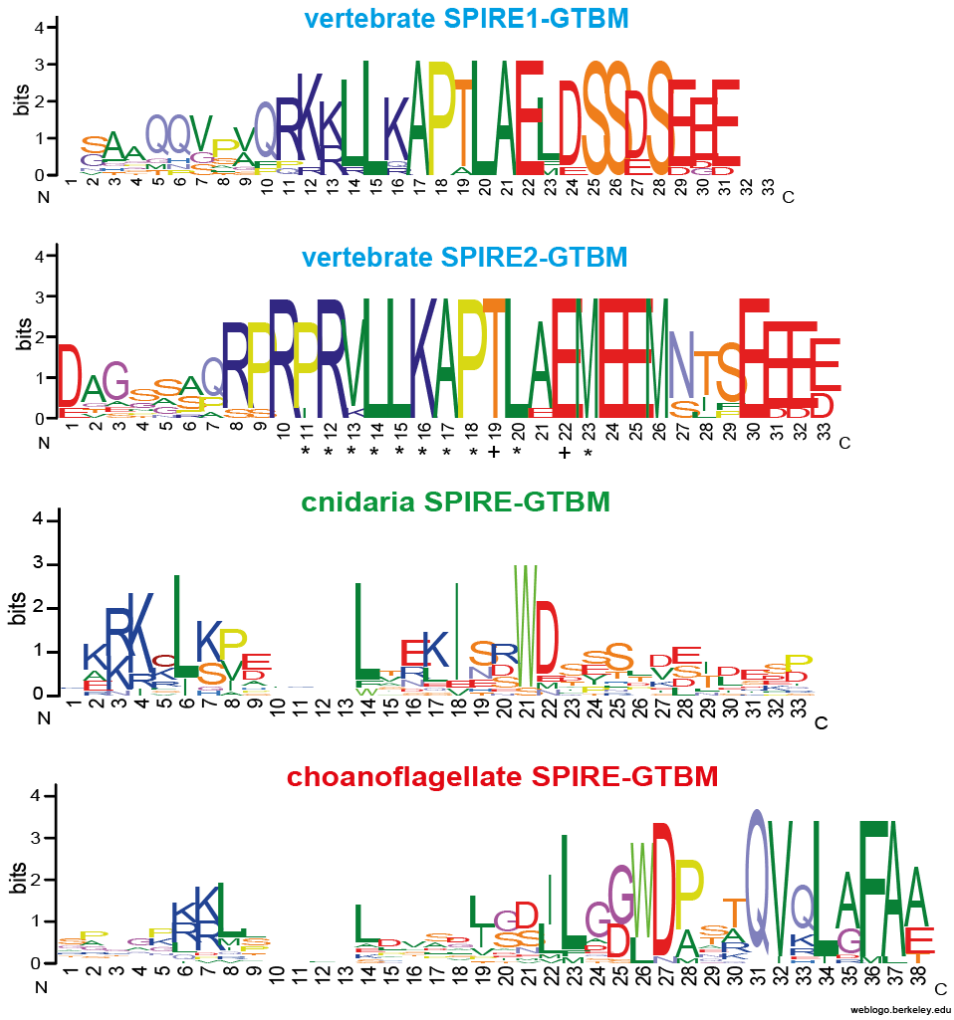

Figure 32: ***The SPIRE GTBM contains highly conserved amino acid clusters with distinct chemical properties****. A multiple protein sequence alignment of the 27 amino acid motif (Kollmar et al., 2024). WebLogos illustrating the amino acid conservation within vertebrate (SPIRE1: 12 sequences; SPIRE2: 10 sequences), cnidarian (13 sequences) and choanoflagellate (18 sequences) all used species see below, residues of SPIRE2 contacting MYO5A within 4Å distance are labelled with '*'; in SPIRE2 exist two conserved residues indicated with '+' stabilise the SPIRE2 conformation (Pylypenko et al., 2016), SPIRE GTBM amino acid sequences generated using weblogo server (weblogo.berkeley.edu) (Crooks et al., 2004). For the vertebrate SPIRE1 weblogo,12 sequences from the following species were used: Homo sapiens, Hs; Panthera leo; Pat; Canis lupus familiares, Caf; Felis catus, Fc; Bos taurus, Bt; Loxodonta africana ,La; Equus caballus, Eqc; Mus musculus; Mm; Brachydanio rerio, Br, A and B isoform; Gallus gallus, Ggg and Xenopus tropicalis, Xt. For the vertebrate SPIRE2 weblogo,10 sequences from the following species were used: Homo sapiens, Hs; Panthera leo; Pat; Felis catus, Fc; Bos taurus, Bt; Loxodonta africana ,La; Equus caballus, Eqc; Mus musculus; Mm; Brachydanio rerio ,Br; Gallus gallus, Ggg and Xenopus tropicalis, Xt. For the cnidarian SPIRE weblogo, 13 sequences from the following species were used: Rhopilema esculentum, Rhes; Hydra magnipapillata, Hm; Hydra oligactis, Hyo; Clytia hemisphaerica, Clh; Podocoryna carnea, Poc; Hydractinia symbiolongicarpus, Hysy; Briareum asbestinum, Bras; Acropora millepora, Acm; Protes australiensis, Poau; Orbicella faveolata, Orfa; Stylophora pistillata, Stp; Nematostella vectensis, Nv and Anthopleura elegantissima, Anel. For the choanoflagellate SPIRE weblogo, 18 sequences from the following species were used: Monosiga brevicollis, Mb; Choanoeca perplexa, Chop; Salpingoeca infusionum, Sinf;* Hartaetosiga gracilis, Hagr; Hartaetosiga balthica, Haba; Salpingoeca rosetta, Sr; Microstomoeca roanoka, Miro; Codosiga hollandica, Codh; Salpingoeca dolichothecata, Sado; Salpingoeca urceolata, Saur; Salpingoeca punica, Spun; Mylnosiga fluctuans, Mvfl; Salpingoeca helianthica, Sahe;

Salpingoeca kvevrii, Sakv; Didymoeca costata, Didc; Stephanoeca diplocostata, Stdi; Diaphanoeca grandis, Digr and Savillea parva, Sapa.

The SPIRE1 and SPIRE2 contain a highly conserved core of five amino acids (LLKAP) in the middle of the GTBM. N-terminal of this core motif the sequence between SPIRE1 and SPIRE2 is less conserved. Three amino acids (PRV) N-terminal of the core in SPIRE2 were identified as interaction sites with MYO5A (Pylypenko et al., 2016). However, these amino acids differ between SPIRE1 and SPIRE2, so this may explain the observed differences in interaction with MYO5A/B/C.

4 Discussion

In this thesis, a possible impact of SPIRE/MYO5 interaction on the differentiation in SPIRE-cell biological functions has been addressed.

Cell biological and biochemical studies on the MYO5/SPIRE interaction during the last decade has revealed partial insights into the underlying molecular mechanisms in the interplay of these two proteins in the intracellular vesicle transport (Welz and Kerkhoff, 2023).

Motor recruitment to specific vesicles plays a crucial role in cellular function and organisation. Targeted recruitment of myosins to vesicles is important for sorting and targeting intracellular cargo within cells. However, the logistics of motor activation can be challenging and vesicle directionality is not well understood. In previous works it could be shown, that SPIRE1 differs in its interaction with various RAB GTPases (Alzahofi et al., 2020; Holthenrich et al., 2022; Lagal et al., 2014; T. Welz), from SPIRE2.

The aim of this thesis was to gain a deeper insight into the protein interaction between MYO5 and SPIRE isoforms. Interactions between the human MYO5 isoforms and SPIRE isoforms were addressed and the affinities of the interactions were measured and compared

4.1 *In silico* RNA expression pattern in humans

Cell biological studies revealed a differentiation of SPIRE1 and SPIRE2 function in melanosome transport and WPB release (Alzahofi et al., 2020; Holthenrich et al., 2022). Using the RNA expression data from the NCBI database, the expression of human SPIRE, MYO5 and FMN genes was analysed to see if SPIRE and it interacting proteins were expressed at similar levels in the distinct tissues.

The advantages of the existing database on RNA expression in different tissues are that it provides the possibility to have a look, if different isoforms of the SPIRE/MYO5/FMN cooperative network are expressed in the same tissue, so interaction partner can be hypothesised.

The RNA expression of the distinct genes was investigated, to make link between already known and suggested SPIRE/FMN/MYO5 isoform protein complexes.

In the mouse brain, a higher expression of *SPIRE1* than *SPIRE2* was observed by (Pleiser et al., 2014; Pleiser et al., 2010; Schumacher et al., 2004). Additionally, (Leader and Leder, 2000) observed a high expression of FMN2 in mouse brain; these detected expression pattern in combination with the high expression of *MYO5A* (Figure 14) gives a hint to a hypothesised protein complex of MYO5A/SPIRE1/FMN2 in neurons. Nevertheless, this observation needs further investigation. However, there are many hints, that this complex plays an important role in the synaptic transmission

or the neuroendocrine system. (Pleiser et al., 2014) could observe in fear-conditioning experiments in mice, that *SPIRE1* mutants show an increased fear-related behaviour. Additionally, a *FMN2*-knock-out mouse has also a fear-related phenotype (Agís-Balboa et al., 2017; Welz and Kerkhoff, 2023) and the loss of FMN2 in human causes intellectual disability (Law et al., 2014). The localisation of FMN2 in neurons (Agís-Balboa et al., 2017) gives a hint, that FMN2 may be involved in a presynaptic vesicle release.

In the skin, the high expression of *SPIRE1*, *MYO5A* and *MYO5B*, shows evidence for the already known protein complex of MYO5A/SPIRE1/FMN1 that is responsible for the melanosome transport in melanocytes (Alzahofi et al., 2020). Therefore, the high expression levels of these genes was not surprising. The also high expression of *MYO5B* could be a hint that there exists another protein SPIRE/MYO5 complex within the melanocytes that may function in distinct vesicle transport processes.

In the small intestine, the expression level of *MYO5B* is the highest, followed by *SPIRE2* and *MYO5C.* These observations are not surprising, the *SPIRE2* expression pattern in the small intestine, was already been shown by (Pleiser et al., 2010). Moreover, the high MYO5B expression makes a link to the existing disease in humans caused by a *MYO5B* mutation, the microvillus inclusion disease (MVID) (Müller et al., 2008). MVID is a life-threatening diarrheal disorder (Müller et al., 2008). In MVID patients nonsense and inactivating mutations and an accompanying loss of function of MYO5B have been identified (Bowman et al., 2022; Hess et al., 2021; Huber, 2016; Müller et al., 2008; Vogel et al., 2016). MYO5B has been identified to interact with SPIRE1 and SPIRE2, which was confirmed in this thesis. The *FMN1* and *FMN2* expression was very low or not detectable at all.

In the thyroid, the high expression levels of *SPIRE1*, *MYO5B* and *MYO5C* give a hint, that this tissue may be similar to the endothelial cells. In the endothelial cells, MYO5C and SPIRE1 build a complex and play a role in WPB release (Holthenrich et al., 2022). These findings can be interesting, because a complex containing MYO5C and SPIRE1 or maybe MYO5B with SPIRE1 can exist and play a similar role in the thyroid, so maybe the release of thyroid hormones. In protein interaction studies performed here, MYO5C also showed a strong interaction with SPIRE2. A possible role of SPIRE and MYO5 interaction in the thyroid gland can be suggest, because *SPIRE2* is also expressed in the thyroid, but not as high as *SPIRE1*. Therefore, further investigations are necessary to gain a deeper understanding of the protein interactions. *FMN1* is expressed; in contrast, *FMN2* was not expressed, so maybe these proteins are not that important in the release process, because there is no movement necessary. In the WPB release FMN1/2 do not show a function, because they are not expressed in the model system (HUVEC cells, human umbilical vein endothelial cells) and the release process functions nevertheless.

In mouse oocytes, the SPIRE1/2/FMN2 organised actin filament mesh derives from cytoplasmic RAB11 vesicles (Pfender et al., 2011; Schuh, 2011). SPIRE 1 and SPIRE2 cooperate with FMN2 to build actin filaments, these filaments serve as tracks to transport the RAB11A vesicles towards the cell cortex via the a long-range transport (Pfender et al., 2011; Schuh, 2011; Welz and Kerkhoff, 2023). For the movement on the new polymerised actin filaments, a model has been proposed in which MYO5B acts in a tripartite with RAB11A and SPIRE1 or SPIRE2 (Welz and Kerkhoff, 2023). Interestingly *MYO5A* is expressed at much higher levels in mouse oocytes than MYO5B yet the RAB11 vesicle transport seems to dependently on MYO5B.
The interaction studies performed here show that SPIRE1 and SPIRE2 interact with MYO5A and MYO5B (Schuh, 2011).

In the pancreas, the high expression levels of *SPIRE1*, *MYO5B* and *MYO5C* give a hint, that this tissue may be also similar to the endothelial cells. In the endothelial cells, MYO5C and SPIRE1 build a complex and play a role in WPB release (Holthenrich et al., 2022). Possibly in the beta-cells of the pancreas MYO5C and SPIRE1 are involved in insulin secretion into the blood.

Maybe a similar release mechanism as shown in the WPB release, building an actin ring like structure between the vesicle membrane and the plasma membrane of the cell organelle, exists in the pancreatic beta-cells and also the thyroid to release insulin or hormones from the organelle into the blood. Because of the low expression levels of *FMN1* and *FMN2* in these two tissues (thyroid, pancreas) the release mechanisms seems to be FMN independent.

Known and suggested protein complexes and their associated cellular functions are shown in the table below (Table 9).

Table 9: Overview on known and suggested protein complexes with their cellular function.

(suggested) protein complex	**(proposed) cellular function**
MYO5A/SPIRE1/FMN1	melanosome transport
MYO5A/SPIRE1/FMN2	presynaptic vesicle release
MYO5B/SPIRE1/2/FMN2	oocytic vesicle transport
MYO5B/SPIRE1/2/FMN?	epithelial development/ apical polarisation
MYO5C/SPIRE1	Weibel-Palade body release
MYO5C/SPIRE1	hormone/ insulin release

4.2 Differentiation of cellular functions of SPIRE1 and SPIRE2

In an earlier study, a difference in the interaction of SPIRE1 and SPIRE2 with RAB-GTPases was observed (done by Dr. Tobias Welz and Dr. Felix Straub; bioRxiv). In GST-pulldowns SPIRE1 was pulled by RAB27A, but not SPIRE2. Thus, one can hypothesise a functional difference between SPIRE1 and SPIRE2, so there are some (sub-)cellular functions specific for SPIRE1 or SPIRE2.

Therefore, in this work, the interaction of the MYO5-GTD-/-cc-GTD isoforms (mammalian MYO5A, MYO5B, MYO5C) with SPIRE1- and SPIRE2-linker/-ΔKW has been investigated using qualitative and quantitative GST-pulldown assays to gain more details of the differentiation of SPIRE1 and SPIRE2 functions. The interaction of all three isoforms of MYO5 with SPIRE1 was weaker and the value of the K_d higher than of the interaction of MYO5 with SPIRE2. The higher dissociation equilibrium constants K_d indicate that the complex of MYO5 with SPIRE1 disassembles faster than the MYO5/SPIRE2 complex.

In melanosome transport, the group of Alistair Hume (Alzahofi et al., 2020) could show, after depleting SPIRE1/2 by siRNA transfection WT melanocytes and rescued them, via infecting the cells with adenoviruses expressing SPIRE1/2. SPIRE1 was almost able to restore the WT equal cytoplasmic dispersion of melanosome in contrast to SPIRE2, which led to hyperdispersion and cortical clustering of the melanosomes.

Another known difference between SPIRE1 and SPIRE2 exists in the release of WPB, where SPIRE2 does not have a function at all, whereas SPIRE1 is involved in the exocytic process (Holthenrich et al., 2022). However, it is also interesting to mention, that in the oocytic vesicle movement, no differences between SPIRE1 and SPIRE2 have been detected (Pylypenko et al., 2016).

In mitochondria, elongation of SPIRE1-assembled actin filaments has been proposed to generate force for mitochondrial division (Welz and Kerkhoff, 2023). The interaction of mitoSPIRE1 with the mitochondrial membrane most likely takes place without the interplay of RAB GTPases, because the mitoSPIRE1 gets integrated in the mitochondrial membrane via sequences encoded by the alternatively spliced exon 13 (Manor et al., 2015). The mitoSPIRE1, as a SPIRE1 isoform contains all the SPIRE1 motifs, so it has the ability to bind to MYO5 and it could be suggested that the mitoSPIRE1 could provide actomyosin structures at mitochondria and therefore could control mitochondrial motility (Welz and Kerkhoff, 2023). RNA interference experiments in cultured *Drosophila* neurons have shown that MYO5 activity opposes microtubule-based axonal transport of mitochondria (Pathak et al., 2010; Welz and Kerkhoff, 2023). To my knowledge at the mitochondria membrane, there is no MYRIP or MLPH localised. A possible MYO5 targeting to mitochondria might therefore be independent of RAB GTPases of other interacting proteins such as MLPH or MYRIP. The presence of MYO5 on mitochondrial membranes would therefore only depend on mitoSPIRE1.

It was observed that in the protein cooperation of MYO5, SPIRE, FMN and RAB-GTPases is often accompanied or supported by cofactors, like the RAB27A effectors MLPH (also known as exophilin-3 or Slac2-a) and MYRIP (also known as exophilin-8 or Slac2-c). The melanosome transport driven by MYO5A and SPIRE1 is MLPH-dependent, which interacts with MYO5A. This can be an explanation, why we observed a weaker interaction between MYO5 and SPIRE1 than with SPIRE2 with MYO5, it seems, that SPIRE1 in melanosome transport does not have to interact that strong with MYO5A, because the cofactor, MLPH contributes to the MYO5A anchoring process. Protein interaction studies suggest that in the case of SPIRE1, MYO5A is indirectly targeted to RAB GTPases, whereas with SPIRE2, MYO5 is directly targeted to RAB GTPases, i.e. by RAB11 which directly interact with MYO5B in oocytic vesicle movement. The two different targeting mechanisms (indirect + MLPH; and direct – MLPH) is shown in the figure below (Figure 33).

Cnidaria and choanoflagellate do not have MLPH or MYRIP, so they do not express these co-factors and the interaction has to go the way of direct targeting of SPIRE and MYO5 and RAB-GTPases. This could also explain, why the investigated interaction of SPIRE and MYO5 in cnidaria (*Nematostella vectensis*) and choanoflagellates (*Salpingoeca rosetta*) resemble in strength to the MYO5/SPIRE2 interactions. Also in choanoflagellates, where SPIRE is suggested to be involved in intracellular transport processes to the apical pole in collaboration with MYO5 and RAB8 (Kollmar et al., 2024). Choanoflagellate SPIRE shows a stronger interaction with MYO5 than it was observed for mammalian SPIRE1/MYO5. Therefore, the SPIRE in vertebrate seems to have evolved from the ancient SPIRE/RAB8 pathway to the more specialised mammalian SPIRE1/RAB27 pathway, which requires the MLPH or MYRIP co-factors for its function in exocytic transport.

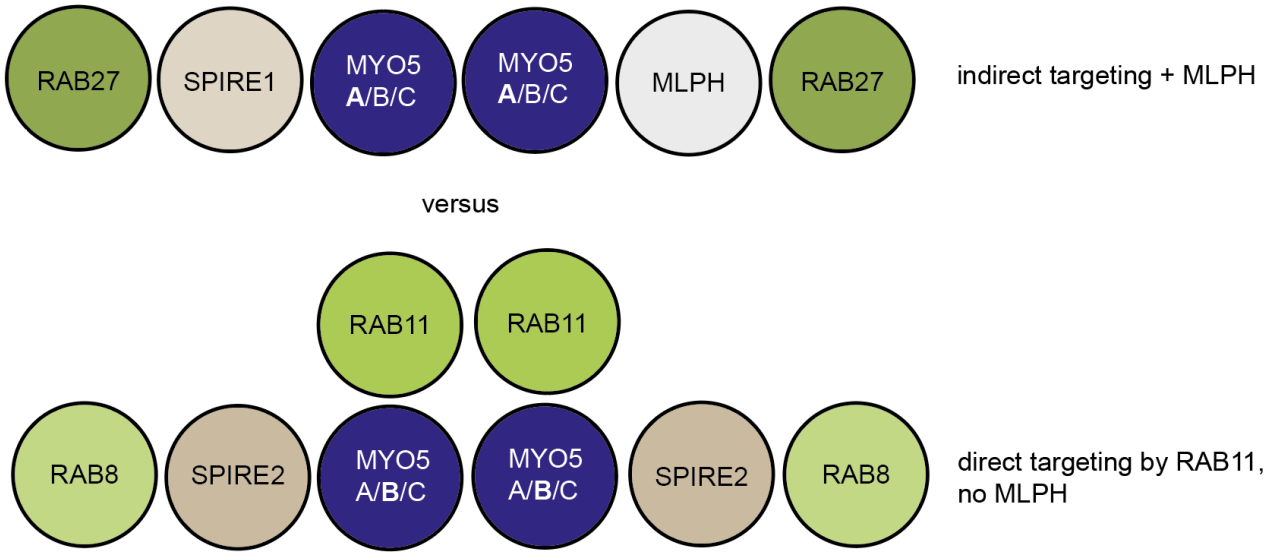

*Figure 33:**Schematic representation of the indirect targeting with MLPH compared to the direct targeting by RAB11 without MLPH** (grey). MYO5 (purple) interacts with RAB27 (green) indirectly via a co-factor, namely MLPH or SPIRE1 (taupe) (upper row), whereas in the direct targeting, MYO5 interacts directly with RAB11 (green) and via SPIRE2 (darker taupe) with RAB8, without MLPH (lower row). MLPH, melanophilin.*

Because of the different interactions of MYO5 isoforms and SPIRE1/2 proteins, the protein sequences of metazoan SPIRE-GTBM and MYO5-GTD-interaction motifs were aligned to have a look if there are differences. Some of the amino acids in the GTBM are conserved throughout evolution. A motif of 26 amino acids in the middle part of the SPIRE2-linker region was identified (Pylypenko et al., 2016), but the characteristics of the amino acids next to this motif are different. The different amino acid characteristics can be an explanation for the different binding strengths between MYO5 and SPIRE1/2 proteins. (Kollmar et al., 2024) have predicted a second helix at the C-terminal end of the GTBM motif in *Monosiga brevicollis* that can lead to changes in the protein folding.

4.3 Colocalisation studies of MYO5-cc-GTD with SPIRE1 and SPIRE2

Despite the measured differences in dissociation equilibrium constants of SPIRE1 compared to SPIRE2 interaction with MYO5A/B/C, the colocalisation experiments do not show a difference in the cellular context. The results of the colocalisation studies of the mammalian SPIRE-ΔKW and MYO5-cc-GTD proteins performed in HeLa cells showed a similar colocalisation of all three MYO5 isoforms with both SPIRE proteins. These results suggest that the vesicle membrane localisation of SPIRE and MYO5 proteins is a more complex mechanism, which is next to the direct interaction of SPIRE and MYO5 influenced by other co-factors such as RAB GTPases and MLPH/MYRIP proteins (Figure 33).

Regarding the different interactions of SPIRE1 and SPIRE2 and different expression levels in tissues, it will be important to analyse the expression levels of the different co-factors in detail for the distinct cell biological mechanisms SPIRE1 and SPIRE2 are involved.

Further crystallisation studies of MYO5 with SPIRE1 and SPIRE2 are necessary in order to make more precise statements with regard to the differences observed in the MYO5/SPIRE interaction. In order to place the measured dissociation constants in a larger framework, the interaction between MYO5 and SPIRE must be measured using a further method and correlated with the previous results.

5 References

Agís-Balboa, R. C., Pinheiro, P. S., Rebola, N., Kerimoglu, C., Benito, E., Gertig, M., Bahari-Javan, S., Jain, G., Burkhardt, S., Delalle, I., Jatzko, A., Dettenhofer, M., Zunszain, P. A., Schmitt, A., Falkai, P., Pape, J. C., Binder, E. B., Mulle, C., Fischer, A., & Sananbenesi, F. (2017). Formin 2 links neuropsychiatric phenotypes at young age to an increased risk for dementia. The EMBO Journal, 36(19), 2815–2828. https://doi.org/10.15252/embj.201796821

Ali, M., Lu, H [H.], Bookwalter, C., Warshaw, D., & Trybus, K. (2008). Myosin V and Kinesin act as tethers to enhance. *PNAS*. 10.1073/pnas.0711531105

Altschul, S., Madden, T., Schäffer, A., Zhang, J [J.], Zhang, Z., Miller, W., & Lipman, D. (1997). Gapped BLAST and PSI-BLAST a new generation of protein database search programs. *Nucleic Acids*.

Alzahofi, N., Welz, T [Tobias], Robinson, C. L., Page, E. L., Briggs, D. A., Stainthorp, A. K., Reekes, J., Elbe, D. A., Straub, F., Kallemeijn, W. W., Tate, E. W., Goff, P. S., Sviderskaya, E. V., Cantero, M., Montoliu, L., Nedelec, F., Miles, A. K., Bailly, M., Kerkhoff, E [Eugen], & Hume, A. N. (2020). Rab27a co-ordinates actin-dependent transport by controlling organelle-associated motors and track assembly proteins. *Nature Communications*, *11*(1), 3495. https://doi.org/10.1038/s41467-020-17212-6

Berg, J., Powell, B., & Cheney, R. (2001). A Millennial Myosin Census. *Molecular Biology of the Cell*(12), 780–794. 10.1091/mbc.12.4.780

Bhabha, G., Johnson, G. T., Schroeder, C. M., & Vale, R. D. (2016). How Dynein Moves Along Microtubules. *Trends in Biochemical Sciences*, *41*(1), 94–105. https://doi.org/10.1016/j.tibs.2015.11.004

Blanchoin, L., Boujemaa-Paterski, R., Sykes, C., & Plastino, J. (2014). Actin Dynamics, Architecture, and Mechanics in Cell Motility. *Physiological Reviews*, *94*(1), 235–263. https://doi.org/10.1152/physrev.00018.2013

Bonfanti, R., Furie, B. C., Furie, B., & Wagner, D. D. (1989). PADGEM (GMP140) is a component of Weibel-Palade bodies of human endothelial cells. *Blood*, *73*(5), 1109–1112. https://doi.org/10.1182/blood.V73.5.1109.1109

Bos, J. L., Rehmann, H., & Wittinghofer, A. (2007). Gefs and GAPs: Critical elements in the control of small G proteins. *Cell*, *129*(5), 865–877. https://doi.org/10.1016/j.cell.2007.05.018

Bowman, D. M., Kaji, I., & Goldenring, J. R. (2022). Altered MYO5B Function Underlies Microvillus Inclusion Disease: Opportunities for Intervention at a Cellular Level. *Cellular and Molecular Gastroenterology and Hepatology*, *14*(3), 553–565. https://doi.org/10.1016/j.jcmgh.2022.04.015

Brunet and King (2017). The Origin of Animal Multicellularity and Cell Differentiation. *Developmental Cell*, *43*(2), 124–140. https://doi.org/10.1016/j.devcel.2017.09.016

Bultema, J. J., Boyle, J. A., Malenke, P. B., Martin, F. E., Dell'Angelica, E. C., Cheney, R. E., & Di Pietro, S. M. (2014). Myosin Vc Interacts with Rab32 and Rab38 Proteins and Works in the Biogenesis and Secretion of Melanosomes. *Journal of Biological Chemistry*, *289*(48), 33513–33528. https://doi.org/10.1074/jbc.M114.578948

Burkhardt, P. (2015). The origin and evolution of synaptic proteins- choanoflagellates lead the way. *The Journal of Experimental Biology*, *218*(Pt 4), 506–514. https://doi.org/10.1242/jeb.110247

Burkhardt, P., Grønborg, M., McDonald, K., Sulur, T., Wang, Q., & King, N [Nicole] (2014). Evolutionary insights into premetazoan functions of the neuronal protein homer. *Molecular Biology and Evolution*, *31*(9), 2342–2355. https://doi.org/10.1093/molbev/msu178

Burkhardt, P., Stegmann, C. M., Cooper, B., Kloepper, T. H., Imig, C., Varoqueaux, F., Wahl, M. C., & Fasshauer, D [Dirk] (2011). Primordial neurosecretory apparatus identified in the choanoflagellate Monosiga brevicollis. *Proceedings of the National Academy of Sciences of the United States of America*, *108*(37), 15264–15269. https://doi.org/10.1073/pnas.1106189108

Carr, M., Leadbeater, B., Hassan, R., Nelson, M., & Baldauf, S. (2008). Melocular phylogeny of choanoflagellates, the sister group of Metazoa. *PNAS*, *105*(43). 10.1073/pnas.0801667105

Cheney, R., O'Shea, M., Heuser, J., Coelho, M., Wolenski, J., Espreafico, E., Forscher, P., Larson, R. E., & Mooseker, M. (1993). Brain Myosin-V Is a Two-Headed Unconventional Myosin with Motor Activity. *Cell*(75). 10.1016/S0092-8674(05)80080-7

Chenna, R., Sugawara, H., Koike, T., Lopez, R., Gibson, T. J., Higgins, D. G., & Thompson, J. D. (2003). Multiple sequence alignment with the Clustal series of programs. *Nucleic Acids Research*, *31*(13), 3497–3500. https://doi.org/10.1093/nar/gkg500

Clamp, M., Cuff, J., Searle, S. M., & Barton, G. J. (2004). The Jalview Java alignment editor. *Bioinformatics (Oxford, England)*, *20*(3), 426–427. https://doi.org/10.1093/bioinformatics/btg430

Clark (1866). Conclusive proofs of the animality of the ciliate sponges and of their affinities with the infusoria flagellata. *American Journal of Science*. https://doi.org/10.2475/ajs.s2-42.126.320

Conte, I. L., Hellen, N., Bierings, R., Mashanov, G. I., Manneville, J.-B., Kiskin, N. I., Hannah, M. J., Molloy, J. E., & Carter, T. (2016). Interaction between MyRIP and the actin cytoskeleton regulates Weibel-Palade body trafficking and exocytosis. *Journal of Cell Science*, *129*(3), 592–603. https://doi.org/10.1242/jcs.178285

Conway, L., Wood, D., Tüzel, E., & Ross, J. L. (2012). Motor transport of self-assembled cargos in crowded environments. *Proceedings of the National Academy of Sciences*, *109*(51), 20814–20819. https://doi.org/10.1073/pnas.1209304109

Correia, S. S., Bassani, S., Brown, T. C., Lisé, M.-F., Backos, D. S., El-Husseini, A., Passafaro, M., & Esteban, J. A. (2008). Motor protein-dependent transport of AMPA receptors into spines during long-term potentiation. *Nature Neuroscience*, *11*(4), 457–466. https://doi.org/10.1038/nn2063

Costes, S. V., Daelemans, D., Cho, E. H., Dobbin, Z., Pavlakis, G., & Lockett, S. (2004). Automatic and quantitative measurement of protein-protein colocalization in live cells. *Biophysical Journal*, *86*(6), 3993–4003. https://doi.org/10.1529/biophysj.103.038422

Crooks, G., Hon, G., Chandonia, J.-M., & Brenner, S. (2004). WebLogo: a sequence logo generator. *Genome Research*. 10.1101/gr.849004

Dagenbach and Endow (2004). A new kinesin tree. *Journal of Cell Science*, *117*(Pt 1), 3–7. https://doi.org/10.1242/jcs.00875

Dahlgaard, K., Raposo, A. A. S. F., Niccoli, T., & St Johnston, D. (2007). Capu and Spire assemble a cytoplasmic actin mesh that maintains microtubule organization in the Drosophila oocyte. *Developmental Cell*, *13*(4), 539–553. https://doi.org/10.1016/j.devcel.2007.09.003

Dominguez, R. (2009). Actin filament nucleation and elongation factors--structure-function relationships. *Critical Reviews in Biochemistry and Molecular Biology*, *44*(6), 351–366. https://doi.org/10.3109/10409230903277340

Dominguez, R. (2016). The WH2 Domain and Actin Nucleation: Necessary but Insufficient. *Trends in Biochemical Sciences*, *41*(6), 478–490. https://doi.org/10.1016/j.tibs.2016.03.004

Espreafico, E., Cheney, R., Matteoli, M., Nascimento, A., Camilli, P. de, Larson, R. E., & Mooseker, M. (1992). Primary Structure and Cellular Localization of Chicken Brain Myosin-V (p190), an Unconventional Myosin with Calmodulin Light Chains. *Journal of Cell Biology*, *119*. 10.1083/jcb.119.6.1541

Fujii, T., Iwane, A. H., Yanagida, T., & Namba, K. (2010). Direct visualization of secondary structures of F-actin by electron cryomicroscopy. *Nature*, *467*(7316), 724–728. https://doi.org/10.1038/nature09372

Fukuda, M. (2008). Regulation of secretory vesicle traffic by Rab small GTPases. *Cellular and Molecular Life Sciences : CMLS*, *65*(18), 2801–2813. https://doi.org/10.1007/s00018-008-8351-4

Geething and Spudich (2007). Identification of a minimal myosin Va binding site within an intrinsically unstructured domain of melanophilin. *The Journal of Biological Chemistry*, *282*(29), 21518–21528. https://doi.org/10.1074/jbc.M701932200

Göhde, R., Naumann, B., Laundon, D., Imig, C., McDonald, K., Cooper, B. H., Varoqueaux, F., Fasshauer, D [Dirk], & Burkhardt, P. (2021). Choanoflagellates and the ancestry of neurosecretory vesicles. *Philosophical Transactions of the Royal Society of London. Series B, Biological Sciences*, *376*(1821), 20190759. https://doi.org/10.1098/rstb.2019.0759

Goley and Welch (2006). The ARP2/3 complex: An actin nucleator comes of age. *Nature Reviews. Molecular Cell Biology*, *7*(10), 713–726. https://doi.org/10.1038/nrm2026

Goligorsky, M. S., Patschan, D., & Kuo, M.-C. (2009). Weibel-Palade bodies--sentinels of acute stress. *Nature Reviews. Nephrology*, *5*(7), 423–426. https://doi.org/10.1038/nrneph.2009.87

Gross, S. P., Tuma, M. C., Deacon, S. W., Serpinskaya, A. S., Reilein, A. R., & Gelfand, V. I. (2002). Interactions and regulation of molecular motors in Xenopus melanophores. *The Journal of Cell Biology*, *156*(5), 855–865. https://doi.org/10.1083/jcb.200105055

Hammer and Sellers (2012). Walking to work: Roles for class V myosins as cargo transporters. *Nature Reviews. Molecular Cell Biology*, *13*(1), 13–26. https://doi.org/10.1038/nrm3248

Hammer and Wagner (2013). Functions of class V myosins in neurons. *The Journal of Biological Chemistry*, *288*(40), 28428–28434. https://doi.org/10.1074/jbc.R113.514497

Hariadi, R. F., Cale, M., & Sivaramakrishnan, S. (2014). Myosin lever arm directs collective motion on cellular actin network. *Proceedings of the National Academy of Sciences*, *111*(11), 4091–4096. https://doi.org/10.1073/pnas.1315923111

Hess, M. W., Krainer, I. M., Filipek, P. A., Witting, B., Gutleben, K., Vietor, I., Zoller, H., Aldrian, D., Sturm, E., Goldenring, J. R., Janecke, A. R., Müller, T., Huber, L. A., & Vogel, G. F. (2021). Advanced Microscopy for Liver and Gut Ultrastructural Pathology in Patients with MVID and PFIC Caused by MYO5B Mutations. *Journal of Clinical Medicine*, *10*(9). https://doi.org/10.3390/jcm10091901

Hirokawa, N., Noda, Y., Tanaka, Y., & Niwa, S. (2009). Kinesin superfamily motor proteins and intracellular transport. *Nature Reviews. Molecular Cell Biology*, *10*(10), 682–696. https://doi.org/10.1038/nrm2774

Hódi, Z., Németh, A. L., Radnai, L., Hetényi, C., Schlett, K., Bodor, A., Perczel, A., & Nyitray, L. (2006). Alternatively spliced exon B of myosin Va is essential for binding the tail-associated light chain shared by dynein. *Biochemistry*, *45*(41), 12582–12595. https://doi.org/10.1021/bi060991e

Holmes, K., Popp, D, Gebhard, W., & Kabsch, W. (1990). Atomic model of the actin filament. *Nature*, *347*. 10.1038/347044a0

Holthenrich, A., Drexler, H., Chehab, T., Naß, J [J.], & Gerke, V [V.] (2019). Proximity proteomics of endothelial Weibel-Palade bodies. *Blood*. 10.1182/blood.2019000786

Holthenrich, A., Terglane, J., Naß, J [Johannes], Mietkowska, M., Kerkhoff, E [Eugen], & Gerke, V [Volker] (2022). Spire1 and Myosin Vc promote Ca2+-evoked externalization of von Willebrand factor in endothelial cells. *Cellular and Molecular Life Sciences : CMLS*, *79*(2), 96. https://doi.org/10.1007/s00018-021-04108-x

Huang, J., Mermall, V., Strobel, M., Russell, L., Mooseker, M., Copeland, N. G., & Jenkins, N. A. (1998). Molecular Genetic Dissection of Mouse Unconventional Myosin-V _ Tail Region Mutations. *Genetics*(148). 10.1093/genetics/148.4.1963

Huber, L. A. (2016). New Mouse Models for Microvillus Inclusion Disease (MVID): Where Do the Inclusions Come From and Are They Cause or Consequence? *Cellular and Molecular Gastroenterology and Hepatology*, *2*(2), 112–113. https://doi.org/10.1016/j.jcmgh.2015.12.012

Hume, A. N., Collinson, L. M., Hopkins, C. R., Strom, M., Barral, D. C., Bossi, G., Griffiths, G. M., & Seabra, M. C. (2002). The leaden gene product is required with Rab27a to recruit myosin Va to melanosomes in melanocytes. *Traffic (Copenhagen, Denmark)*, *3*(3), 193–202. https://doi.org/10.1034/j.1600-0854.2002.030305.x

Hume and Seabra (2011). Melanosomes on the move: A model to understand organelle dynamics. *Biochemical Society Transactions*, *39*(5), 1191–1196. https://doi.org/10.1042/BST0391191

Jahn, R [R.], and, & and T C Sudhof (1994). Synaptic Vesicles and Exocytosis. *Neuroscience*.

Kerkhoff, E [E.], Simpson, J., Leberfinger, C., Otto, I., Doerks, T., Bork, P [P.], RApp, U., Raabe, T., & Pepperkok, R. (2001). The Spir actin organizers are involved in vesicle transport processes. *Brief Communication*. 10.1016/s0960-9822(01)00602-9

Kerkhoff, E [Eugen] (2006). Cellular functions of the Spir actin-nucleation factors. *Trends in Cell Biology*, *16*(9), 477–483. https://doi.org/10.1016/j.tcb.2006.07.005

King, N [N.], Westbrook, M. J., Young, S. L., Kuo, A., Abedin, M., Chapman, J., Fairclough, S., Hellsten, U., Isogai, Y., Letunic, I., Marr, M., Pincus, D., Putnam, N., Rokas, A., Wright, K. J., Zuzow, R., Dirks, W., Good, M., Goodstein, D., . . . Rokhsar, D. (2004). The unicellular ancestry of animal development. *Developmental Cell*, *7*(3), 313–325. https://doi.org/10.1016/j.devcel.2004.08.010

King, N [Nicole], Westbrook, M. J., Young, S. L., Kuo, A., Abedin, M., Chapman, J., Fairclough, S., Hellsten, U., Isogai, Y., Letunic, I., Marr, M., Pincus, D., Putnam, N., Rokas, A., Wright, K. J., Zuzow, R., Dirks, W., Good, M., Goodstein, D., . . . Rokhsar, D. (2008). The genome of the choanoflagellate Monosiga brevicollis and the origin of metazoans. *Nature*, *451*(7180), 783–788. https://doi.org/10.1038/nature06617

Klöpper, T., Kienle, N., Fasshauer, D [D.], & Munro, S. (2012). Untangling the evolution of Rab G proteins: implications of a comprehensive genomic analysis. *BMC Biology*(10). 10.1186/1741-7007-10-71

Klumpp and Lipowsky (2005). Cooperative cargo transport by several molecular motors. *PNAS*.

Kneussel, M., & Wagner, W. (2013). Myosin motors at neuronal synapses: Drivers of membrane transport and actin dynamics. *Nature Reviews. Neuroscience*, *14*(4), 233–247. https://doi.org/10.1038/nrn3445

Kollmar, M., Welz, T [Tobias], Ravi, A., Kaufmann, T., Alzahofi, N., Hatje, K., Alghamdi, A., Kim, J., Briggs, D. A., Samol-Wolf, A., Pylypenko, O., Hume, A. N., Burkhardt, P., Faix, J., & Kerkhoff, E [Eugen] (2024). Actomyosin organelle functions of SPIRE actin nucleators precede animal evolution. *Communications Biology*, *7*(1), 832. https://doi.org/10.1038/s42003-024-06458-1

Kollmar, M., Welz, T [Tobias], Straub, F., Alzahofi, N., Hatje, K., Briggs, D. A., Samol-Wolf, A., Burkhardt, P., Hume, A., & Kerkhoff, E [Eugen] (2019). Animal evolution coincides with a novel degree of freedom in exocytic transport processes. *BioRxiv : The Preprint Server for Biology*. Advance online publication. https://doi.org/10.1101/591974

Korobova, F., Ramabhadran, V., & Higgs, H. (2013). An Actin-Dependent Step in Mitochondrial Fission Mediated by the ER-Associated Formin INF2. *Science (New York, N.Y.)*, *339*(6118), 460–464. https://doi.org/10.1126/science.1227299

Krementsov, D. N., Krementsova, E. B., & Trybus, K. M. (2004). Myosin V: Regulation by calcium, calmodulin, and the tail domain. *The Journal of Cell Biology*, *164*(6), 877–886. https://doi.org/10.1083/jcb.200310065

Lagal, V., Abrivard, M., Gonzalez, V., Perazzi, A., Popli, S., Verzeroli, E., & Tardieux, I. (2014). Spire-1 contributes to the invadosome and its associated invasive properties. *Journal of Cell Science*, *127*(Pt 2), 328–340. https://doi.org/10.1242/jcs.130161

Lambert, J., et al. (1998). Human Myosin V Gene Produces Different Transcripts in a Cell Type-Specific Manner. *Biochemical and Biophysical Research Communications*(252). 10.1006/bbrc.1998.9644

Lang, B., O'Kelly, C., Nerad, T., Gray, M., & Burger, G [G.] (2002). The Closest Unicellular Relatives of Animals. *Current Biology : CB*. 10.1016/s0960-9822(02)01187-9

Langford, G. (1995). Actin- and microtubule-dependent organelle motors: interrelationships between the two motility systems. *Current Opinion in Cell Biology*, *7*.

Law, R., Dixon-Salazar, T., Jerber, J., Cai, N., Abbasi, A. A., Zaki, M. S., Mittal, K., Gabriel, S. B., Rafiq, M. A., Khan, V., Nguyen, M., Ali, G., Copeland, B., Scott, E., Vasli, N., Mikhailov, A., Khan, M. N., Andrade, D. M., Ayaz, M., . . . Gleeson, J. G. (2014). Biallelic truncating mutations in FMN2, encoding the actin-regulatory protein Formin 2, cause nonsyndromic autosomal-recessive intellectual disability. *American Journal of Human Genetics*, *95*(6), 721–728. https://doi.org/10.1016/j.ajhg.2014.10.016

Leader and Leder (2000). Formin-2, a novel formin homology protein of the cappuccino subfamily, is highly expressed in the developing and adult central nervous system. *Mechanisms of Development.* Advance online publication. https://doi.org/10.7554/eLife.49030.001

Li, X.-D., Mabuchi, K., Ikebe, R., & Ikebe, M. (2004). Ca2+-induced activation of ATPase activity of myosin Va is accompanied with a large conformational change. *Biochemical and Biophysical Research Communications*, *315*(3), 538–545. https://doi.org/10.1016/j.bbrc.2004.01.084

Lindsay, A., Jollivet, F., Horgran, C., Khan, A., Raposo, G., McCaffrey, M., & Goud, B [B.] (2013). Identification and characterization of multiple novel RAB-myosin Va interactions. *Molecular Biology of the Cell*. 10.1091/mbc.E13-05-0236

Lisé, M.-F., Wong, T. P., Trinh, A., Hines, R. M., Liu, L., Kang, R., Hines, D. J., Lu, J [Jie], Goldenring, J. R., Wang, Y. T., & El-Husseini, A. (2006). Involvement of myosin Vb in glutamate receptor trafficking. *The Journal of Biological Chemistry*, *281*(6), 3669–3678. https://doi.org/10.1074/jbc.M511725200

Lu, H [Hailong], Krementsova, E. B., & Trybus, K. M. (2006). Regulation of Myosin V Processivity by Calcium at the Single Molecule Level. *Journal of Biological Chemistry*, *281*(42), 31987–31994. https://doi.org/10.1016/S0021-9258(19)84112-1

Manor, U., Bartholomew, S., Golani, G., Christenson, E., Kozlov, M., Higgs, H., Spudich, J., & Lippincott-Schwartz, J. (2015). A mitochondria-anchored isoform of the actin-nucleating spire protein regulates mitochondrial division. *ELife*.

Martin-Belmonte and Perez-Moreno (2012). Epithelial cell polarity, stem cells and cancer. *Nature Reviews Cancer*, *12*(1), 23–38. https://doi.org/10.1038/nrc3169

McCormack, J. J., Da Lopes Silva, M., Ferraro, F., Patella, F., & Cutler, D. F. (2017). Weibel-Palade bodies at a glance. *Journal of Cell Science*, *130*(21), 3611–3617. https://doi.org/10.1242/jcs.208033

McEver, R. P., Beckstead, J. H., Moore, K. L., Marshall-Carlson, L., & Bainton, D. F. (1989). Gmp-140, a platelet alpha-granule membrane protein, is also synthesized by vascular endothelial cells and is localized in Weibel-Palade bodies. *The Journal of Clinical Investigation*, *84*(1), 92–99. https://doi.org/10.1172/JCI114175

Mercer, J., Seperack, P., Stroble, M., Copeland, N. G., & Jenkins, N. A. (1991). Novel myosin heavy chain encoded by murine dilute coat colour locus. *Nature*, *349*. 10.1038/349709a0

Miki, H., Okada, Y., & Hirokawa, N. (2005). Analysis of the kinesin superfamily: Insights into structure and function. *Trends in Cell Biology*(9), 467–476. https://doi.org/10.1016/j.tcb.2005.07.006

Millard and Martin (2008). Dynamic analysis of filopodial interactions during the zippering phase of Drosophila dorsal closure. *Development (Cambridge, England)*, *135*(4), 621–626. https://doi.org/10.1242/dev.014001

Müller, T., Hess, M. W., Schiefermeier, N., Pfaller, K., Ebner, H. L., Heinz-Erian, P., Ponstingl, H., Partsch, J., Röllinghoff, B., Köhler, H., Berger, T., Lenhartz, H., Schlenck, B., Houwen, R. J., Taylor, C. J., Zoller, H., Lechner, S., Goulet, O., Utermann, G., . . . Janecke, A. R. (2008). Myo5b mutations cause microvillus inclusion disease and disrupt epithelial cell polarity. *Nature Genetics*, *40*(10), 1163–1165. https://doi.org/10.1038/ng.225

Müller and Goody (2018). Molecular control of Rab activity by GEFs, GAPs and GDI. *Small GTPases*, *9*(1-2), 5–21. https://doi.org/10.1080/21541248.2016.1276999

Nascimento, A., Amaral, R., Bizario, J., Larson, R. E., & Espreafico, E. (1997). Subcellular Localization of Myosin-V in the B16. *Molecular Biology of the Cell*.

Nelson, S. R., Trybus, K. M., & Warshaw, D. M. (2014). Motor coupling through lipid membranes enhances transport velocities for ensembles of myosin Va. *Proceedings of the National Academy of Sciences of the United States of America*, *111*(38), E3986-95. https://doi.org/10.1073/pnas.1406535111

Nightingale, T., Pattni, K., Hume, A [A.], Seabra, M. C., & Cutler, D. F. (2009). Rab27a and MyRIP regulate the amount and multimeric state of VWF released from endothelial cells. *Blood*. 10.1182/blood-2008-09-181206

Nightingale and Cutler (2013). The secretion of von Willebrand factor from endothelial cells; an increasingly complicated story. *Journal of Thrombosis and Haemostasis : JTH*, *11 Suppl 1*(Suppl 1), 192–201. https://doi.org/10.1111/jth.12225

Oda, T., Iwasa, M., Aihara, T., Maéda, Y., & Narita, A. (2009). The nature of the globular- to fibrous-actin transition. *Nature*, *457*(7228), 441–445. https://doi.org/10.1038/nature07685

Odronitz and Kollmar (2006). Pfarao: A web application for protein family analysis customized for cytoskeletal and motor proteins (CyMoBase). *BMC Genomics*, *7*, 300. https://doi.org/10.1186/1471-2164-7-300

Odronitz and Kollmar (2007). Drawing the tree of eukaryotic life based on the analysis of 2,269 manually annotated myosins from 328 species. *Genome Biology*. 10.1186/gb-2007-8-9-r196

Otomo, T., Tomchick, D., Otomo, C., Panchal, S., Machius, M., & Rosen, M. (2005). Structural basis of actin filament nucleation and processive capping by a formin homology 2 domain. *Nature*.

Pantaloni and Carlier (1993). Dominique Pantaloni How profilin promotes actin filament assembly in the presence of thymosin β4. *Cell*. https://doi.org/10.1016/0092-8674(93)90544-Z

Pathak, D., Sepp, K. J., & Hollenbeck, P. J. (2010). Evidence that myosin activity opposes microtubule-based axonal transport of mitochondria. *The Journal of Neuroscience : The Official Journal of the Society for Neuroscience*, *30*(26), 8984–8992. https://doi.org/10.1523/JNEUROSCI.1621-10.2010

Pavlos, N. J., Grønborg, M., Riedel, D., Chua, J. J. E., Boyken, J., Kloepper, T. H., Urlaub, H., Rizzoli, S. O., & Jahn, R [Reinhard] (2010). Quantitative analysis of synaptic vesicle Rabs uncovers distinct yet overlapping roles for Rab3a and Rab27b in Ca2+-triggered exocytosis. *The Journal of Neuroscience : The Official Journal of the Society for Neuroscience*, *30*(40), 13441–13453. https://doi.org/10.1523/JNEUROSCI.0907-10.2010

Pechlivanis, M., Samol, A., & Kerkhoff, E [Eugen] (2009). Identification of a short Spir interaction sequence at the C-terminal end of formin subgroup proteins. *The Journal of Biological Chemistry*, *284*(37), 25324–25333. https://doi.org/10.1074/jbc.M109.030320

Pfeffer, S. R. (2005). Structural clues to Rab GTPase functional diversity. *The Journal of Biological Chemistry*, *280*(16), 15485–15488. https://doi.org/10.1074/jbc.R500003200

Pfender, S., Kuznetsov, V., Pleiser, S., Kerkhoff, E [Eugen], & Schuh, M. (2011). Spire-type actin nucleators cooperate with Formin-2 to drive asymmetric oocyte division. *Current Biology : CB*, *21*(11), 955–960. https://doi.org/10.1016/j.cub.2011.04.029

Pleiser, S., Banchaabouchi, M. A., Samol-Wolf, A., Farley, D., Welz, T [Tobias], Wellbourne-Wood, J., Gehring, I., Linkner, J., Faix, J., Riemenschneider, M. J., Dietrich, S., & Kerkhoff, E [Eugen] (2014). Enhanced fear expression in Spir-1 actin organizer mutant mice. *European Journal of Cell Biology*, *93*(5-6), 225–237. https://doi.org/10.1016/j.ejcb.2013.11.001

Pleiser, S., Rock, R., Wellmann, J., Gessler, M., & Kerkhoff, E [Eugen] (2010). Expression patterns of the mouse Spir-2 actin nucleator. *Gene Expression Patterns : GEP*, *10*(7-8), 345–350. https://doi.org/10.1016/j.gep.2010.08.001

Pollard, T. D. (2007). Regulation of actin filament assembly by Arp2/3 complex and formins. *Annual Review of Biophysics and Biomolecular Structure*, *36*, 451–477. https://doi.org/10.1146/annurev.biophys.35.040405.101936

Pollard, T. D. (2010). A guide to simple and informative binding assays. *Molecular Biology of the Cell*, *21*(23), 4061–4067. https://doi.org/10.1091/mbc.E10-08-0683

Pollard, T. D. (2016). Actin and Actin-Binding Proteins. *Cold Spring Harbor Perspectives in Biology*, *8*(8). https://doi.org/10.1101/cshperspect.a018226

Pollard and Beltzner (2002). Structure and function of the Arp2/3 complex. *Current Biology in Structural Biology*.

Pollard and Cooper (2009). Actin, a central player in cell shape and movement. *Science (New York, N.Y.)*, *326*(5957), 1208–1212. https://doi.org/10.1126/science.1175862

Pompey, S. N., Michaely, P., & Luby-Phelps, K. (2013). Quantitative fluorescence co-localization to study protein-receptor complexes. *Methods in Molecular Biology (Clifton, N.J.)*, *1008*, 439–453. https://doi.org/10.1007/978-1-62703-398-5_16

Provance, D. (1999). Myosin-V head to tail. *Cellular and Molecular Life Sciences : CMLS*(56). 10.1007/s000180050425

Pylypenko, O., Attanda, W., Gauquelin, C., Lahmani, M., Coulibaly, D., Baron, B., Hoos, S., Titus, M. A., England, P., & Houdusse, A. M. (2013). Structural basis of myosin V Rab GTPase-dependent cargo recognition. *Proceedings of the National Academy of Sciences of the United States of America*, *110*(51), 20443–20448. https://doi.org/10.1073/pnas.1314329110

Pylypenko, O., Welz, T [Tobias], Tittel, J., Kollmar, M., Chardon, F., Malherbe, G., Weiss, S., Michel, C. I. L., Samol-Wolf, A., Grasskamp, A. T., Hume, A., Goud, B [Bruno], Baron, B., England, P., Titus, M. A., Schwille, P., Weidemann, T., Houdusse, A., & Kerkhoff, E [Eugen] (2016). Coordinated recruitment of Spir actin nucleators and myosin V motors to Rab11 vesicle membranes. *ELife*, *5.* https://doi.org/10.7554/eLife.17523

Qualmann and Kessels (2009). New players in actin polymerization--WH2-domain-containing actin nucleators. *Trends in Cell Biology*, *19*(6), 276–285. https://doi.org/10.1016/j.tcb.2009.03.004

Quinlan, M. E. (2013). Direct interaction between two actin nucleators is required in Drosophila oogenesis. *Development (Cambridge, England)*, *140*(21), 4417–4425. https://doi.org/10.1242/dev.097337

Quinlan, M. E., Hilgert, S., Bedrossian, A., Mullins, R. D., & Kerkhoff, E [Eugen] (2007). Regulatory interactions between two actin nucleators, Spire and Cappuccino. *The Journal of Cell Biology*, *179*(1), 117–128. https://doi.org/10.1083/jcb.200706196

Quinlan and Kerkhoff (2005). Drosophila Spire is an actin. *Nature*.

Quinlan and Kerkhoff (2008). Actin nucleation bacteria get in-Spired. *Nature Cell Biology*, *10*. 10.1038/ncb0108-13

Ramabhadran, V., Korobova, F, Rahme, G., & Higgs, H. (2011). Splice variant-specific cellular function of the formin INF2 in maintenance of Golgi architecture. *Molecular Biology of the Cell*. 10.1091/mbc.E11-05-0457

Ramalho, J. S., Lopes, V. S., Tarafder, A. K., Seabra, M. C., & Hume, A. N. (2009). Myrip uses distinct domains in the cellular activation of myosin VA and myosin VIIA in melanosome transport. *Pigment Cell & Melanoma Research*, *22*(4), 461–473. https://doi.org/10.1111/j.1755-148X.2009.00567.x

Reiner and Lundquist (2018). Small GTPases. *WormBook : The Online Review of C. Elegans Biology*, *2018*, 1–65. https://doi.org/10.1895/wormbook.1.67.2

Rodriguez and Cheney (2002). Human myosin-Vc is a novel class V myosin expressed in epithelial cells. *Journal of Cell Science*. 10.1242/jcs.115.5.991

Rojas, A. M., Fuentes, G., Rausell, A., & Valencia, A. (2012). The Ras protein superfamily: Evolutionary tree and role of conserved amino acids. *The Journal of Cell Biology*, *196*(2), 189–201. https://doi.org/10.1083/jcb.201103008

Roland, J. T., Lapierre, L. A., & Goldenring, J. R. (2009). Alternative splicing in class V myosins determines association with Rab10. *The Journal of Biological Chemistry*, *284*(2), 1213–1223. https://doi.org/10.1074/jbc.M805957200

Romero, S., Le Clainche, C., Didry, D., Egile, C., Pantaloni, D., & Carlier, M.-F. (2004). Formin is a processive motor that requires profilin to accelerate actin assembly and associated ATP hydrolysis. *Cell*, *119*(3), 419–429. https://doi.org/10.1016/j.cell.2004.09.039

Ross, J. L., Ali, M. Y., & Warshaw, D. M. (2008). Cargo transport: Molecular motors navigate a complex cytoskeleton. *Current Opinion in Cell Biology*, *20*(1), 41–47. https://doi.org/10.1016/j.ceb.2007.11.006

Rottner, K [Klemens], Faix, J., Bogdan, S., Linder, S., & Kerkhoff, E [Eugen] (2017). Actin assembly mechanisms at a glance. *Journal of Cell Science*, *130*(20), 3427–3435. https://doi.org/10.1242/jcs.206433

Ruiz-Trillo, I., Roger, A. J., Burger, G [Gertraud], Gray, M. W., & Lang, B. F. (2008). A phylogenomic investigation into the origin of metazoa. *Molecular Biology and Evolution*, *25*(4), 664–672. https://doi.org/10.1093/molbev/msn006

Sato, O., Li, X.-D., & Ikebe, M. (2007). Myosin Va becomes a low duty ratio motor in the inhibited form. *The Journal of Biological Chemistry*, *282*(18), 13228–13239. https://doi.org/10.1074/jbc.M610766200

Schneider and Stephens (1990). Sequence logos _ a new way to display consensus. *Nucleic Acids*. 10.1093/nar/18.20.6097

Schönichen and Geyer (2010). Fifteen formins for an actin filament: A molecular view on the regulation of human formins. *Biochimica Et Biophysica Acta*, *1803*(2), 152–163. https://doi.org/10.1016/j.bbamcr.2010.01.014

Schuh, M. (2011). An actin-dependent mechanism for long-range vesicle transport. *Nature Cell Biology*, *13*(12), 1431–1436. https://doi.org/10.1038/ncb2353

Schultz, D. T., Haddock, S. H. D., Bredeson, J. V., Green, R. E., Simakov, O., & Rokhsar, D. S. (2023). Ancient gene linkages support ctenophores as sister to other animals. *Nature*, *618*(7963), 110–117. https://doi.org/10.1038/s41586-023-05936-6

Schumacher, N., Borawski, J. M., Leberfinger, C. B., Gessler, M., & Kerkhoff, E [Eugen] (2004). Overlapping expression pattern of the actin organizers Spir-1 and formin-2 in the developing mouse nervous system and the adult brain. *Gene Expression Patterns : GEP*, *4*(3), 249–255. https://doi.org/10.1016/j.modgep.2003.11.006

Sckolnick, M., Krementsova, E. B., Warshaw, D. M., & Trybus, K. M. (2013). More than just a cargo adapter, melanophilin prolongs and slows processive runs of myosin Va. *The Journal of Biological Chemistry*, *288*(41), 29313–29322. https://doi.org/10.1074/jbc.M113.476929

Sebé-Pedrós, A., Burkhardt, P., Sánchez-Pons, N., Fairclough, S. R., Lang, B. F., King, N [Nicole], & Ruiz-Trillo, I. (2013). Insights into the origin of metazoan filopodia and microvilli. *Molecular Biology and Evolution*, *30*(9), 2013–2023. https://doi.org/10.1093/molbev/mst110

Seperack, P., Mercer, J., Stroble, M., & Copeland, N:, Jenkins, N. (1995). Retroviral sequences located within an intron of the dilute gene alter dilute expression in a tissue specific manner. *The EMBO Journal*, *14*. 10.1002/j.1460-2075.1995.tb07227.x

Sept and McCammon (2001). Thermodynamics and Kinetics of Actin Filament Nucleation.

Shalmi and Goetze (2021). Von Willebrand Factor Activity in Thrombosis: An Overlooked Target for Intervention? *JACC. Basic to Translational Science*, *6*(7), 595–597. https://doi.org/10.1016/j.jacbts.2021.05.003

Sladewski, T. E., Krementsova, E. B., & Trybus, K. M. (2016). Myosin Vc Is Specialized for Transport on a Secretory Superhighway. *Current Biology : CB*, *26*(16), 2202–2207. https://doi.org/10.1016/j.cub.2016.06.029

Small, J. V., Stradal, T., Vignal, E., & Rottner, K [K.] (2002). The lamellipodium: where motility begins. *Trends in Cell Biology*. https://doi.org/10.1016/S0962-8924(01)02237-1

Springer, T. (2014). von Willebrand factor, Jedi knight of the bloodstream. *Blood*(124). 10.1182/blood-2014-05-378638

Stenmark, H. (2009). Rab GTPases as coordinators of vesicle traffic. *Nature Reviews. Molecular Cell Biology*, *10*(8), 513–525. https://doi.org/10.1038/nrm2728

Straub, F., Welz, T [Tobias], Alberico, H., Brandão, R. O., Huber, A., Samol-Wolf, A., Brakebusch, C., Woods, D., Kollmar, M., Martin-Gonzalez, J., & Kerkhoff, E [Eugen] (2020). The SPIRE1 actin nucleator coordinates actin/myosin functions in the regulation of mitochondrial motility. Advance online publication. https://doi.org/10.1101/2020.06.19.161109

Strom, Hume, Tarafder, Barkagianni, & Seabra (2002). A family of RAB27-binding proteins. *Journal of Biological Chemistry*, *277*(28), i–ii. https://doi.org/10.1016/S0021-9258(19)66425-2

Tabb et al (1998). Transport of ER vesicles on actin filaments in neurons by myosin V. *Journal of Cell Science*.

Tilelli, C. Q., Martins, A. R., Larson, R. E., & Garcia-Cairasco, N. (2003). Immunohistochemical localization of myosin Va in the adult rat brain. *Neuroscience*, *121*(3), 573–586. https://doi.org/10.1016/s0306-4522(03)00546-3

Tittel, J., Welz, T [Tobias], Czogalla, A., Dietrich, S., Samol-Wolf, A., Schulte, M., Schwille, P., Weidemann, T., & Kerkhoff, E [Eugen] (2015). Membrane targeting of the Spir·formin actin

nucleator complex requires a sequential handshake of polar interactions. *The Journal of Biological Chemistry*, *290*(10), 6428–6444. https://doi.org/10.1074/jbc.M114.602672

Tóth, J., Kovács, M., Wang, F., Nyitray, L., & Sellers, J. R. (2005). Myosin V from Drosophila reveals diversity of motor mechanisms within the myosin V family. *The Journal of Biological Chemistry*, *280*(34), 30594–30603. https://doi.org/10.1074/jbc.M505209200

Vale, R. (2003). The Molecular Motor Toolbox for Intracellular Transport. *Cell*. 10.1016/s0092-8674(03)00111-9

Vale and Fletterick (1997). The design plan of kinesin motors. *Cell Dev. Biol,* 13. 10.1146/annurev.cellbio.13.1.745

van den Bossche, K., Naeyaert, J.-M., & Lambert, J. (2006). The quest for the mechanism of melanin transfer. *Traffic (Copenhagen, Denmark)*, *7*(7), 769–778. https://doi.org/10.1111/j.1600-0854.2006.00425.x

van Mourik, J. A., Romani de Wit, T., & Voorberg, J. (2002). Biogenesis and exocytosis of Weibel-Palade bodies. *Histochemistry and Cell Biology*, *117*(2), 113–122. https://doi.org/10.1007/s00418-001-0368-9

Vavylonis, D., Kovar, D. R., O'Shaughnessy, B., & Pollard, T. D. (2006). Model of formin-associated actin filament elongation. *Molecular Cell*, *21*(4), 455–466. https://doi.org/10.1016/j.molcel.2006.01.016

Viveiros, R., Hutter, H., & Moerman, D. G. (2011). Membrane extensions are associated with proper anterior migration of muscle cells during Caenorhabditis elegans embryogenesis. *Developmental Biology*, *358*(1), 189–200. https://doi.org/10.1016/j.ydbio.2011.07.026

Vizcarra, C. L., Kreutz, B., Rodal, A. A., Toms, A. V., Lu, J [Jun], Zheng, W., Quinlan, M. E., & Eck, M. J. (2011). Structure and function of the interacting domains of Spire and Fmn-family formins. *Proceedings of the National Academy of Sciences of the United States of America*, *108*(29), 11884–11889. https://doi.org/10.1073/pnas.1105703108

Vogel, G. F., Hess, M. W., Pfaller, K., Huber, L. A., Janecke, A. R., & Müller, T. (2016). Towards understanding microvillus inclusion disease. *Molecular and Cellular Pediatrics*, *3*(1), 3. https://doi.org/10.1186/s40348-016-0031-0

Wagner, W., Fodor, E., Ginsburg, A., & Hammer, J. A. (2006). The binding of DYNLL2 to myosin Va requires alternatively spliced exon B and stabilizes a portion of the myosin's coiled-coil domain. *Biochemistry*, *45*(38), 11564–11577. https://doi.org/10.1021/bi061142u

Wagner et al (1982). Immunolocalization of von Willebrand Protein in Weibel-Palade Bodies of Human Endothelial Cells. *Journal of Cell Biology*. https://doi.org/10.1083/jcb.95.1.355

Wallar and Alberts (2003). The formins: Active scaffolds that remodel the cytoskeleton. *Trends in Cell Biology*, *13*(8), 435–446. https://doi.org/10.1016/s0962-8924(03)00153-3

Wang, F., Thirumurugan, K., Stafford, W. F., Hammer, J. A., Knight, P. J., & Sellers, J. R. (2004). Regulated Conformation of Myosin V. *Journal of Biological Chemistry*, *279*(4), 2333–2336. https://doi.org/10.1074/jbc.C300488200

Wang, S., Hu, C., Wu, F., & He, S. (2017). Rab25 GTPase: Functional roles in cancer. *Oncotarget*. 10.18632/oncotarget.19571

Wang, Z., Edwards, J. G., Riley, N., Provance, D. W., Karcher, R., Li, X.-D., Davison, I. G., Ikebe, M., Mercer, J. A., Kauer, J. A., & Ehlers, M. D. (2008). Myosin Vb mobilizes recycling endosomes and AMPA receptors for postsynaptic plasticity. *Cell*, *135*(3), 535–548. https://doi.org/10.1016/j.cell.2008.09.057

Wasmeier, C., Hume, A. N., Bolasco, G., & Seabra, M. C. (2008). Melanosomes at a glance. *Journal of Cell Science*, *121*(Pt 24), 3995–3999. https://doi.org/10.1242/jcs.040667

Watanabe, S., Mabuchi, K., Ikebe, R., & Ikebe, M. (2006). Mechanoenzymatic characterization of human myosin Vb. *Biochemistry*, *45*(8), 2729–2738. https://doi.org/10.1021/bi051682b

Wellington and Manseau (1999). Spire contains actin binding domains and is related to ascidian posterior end mark-5. *Developmental Biology*. https://doi.org/10.1242/dev.126.23.5267

Welz, T [T.]. Dissertation_Tobias Welz: Mechanisms of force generation for vesicle transport processes: identification and characterisation of the Spir actin nucleator-myosin V motor protein complex. 10.5283/epub.36856

Welz, T [Tobias], Wellbourne-Wood, J., & Kerkhoff, E [Eugen] (2014). Orchestration of cell surface proteins by Rab11. *Trends in Cell Biology*, *24*(7), 407–415. https://doi.org/10.1016/j.tcb.2014.02.004

Welz and Kerkhoff (2017). Exploring the iceberg: Prospects of coordinated myosin V and actin assembly functions in transport processes. *Small GTPases*, *10*(2), 111–121. https://doi.org/10.1080/21541248.2017.1281863

Welz and Kerkhoff (2023). The role of SPIRE actin nucleators in cellular transport processes. *Journal of Cell Science*, *136*(6). https://doi.org/10.1242/jcs.260743

Wöllert, T., Patel, A., Lee, Y.-L., Provance, D. W., Vought, V. E., Cosgrove, M. S., Mercer, J. A., & Langford, G. M. (2011). Myosin5a tail associates directly with Rab3A-containing compartments in neurons. *The Journal of Biological Chemistry*, *286*(16), 14352–14361. https://doi.org/10.1074/jbc.M110.187286

Xue and Robinson (2013). Guardians of the actin monomer. *European Journal of Cell Biology*, *92*(10-11), 316–332. https://doi.org/10.1016/j.ejcb.2013.10.012

Yao, L.-L., Cao, Q.-J., Zhang, H.-M., Zhang, J [Jie], Cao, Y., & Li, X.-D. (2015). Melanophilin Stimulates Myosin-5a Motor Function by Allosterically Inhibiting the Interaction between the Head and Tail of Myosin-5a. *Scientific Reports*, *5*, 10874. https://doi.org/10.1038/srep10874

Zeth, K., Pechlivanis, M., Samol, A., Pleiser, S., Vonrhein, C., & Kerkhoff, E [Eugen] (2011). Molecular basis of actin nucleation factor cooperativity: Crystal structure of the Spir-1 kinase non-catalytic C-lobe domain (KIND)•formin-2 formin SPIR interaction motif (FSI) complex. *The Journal of Biological Chemistry*, *286*(35), 30732–30739. https://doi.org/10.1074/jbc.M111.257782

Zhang, N., Yao, L.-L., & Li, X.-D. (2018). Regulation of class V myosin. *Cellular and Molecular Life Sciences : CMLS*, *75*(2), 261–273. https://doi.org/10.1007/s00018-017-2599-5

Zhao, L., Koslovky, J., Reinhard, J., Bähler, M., Witt, A., Provance W. Jr., & Mercer, J. (1996). Cloning and characterization of myr 6, an unconventional myosin of the dilute_myosin-V family. *Cell Biology*, *93*. 10.1073/pnas.93.20.10826

Zhao, S., Ye, Z., & Stanton, R. (2020). Misuse of RPKM or TPM normalization when comparing across samples and sequencing protocols. *RNA*. 10.1261/rna.074922.120

Zhao, Y., Li, M.-C., Konaté, M. M., Chen, L., Das, B., Karlovich, C., Williams, P. M., Evrard, Y. A., Doroshow, J. H., & McShane, L. M. (2021). Tpm, FPKM, or Normalized Counts? A Comparative Study of Quantification Measures for the Analysis of RNA-seq Data from the NCI Patient-Derived Models Repository. *Journal of Translational Medicine*, *19*(1), 269. https://doi.org/10.1186/s12967-021-02936-w

Zhen and Stenmark (2015). Cellular functions of Rab GTPases at a glance. *Journal of Cell Science*, *128*(17), 3171–3176. https://doi.org/10.1242/jcs.166074

6 Supplement

6.1 Sequence related data

SPIRE1, *homo sapiens* (742 amino acids) Isoform B

NP_064533.3; NM_020148.3

MAQAAGPAGGGEPRTEAVGGEGPREPGAAGGAAGGSRDALSLEEILRLYNQPINEEQAWAVCYQCCGS
LRAAARRRQPRHRVRSAAQIRVWRDGAVTLAPAADDAGEPPPVAGKLGYSQCMETEVIESLGIIIYKA
LDYGLKENEERELSPPLEQLIDHMANTVEADGSNDEGYEAAEEGLGDEDEKRKISAIRSYRDVMKLCA
AHLPTESDAPNHYQAVCRALFAETMELHTFLTKIKSAKENLKKIQEMEKSDESSTDLEELKNADWARF
WVQVMRDLRNGVKLKKVQERQYNPLPIEYQLTPYEMLMDDIRCKRYTLRKVMVNGDIPPRLKKSAHEI
ILDFIRSRPPLNPVSARKLKPTPPRPRSLHERILEEIKAERKLRPVSPEEIRRSRLAMRPLSMSYSFD
LSDVTTPESTKNLVESSMVNGGLTSQTKENGLSTSQQVPAQRKKLLRAPTLAELDSSESEEETLHKST
SSSSVSPSFPEEPVLEAVSTRKKPPKFLPISSTPQPERRQPPQRRHSIEKETPTNVRQFLPPSRQSSR
SLEEFCYPVECLALTVEEVMHIRQVLVKAELEKYQQYKDIYTALKKGKLCFCCRTRRFSFFTWSYTCQ
FCKRPVCSQCCKKMRLPSKPYSTLPIFSLGPSALQRGESSMRSEKPSTAHHRPLRSIARFSSKSKSMD
KSDEELQFPKELMEDWSTMEVCVDCKKFISEIISSSRRSLVLANKRARLKRKTQSFYMSSPGPSEYCP
SERTISEI

linker

KIND **WH2** **GTBM** **SPIRE-box** **FYVE-type**

SPIRE2, *homo sapiens* (728 amino acids)

CAD19439.1; AJ422077.1

MARAGSCGGAAAGAGRPEPWELSLEEVLKAYEQPLNEEQALAVCFQGCRGLRGSPGRRLRDTGDLLLR
GDGSVGAREPEAAEPATMVVPLASSEAQTVQSLGFAIYRALDWGLDESEERELSPQLERLIDLMANND
SEDSGCGAADEGYGGPEEEEEAEGVPRSVRTFAQAMRLCAARLTDPRGAQAHYQAVCRALFVETLELR
AFLARVREAKEMLQKLREDEPHLETPRAELDSLGHTDWARLWVQLMRELRRGVKLKKVQEQEFNPLPT
EFQLTPFEMLMQDIRARNYKLRKVMVDGDIPPRVKKDAHELILDFIRSRPPLKQVSERRLRPLPPKQR
SLHEKILEEIKQERRLRPVRGEGWAARGFGSLPCILNACSGDAKSTSCINLSVTDAGGSAQRPRPRVL
LKAPTLAEMEEMNTSEEEESPCGEVTLKRDRSFSEHDLAQLRSEVASGLQSATHPPGGTEPPRPRAGS
AHVWRPGSRDQGTCPASVSDPSHPLLSNRGSSGDRPEASMTPDAKHLWLEFSHPVESLALTVEEVMDV
RRVLVKAEMEKFLQNKELFSSLKKGKICCCCRAKFPLFSWPPSCLFCKRAVCTSCSIKMKMPSKKFGH
IPVYTLGFESPQRVSAAKTAPIQRRDIFQSLQGPQWQSVEEAFPHIYSHGCVLKDVCSECTSFVADVV
RSSRKSVDVLNTTPRRSRQTQSLYIPNTRTLDFK

linker

KIND **WH2** **GTBM** **SPIRE-box** **FYVE-type**

SPIRE, *Nematostella vectensis* (650 amino acids)

XP_032234162.2; XM_032378271.2

MESMSIYEILKNFRAPLSEEQAWAVCYQCTRELVSQRETGFQTFQKNIIDIQLSTTKILKDGSVEFTS
ISPTETPQKENEVLFRLGSLVYECLDFGMEVCMERELDPALEKLITEMTCEQGDEGISVPEYCDDKHT
GIRGTSPPKKERRLSSKGVSSKDMSLERVLQSCTEHLAGDQAKSQVHFKAVCRALVNEAIELTAFLNH
LYNGHEIMAQTSGQGVGLTNWAYLQSLHAAEWAQLWLQAMRELRQGVTLRHVVHNKLPPASFEMTPFE
MLLDDIRYRRFNLNHVSIQQNTLNKSKDAHDVILDFIRSRPPLARVSERKMNPVAENSPNLHDKLLTE
IKSCKKLKPTPQPVLKTVQEIYYGEDLNLVPNDISASVTHKRRRLKPDLEFVEKISRWDSPTPDSSPE
EEQIPRSSVVEIKSVRSRSLPTSPRAELFEQFDSVADVKQFDSSRSSGFYEPGSSQSSLDSVEDNSCV
RNGKFSGNYTLGFDDNPIFPPSLRNLQNMKVTAKIYMTLNEVRHMCKTLAMLELENFDPDDPTYRSLI
SGQLCFCCRKRKFSLFGEWSRPCYICESCVCSHCLHKVETSSSYVFMENECTNKRDGFCDSSPYFPVC
ASSMPNSFSSPALTTHCMPTKTHRVCLTCKRFISKHC

linker

KIND WH2 GTBM SPIRE-box FYVE-type

SPIRE, *Salpingoeca rosetta* (683 amino acids)

XP_004990203.1; XM_004990146.1

MPSVHHILTTLNAPLDEEQLWALALLLGAHMDALKPSFPDLSDPQHLTFLINANTAIIEPSGHVTLDM
STLGNEDQTLPFLADEVKERQPSTDLEKAHVFSIGALLFTAADFSLMEDEEPSLSEDLEALITQMTDE
CMEDRHTLEAAIQACRAHVEDNEAVEVLKDLVALAISIEKADGQIPAELLSGRATTSSSPDSGYTQDA
TAFDETRDLHASLMREIQAKPDLKDGSKRALTGPAPYVTPHEQLLDDIRRSSVASLNKTPAPTPTRLS
HSTPDTHAADTLPTRGAYSRHGYQQHGSARSQMSSHGGTPLRLSTAASTESLPGAHQHTHSQRQSLAA
ASQHNRSTASMGTPGYGGDSTHNGGGGGGDGRKKRMPVRLALDSSALGSILGGLDATTQVKLAFAEQQ
AKTPTASSPAHNRTASGNSGSNHERTGQADAHSSSGSRGGDGGDGGGGGDRPATAGVRGSGRGGGGGD
GDGSNLIPTTRQSLSGQSSLSSPSSPSSSSAVTLPARPSTASSSLSHSQQRQQQQNGGTPPKPQEECS
FVGFEEHRHISTTLFKAELDDLMYQNEKQYNAIAQKKLCPICRKTRFTLLTRGRECPMCTRFACRDCR
SDVTMPAHMRATPSADSSSSGNGATTASSSSGNGSGSSHVTSVSSSAGKPFTINLCNECKKQLGGIRT
KRM

linker

KIND WH2 GTBM SPIRE-box FYVE-type

Myosin 5A, Mus musculus, Transcript variant X1 (1880 amino acids)
XP_ 006510890.1; XM_006510827.2

MAASELYTKFARVWIPDPEEVWKSAELLKDYKPGDKVLLLHLEEGKDLEYRLDPKTGELPHLRNPDIL
VGENDLTALSYLHEPAVLHNLRVRFIDSKLIYTYCGIVLVAINPYEQLPIYGEDIINAYSGQNMGDMD
PHIFAVAEEAYKQMARDERNQSIIVSGESGAGKTVSAKYAMRYFATVSGSASEANVEEKVLASNPIME
SIGNAKTTRNDNSSRFGKYIEIGFDKRYRIIGANMRTYLLEKSRVVFQAEEERNYHIFYQLCASAKLP
EFKMLRLGNADSFHYTKQGGSPMIEGVDDAKEMAHTRQACTLLGISESYQMGIFRILAGILHLGNVGF
ASRDSDSCTIPPKHEPLTIFCDLMGVDYEEMCHWLCHRKLATATETYIKPISKLQATNARDALAKHIY
AKLFNWIVDHVNQALHSAVKQHSFIGVLDIYGFETFEINSFEQFCINYANEKLQQQFNMHVFKLEQEE
YMKEQIPWTLIDFYDNQPCINLIESKLGILDLLDEECKMPKGTDDTWAQKLYNTHLNKCALFEKPRMS
NKAFIIKHFADKVEYQCEGFLEKNKDTVFEEQIKVLKSSKFKMLPELFQDDEKAISPTSATSSGRTPL
TRVPVKPTKGRPGQTAKEHKKTVGHQFRNSLHLLMETLNATTPHYVRCIKPNDFKFPFTFDEKRAVQQ
LRACGVLETIRISAAGFPSRWTYQEFFSRYRVLMKQKDVLGDRKQTCKNVLEKLILDKDKYQFGKTKI
FFRAGQVAYLEKLRADKLRAACIRIQKTIRGWLLRKRYLCMQRAAITVQRYVRGYQARCYAKFLRRTK
AATTIQKYWRMYVVRRRYKIRRAATIVIQSYLRGYLTRNRYRKILREYKAVIIQKRVRGWLARTHYKR
TMKAIVYLQCCFRRMMAKRELKKLKIEARSVERYKKLHIGMENKIMQLQRKVDEQNKDYKCLMEKLTN
LEGVYNSETEKLRNDVERLQLSEEEAKVATGRVLSLQEEIAKLRKDLEQTRSEKKSIEERADKYKQET
DQLVSNLKEENTLLKQEKETLNHRIVEQAKEMTETMERKLVEETKQLELDLNDERLRYQNLLNEFSRL
EERYDDLKEEMTLMLNVPKPGHKRTDSTHSSNESEYTFSSEFAETEDIAPRTEEPIEKKVPLDMSLFL
KLQKRVTELEQEKQLMQDELDRKEEQVFRSKAKEEERPQIRGAELEYESLKRQELESENKKLKNELNE
LRKALSEKSAPEVTAPGAPAYRVLMEQLTSVSEELDVRKEEVLILRSQLVSQKEAIQPKDDKNTMTDS
TILLEDVQKMKDKGEIAQAYIGLKETNRSSTMDYQELNEDGELWMVYEGLKQANRLLESQLQSQKRSH
ENEAEALRGEIQSLKEENNRQQQLLAQNLQLPPEARIEASLQHEITRLTNENLYFEELYADDPKKYQS
YRISLYKRMIDLMEQLEKQDKTVRKLKKQLKVFAKKIGELEVGQMENISPGQIIDEPIRPVNIPRKEK
DFQGMLEYKREDEQKLVKNLILELKPRGVAVNLIPGLPAYILFMCVRHADYLNDDQKVRSLLTSTINS
IKKVLKKRGDDFETVSFWLSNTCRFLHCLKQYSGEEGFMKHNTSRQNEHCLTNFDLAEYRQVLSDLAI
QIYQQLVRVLENILQPMIVSGMLEHETIQGVSGVKPTGLRKRTSSIADEGTYTLDSILRQLNSFHSVM
CQHGMDPELIKQVVKQMFYIVGAITLNNLLLRKDMCSWSKGMQIRYNVSQLEEWLRDKNLMNSGAKET
LEPLIQAAQLLQVKKKTDDDAEAICSMCNALTTAQIVKVLNLYTPVNEFEERVSVSFIRTIQMRLRDR
KDSPQLLMDAKHIFPVTFPFNPSSLALETIQIPASLGLGFIARV

motor IQ/IQ GTD

Myosin 5A, *homo sapiens,* Transcript variant_X2 X1 (1877 amino acids)
XP_011519909.2; XM_011521607.3

MLTCLDETALKFARVWIPDPEEVWKSAELLKDYKPGDKVLLLHLEEGKDLEYHLDPKTKELPHLRNPD
ILVGENDLTALSYLHEPAVLHNLRVRFIDSKLIYTYCGIVLVAINPYEQLPIYGEDIINAYSGQNMGD
MDPHIFAVAEEAYKQMARDERNQSIIVSGESGAGKTVSAKYAMRYFATVSGSASEANVEEKVLASNPI
MESIGNAKTTRNDNSSRFGKYIEIGFDKRYRIIGANMRTYLLEKSRVVFQAEEERNYHIFYQLCASAK
LPEFKMLRLGNADNFNYTKQGGSPVIEGVDDAKEMAHTRQACTLLGISESHQMGIFRILAGILHLGNV
GFTSRDADSCTIPPKHEPLCIFCELMGVDYEEMCHWLCHRKLATATETYIKPISKLQATNARDALAKH
IYAKLFNWIVDNVNQALHSAVKQHSFIGVLDIYGFETFEINSFEQFCINYANEKLQQQFNMHVFKLEQ
EEYMKEQIPWTLIDFYDNQPCINLIESKLGILDLLDEECKMPKGTDDTWAQKLYNTHLNKCALFEKPR
LSNKAFIIQHFADKVEYQCEGFLEKNKDTVFEEQIKVLKSSKFKMLPELFQDDEKAISPTSATSSGRT
PLTRTPAKPTKGRPGQMAKEHKKTVGHQFRNSLHLLMETLNATTPHYVRCIKPNDFKFPFTFDEKRAV
QQLRACGVLETIRISAAGFPSRWTYQEFFSRYRVLMKQKDVLSDRKQTCKNVLEKLILDKDKYQFGKT
KIFFRAGQVAYLEKLRADKLRAACIRIQKTIRGWLLRKKYLRMRKAAITMQRYVRGYQARCYAKFLRR
TKAATIIQKYWRMYVVRRRYKIRRAATIVLQSYLRGFLARNRYRKILREHKAVIIQKRVRGWLARTHY
KRSMHAIIYLQCCFRRMMAKRELKKLKIEARSVERYKKLHIGMENKIMQLQRKVDEQNKDYKCLVEKL
TNLEGIYNSETEKLRSDLERLQLSEEEAKVATGRVLSLQEEIAKLRKDLEQTRSEKKCIEEHADRYKQ
ETEQLVSNLKEENTLLKQEKEALNHRIVQQAKEMTETMEKKLVEETKQLELDLNDERLRYQNLLNEFS
RLEERYDDLKEEMTLMVHVPKPGHKRTDSTHSSNESEYIFSSEIAEMEDIPSRTEEPSEKKVPLDMSL
FLKLQKRVTELEQEKQVMQDELDRKEEQVLRSKAKEEERPQIRGAELEYESLKRQELESENKKLKNEL
NELRKALSEKSAPEVTAPGAPAYRVLMEQLTSVSEELDVRKEEVLILRSQLVSQKEAIQPKNTMTDST
ILLEDVQKMKDKGEIAQAYIGLKETNRSSALDYHELNEDGELWLVYEGLKQANRLLESQLQSQKRSHE
NEAEALRGEIQSLKEENNRQQQLLAQNLQLPPEARIEASLQHEITRLTNENLYFEELYADDPKKYQSY
RISLYKRMIDLMEQLEKQDKTVRKLKKQLKVFAKKIGELEVGQMENISPGQIIDEPIRPVNIPRKEKD
FQGMLEYKKEDEQKLVKNLILELKPRGVAVNLIPGLPAYILFMCVRHADYLNDDQKVRSLLTSTINSI
KKVLKKRGDDFETVSFWLSNTCRFLHCLKQYSGEEGFMKHNTSRQNEHCLTNFDLAEYRQVLSDLAIQ
IYQQLVRVLENILQPMIVSGMLEHETIQGVSGVKPTGLRKRTSSIADEGTYTLDSILRQLNSFHSVMC
QHGMDPELIKQVVKQMFYIIGAITLNNLLLRKDMCSWSKGMQIRYNVSQLEEWLRDKNLMNSGAKETL
EPLIQAAQLLQVKKKTDDDAEAICSMCNALTTAQIVKVLNLYTPVNEFEERVSVSFIRTIQMRLRDRK
DSPQLLMDAKHIFPVTFPFNPSSLALETIQIPASLGLGFISRV

GTD

motor IQ/IQ GTD

Myosin 5B, *homo sapiens* (1848 amino acids)
NP_001073936.1; NM_001080467.2

MSVGELYSQCTRVWIPDPDEVWRSAELTKDYKEGDKSLQLRLEDETILEYPIDVQRNQLPFLRNPDIL
VGENDLTALSYLHEPAVLHNLKVRFLESNHIYTYCGIVLVAINPYEQLPIYGQDVIYTYSGQNMGDMD
PHIFAVAEEAYKQMARDEKNQSIIVSGESGAGKTVSAKYAMRYFATVGGSASETNIEEKVLASSPIME
AIGNAKTTRNDNSSRFGKYIQIGFDKRYHIIGANMRTYLLEKSRVVFQADDERNYHIFYQLCAAAGLP
EFKELALTSAEDFFYTSQGGDTSIEGVDDAEDFEKTRQAFTLLGVKESHQMSIFKIIASILHLGSVAI
QAERDGDSCSISPQDVYLSNFCRLLGVEHSQMEHWLCHRKLVTTSETYVKTMSLQQVINARNALAKHI
YAQLFGWIVEHINKALHTSLKQHSFIGVLDIYGFETFEVNSFEQFCINYANEKLQQQFNSHVFKLEQE
EYMKEQIPWTLIDFYDNQPCIDLIEAKLGILDLLDEECKVPKGTDQNWAQKLYDRHSSSQHFQKPRMS
NTAFIIVHFADKVEYLSDGFLEKNRDTVYEEQINILKASKFPLVADLFHDDKDPVPATTPGKGSSSKI
SVRSARPPMKVSNKEHKKTVGHQFRTSLHLLMETLNATTPHYVRCIKPNDEKLPFHFDPKRAVQQLRA
CGVLETIRISAAGYPSRWAYHDFFNRYRVLVKKRELANTDKKAICRSVLENLIKDPDKFQFGRTKIFF
RAGQVAYLEKLRADKFRTATIMIQKTVRGWLQKVKYHRLKGATLTLQRYCRGHLARRLAEHLRRIRAA
VVLQKHYRMQRARQAYQRVRRAAVVIQAFTRAMFVRRTYRQVLMEHKATTIQKHVRGWMARRHFQRLR
DAAIVIQCAFRMLKARRELKALRIEARSAEHLKRLNVGMENKVVQLQRKIDEQNKEFKTLSEQLSVTT
STYTMEVERLKKELVHYQQSPGEDTSLRLQEEVESLRTELQRAHSERKILEDAHSREKDELRKRVADL
EQENALLKDEKEQLNNQILCQSKDEFAQNSVKENLMKKELEEERSRYQNLVKEYSQLEQRYDNLRDEM
TIIKQTPGHRRNPSNQSSLESDSNYPSISTSEIGDTEDALQQVEEIGLEKAAMDMTVFLKLQKRVREL
EQERKKLQVQLEKREQQDSKKVQAEPPQTDIDLDPNADLAYNSLKRQELESENKKLKNDLNELRKAVA
DQATQNNSSHGSPDSYSLLLNQLKLAHEELEVRKEEVLILRTQIVSADQRRLAGRNAEPNINARSSWP
NSEKHVDQEDAIEAYHGVCQTNSKTEDWGYLNEDGELGLAYQGLKQVARLLEAQLQAQSLEHEEEVEH
LKAQLEALKEEMDKQQQTFCQTLLLSPEAQVEFGVQQEISRLTNENLDLKELVEKLEKNERKLKKQLK
IYMKKAQDLEAAQALAQSERKRHELNRQVTVQRKEKDFQGMLEYHKEDEALLIRNLVTDLKPQMLSGT
VPCLPAYILYMCIRHADYTNDDLKVHSLLTSTINGIKKVLKKHNDDFEMTSFWLSNTCRLLHCLKQYS
GDEGFMTQNTAKQNEHCLKNFDLTEYRQVLSDLSIQIYQQLIKIAEGVLQPMIVSAMLENESIQGLSG
VKPTGYRKRSSSMADGDNSYCLEAIIRQMNAFHTVMCDQGLDPEIILQVFKQLFYMINAVTLNNLLLR
KDVCSWSTGMQLRYNISQLEEWLRGRNLHQSGAVQTMEPLIQAAQLLQLKKKTQEDAEAICSLCTSLS
TQQIVKILNLYTPLNEFEERVTVAFIRTIQAQLQERNDPQQLLLDAKHMFPVLFPFNPSSLTMDSIHI
PACLNLEFLNEV

GTD

motor IQ/IQ GTD

Myosin 5C, *homo sapiens* (1742 amino acids)
NP_061198; NM_018728.4

MAVAELYTQYNRVWIPDPEEVWKSAEIAKDYRVGDKVLRLLLEDGTELDYSVNPESLPPLRNPDILVG
ENDLTALSYLHEPAVLHNLRIRFAESKLIYTYSGIILVAMNPYKQLPIYGDAIIHAYSGQNMGDMDPH
IFAVAEEAYKQMARNNRNQSIIVSGESGAGKTVSARYAMRYFATVSKSGSNAHVEDKVLASNPITEAV
GNAKTTRNDNSSRFGKYTEISFDEQNQIIGANMSTYLLEKSRVVFQSENERNYHIFYQLCASAQQSEF
KHLKLGSAEEFNYTRMGGNTVIEGVNDRAEMVETQKTFTLLGFKEDFQMDVFKILAAILHLGNVQITA
VGNERSSVSEDDSHLKVFCELLGLESGRVAQWLCNRKIVTSSETVVKPMTRPQAVNARDALAKKIYAH
LFDFIVERINQALQFSGKQHTFIGVLDIYGFETFDVNSFEQFCINYANEKLQQQFNMHVFKLEQEEYM
KEDIPWTLIDFYDNQPVIDLIEAKMGILELLDEECLLPHGTDENWLQKLYNNFVNRNPLFEKPRMSNT
SFVIQHFADKVEYKCEGFLEKNRDTVYDMLVEILRASKFHLCANFFQENPTPPSPFGSMITVKSAKQV
IKPNSKHFRTTVGSKFRSSLYLLMETLNATTPHYVRCIKPNDEKLPFEFDSKRIVQQLRACGVLETIR
ISAQSYPSRWTYIEFYSRYGILMTKQELSFSDKKEVCKVVLHRLIQDSNQYQFGKTKIFFRAGQVAYL
EKLRLDKLRQSCVMVQKHMRGWLQRKKFLRERRAALIIQQYFRGQQTVRKAITAVALKEAWAAIIIQK
HCRGYLVRSLYQLIRMATITMQAYSRGFLARRRYRKMLEEHKAVILQKYARAWLARRRFQSIRRFVLN
IQLTYRVQRLQKKLEDQNKENHGLVEKLTSLAALRAGDVEKIQKLEAELEKAATHRRNYEEKGKRYRD
AVEEKLAKLQKHNSELETQKEQIQLKLQEKTEELKEKMDNLTKQLFDDVQKEERQRMLLEKSFELKTQ
DYEKQIQSLKEEIKALKDEKMQLQHLVEGEHVTSDGLKAEVARLSKQVKTISEFEKEIELLQAQKIDV
EKHVQSQKREMREKMSEITKQLLESYDIEDVRSRLSVEDLEHLNEDGELWFAYEGLKKATRVLESHFQ
SQKDCYEKEIEALNFKVVHLSQEINHLQKLFREENDINESIRHEVTRLTSENMMIPDFKQQISELEKQ
KQDLEIRLNEQAEKMKGKLEELSNQLHRSQEEEGTQRKALEAQNEIHTKEKEKLIDKIQEMQEASDHL
KKQFETESEVKCNFRQEASRLTLENRDLEEELDMKDRVIKKLQDQVKTLSKTIGKANDVHSSSGPKEY
LGMLQYKREDEAKLIQNLILDLKPRGVVVNMIPGLPAHILFMCVRYADSLNDANMLKSLMNSTINGIK
QVVKEHLEDFEMLSFWLSNTCHFLNCLKQYSGEEEFMKHNSPQQNKNCLNNFDLSEYRQILSDVAIRI
YHQFIIIMEKNIQPIIVPGMLEYESLQGISGLKPTGFRKRSSSIDDTDGYTMTSVLQQLSYFYTTMCQ
NGLDPELVRQAVKQLFFLIGAVTLNSLFLRKDMCSCRKGMQIRCNISYLEEWLKDKNLQNSLAKETLE
PLSQAAWLLQVKKTTDSDAKEIYERCTSLSAVQIIKILNSYTPIDDFEKRVTPSFVRKVQALLNSRED
SSQLMLDTKYLFQVTFPFTPSPHALEMIQIPSSFKLGFLNRL

GTD

motor IQ/IQ GTD

Myosin 5, *Nematostella vectensis* (1828 amino acids) isoform X1
XP_048581654; XM_048725697.1

MTTLELYTKGARVWIPHPDLVWIGGELTKDIEDKILEILLEDGREIIIDTRKSRLPPLRNPEILVGEN
DLTTLSYLHEPAVLHNLNVRFIQSNAIYTYCGIVLVAINPYEELPLYGPDIVAAYRGRSMGDMDPHIF
AVAEDAFQSMIRDERNQSVIVSGESGAGKTVSAKYAMRYFSAVGGASTETQIEKKVIATNPIMEAIGN
AKTIRNDNSSRFGKYLEISFDRNHHIIGAHMRTYLLEKSRVVFQAAEERNYHVFYQMCAACDLPEMKD
FRLAHPDNFSYLNQGDAPVVDSIDDADCFEELREALSMVGINDDEQLMLFRILSAILHLGNVEILQAG
DDECTVEENDFHLEMTAVLLGIDKNQLRKWLCNRKIVTVGEVLIKPLSITEANYGREAISKRIYSQLF
KWVVNTINCTLTSTSKPHSFIGVLDIYGFETFEINSFEQFCINYANEKLQQQFTQHVFKLEQDEYVRE
EIQWSFINFYDNQPCIDLIEAKLGILDLLDEECKMPKGSDSQWAQKLYKQHLQKSKHFSKPRMSNLAF
VIHHFADHVEYFVSGFVEKNRDTVNDEHLALLRASEYDLVSEVIQCMDRDEMVGEMFTENDAHSAPRK
RAASRAGKQGGKGGKMFKSVGSQFSVSLSKLMETLNSTTPHYVRCIKPNDTKAPFEFHPKRSIQQLRA
CGVLETIRISAAGYPSRWTYREFFARYIMLLPSKKINRKKPRETIKLILETFIKDEDMFQMGKTKIFF
RAGQVAYLEKLRGDKLRRSCVMIQKNYRCYREHKLYLRMRKAAILIQAWVRGDQARNLARSLRRNKSA
TTIQRYYRGFHLRQAYLRKHAAILTIQSYARGMSARRQRQVLLYNAKAGVIQRCWRGYKGRQKYRNYF
KKIIFLQSCVRRMRARKELKKLKIEARSVEHFKALNKGMENKIIELQQRLDQEVKKKELAQAAERDLS
EARKELDEARKWKGHYESSSARLVEMELVVSELRDELKRSMEARERVEKETKEEIEEKDEEIKSLRDV
IEQLREQVAEANSRAADEVASRDATLDERLEEQRVQILSEFEAERLNHQRVLRDYSRLEQRYQNLQDE
LEIVQTSPQKPLRSLDSVSTASSETSLVDALEKELREQEAEEPDEVRSIITKSQLFVRLRSKVMDLEN
RLVDAQSQLNKQSGETSAPNVPSIKVEEGDAWKQKTGKLQEIMKERDALKEEKEKVEAEQKKMGSELV
LLRKLVSQRNVDKEAEWDLISEKMKEIKDDRDLLEREKERLRKQLIDMASVAKDLREIDELLKFNPDE
SAYVLQAESLKKANNVLQIELEELIKKEKSLKEANENLWRDKAKLQKGRTSSVHAMDSSFQQEVTRLV
TENVDLREQVERLEKENATLRKDQSSLMPFRGRAQSMKADLLTEQKRRSHSVWAGQEPRAGKLVMRHA
GLLRKSPSRDEDFLPLPLQAKQRKAHGMIEYSAEDEEKIIKSLITDMNPSSVSDSIPGLPAHILFMCI
RHVDHMNDDRRMQSLLINSMNSIRNVIKKNPNLDMLAFWLANTLRLLHDMKQYSGDRAFQVHNTPEQN
EHCLKNFDLTEYRQVLSDLSIHIYQDLVKAIWDSINGMIVPGILEYESIPGVSSSKPFGGRSRGSEDI
SVKRITKKLSQVLNILNAHCVDPEIIKQCFRQVFYYIGANLMNNILLRKDMCHWSRGMQIRFNLSQLE
DWVRVNQLEGSGIVEALECITQATQLLQVNKKTLEDVDAICEVCSALNTLQVQKILSMYTPANEYEAR
VPSSVIRAVVERGHNKTDPMYLMLDTAYLFPVTLPFTPSAVSLETINIPELPGLDFLKVV

GTD

motor IQ/IQ GTD

Myosin 5, *Salpingoeca rosetta* (1921 amino acids)
XP_004997168.1; XM_004997111.1

MEAFSQGTRVWVPHDELVWKPAVVEALNTEERAITLRTEDGEEQQVAVKEDDSNLPPLRNPDILVGSD
DLTDLSYLHEPAVVHNLQVRFKEQQTIYTYCGIVLVALNPYSSLPIYSNDIIHAYSGRSLGELDPHIF
AVAEEAFRCMGRHSKNQSIIVSGESGAGKTVSAKYAMRYFATVGGAEAETQIEKKVLASNPVMESIGN
AKTIRNDNSSRFGKYIEILFNKHDHIIGAEMRTYLLEKSRVVFQAKSERNYHIFYQLCASADRPELEA
LELSEADDFFYTNQGEEAEIENVDDAADFERTKDALSLLGISDDDQQQIFCILAAILHMGNIEIKQRS
RRSDDARIPVEDTHVPVVSRLLGVEANMLTKWITHRKIQTGREVFTKPQTADNALRARDALAKHIYAH
VFDWLVSRINESLAHGSKQKDKRFIGVLDIYGFETFKVNSFEQFCINYANEKLQQQFNLHVFKLEQDE
YIKEKIQWSFIDFYDNQPCIDLIEDKLGVLSLLDEETKMPKGSDDNWATKMYASLTDRHHFEKPRLSN
TSFIVKHYADKVAYEVTGFMEKNKDTIYEEHLIMLRGSTSPFIAELFAAKGEGKASIDIRKATVSSQF
KNSLSSLMETLNATEPHYVRCIKPNDAKQPFEINPQRLVQQLRACGVLETIRISAAGYPSRWSYREFL
DRYRLLATSAAPLKSAEVKDACRAILQPLIADEDKYQFGQTKLFFRAGQVAYLEKLRSDKMKLCCVRI
QACVRRWLASRRYQRIKTAALGVQTYGRGLLARVRAQRLRERAAATKIQATFRAHRQRRQYAVTMAAV
VRLQAAYRALKARRALSGLRREAAALKIQSTWRMWAVRRQFLTKRNAAVTIQCAVRQMLARRVFKQLK
IEARSVAGMKAKTVGLEKKIFELQQTMDRRIQEAHEKQAAEVARLKEQLAAAEAKESTSTQASASEIE
RLRARNDELEQELESTSTERDALQSKYDEETAAAAAEHQSLKAKLEEMTQTLQMTTEAAKGSEGLAEQ
LEALNRRNMQLQSELADERAALQLKIKTQAEAEERVKALEHELLRAEMKALHDDDGNDDGVDRGARGE
YVEVRPQSPNGRTHTAATGEYMEVGGRVSPSKLNSSVDAGEELDQAASNAIIQQLRSDLAAAEAEAKR
LHKQQQQQQQQQQQPVEVEGQAAGKTATVTATATAAGETKSESEQLEGESETENALAVAAAAAVQREQ
ELTAEMEELKGEQRTHARRTEPHRGNSKEDKEEGEQRDLQAELREASTNIARLQLANRMLNDKVQALE
KAKVSAESRLKRLTGGDGELDPQVLQQEVAALQQHVQQLQGERAGLVSRTELEQAQADYEQLLKQFRA
LQDDYNRFMTDHCMEDLAKAKTDLQQRNHGLEEELKSLRSRVKDYEHDLTAARAEVSDLQAEKKQTNE
RVLALKQALTRQMPAESGSASSDGALLQEEVRILIDENLAMREQIEVLEERLQAALNGDVSGAAPGSG
SGGRDGSAQQPGRGGAGGGVGDGHQQQHQQHQSYGGSGAHGAGSQQLHQRKQMLGMLKFQEKDTQRVV
SELVSKLQPADVDGCMPCIPAHLLFMCVLYADYEENASMLQGLLTKAMTAMKNVVQDNAADLGRLAFW
LANGYRLLTNMKQFSGEPQFASPDDKDSATLKTFDLQEYRIVLSDLLVQIYHFVVKHIEHQLAGMIVP
GMLEHESLPTSNTSMPSRRRGRSKVDCKVEDILRLLTRVHGLLTEHCVEPRLVQQVFRQLFYIINATM
CNHLLLRKDLVRLTKGMQVRYNISKLEDWARDHNLEQICSSLVEAVQITQLLQCNKSKPDDIDTIFET
CTKLKPLQIQKVLQMYTPEDFEERVPAALIRAAQARVDAEAGGGTKLLLDTSFIHPVTFPFTPSSPRF
PTLDIPPTIKLDFVTKI

GTD

motor IQ/IQ GTD

6.2 Overview on cloning vectors

6.2.1 pAcGFP1-C1

The eukaryotic expression vector pAcGFP1-C1 was used to generate N-terminal AcGFP1-tagged SPIRE and myosin 5 proteins for ectopic expression in HEK 293 (ATCC 293) and HeLa cells (ATCC CCL-2). Gene expression is regulated by the strong CMV promoter. A kanamycin resistance gene is present for bacterial selection. The AcGFP1 cassette was substituted by an mScarlet-I cassette (released with *Age*I / *Bspl*) to generate pmScarlet-I-C1 expression vectors.

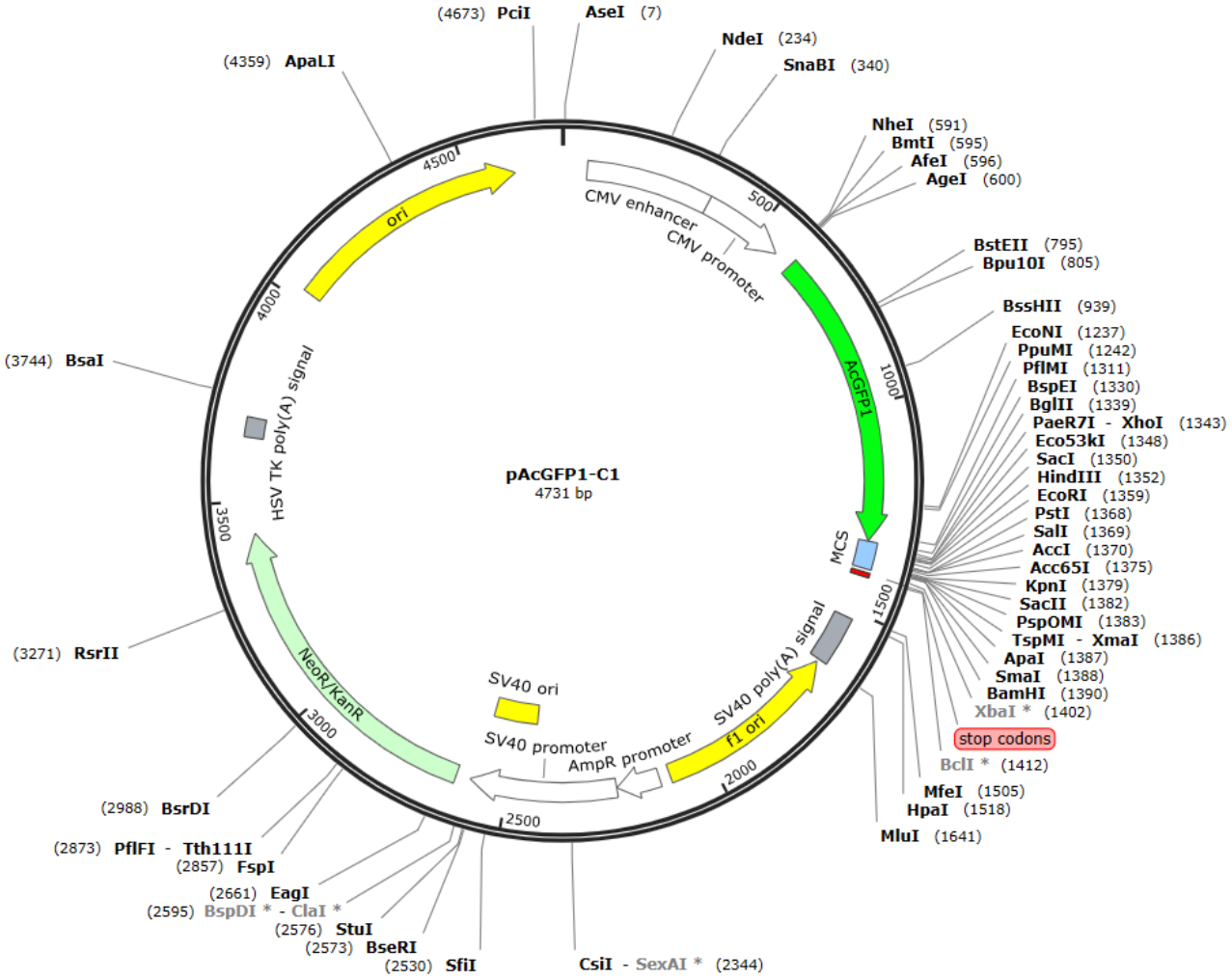

6.2.2 pGEX-4T1-NTEV

The bacterial expression vector pGEX-4T1-NTEV used here is based on the pGEX-4T1 vector which was modified by introducing a TEV (Tobacco Etch Virus) nuclear-inclusion-a endopeptidase site downstream of the GST coding sequence for cleavage of the GST tag following protein purification. This vector was used to generate N-terminal GST-tagged myosin 5 proteins for expression of recombinant proteins in *E.coli* and subsequent protein purification. Gene expression is regulated by the tac promoter, a ubiquitous *E.coli* promoter. An ampicillin resistance gene is present for bacterial selection.

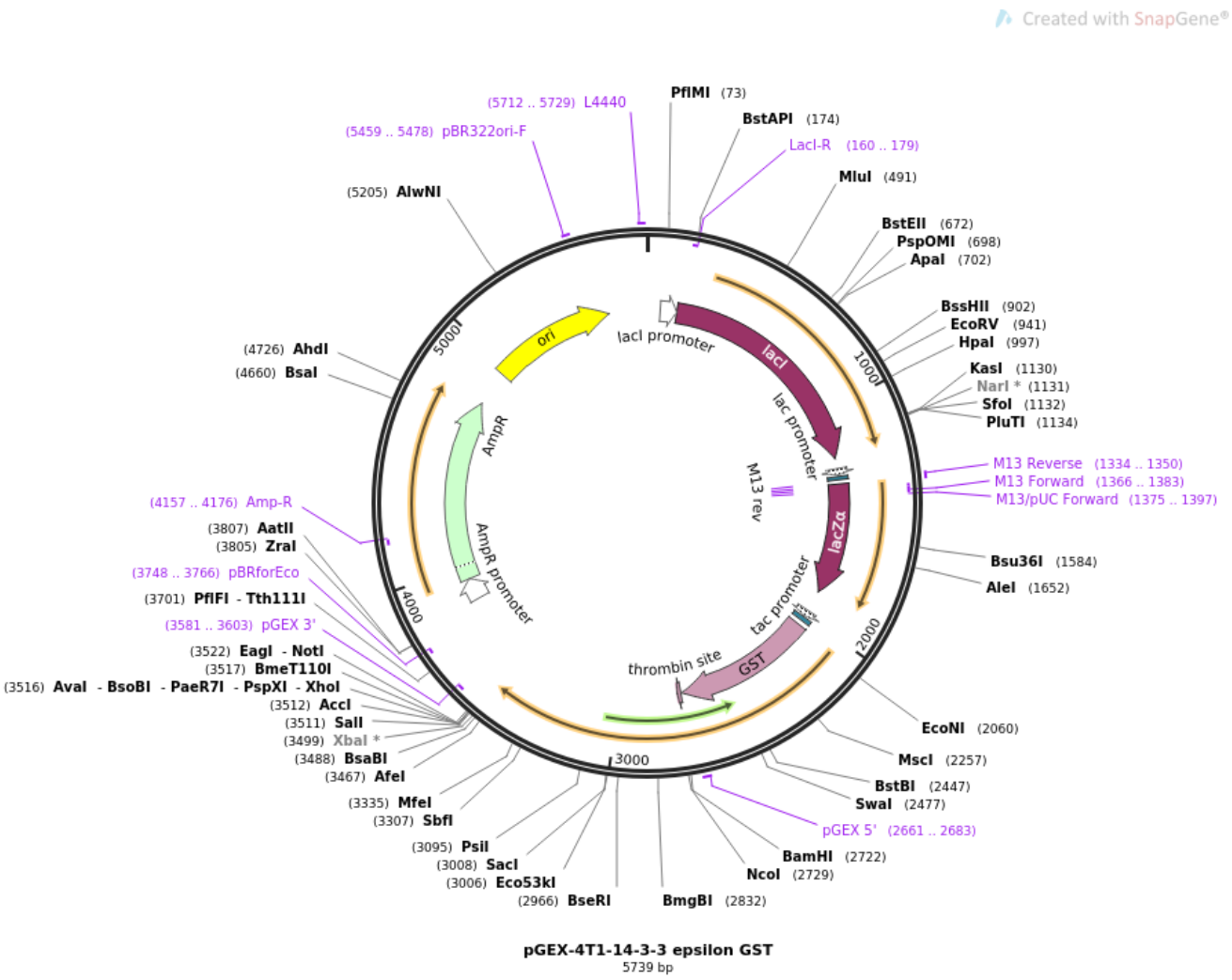

6.2.3 pProEX-HTb

The bacterial expression vector pProEX-HTb used here was modified by inserting the coding sequence of the mScarlet-I red fluorescent protein at the beginning of the multiple cloning site (EcoRI / *Kpn*I _ EcoRI/ HindIII). This vector was used to generate N-terminal His_6-mScarlet-I-tagged SPIRE peptides for expression of recombinant proteins in *E.coli* and subsequent protein purification. Gene expression is regulated by the trc promoter, a ubiquitous *E.coli* promoter. A TEV site is present downstream of the His_6 amino acid sequence for cleavage of the His_6 tag following protein purification. An ampicillin resistance gene allows for bacterial selection.

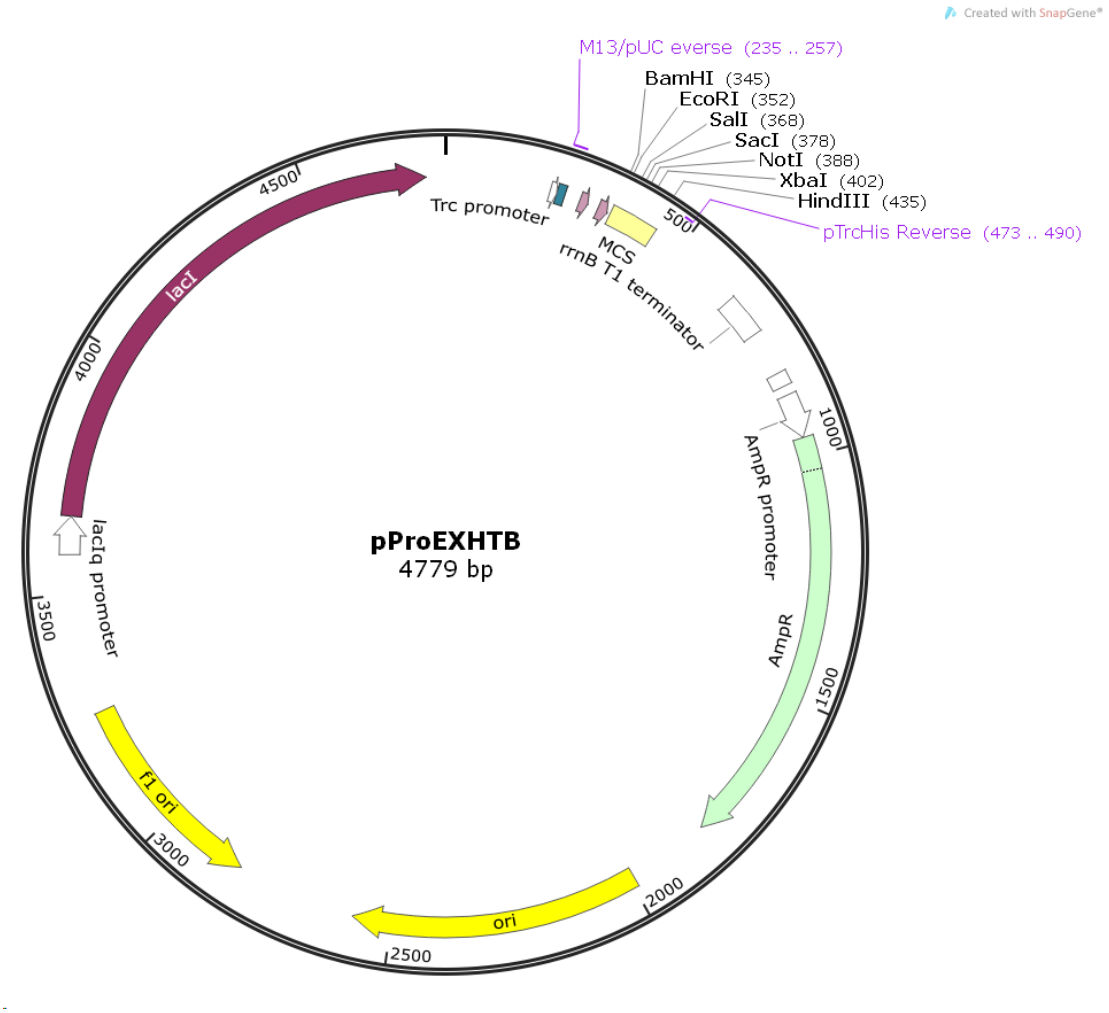

6.3 Expression vectors used in this thesis

6.3.1 Eucaryotic expression vectors

Construct name	Expression vector	Boundaries	Purpose
GFP-MYO5A-cc-GTD	peGFP-C2-mm-MYO5A-cc-GTD	aa 1260 – 1880 (EcoRI/ SalI)	Colocalisation, fluorescent microscopy
GFP-MYO5B-cc-GTD	pAcGFP1-C1-Hs-MYO5B-cc-GTD	aa 904 – 1848 (HindIII/SalI)	Colocalisation, fluorescent microscopy
GFP-MYO5C-cc-GTD	pAcGFP1-C1-Hs-MYO5C-cc-GTD	aa 889 – 1742 (XhoI/ EcoRI)	Colocalisation, fluorescent microscopy
GFP-Hs-SPIRE1-fl	pAcGFP1-C1-Hs-SPIRE1-fl	aa 1 – 742 (BamHI/ KpnI)	GST-pulldown Assay from HEK lysates
GFP-Hs-SPIRE1-ΔKW	pAcGFP1-C1-Hs-ΔKW	aa 388 – 742 (KpnI/ BamHI)	GST-pulldown Assay from HEK lysates
GFP-Hs-SPIRE2-fl	pAcGFP1-C1-Hs-SPIRE2-fl	aa 1 – 728 (BamHI/ XbaI)	GST-pulldown Assay from HEK lysates
GFP-Hs-SPIRE2-ΔKW	pAcGFP1-C1-Hs-SPIRE2-ΔKW	aa 375 – 728 (XhoI/ KpnI)	GST-pulldown Assay from HEK lysates
GFP	pAcGFP1-C1		GST-pulldown Assay from HEK lysates as control

Table 10: Overview on eukaryotic expression vectors. aa, amino acid.

6.3.2 Bacterial expression vectors

Construct name	Expression vector	Boundaries	Purification	Purpose
His_6-mScarlet-I-Hs-SPIRE1-linker	pProEX-HTb-mScarlet-I-Hs-SPIRE1-linker	aa 388 – 528 (EcoRI/ KpnI)	Ni-NTA Agarose, Superdex 200	GST-pulldown, Binding assays, quantitative pulldown/supernatant depletion assay
His_6-mScarlet-I-Hs-SPIRE2-linker	pProEX-HTb-mScarlet-I-Hs-SPIRE2-linker	aa 375 – 533 (EcoRI/ HindIII)	Ni-NTA Agarose, Superdex 200	GST-pulldown, Binding assays, quantitative pulldown/supernatant depletion assay
GST-Hs-MYO5A-GTD	pGEX-4T1-NTEV-Hs-MYO5A-GTD	aa 1495 – 1880 (BamHI/ EcoRI)	GSH Sepharose 4B, Superdex 200	GST-pulldown, Binding assays, quantitative pulldown/supernatant depletion assay
GST-Hs-MYO5B-GTD	pGEX-4T1-NTEV-Hs-MYO5B-GTD	aa 1467 – 1848 (BamHI/ XhoI)	GSH Sepharose 4B, Superdex 200	GST-pulldown, Binding assays, quantitative pulldown/supernatant depletion assay
GST-Hs-MYO5C-GTD	pGEX-4T1-NTEV-Hs-MYO5C-GTD	aa 1358 – 1742 (BamHI/ XhoI)	GSH Sepharose 4B, Superdex 200	GST-pulldown, Binding assays, quantitative

				pulldown/supernatant depletion assay
GST-Sr-MYO5-GTD	pGEX-4T1-NTEV-Sr-MYO5-GTD	aa 1547 - 1921 (BamHI/ EcoRI)	GSH Sepharose 4B, Superdex 200	GST-pulldown, Binding assays, quantitative pulldown/supernatant depletion assay
GST-Nv-MYO5-GTD	pGEX-4T1-NTEV-Nv-MYO5-GTD	aa 1455 - 1828 (BamHI/ EcoRI)	GSH Sepharose 4B, Superdex 200	GST-pulldown, Binding assays, quantitative pulldown/supernatant depletion assay
His_6-mScarlet-I-Sr-SPIRE-linker	pProEX-HTb-mScarlet-I- Sr-SPIRE-linker	aa 269 – 540 (EcoRI/ HindIII)	Ni-NTA Agarose, Superdex 200	GST-pulldown, Binding assays, quantitative pulldown/supernatant depletion assay
His_6-mScarlet-I-Nv-SPIRE-linker	pProEX-HTb-mScarlet-I- Nv-SPIRE-linker	aa 357 – 500 (EcoRI/ KpnI)	Ni-NTA Agarose, Superdex 200	GST-pulldown, Binding assays, quantitative pulldown/supernatant depletion assay
His_6-mScarlet-I	pProEX-Htb-mScarlet-I	aa 1 -234 (BamHI/ KpnI)	Ni-NTA Agarose, Superdex 200	GST-pulldown
GST	pGEX-4T1-NTEV		GSH Sepharose 4B, Superdex 200	GST-pulldown

Table 11: Overview on bacterial expression vectors (*), these expression vectors were generated and kindly provided by;. aa, amino acid.

6.4 Single graphs of RNA expression pattern

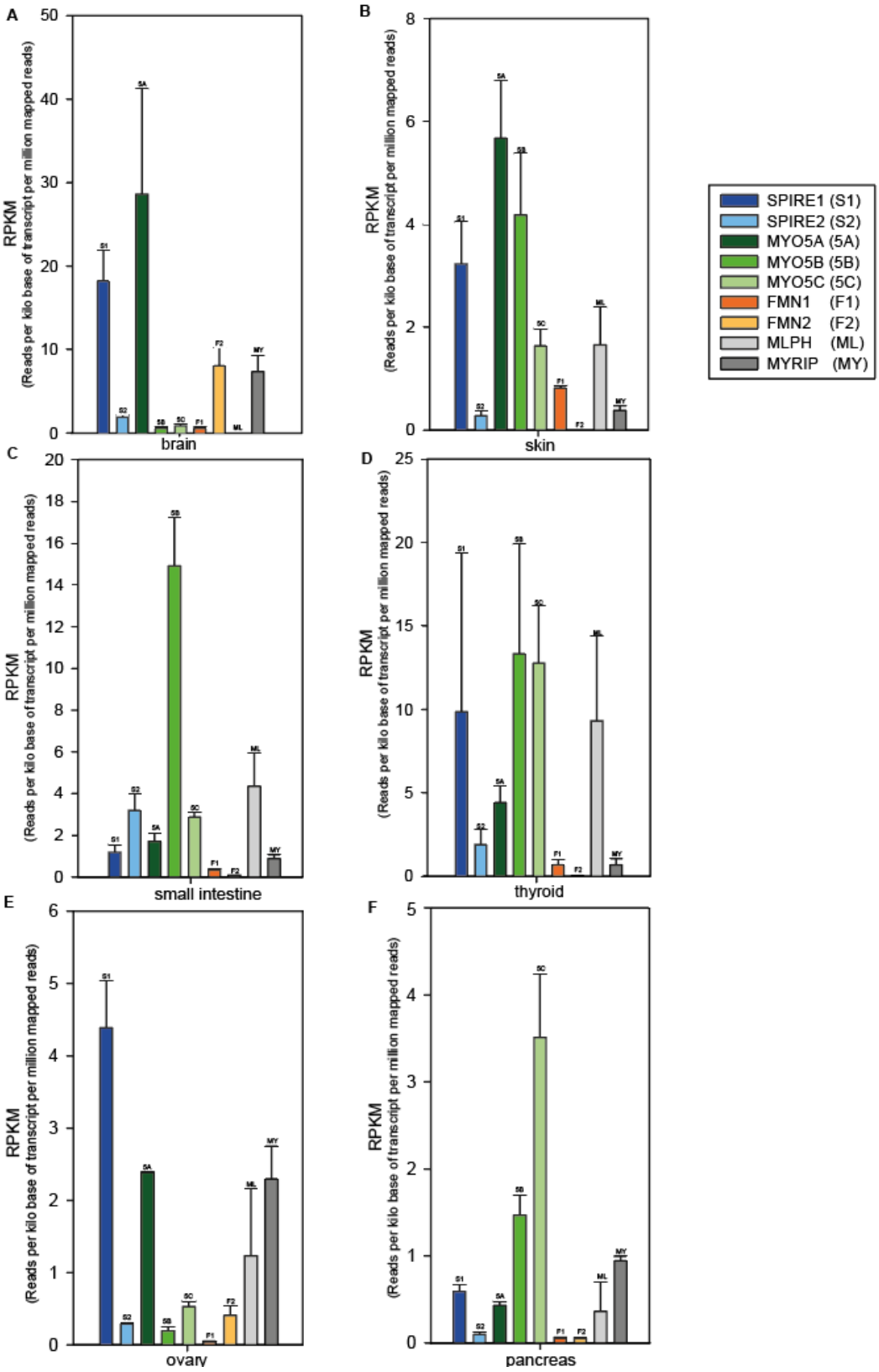

*Figure 34: **Single graphs of RNA-Expression** of SPIRE1, SPIRE2, MYO5A, MYO5B, MYO5C, FMN1, FMN2, MLPH and MYRIP in the six different tissues. A) brain; B) skin; C) small intestine; D) thyroid; E) ovary; F) pancreas; Error bars represent SEM. Data from the in silico RNA-seq data base from the NCBI.*

6.5 Pulldown with purified proteins Nv-/Sr-MYO5-GTD with Nv-/Sr-SPIRE-linker

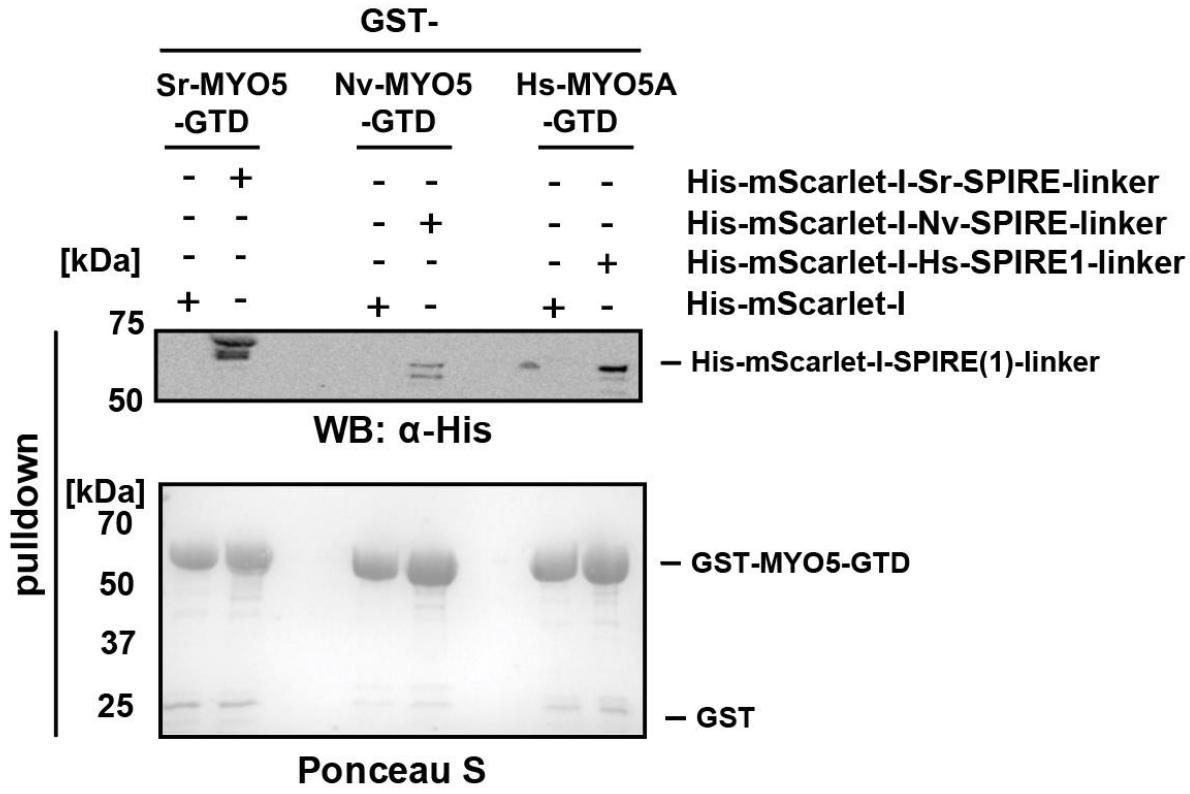

Figure 35: ***Nv/Sr/Hs-MYO5A-GTD interacts with Nv/Sr/Hs-SPIRE1-linker:*** *GST-Pulldown-Assay with purified GST-Nv/Sr/Hs-MYO5A with purified His-mScarlet-I-Nv/Sr/Hs-SPIRE1-linker and as a control functions mScarlet-I. GST-tagged proteins were immobilised on GSH-beads and incubated with His-mScarlet-I-SPIRE1/2-linker and His-mScarlet-I on a rotating wheel at 4°C. GTD, globular tail domain.*

6.6 Single graphs and raw data of the quantitative pulldown assays: MYO5 – SPIRE interaction

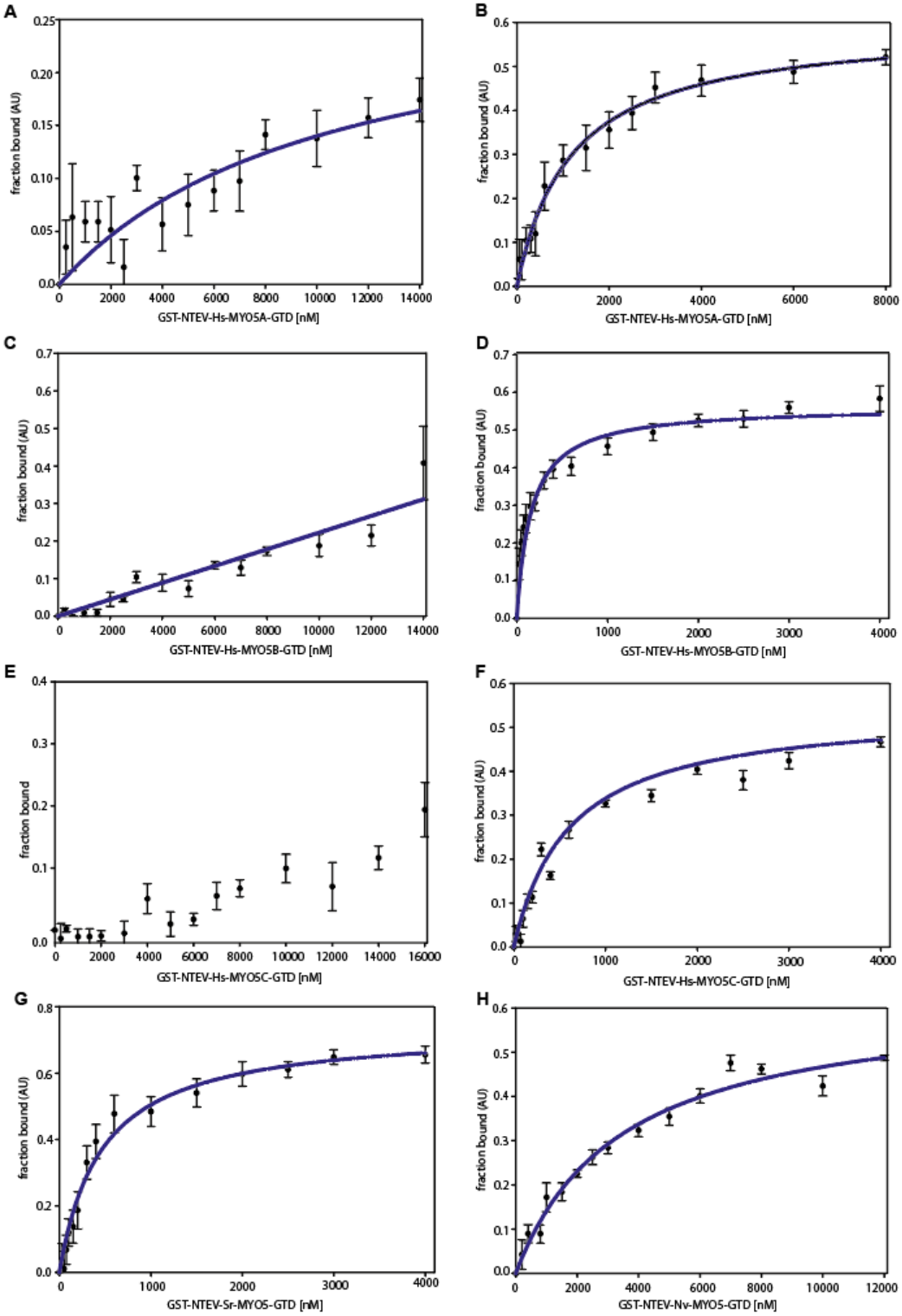

*Figure 36: **Single graphs of MYO5-GTD – SPIRE-linker quantitative pulldown assays**. A) GST-NTEV-Hs-MYO5A-GTD/mScarlet-I-Hs-SPIRE1-linker; B) GST-NTEV-Hs-MYO5A-GTD/mScarlet-I-Hs-SPIRE2-linker; C) GST-NTEV-Hs-MYO5B-GTD/mScarlet-I-Hs-SPIRE1-linker; D) GST-NTEV-Hs-MYO5A-GTD/mScarlet-I-Hs-SPIRE2-linker; E) GST-NTEV-Hs-MYO5C-GTD/mScarlet-I-Hs-SPIRE1-linker; F) GST-NTEV-Hs-MYO5C-GTD/mScarlet-I-Hs-SPIRE2-linker; G) GST-NTEV-Sr-MYO5-GTD/mScarlet-I-Sr-SPIRE-linker; H) GST-NTEV-Nv-MYO5-GTD/mScarlet-I-Nv-SPIRE-linker. Hs, Homo sapiens; Sr, Salpingoeca rosetta; Nv, Nematostella vectensis. Error bars represent SEM; N = 5 experimental repeats.*

Table 12: raw data of the quantitative pulldown assays.

GST-Hs-MYO5A-GTD / His-mScarlet-I-Hs-SPIRE1-linker																
	0 nM	250 nM	500 nM	1000 nM	1500 nM	2000 nM	2500 nM	3000 nM	4000 nM	5000 nM	6000 nM	7000 nM	8000 nM	10000 nM	12000 nM	14000 nM
experiment 1	58,1665964	53,6511297	49,1277964	53,628363	51,6844964	55,3306964	55,2291964	53,9459297	54,807163	54,6190297	52,4414964	52,4464297	50,341763	52,8970297	50,1035297	49,3378964
$(y_0 - y_c)/y_0$	0	0,0776	0,1554	0,078	0,078	0,0488	0,0505	0,0726	0,0578	0,061	0,0984	0,0983	0,1345	0,0906	0,1386	0,1518
experiment 2	67,3667446	67,0194779	63,0848113	63,5223779	67,6393779	61,6087779	65,0253446	58,7870779	62,6392446	56,7561779	60,3241113	58,2853446	56,9440113	53,8394779	55,3133113	52,2542779
$(y_0 - y_c)/y_0$	0	5,15E-03	0,0636	0,0571	0,0571	0,0855	0,0348	0,1274	0,0702	0,1575	0,1045	0,1348	0,1547	0,2008	0,1789	0,2243
experiment 3	78,9003385	70,1785718	64,9423385	69,3804385	68,4462385	67,0602385	73,6996718	68,6452718	67,7788052	69,0958385	67,5429052	65,2661052	64,0360052	62,7862385	63,2813718	61,5486052
$(y_0 - y_c)/y_0$	0	0,1105	0,1769	0,1207	0,1207	0,1501	0,0659	0,13	0,141	0,1243	0,1439	0,1728	0,1884	0,2042	0,198	0,2199
experiment 4	35,6329712	36,5847379	39,3771379	35,3089045	35,6113379	36,4930379	38,5401379	32,5858712	35,7928045	34,4424712	33,2135379	32,9066712	31,5006379	32,2807045	32,2889379	30,1204379
$(y_0 - y_c)/y_0$	0	-0,0267	-0,1051	9,09E-03	9,09E-03	-0,0241	-0,0816	0,0855	-4,49E-03	0,0334	0,0679	0,0765	0,116	0,0941	0,0938	0,1547
experiment 5	52,814809	52,3589423	51,473509	51,191109	52,6989423	53,0103756	52,229809	48,2704423	51,8338756	52,857509	51,3879756	52,5882423	46,8728423	47,6240423	43,4950756	46,4857423
$(y_0 - y_c)/y_0$	0	8,63E-03	0,0254	0,0307	0,0307	-3,70E-03	0,0111	0,086	0,0186	-8,08E-04	0,027	4,29E-03	0,1125	0,0983	0,1765	0,1198

GST-Hs-MYO5A-GTD / His-mScarlet-I-Hs-SPIRE2-linker																
	0 nM	25 nM	50 nM	100 nM	200 nM	300 nM	400 nM	600 nM	1000 nM	1500 nM	2000 nM	2500 nM	3000 nM	4000 nM	6000 nM	8000 nM
experiment 1	35,4770847	33,6068513	36,5617847	34,937118	32,1934513	34,8385847	35,4273847	34,1929513	26,2200513	26,975318	23,5966847	24,8770847	22,1766847	21,6494513	20,6046513	17,063918
$(y_0 - y_c)/y_0$	0	0,0527	-0,0306	-0,0306	0,0926	0,018	1,40E-03	0,0362	0,2609	0,2396	0,3349	0,2988	0,3749	0,3898	0,4192	0,519
experiment 2	44,5516041	48,3006708	37,6500375	40,1287041	40,4266041	37,5445041	39,8727708	31,2884708	29,0439708	35,3232041	29,7348708	25,5558708	23,4812375	23,6544041	19,3837041	20,2825375
$(y_0 - y_c)/y_0$	0	-0,0842	0,1549	0,1549	0,0926	0,1573	0,105	0,2977	0,3481	0,2071	0,3326	0,4264	0,4729	0,4691	0,5649	0,5447
experiment 3	29,9908785	33,8274119	31,1976452	30,1871785	29,5155119	27,6048452	28,8707452	23,7871452	24,3369785	21,5469452	21,6195452	20,4097119	18,9160119	18,1554119	16,2233452	16,1115452
$(y_0 - y_c)/y_0$	0	-0,1279	-0,0402	-0,0402	0,0159	0,0796	0,0373	0,2069	0,1885	0,2816	0,2791	0,3195	0,3693	0,3946	0,4591	0,4628
experiment 4	37,9153255	35,7205922	36,5264588	37,7729255	33,3663922	34,5314922	31,4846255	28,9258255	28,4975255	24,7536588	25,9488588	21,8759588	19,2100588	18,4844922	20,1653588	18,3867922
$(y_0 - y_c)/y_0$	0	0,0579	0,0366	0,0366	0,12	0,0892	0,1696	0,2371	0,2484	0,3471	0,3156	0,423	0,4933	0,5125	0,4681	0,5151
experiment 5	22,2207774	21,9435108	18,0764441	20,6004108	17,7883774	17,8455108	15,8856108	14,1809774	13,6671774	11,1304441	10,7174674	11,0322774	9,98991077	9,39596411	10,5120208	9,68563744
$(y_0 - y_c)/y_0$	0	0,0125	0,1865	0,1865	0,1995	0,1969	0,2851	0,3618	0,3849	0,4991	0,5177	0,5035	0,5504	0,5772	0,5269	0,5641

GST-Hs-MYO5B-GTD / His-mScarlet-I-Hs-SPIRE1-linker																
	0 nM	250 nM	500 nM	1000 nM	1500 nM	2000 nM	2500 nM	3000 nM	4000 nM	5000 nM	6000 nM	7000 nM	8000 nM	10000 nM	12000 nM	14000 nM
experiment 1	39,2668425	38,4129758	37,0182092	38,1421092	35,8268092	34,5462425	36,5623758	33,6779758	32,8197092	37,9453425	33,9732092	36,0377092	32,4568092	33,9431758	33,9714425	30,5668092
$(y_0 - y_c)/y_0$	0	0,0217	0,0573	0,0286	0,0286	0,1202	0,0689	0,1423	0,1642	0,0337	0,1348	0,0822	0,1734	0,1356	0,1349	0,2216
experiment 2	82,0013992	79,6281659	82,8535992	79,3681992	77,1119992	79,5601325	79,8155325	77,7993325	79,7239992	81,0891659	73,9619992	65,4827992	71,1981659	73,9468325	69,0748659	62,5294325
$(y_0 - y_c)/y_0$	0	0,0289	-0,0104	0,0321	0,0321	0,0298	0,0267	0,0512	0,0278	0,0111	0,098	0,2014	0,1317	0,0982	0,1576	0,2375
experiment 3	83,3763311	82,9287978	86,4653645	83,3701645	79,7263978	81,6525978	79,7802645	74,0043311	77,3005645	74,8108645	70,8437978	73,3140978	68,4567978	63,9766645	62,4456978	29,5382978
$(y_0 - y_c)/y_0$	0	5,37E-03	-0,037	7,40E-05	7,40E-05	0,0207	0,0431	0,1124	0,0729	0,1027	0,1503	0,1207	0,1789	0,2327	0,251	0,6457
experiment 4	83,3763311	82,9287978	86,4653645	83,3701645	79,7263978	81,6525978	79,7802645	74,0043311	77,3005645	74,8108645	70,8437978	73,3140978	68,4567978	63,9766645	62,4456978	29,5382978
$(y_0 - y_c)/y_0$	0	5,37E-03	-0,037	7,40E-05	7,40E-05	0,0207	0,0431	0,1124	0,0729	0,1027	0,1503	0,1207	0,1789	0,2327	0,251	0,6457
experiment 5	61,8949565	60,6464898	65,2011565	62,7940565	60,3701898	59,7573898	59,2829231	55,6338565	55,1125231	54,6967231	52,9678231	54,4852898	49,4272898	47,0616898	44,6568898	44,0092231
$(y_0 - y_c)/y_0$	0	0,0202	-0,0534	-0,0145	-0,0145	0,0345	0,0422	0,1012	0,1096	0,1163	0,1442	0,1197	0,2014	0,2397	0,2785	0,289

GST-Hs-MYO5B-GTD / His-mScarlet-I-Hs-SPIRE2-linker																
	0 nM	25 nM	50 nM	75 nM	100 nM	150 nM	200 nM	300 nM	400 nM	600 nM	1000 nM	1500 nM	2000 nM	2500 nM	3000 nM	4000 nM
experiment 1	60,3411311	54,2419811	50,3053811	42,5717811	42,6760811	39,4390311	38,7690811	37,8128311	37,5797311	36,9849811	32,7019311	27,8773811	27,8403811	27,4357311	25,4252311	22,2931311
$(y_0 - y_c)/y_0$	0	0,1011	0,1663	0,2945	0,2928	0,3464	0,3575	0,3733	0,3772	0,3871	0,458	0,538	0,5386	0,5453	0,5786	0,6305
experiment 2	65,6129552	60,4808552	59,8074552	55,7340552	53,0778552	51,0660052	45,9678552	41,3135552	42,0224552	43,1855052	36,8694552	33,2332552	35,1720052	32,9033052	26,4749052	28,9953552
$(y_0 - y_c)/y_0$	0	0,0782	0,0885	0,1506	0,191	0,2217	0,2994	0,3703	0,3595	0,3418	0,4381	0,4935	0,4639	0,4985	0,5965	0,5581
experiment 3	66,2362664	62,7293331	52,4251331	52,9228664	55,7860331	53,3422664	51,0842664	47,7996331	43,2755331	41,7947664	40,8819998	38,1635331	32,1643331	35,7833331	32,8513331	35,6569664
$(y_0 - y_c)/y_0$	0	0,0529	0,2085	0,201	0,1578	0,1947	0,2288	0,2783	0,3466	0,369	0,3828	0,4238	0,5144	0,4598	0,504	0,4617
experiment 4	66,6297999	48,8475999	47,5806332	44,9480332	44,8510999	41,6014666	45,0201666	40,0327666	39,1366666	36,7138332	33,2094332	30,5809999	29,6467666	28,7276999	29,8180999	23,4127999
$(y_0 - y_c)/y_0$	0	0,2669	0,2859	0,3254	0,3269	0,3756	0,3243	0,3992	0,4126	0,449	0,5016	0,541	0,5551	0,5688	0,5525	0,6486
experiment 5	74,8601423	58,3654423	56,0714089	57,1258423	48,7727089	49,0526423	50,9685423	44,5265089	38,8874089	39,7007089	37,4321423	39,6514423	33,5976423	31,9177423	32,8427089	28,9944423
$(y_0 - y_c)/y_0$	0	0,2203	0,251	0,2369	0,3485	0,3447	0,3191	0,4052	0,4805	0,4697	0,5	0,4703	0,5512	0,5736	0,5613	0,6127

GST-Hs-MYO5C-GTD / His-mScarlet-I-Hs-SPIRE1-linker																
	0 nM	250 nM	500 nM	1000 nM	1500 nM	2000 nM	3000 nM	4000 nM	5000 nM	6000 nM	7000 nM	8000 nM	10000 nM	12000 nM	14000 nM	16000 nM
experiment 1	63,0942027	60,710636	62,504336	61,6235027	61,5356693	63,3158693	65,4899693	62,5424027	59,5003027	63,3570693	59,1875027	56,6517027	56,089936	56,4663693	56,4514693	52,2620027
$(y_0 - y_c)/y_0$	0	0,0378	9,35E-03	0,0233	0,0247	-3,51E-03	-0,038	8,75E-03	0,057	-4,17E-03	0,0619	0,1021	0,111	0,105	0,1053	0,1717
experiment 2	52,8436723	55,315939	52,695339	52,316139	53,9246723	53,797239	49,4098057	46,4798723	49,9425723	52,840639	48,4968723	49,163839	44,321039	43,1168057	43,3087057	34,259239
$(y_0 - y_c)/y_0$	0	-0,0468	2,81E-03	0,01	0,01	-0,018	0,065	0,1204	0,0549	5,74E-05	0,0823	0,0696	0,1613	0,1841	0,1804	0,3517
experiment 3	131,052141	141,548808	132,926141	135,366474	131,881474	134,444141	135,544141	118,828474	130,909141	124,303808	115,361808	120,381808	114,516474	136,131808	113,818474	103,133108
$(y_0 - y_c)/y_0$	0	-0,0801	-0,0143	-0,0329	-0,0329	-0,0259	-0,0343	0,0933	1,09E-03	0,0515	0,1197	0,0814	0,1262	-0,0388	0,1315	0,213
experiment 4	122,506675	125,470675	120,492675	123,688675	122,526675	119,885342	121,190675	118,478675	126,696009	119,822675	122,235009	114,718342	114,332342	111,129009	114,129342	106,230342
$(y_0 - y_c)/y_0$	0	-0,0242	0,0164	-9,65E-03	-9,65E-03	0,0214	0,0107	0,0329	-0,0342	0,0219	2,22E-03	0,0636	0,0667	0,0929	0,0684	0,1329
experiment 5	123,144147	117,437814	123,55548	128,46548	120,699814	125,66848	126,635814	123,37748	126,699147	120,90948	121,951814	120,80648	119,31048	122,215814	111,314814	110,810814
$(y_0 - y_c)/y_0$	0	0,0463	-3,34E-03	-0,0432	-0,0432	-0,0205	-0,0284	-1,89E-03	-0,0289	0,0181	9,68E-03	0,019	0,0311	7,54E-03	0,0961	0,1002

GST-Hs-MYO5C-GTD / His-mScarlet-I-Hs-SPIRE2-linker																
	0 nM	25 nM	50 nM	75 nM	100 nM	150 nM	200 nM	300 nM	400 nM	600 nM	1000 nM	1500 nM	2000 nM	2500 nM	3000 nM	4000 nM
experiment 1	57,0347801	53,7190801	56,7931135	57,7987801	54,3285135	51,9002801	52,2583801	41,2933135	46,6943135	40,8041801	37,6960468	36,0138801	32,4852135	34,7068468	33,0836135	27,9721801
$(y_0 - y_c)/y_0$	0	0,0581	4,24E-03	-0,0134	0,0474	0,09	0,0837	0,276	0,1813	0,2846	0,3391	0,3686	0,4304	0,3915	0,4199	0,5096
experiment 2	56,2740913	52,6352247	54,8020913	53,2966247	50,7354247	49,562558	47,1032247	45,5584247	46,6824913	38,4847913	36,9246913	35,1926913	31,9696913	31,751758	29,437458	30,379758
$(y_0 - y_c)/y_0$	0	0,0647	0,0262	0,0529	0,0984	0,1193	0,163	0,1904	0,1704	0,3161	0,3438	0,3746	0,4319	0,4358	0,4769	0,4601
experiment 3	56,1668453	55,2598786	55,6075786	55,0661119	55,3717786	53,5208786	50,0477786	44,2153453	48,6517119	39,9213786	39,2919119	38,8505119	34,3296453	35,8407119	30,9593453	29,9934453
$(y_0 - y_c)/y_0$	0	0,0161	0,01	0,0196	0,0142	0,0471	0,1089	0,2128	0,1338	0,2892	0,3004	0,3083	0,3888	0,3619	0,4488	0,466
experiment 4	48,8411624	50,4243624	48,7612624	50,4680624	46,7360624	42,8570958	43,3397624	37,7977291	40,3223291	38,6190624	33,3768291	33,3921958	30,3919624	33,8138958	30,7940958	27,0947624
$(y_0 - y_c)/y_0$	0	-0,0324	1,64E-03	-0,0333	0,0431	0,1225	0,1126	0,2261	0,1744	0,2093	0,3166	0,3163	0,3777	0,3077	0,3695	0,4452
experiment 5	59,5612981	57,0547981	53,0715314	57,3019647	52,5396314	51,0730314	53,6330314	47,2437314	50,2967981	45,6011647	39,6670314	38,4133981	36,1237314	35,4373647	35,4493314	32,5189314
$(y_0 - y_c)/y_0$	0	0,0421	0,109	0,0379	0,1179	0,1425	0,0995	0,2068	0,1555	0,2344	0,334	0,3551	0,3935	0,405	0,4048	0,454

GST-Nv-MYO5-GTD / His-mScarlet-I-Nv-SPIRE-linker																
	0 nM	200 nM	400 nM	800 nM	1000 nM	1500 nM	2000 nM	2500 nM	3000 nM	4000 nM	5000 nM	6000 nM	7000 nM	8000 nM	10000 nM	12000 nM
experiment 1	25,5194302	25,5144302	24,9135302	23,4049635	20,6754968	20,3821302	19,9412968	18,0187635	18,2695302	17,2345302	17,0158635	14,5824635	14,4815302	14,7406302	12,8048635	13,0106302
$(y_0 - y_c)/y_0$	0	1,96E-04	0,0237	0,0237	0,1898	0,2013	0,2186	0,2939	0,2841	0,3247	0,3332	0,4286	0,4325	0,4224	0,4982	0,4902
experiment 2	27,8996387	23,070272	23,680272	23,3461387	20,1337053	21,211272	22,2011387	19,711072	19,826472	17,8891053	15,865472	15,8652387	13,8134387	15,2395053	15,6750387	13,9998387
$(y_0 - y_c)/y_0$	0	0,1731	0,1512	0,1512	0,2784	0,2397	0,2042	0,2935	0,2894	0,3588	0,4313	0,4313	0,5049	0,4538	0,4382	0,4982
experiment 3	26,7711709	26,6053709	24,1761709	23,0525376	22,5884042	21,8913376	20,2166042	19,7496042	18,5513042	17,9164042	18,0081042	15,9849376	13,2693376	13,9656042	15,7545042	14,0728042
$(y_0 - y_c)/y_0$	0	6,19E-03	0,0969	0,0969	0,1562	0,1823	0,2448	0,2623	0,307	0,3308	0,3273	0,4029	0,5043	0,4783	0,4115	0,4743
experiment 4	44,7614261	44,5865595	39,3366595	44,3557595	40,6545928	39,5154928	38,6949928	36,0506261	32,5046261	33,1478261	29,9120261	30,2488595	26,1261595	26,0520928	24,9762928	23,8823928
$(y_0 - y_c)/y_0$	0	3,90E-03	0,1212	0,1212	0,0917	0,1172	0,1355	0,1946	0,2738	0,2595	0,3317	0,3242	0,4163	0,418	0,442	0,4665
experiment 5	25,7154439	25,0672106	23,7184772	23,2696439	23,6954439	22,7915439	20,2471772	20,5557772	19,7384439	18,7157772	16,6582439	16,9271106	14,5822772	13,4156772	16,4839439	12,8949106
$(y_0 - y_c)/y_0$	0	0,0252	0,0777	0,0777	0,0786	0,1137	0,2126	0,2006	0,2324	0,2722	0,3522	0,3418	0,4329	0,4783	0,359	0,4986

GST-Sr-MYO5-GTD / His-mScarlet-I-Sr-SPIRE-linker																
	0 nM	25 nM	50 nM	75 nM	100 nM	150 nM	200 nM	300 nM	400 nM	600 nM	1000 nM	1500 nM	2000 nM	2500 nM	3000 nM	4000 nM
experiment 1	13,5719496	14,1982162	14,9876829	14,0258162	13,3394162	13,4723162	12,1931829	9,13730956	7,77808289	8,01845623	6,92535623	6,28292956	5,46616289	4,89392289	5,27059623	5,14369289
$(y_0 - y_c)/y_0$	0	-0,0461	-0,1043	-0,0334	0,0171	7,34E-03	0,1016	0,3268	0,4269	0,4092	0,4897	0,5371	0,5972	0,6394	0,6117	0,621
experiment 2	13,8468977	14,3217643	14,0332977	13,154631	11,0062643	11,7845977	9,992251	7,464771	8,48224433	6,12678433	6,54576433	7,11947433	5,095451	6,052291	5,68401433	4,85667767
$(y_0 - y_c)/y_0$	0	-0,0343	-0,0135	0,05	0,2051	0,1489	0,2784	0,4609	0,3874	0,5575	0,5273	0,4858	0,632	0,5629	0,5895	0,6493
experiment 3	12,3436774	13,5949441	12,6368108	10,7625741	11,9800774	9,73104077	10,5224474	8,37156743	6,56281077	5,29938077	5,26441077	4,05421743	4,56811743	4,7010041	4,18138077	4,0447841
$(y_0 - y_c)/y_0$	0	-0,1014	-0,0237	0,1281	0,0295	0,2117	0,1475	0,3218	0,4683	0,5707	0,5735	0,6716	0,6299	0,6192	0,6613	0,6723
experiment 4	16,7922546	16,700888	13,3689546	15,2889213	13,3327546	12,1989546	10,9071813	10,253858	8,58875463	7,3294813	8,08432463	6,9807713	5,53394797	5,37590797	4,74452797	4,31874463
$(y_0 - y_c)/y_0$	0	5,44E-03	0,2039	0,2039	0,206	0,2735	0,3505	0,3894	0,4885	0,5635	0,5186	0,5843	0,6704	0,6799	0,7175	0,7428
experiment 5	18,3700501	13,2918834	18,5157501	17,1730501	15,7421834	17,4615501	17,3243501	15,5061501	14,6781167	13,1186501	12,6304834	10,5940501	9,94252007	8,27697007	6,21536007	7,49716007
$(y_0 - y_c)/y_0$	0	0,2764	-7,93E-03	-7,93E-03	0,1431	0,0495	0,0569	0,1559	0,201	0,2859	0,3124	0,4233	0,4588	0,5494	0,6617	0,5919

Table 13: Raw data for RNA expression level analysis for the six chosen tissues, in RPKM (reads per kilo base of transcript per million mapped reads).

RPKM	SPIRE1	SEM SPIRE1	SPIRE2	SEM SPIRE2	MYO5A	SEM MYO5A	MYO5B	SEM MYO5B	MYO5C	SEM MYO5C	FMN1	SEM FMN1	FMN2	SEM FMN2
brain	18,208	3,697	1,880	0,242	28,595	12,662	0,539	0,243	0,835	0,168	0,571	0,190	8,016	2,119
skin	3,233	0,820	0,278	0,100	5,676	1,127	4,180	1,199	1,638	0,332	0,818	0,054	0,000	0,000
small intestine	1,179	0,379	3,196	0,793	1,720	0,381	14,911	2,325	2,873	0,222	0,337	0,086	0,068	0,024
thyroid	9,853	9,526	1,904	0,896	4,421	0,994	13,338	6,557	12,775	3,430	0,683	0,307	0,036	0,020
ovary	4,385	0,650	0,289	0,013	2,383	0,013	0,188	0,067	0,533	0,069	0,037	0,013	0,406	0,133
pancreas	0,590	0,081	0,096	0,035	0,434	0,043	1,469	0,234	3,509	0,736	0,056	0,008	0,050	0,021

6.7 Colocalisation images of whole cells with insets of GFP-MYO5-cc-GTD with mScarlet-I-SPIRE1/2-ΔKW in HeLa cells

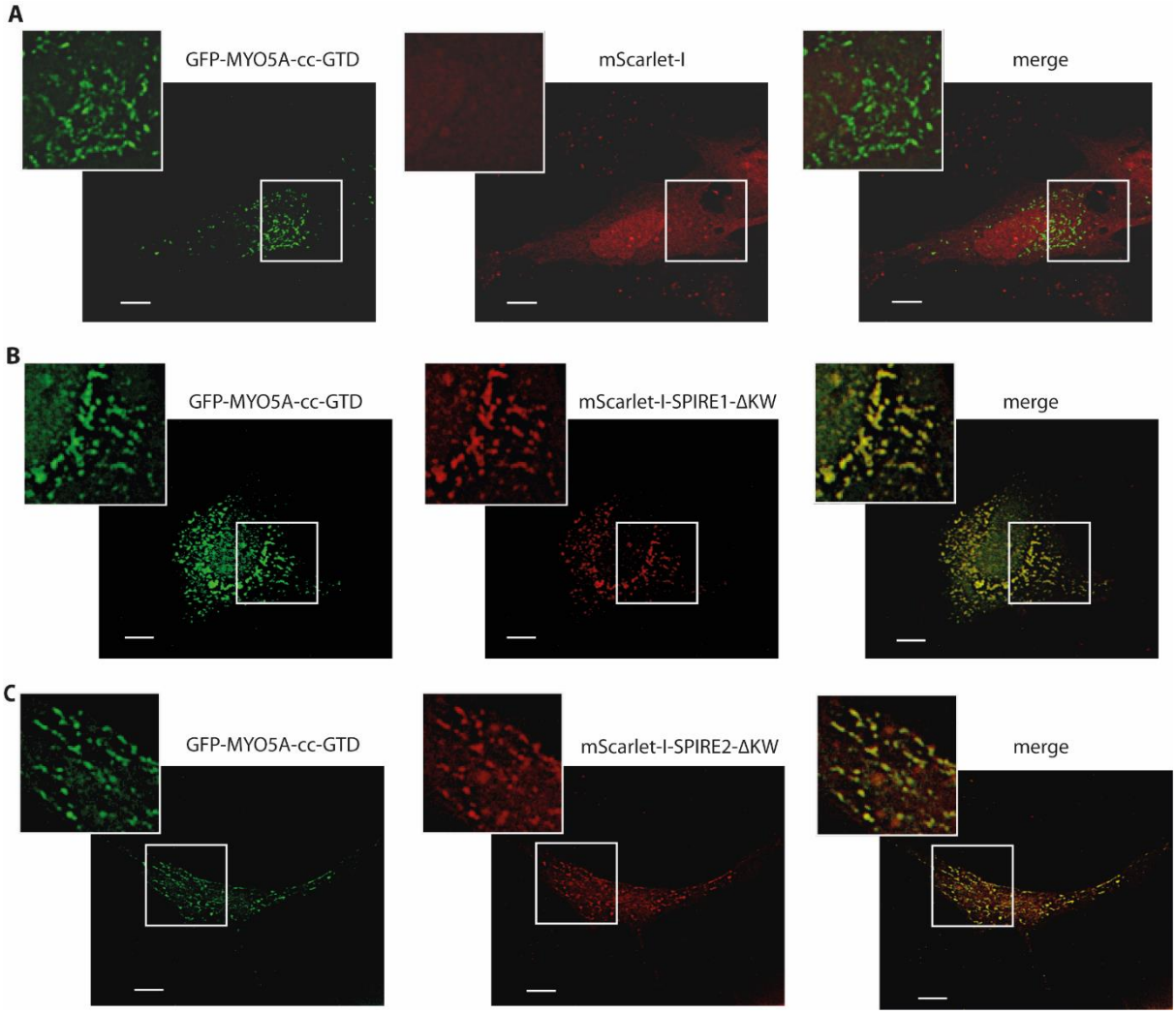

Figure 37: ***Myosin5A-cc-GTD and SPIRE-1-ΔKW and SPIRE-2-ΔKW colocalise at vesicle membranes****. GFP-tagged Myo5A-cc-GTD (GFP-Myo5A-cc-GTD; green) A) GFP-tagged-MYO5A-cc-GTD does not colocalise with mScarlet-I (pm-Scarlet-I; red) B), GFP-tagged-MYO5A-cc-GTD colocalise with mScarlet-I-SPIRE1-ΔKW (pm-Scarlet-I-Hs-SPIRE1-ΔKW; red)* ***C****) GFP-tagged-MYO5B-cc-GTD colocalise with mScarlet-I-SPIRE2-ΔKW (pm-Scarlet-I-Hs-SPIRE2-ΔKW; red) at vesicle membranes when transiently co-expressed in HeLa cells, as indicated by overlapping punctae (merge; yellow; see also higher magnification in insets). 5 cells were recorded for each condition and one representative cell is presented here.* Scale bars *represent 10 µm.*

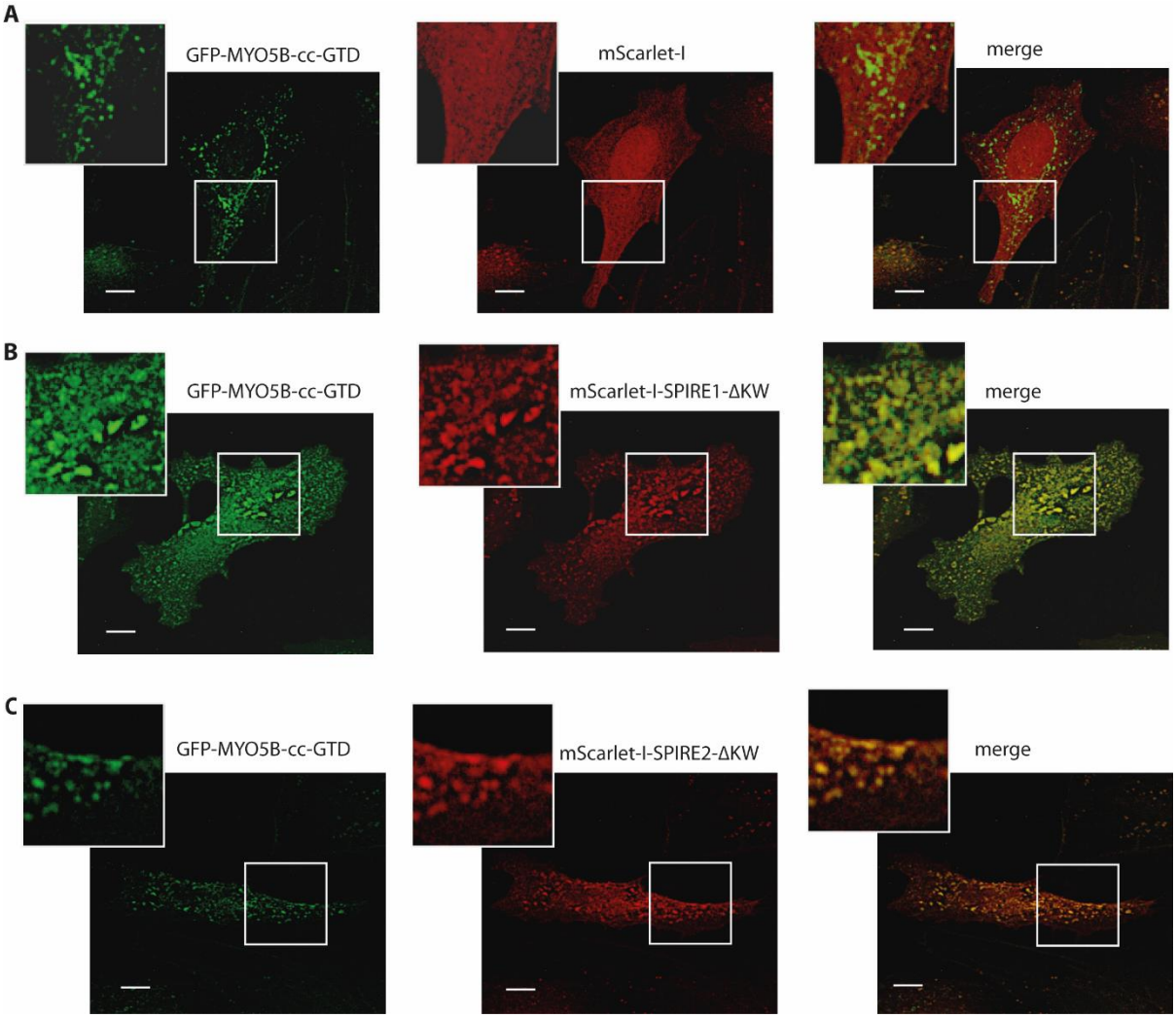

Figure 38: ***Myosin5B-cc-GTD and SPIRE-1-ΔKW and SPIRE-2-ΔKW colocalise at vesicle membranes.*** *GFP-tagged Myo5B-cc-GTD (AcGFP1-C1-Myo5B-cc-GTD; green)* ***A****) GFP-tagged-MYO5B-cc-GTD does not colocalise with mScarlet-I (pm-Scarlet-I; red)* **B***), GFP-tagged-MYO5B-cc-GTD colocalise with mScarlet-I-SPIRE1-ΔKW (pm-Scarlet-I-Hs-SPIRE1-ΔKW; red)* ***C****) GFP-tagged-MYO5B-cc-GTD colocalise with mScarlet-I-SPIRE2-ΔKW (pm-Scarlet-I-Hs-SPIRE2-ΔKW; red) at vesicle membranes when transiently co-expressed in HeLa cells, as indicated by overlapping punctae (merge; yellow; see also higher magnification in insets). 5 cells were recorded for each condition and one representative cell is presented here.* Scale bars *represent 10 µm.*

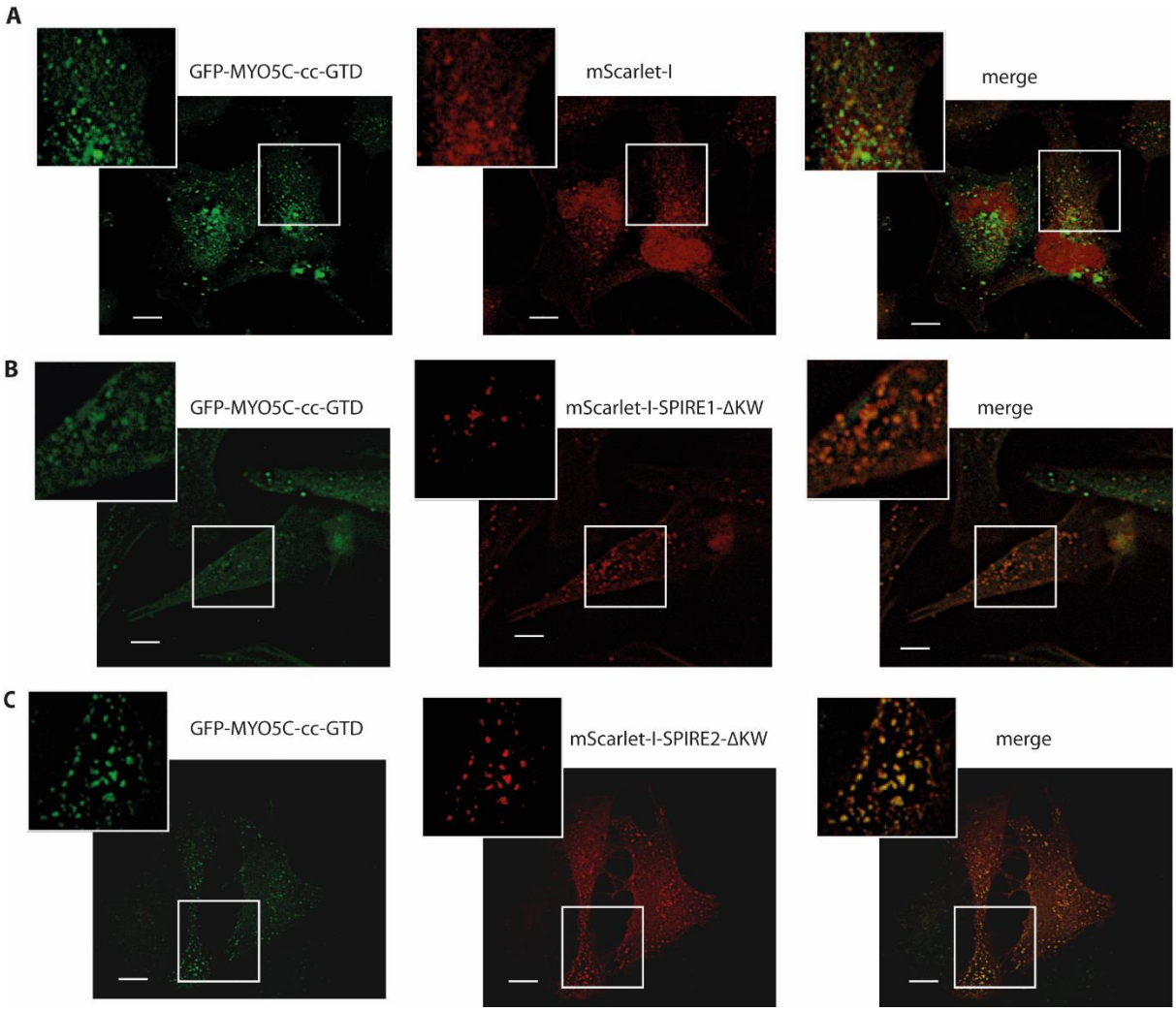

Figure 39: ***Myosin5C-cc-GTD and SPIRE-1-ΔKW and SPIRE-2-ΔKW colocalise at vesicle membranes.*** *GFP-tagged Myo5C-cc-GTD (AcGFP1-C1-Myo5C-cc-GTD; green)* ***A****) GFP-tagged-MYO5C-cc-GTD does not colocalise with mScarlet-I (pm-Scarlet-I; red)* **B***), GFP-tagged-MYO5C-cc-GTD colocalise with mScarlet-I-SPIRE1-ΔKW (pm-Scarlet-I-Hs-SPIRE1-ΔKW; red)* ***C****) GFP-tagged-MYO5C-cc-GTD colocalise with mScarlet-I-SPIRE2-ΔKW (pm-Scarlet-I-Hs-SPIRE2-ΔKW; red)at vesicle membranes when transiently co-expressed in HeLa cells, as indicated by overlapping punctae (merge; yellow; see also higher magnification in insets). 5 cells were recorded for each condition and one representative cell is presented here.* Scale bars *represent 10 µm.*

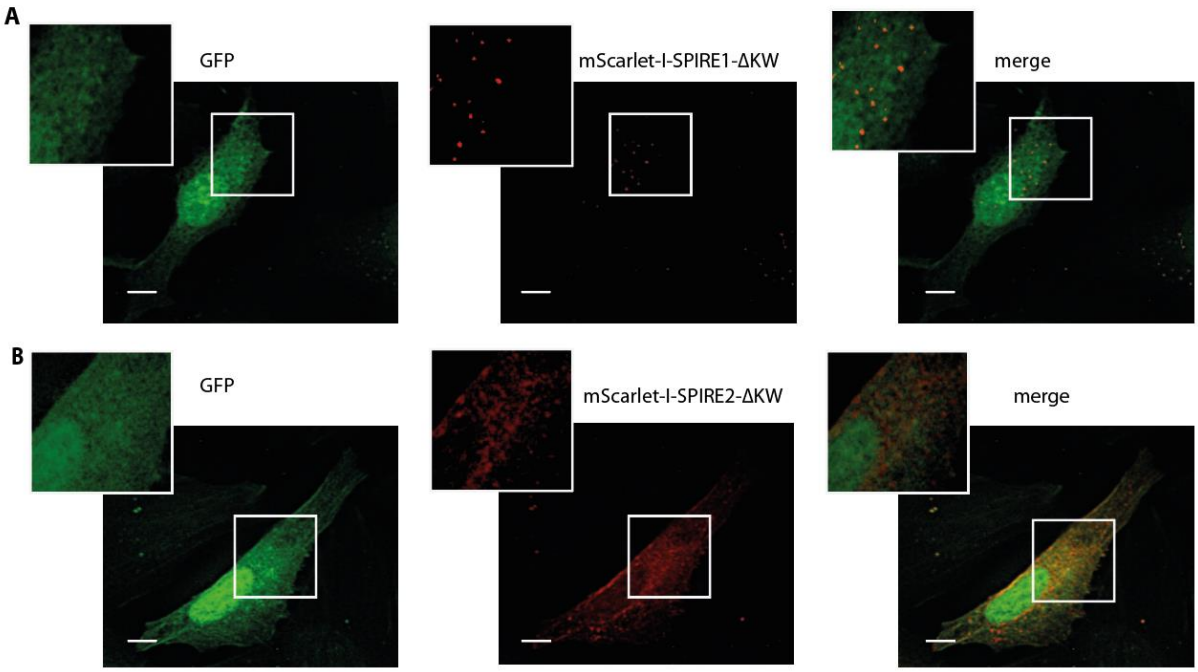

Figure 40: ***GFP and SPIRE-1-ΔKW and SPIRE-2-ΔKW do not colocalise at vesicle membranes.*** *GFP (green)* ***A****) GFP does not colocalise with mScarlet-I-SPIRE1-ΔKW (mScarlet-I-SPIRE1/2-ΔKW; red)* **B***) GFP does not colocalise with mScarlet-I-SPIRE2-ΔKW (mScarlet-I-SPIRE2-ΔKW; red) at vesicle membranes when transiently co-expressed in HeLa cells, as indicated by overlapping punctae (merge; yellow; see also higher magnification in insets). 5 cells were recorded for each condition and one representative cell is presented here.* Scale bars *represent 10 µm.*

6.8 Buffers, solutions and media

Agar selection plates for bacterial culture	- 25 g LB_0 medium - 13 g select agar - Fill up with H_2O to 1 l - Autoclave for 20 min at 121°C - Cool to approx. 42°C - Add antibiotics (10% Amp or 25 mg/ml Kan)
Agarose solution for gel electrophoresis	- Dissolve needed amount of agarose in 0.5x TBE buffer by boiling and shaking (1%- 2%)
Ampicillin solution (10%)	- 1 g Ampicillin sodium salt in 10 ml H_2O - Filter sterile and store aliquots à 1 ml at-20°C
APS solution (10%)	- Dissolve 10% Ammoniumpersulfat (w/v) in H_2O - Store at 4°C
ß-Mercaptoethanol solution (12.8M)	- Mix stock solution in H_2O to receive 12.8 M
Coomassie staining solution	- 10% acetic acid - 40% ethanol - 0.6% (w/v) Coomassie brilliant blue G250 - 0.6% (w/v) Coomassie brilliant blue R250
Chloramphenicol solution	- Dissolve 34 mg/ml in ethanol
DNA ladder (1 kb) for agarose gel electrophoresis	- 100 µl 6x Tri Track DNA loading buffer - 100 µl 1kb ladder (Thermo Fisher) - 400 µl H_2O
DNA loading dye (6x)	- 10 mM Tris-HCl, pH 7.6 - 0.03% Bromophenol blue - 60% glycerol - 60 mM EDTA
FCSIII for cell culture	- Inactivate at 56°C (water bath) for 30 min - Store 50 ml aliquots at-20°C
Full Medium for cell culture	- DMEM - 10% FCSIII - 2 mM L-Glutamine - 100 units/ ml Penicillin - 100 µg/ ml Streptomycin
IPTG stock solution (0.1 M)	- Dissolve in sterile H_2O - Filter sterile, store 2 ml aliquots at-20°C
Kanamycin stock solution (25 mg/ml)	- Dissolve Kanamycin monosulfate in H_2O - Filter sterile and store 2 ml aliquots at-20°C
LB medium (Luria/ Miller)	- Dissolve 25 g/ l in H_2O (10g/l Trypton; 3g/l yeast extract; 10g/l NaCl) - Autoclave for 20 min at 121°C
Mowiol solution	- Dissolve 15 g Mowiol 4-88 in 70 ml H_2O - Add 30 mL glycerol - Add 2.5% (w/v) n-propylgallat - Centrifuge at 17,300 x g for 15 min - Store 1 ml aliquots at-20°C
Paraformaldehyde solution (3.7%)	- Dissolve 7.4 g paraformaldehyde in 100 ml 1x PBS - Add 2 drops 10 M NaOH - Incubate at 60°C for at least 30 min - Add 100 ml 1x PBS, adjust to pH 7.4 - Store 10 ml aliquots at-20°C
PBS (2x) for protein purification	- 2300 mg/ l = 16.2 mM Na_2HPO_4

	- 400 mg/ l = 5.4 mM KCl - 400 mg/ l = 2.94 KH_2PO_4 - 16000 mg/ l = 275 mM NaCl
PBS (10x)	- Dissolve 95.5 g PBS powder in 1 l H_2O
PBST (1x; 0.05% Tween20)	- Add 0.05% Tween20 to 1x PBS (100ml 10xPBS + 900ml H_2O)
PMSF stock solution (0.1 M)	- Dissolve in ethanol - Store 2 ml aliquots at-20°C
Ponceau S staining solution	- 5% acetic acid - 0.1% (w/v) Ponceau S
Pulldown buffer	- 25 mM Tris-HCl, pH 7.4 - 150 mM NaCl - 5 mM $MgCl_2$ - 0.1% NP-40 - 10% glycerol
SDS-PAGE-buffer (10x)	- 250 mM Tris - 1.9 M glycine - 1% SDS (w/v)
SDS protein sample buffer (5x) **Laemmli buffer**	- 100 mM Tris-HCl, pH 6.8 - 50% glycerol (v/v) - 15% SDS (w/v) - 25% ß-Mercaptoethanol (v/v) - 0.025% bromophenol blue (w/v) - Store 1 ml aliquots at-20°C
Transfer buffer (10x)	- 250 mM Tris - 1.92 M glycine
Transfer buffer (1x)	- 25 mM Tris - 192 mM glycine - 20% methanol
Tris-EDTA, pH 8.0 **For plasmid DNA storage**	- 20 mM Tris - 1 mM EDTA - adjust to pH 8.0 with HCl - autoclave
Triton X-100 (0.2%)	- 0.2% in 1x PBS
Tween20 (10%)	- dilute Tween20 in 1x PBS

Table 14: Overview on buffers, solutions and media.

6.9 SDS polyacrylamide gels

Separating gel

	10 %	**12 %**
H_2O	4.8 ml	4.1 ml
3 M Tris pH 9.0	1.3 ml	1.3 ml
Acrylamide30	3.5 ml	4.2 ml
20% SDS	50 µl	50 µl
TEMED	10 µl	10 µl
10% APS	50 µl	50 µl

Table 15: Preparation of SDS separation gels.

Stacking gel

H_2O	2.6 ml
1 M Tris pH 9.0	420 µl
Acrylamide30	550 µl
20% SDS	17 µl
TEMED	5 µl
10% APS	33 µl

Table 16: Preparation of SDS stacking gels.

6.10 Primer

Primer name	Tm (°C)	Primer sequence (5' > 3')
Cloning primer		
EcoRI-HsSpire1-388-5' (388-528aa)	69.9	g gaa ttc cca gag gag att aga cgt agc
HsSpire1-528-Stop-KpnI-3' (388-528aa)	83.8	gg ggt acc tca act ctg cct gga agg cgg cag
EcoRI-HsSpire2-375-5' (375-533 aa	88.5	g gaa ttc ggc gag ggc tgg gct gcc cgc
HsSpire2-533-Stop-HindIII-3' (388- 528 aa)	84.7	ccc aag ctt tca atc ggg ggt cat gga ggc ctc
BamHI-HsMyoVc-GTD-5'	78.7	cg gga tcc gag tac ctt gga atg ctg caa tac
HsMyoVc-GTD-Stop-XhoI-3'	73.1	ccg ctc gag tac taa cct att cag aaa gcc tag
XhoI-HsMyoVc-GTD-5'	80.8	ccg ct cga gct gag tac ctt gga atg ctg caa tac
HsMyoVc-GTD-Stop-BamHI-3'	71.6	cg gga tcc cta taa cct att cag aaa gcc tag
XhoI-HsMyoVc-cc-GTD-5'	83.3	ccg ct cga gct cag ggt cca gcg ttt gca gaa
HsMyoVc-GTD-intEcoRI-3'	68.8	g gaa ttc ctc ttc tcc gct gta ctg
EcoRI-NvSPIRE-357-5'	77.1	g gaa ttc aca gtg cag gaa att tac tac
NvSPIRE-500-Stop-KpnI-3'	84.7	gg ggt acc tca tcg tag gga ggg cgg gaa aat ggg
EcoRI-SrSPIRE-269-5'	78.6	g gaa ttc acg cgc ctc tca cac agc acg cca
SrSPIRE-540-Stop-HindIII-3'	79.1	ccc aag ctt tca ttg tgg ttt cgg cgg tgt ccc tcc

Table 17: Overview on primers used in this thesis. Tm, melting temperature.

6.11 Antibodies

6.11.1 Primary antibodies

Antibody	Species/ clonality	Purpose	Company	Order number
Living Colors® Full-length GFP antibody	rabbit polyclonal	Western blot	TakaraBio/Clontech	632592
Penta-His™ Antibody, BSA-free	mouse monoclonal	Western blot	QIAGEN	34660

Table 18: Overview on primary antibodies.

6.11.2 Secondary antibodies

Antibody	Species/ clonality	Purpose	Company	Order number
ECL ® anti-rabbit IgG, HRP-linked	donkey	Western blot	GE Healtcare Life Sciences	NA934-1ML
ECL ® anti-mouse IgG, HRP-linked	sheep	Western blot	GE Healtcare Life Sciences	NA931-1ML

Table 19: Overview on secondary antibodies.

6.12 Chemicals and reagents

6.12.1 Restriction endonucleases

Restriction endonuclease	Concentration	Company	Order number
***Bam*HI-HF**	20,000 units/ ml	NEB	R3136S
***Eco*RI-HF**	20,000 units/ ml	NEB	R3101S
***Hind*III-HF**	20,000 units/ ml	NEB	R3104S
***Kpn*I-HF**	20,000 units/ ml	NEB	R3142L
***Sac*I**	20,000 units/ ml	NEB	R0156L
***Xho*I**	20,000 units/ ml	NEB	R0146L

Table 20: Overview on restriction endonucleases.

6.12.2 DNA polymerases

DNA polymerase	Concentration/ volume	Company	Order number
AccuPrimeTM Pfx DNA Polymerase	2.5 units/ µl	ThermoFisher	12344-024

Table 21: Overview on DNA polymerases.

6.12.3 Enzymes

Enzyme	Concentration	Company	Order number
Quick CIP (Alkaline Phosphatase, Calf Intestinal)	5,000 units/ml	NEB	M0525S
T4 DNA Ligase	400,000 units/ml	NEB	M0202S

Table 22: Overview on further used enzymes.

6.12.4 Chemicals

Article	Quantity	Company	Order number
1,4-Dithioerythriol (DTE)	5 g	Sigma-Aldrich	D8255-5G
Acetic acid, Rotipuran, 100%, p.a.	1 l	Carl Roth	3738.1
Albumin standard (2.0 mg/ml)	10 x 1 ml	ThermoFisher	23209
Ammoniumpersulfat	100 g	Sigma-Aldrich	A3678
Ampicillin sodium salt	25 g	Sigma-Aldrich	A9518-25G
ß-Mercaptoethanol	100 ml	Carl Roth	4227.3
Boric acid	1 kg	Sigma-Aldrich	B0252-1KG
Brilliant Blue G 250	10 g	Carl Roth	9598.1
Brilliant Blue R 250	10 g	Carl Roth	3862.1
Bromophenol blue sodium salt	10 g	Carl Roth	A512.1
Chloramphenicol	25 g	Sigma-Aldrich	C0378-25G
Coomassie Plus Protein Assay Reagent for Bradford assays	950 ml	ThermoFisher	1856210
cOmplete Mini, EDTA-free	25 tabs	Roche	11836170001
DL-Dithiothreitol (DTT)	5 g	Sigma-Aldrich	D0632-5G
dNTP solution set	25 µM each	NEB	N0446S
Ethanol >99.8%, p.a.	2.5 l	Carl Roth	9065.2
Ethanol >99.8% + 1 % MEK	2.5 l	Carl Roth	K928.1
Ethidiumbromide solution, 0.5%	15 ml	Carl Roth	HP46.1
Glycerine-solution for microscopy		Leica	11513872
Glutathione Sepharose 4B	10 ml	GE Healthcare Life Sciences	17-0756-01
Glycine, 99%	5 kg	Carl Roth	3790.3
Hydrochloric acid, Rotipuran, 25%	1 l	Carl Roth	6331.1
Immersion liquid, Type F		Leica	11513859
Imidazole	500 g	Sigma-Aldrich	56750-500G
Isopropyl-ß-D-1-thiogalactopyranoside (IPTG)	5 g	Sigma-Aldrich	I6758-5G
Isopropanol, > 99.5%	2.5 l	Carl Roth	9866.5
Kanamycin B sulfate salt	250 mg	Sigma-Aldrich	B5264-250MG
LB-Medium (Luria/ Miller; 10 g/ l NaCl)	5 kg	Carl Roth	X968.4
L-Glutathione reduced, >98%	25 g	Sigma-Aldrich	G4251-25G
Luminata™ Forte Western HRP Substrate	100 ml	Merck-Millipore	WBLUF0100
Magnesium chloride hexahydrate	100 g	Sigma-Aldrich	M2670-100G
Methanol, LiChrosolv	2.5 l	Merck-Millipore	1.06007.2500
Milk powder	1 kg	Carl Roth	T145.3
MOWIOL 4-88 Reagent	100 g	Calbiochem	475904
Ni-NTA Agarose	25 ml	Qiagen	1018244
Nonidet P-40 BioChemica (NP-40)	500 ml	AppliChem	A1694,0500
Paraformaldehyde	250 g	Carl Roth	0335.1
PBS-Buffer powder	10 l	AppliChem	A0965,9010
ThermoFisher 1kb DNA Ladder	5 x 50 µg	ThermoFisher	SM0242
Phenylmethylsulfonylfluorid, PMSF	5 g	Sigma-Aldrich	P-7626-5G
Ponceau S, pratical grade	50 g	Sigma-Aldrich	P3504-50G
Protran® Nitrocellulose Blotting Membrane BA85, 0.45 µm		GE Healthcare LifeScience Amersham	10401196

Precision Plus Protein Dual Color Standards	500 µl	Bio-Rad	161-0374
Rotiphorese Gel 30, Acrylamid/ Bis-Acrylamid solution	500 ml	Carl Roth	3029.1
Rubidium chloride, >99%, p.a.	25 g	Carl Roth	4471.3
Select agar	1 kg	Sigma-Aldrich	A5054-1KG
Sodium chloride, >98%	1 kg	Sigma-Aldrich	S3014-1KG
Sodium dodecyl sulfate (SDS)	500 g	Sigma-Aldrich	L4390-500G
Sodium fluoride	100 g	Fluka	71519
Sodium hydroxide pellets	1 kg	Merck	1.06462
Sodium orthovanadate	10 g	Sigma-Aldrich	450243-10G
TEMED	100 ml	Sigma-Aldrich	T9281
Triton X-100, for molecular biology	100 ml	Sigma-Aldrich	T8787-100ML
Trizma base	1 kg	Sigma	T1503-1KG
Tween 20, BioChemica	500 ml	AppliChem	A1389,0500
UltraPure™ Agarose	500 g	Invitrogen	15510-027

Table 23: Overview on chemicals.

6.13 Cell culture media, reagents and supplements

Article	Quantity	Company	Order number
D-MEM (HG) W/O NA PYR (CE)	500 ml	ThermoFisher	41965-062
Dimethyl sulfoxide (DMSO), Hybri-Max	5 x 10 ml	Sigma-Aldrich	D2650
HyClone FetalClone III Serum (FCS III) Lot: AD23319274	500 ml	GE Healthcare Life Sciences	SH30109.03
jetOPTIMUS®	0.75 ml	Polyplus	101000025
L-Glutamine; 200 mM	100 ml	ThermoFisher	25030024
Lipofectamine2000 reagent	1 ml	ThermoFisher	18324012
Dulbecco's Phosphate Buffered Saline (PBS)	500 ml	Sigma-Aldrich	D8537
Penicillin/ Streptomycin solution	100 ml	ThermoFisher	15140122
Poly-L-Lysine	50 ml	Sigma-Aldrich	P4707
Trypan Blue solution (0.4%, sterile-filtered, suitable for cell culture)	100 ml	Sigma-Aldrich	T8154-100ML
Trypsin-EDTA (0.05%)	100 ml	ThermoFisher	25300054
Waster, sterile filtered, BioReagent, suitable for cell culture	1 l	Sigma-Aldrich	W3500-1L

Table 24: Overview on cell culture media, reagents and supplements.

6.14 Kits

Kit	Company	Order number
NucleoSpin® Gel and PCR Clean-up	Macherey-Nagel	REF 740609.50
QIAGEN® Plasmid Maxi Kit (25)	Qiagen	12163
QIAprep Spin Miniprep Kit (250)	Qiagen	27106

Table 25: Overview on kits.

6.15 Equipment

Article	Company	Order number
ÄKTApurifier	GE Healthcare Life Sciences	
Cell counting Chamber (Neubauer, depth: 0.1 mm; 0.0025 mm²)	Marienfeld-Superior	0640010
Centrifuge, 5417 R, refrigerated	Eppendorf	
Centrifuge, 5424	Eppendorf	
Centrifuge, Multifuge 1-s-r, refrigerated	Heraeus	75004331
Centrifuge, refrigerated, BC Avanti J-26 XP	Beckman Coulter	JXS 10 G30
Centrifuge bottle, polycarbonate, 50 ml	Beckman Coulter	357000
Centrifuge bottle, polycarbonate, 250 ml	Heraeus	
Centrifuge bottle, polypropylene, 1000 ml	Beckman Coulter	366752
E-Box 3026 WL-26M (UV-Transilluminator)	PeqLab	
Forma Orbital Shaker, 37°C	Thermo Scientific	
Forma Orbital Shaker, refrigerated	Thermo Scientific	
GeneQuant 1300	GE Healthcare Life Sciences	28-9182-13
ImageQuant LAS 4000	GE Healthcare Life Sciences	28-9558-10
JA-25.50 rotor for Avanti J-26 XP	Beckman Coulter	S/N 10E 2140
JLA-8.1000 rotor for Avanti J-26 SP	Beckman Coulter	969329
High Load™ 16/60 Superdex 200 pg	GE Healtcare Life Sciences	28989335
Leica AF6000 LX Life Cell Imaging System	Leica	
Mastercycler en gradient S	Eppendorf	5345 000.510
Mini Trans-Blot® Cell	Bio-Rad	170-3930
PowerPac™ 300	Bio-Rad	165-5051
PowerPac™ Basic Power Supply	Bio-Rad	164-5050
VarioScan	ThermoFisher	9001272
Water bath	Memmert	

Table 26: Overview on used equipment.

6.16 Disposable materials

Article	Company	Order number
Amicon Ultra, 30K, Centrifugal filters	Millipore	UFC803024
Amicon Ultra, 30K, Centrifugal filters	Millipore	UFC903024
Autoclave indicator tape (12°C)	A. Hartenstein	STKD
Blotting papers, Grade 3 MM Chr	Whatman	3030.917
Cell culture dish (100x 20 mm)	Greiner Bio-One	664160
Cell culture plate (6-well)	Greiner Bio-One	657160
Cell culture plate (6-well)	TPP	Z707759
Cellstar tubes, canonical (15 ml)	Greiner Bio-One	188261
Cellstar tubes, canonical (50 ml)	Greiner Bio-One	227261
CryoTube Vials (1 ml)	Nunc	366656
Microscope cover glasses, 15 mm	A. Hartenstein	DKR2
Microscope slides, Menzel-Gläser, Superfrost Plus	Thermo Scientific	J1800AMNZ
Needles, BD Microlance 3, 20G x 1.5''	BD Biosciences	301300
Parafilm® "M" Laboratory Film	Pechiney Plastic Packaging	PM-996
Pasteur pipettes	A. Hartenstein	PP07
PCR SoftTubes (0.2 ml)	Biozym	710920

Petri dishes (94 x 16 mm)	A. Hartenstein	PP90
Pipette tips, blue (100 – 1000 µl)	Axygen	T-1000-B
Pipette tips, blue (100 – 1000 µl)	Sarstedt	70.3050.020
Pipette tips, white (0.5 – 10 µl)	Axygen	T-300
Pipette tips, yellow (2 – 200 µl)	Sarstedt	70.760.002
Reaction tubes (1.5 ml)	A. Hartenstein	RK1G
Reaction tubes (2.0 ml)	A. Hartenstein	RK2G
Syringe (2 ml)	BD Biosciences	237
Syringe (10 ml)	BD Biosciences	274
Syringe with needle, 1 ml 26G x 3/8'', Luer	BD Biosciences	300015
T75 cell culture flask (75 cm², 250 ml)	Sarstedt	83.1813.002
Transfection tubes (5 ml, 75 x 12 mm)	Sarstedt	55.476.013
Ventilation cap tubes (14 ml)	Sarstedt	62.515.006
Videoprinter paper	VWR	PEQRCD80E1091

Table 27: Overview on desposables.

7 List of abbreviations

A

Aa – Amino acid

AAA – ATPases Associated with Diverse Activities

ABD – F-actin binding domain

AcGFP – Aequorea coerulescens GFP

ADF – Actin depolymerising factor

ADP – Adenosine diphosphate

AMPA – α-amino-3-hydroxy-5-methyl-4-isoxazoleporpionic acid

Arf – ADP-ribosylation factor

Arp2/3 – Actin-related protein 2/3

ARPC – Arp complex protein

ATP – Adenosine triphosphate

B

Bp – Base pair

Br – Brachydanio rerio

BSA – Bovine serum albumin

C

cAMP – cyclic adenosine monophosphate

Capu – Cappucino

cDNA – Complementary DNA

CIP – Calf intestinal alkaline phosphatase

CMV – Cytomegalovirus

CobI – Cordon-bleu

Co-IP – Co-immunoprecipitation

Crag – Calmodulin-binding protein related to a Rab3 GDP/ GTP exchange protein

CRISPR – Clustered Regulatory Interspaced Short Palindromic Repeats

CV – Column volume

Cy5 – Cyanine dye 5

D

DENN – differentially expressed in normal and neoplastic cells

DFV – Discoidal/ fusiform.shaped vesicle

DLC2 – Dynein light chain 2

DLIC – Dynein light intermediate chain

DMEM – Dulbecco's modified eagle's medium

Dm-Myo5 – Drosophila myosin 5

DMSO – Dimethylsulfoxide

dNTP – 2'-Desoxyribonucleosid -5'-triphosphate

DTE – 1,4-Dithioerythritol

E

EB – Elution buffer

ECM – Extracellular matrix

EDTA – Ethylenediaminetetraacetate

EE – Early endosome

EEA1 – Early endosome antigen 1

EFBD – exon-F binding domain

EGF – Epidermal growth factor

eGFP – Enhanced GFP

EHD1 – Eps-15-homology domain-containing protein 1

EHD3 – Eps-15-homology domain-containing protein 3

ER – Endoplasmatic reticulum

F

F-actin – Filamentous actin

FCCS – Fluorescence cross-correlation spectroscopy

FCS – Fluorescence correlation spectroscopy

FCSIII – Fetal calf serum III

FH – Formin-homology domain

FL – Full length

FMN – Formin family formin

FMN-1 – Formin-2

FSI – Formin/ Spir interaction sequence

FYVE – Fab1, YOTB/ ZK632.12, Vac1, EEA1

G

G-actin – Globular actin

GAP – GTPase activating protein

GDF – GDI displacement factor

GDI – Guanine nucleotide dissociation inhibitor

GDP – Guanosine diphosphate

GEF – Guanine nucleotide exchange factor

GFP – Green fluorescent protein

Gg – Gallus gallus

GluA1 – Glutamate ionotropic receptor AMPA type subunit 1

GLUT4 – Glucose transporter type 4

GS – Griscelli syndrome

GST – Glutathione-S-transferase

GTBM – Globular tail domain binding motif

GTP – Guanosine triphosphate

H

HCl – Hydrochloric acid

HEK 293 – Human embryonic kidney 293 cells

HPLC – High pressure liquid chromatography

HRP – Horse-radish-peroxidase

Hs – Homo sapiens

I

IC – Intermediate compartment

Ile – Isoleucine

INF2 – Inverted formin 2

IPTG – Isopropyl-ß-D-thiogalactopyranoside

IG motif – Isoleucine glutamine motif

K

KCl – Potassium chloride

kDA – Kilodalton

KH_2PO_4 – Potassium dihydrogen phosphate

KIF – Kinesin superfamily

KIND – Kinase non-catalytic C-lobe domain

KW – KIND-WH2

L

LB_0 – Lysogeny broth

LE/ MVB – Late endosome/ multi-vesicular body

M

mA – Milliampere

MaxiPrep – Plasmid – Maxi- Purification

MDa – Megadalton

$MgCl_2$ – Magnesium chloride

MLPH – Melanophilin

mM – Millimolar

Mm – Mus musculus

MMP – Matrix metalloproteinase

mRNA – Messenger RNA

MYO5A – Myosin 5A

MYO5B – Myosin 5B

MYO5C – Myosin 5C

MYRIP – Myosin and Rab interacting protein

N

Na_2HPO_4 – Sodium hydrogen phosphate

Na_3VO_4 – Sodium orthovanadate

NaCL – Sodium chloride

NaF – Sodium fluoride

NEB – New England Biolabs

NPF – Nucleation promoting factor

NT3 - Wash Buffer

NTA – Nitrilotetraacetat

NTI – Binding Buffer

O

oN – Over night

P

PAGE – Polyacrylamide gelelectrophoresis

PBS – Phosphate buffered saline

PBST – PBS/ Tween20

PCC – Pearson Correlation Coefficient

PCR – Polymerase chain reaction

Phe – Phenylalanine

P_i – Inorganic phosphatate

PIP2 – Phosphatidylinositol-3,4,5-trisphosphate

PMSF – Phenylmethylsulfonylfluoride

PSD – Postsynaptic densities

R

Rab – Ras-like in brain

Ran – Ras-like nuclear

Ras – Rat sarcoma

RCP – Rab coupling protein

RE – Recycling endosome

Rho – Ras homology

RPKM – reads per kilo base of transcript per million mapped reads

RT – Room temperature

S

SB – Spir-box

SDS – Sodium dodecyl sulfate

SEC – Size exclusion chromatography

SEM – Standard error of mean

SF – SB-FYVE

SHD – Synaptotagmin homology domains

SNARE – Soluble NSF Attachment Protein Receptor

SPIRE1/2-ΔKW – Spire-1/2-KIND-WH2

SPIRE1/2-MSF – Spire-1/2-GTBM-SB-FYVE

T

T_A Annealing temperature

TBC – Tre2/Bub2/Cdc16

TBE – Tris-borated-EDTA

t_E – Elongation time

TEV – Tobacco Ech Virus

TGN – Trans-Golgi network

TH1 – Tail homology 1 domain

TIRF – Total internal reflection

TLR4 – Toll-like receptor 4

Tm – Melting temperature

V

Val – Valine

W

WASP – Wiskott-Aldrich syndrome protein

WAVE – WASP-familiy verprolin homology

WH2 – Wiskott-Aldrich syndrome protein homology

8 List of figures

Figure 1: The highways and local roads model of mammalian exocytic transport processes. 12
Figure 2: Actin filament polymerisation and depolymerisation. 14
Figure 3: Actin nucleation factors 15
Figure 4: Isoforms of vertebrate SPIRE1 16
Figure 5: RAB GTPase cycle 18
Figure 6: Mammalian class-5 myosin actin motor proteins 20
Figure 7: Structure and conformations of MYO5A and SPIRE2 23
Figure 8: Diagram showing the general structure of the SPIRE protein 24
Figure 9: RAB/SPIRE/MYO5 motor protein complexes 26
Figure 10: Different known protein complexes and their functions 27
Figure 11: *Model of a proposed RAB8/SPIRE/MYO5/FMN protein complex in choanoflagellates* 31
Figure 12: Method of the Protein Purification using ÄKTA purifier system. 51
Figure 13: Fluorometric measurement protocol and black 96 well plate layout 55
Figure 14: RNA expression of SPIRE1, SPIRE2, MYO5A, MYO5B, MYO5C, FMN1, FMN2, MLPH and MYRIP 60
Figure 15: Overview on mammalian myosin 5A, myosin 5B and myosin 5C protein fragments used in this thesis. 62
Figure 16: Overview on SPIRE1/2-linker, Sr-SPIRE-linker, Nv-SPIRE-linker protein fragments used in this thesis. 63
Figure 17: Overview on SPIRE1/2 protein fragments used in this thesis. 63
Figure 18: Protein purification steps of GST-NTEV-Hs-MYO5B-GTD. 64
Figure 19: Chromatogram for size exclusion chromatography of His_6-mScarlet-I-Nv-SPIRE-linker. 65
Figure 20: SDS-PAGE of His_6-mScarlet-I-Nv-SPIRE-linker after size exclusion chromatography. 65
Figure 21: Protein quality control of used purified proteins: 66
Figure 22: SPIRE1 and SPIRE2 interact with MYO 5A-GTD. 67
Figure 23: SPIRE1 and SPIRE2 interact with MYO5B-GTD. 68
Figure 24: SPIRE1 and SPIRE2 interact with MYO5C-GTD. 69
Figure 25: Schematic representation of GTD- and linker-region. 70
Figure 26: MYO5A/B/C-GTD interacts with SPIRE1/2-linker: 70
Figure 27: Schematic representation of GTD- and linker-region. 71
Figure 28: Scheme of the quantitative binding assay: 73

Figure 29: Quantitative binding assays of GST-NTEV-Hs-MYO5-GTD with His_6-mScarlet-I-Hs-SPIRE1/2-linker..... 74
Figure 30: Quantitative pulldowns of GST-NTEV-Hs-MYO5A-GTD with His-mScarlet-I-Hs-SPIRE1/2-linker with the measured dissociation constants, K_d..... 75
Figure 31: MYO5-cc-GTD and SPIRE1-ΔKW and SPIRE2-ΔKW colocalise at vesicle membranes..... 78
Figure 32: The SPIRE GTBM contains highly conserved amino acid clusters with distinct chemical properties..... 81
Figure 33:Schematic representation of the indirect targeting with MLPH compared to the direct targeting by RAB11 without MLPH..... 88
Figure 34: Single graphs of RNA-Expression..... 118
Figure 35: Nv/Sr/Hs-MYO5A-GTD interacts with Nv/Sr/Hs-SPIRE1-linker:..... 119
Figure 36: Single graphs of MYO5-GTD – SPIRE-linker quantitative pulldown assays..... 120
Figure 37: Myosin5A-cc-GTD and SPIRE-1-ΔKW and SPIRE-2-ΔKW colocalise at vesicle membranes. 126
Figure 38: Myosin5B-cc-GTD and SPIRE-1-ΔKW and SPIRE-2-ΔKW colocalise at vesicle membranes. 127
Figure 39: Myosin5C-cc-GTD and SPIRE-1-ΔKW and SPIRE-2-ΔKW colocalise at vesicle membranes. 128
Figure 40: GFP and SPIRE-1-ΔKW and SPIRE-2-ΔKW do not colocalise at vesicle membranes..... 129

9 List of tables

Table 1: Protocol of PCR-mixture 36
Table 2: PCR cycling protocol 36
Table 3 : Protocol for plasmid DNA vector digest. Enzyme 37
Table 4: Protocol for insert digest. Enzyme: 37
Table 5 : Protocol for ligation of digested plasmid DNA vectors and DNA- inserts 38
Table 6: Protocol for digest. 41
Table 7: Overview of the measured equilibrium dissociation constants (K_d) of the MYO5-GTD: SPIRE-linker interactions 76
Table 8: Comparison of measured dissociation constants (K_d) 77
Table 9: Overview on known and suggested protein complexes with their cellular function. 85
Table 10: Overview on eukaryotic expression vectors. aa, amino acid. 116
Table 11: Overview on bacterial expression vectors 117
Table 12: raw data of the quantitative pulldown assays. 121
Table 13: Raw data for RNA expression level analysis 125
Table 14: Overview on buffers, solutions and media. 131
Table 15: Preparation of SDS separation gels. 131
Table 16: Preparation of SDS stacking gels. 132
Table 17: Overview on primers used in this thesis. Tm, melting temperature. 132
Table 18: Overview on primary antibodies. 132
Table 19: Overview on secondary antibodies. 133
Table 20: Overview on restriction endonucleases. 133
Table 21: Overview on DNA polymerases. 133
Table 22: Overview on further used enzymes. 133
Table 23: Overview on chemicals. 135
Table 24: Overview on cell culture media, reagents and supplements 135
Table 25: Overview on kits. 135
Table 26: Overview on used equipment. 136
Table 27: Overview on desposables 137

10 Acknowledgements

Zuallererst möchte ich mich bei meinem Doktorvater Prof. Dr. Eugen Kerkhoff für die Möglichkeit bedanken, meine Doktorarbeit in seinem Labor am Universitätsklinikum anzufertigen. Danke für deine Unterstützung, die klärenden Gespräche und wissenschaftlichen Diskussionen. Vielen Dank auch für die Möglichkeiten die Welt der Wissenschaft bei Konferenzen im In- und Ausland näher kennenzulernen.

Ein ganz großer Dank geht an Dr. Tobias Welz. Ohne dich, deine Hilfe in allen Laborangelegenheiten vom ersten Tag an und deine Geduld, die Zusammenhänge auch mehrmals zu erklären und dabei immer ruhig zu bleiben. Danke, dass du dir immer Zeit für mich genommen hast, auch für das Korrekturlesen! Ohne dich und dein umfassendes Wissen wäre diese Arbeit nicht so zustande gekommen, wie sie jetzt hier liegt.

Im Labor gilt ein ganz großer Dank Annette Samol-Wolff. Du bist für uns alle im Labor unglaublich wichtig, durch deine mentale und wissenschaftliche unmittelbare Unterstützung. Vielen lieben Dank dafür! Ein großer Dank geht auch an Antonia Heinrich. Für deine mentale Unterstützung im Labor und auch außerhalb des Labors! Vielen Dank für die wunderschöne Zeit in Helsinki!

Thank you Prof. Dr. Stephan Schneuwly and Prof. Dr. Alistair Hume for helping me as my mentors during the last three years. Thank you for your support, your ideas, and the discussions during our meetings and your knowledge!

I would like to thank my thesis committee Prof. Dr. Eugen Kerkhoff, Prof. Dr. Stephan Schneuwly, Prof. Dr. Alistair Hume, Prof. Dr. Oliver Bosch and Prof. Dr. Gernot Längst for giving me the opportunity to do my colloquium to reach my goal to finish my doctoral thesis.

Ein Dank geht auch an meine Labornachbarn Dr. Laura Ammer, Birgit Jachnik, Dr. Arabel Vollmann-Zwerenz, Eva Herschberger, Jeanne und Annette Lohmeier (Lohmi) für die gute Zusammenarbeit, eure Hilfsbereitschaft, die schöne Zeit in der Küche bei Kaffee und Kuchen ☺ Ihr werdet mir fehlen!

Vielen Dank an die AG Bruckmann für die Proteinanalyse. Danke an Frau Dr. Bruckmann für die Möglichkeit der Überprüfung der Proteine. Mein besonderer Dank gilt Patricia Luckner für die klärenden und angenehmen Gespräche sowie Ihre Hilfe in allen Fragen.

In dieser Zeit waren für mich waren meine Freunde sehr wichtig, allen voran Julia <3 und Chris. Vielen lieben Dank, dass ihr einfach immer für mich da seid! Für all die schönen Stunden an der Donau oder am Bismarkplatz, Hauptsache Wein ist dabei ☺ Dziękuję! Und vielen Dank fürs Korrekturlesen ☺ Melina und Jaki für die schönen Stunden, die wir zusammen verbracht haben und ich mal nicht an die Arbeit denken musste ☺. Helena, du denkst immer aus der Ferne an mich. Vielen Dank meine Liebe! ☺ Annkathrin und Noah, ihr bringt mich durch unsere Videocalls immer auf andere Gedanken! ☺

Und zuletzt möchte ich mich von Herzen bei meinem Freund Tobi und meiner Familie bedanken!!! Tobi, danke, dass wir uns gefunden haben, dass du immer hinter mir stehst und für mich da bist!! <3 Mama, Papa ohne eure Unterstützung hätte ich dieses Studium nicht absolvieren können! Mama, Papa und Patrick, ohne unsere wöchentlichen Telefonate hätte ich diese teilweise stressige Zeit nicht durchgestanden. Ihr seid mein Fels in der Brandung und ihr seid immer für euch da. Ich kann mich immer auf euch verlassen und liebe euch über alles!! <3